Microscopic description and simulation of ultracold atoms in optical resonators

Dissertation
zur Erlangung des akademischen Grades
Doktor der Naturwissenschaften

eingereicht an der
Fakultät für Mathematik, Informatik und Physik
der Leopold-Franzens-Universität Innsbruck

von
Mag. rer. nat. Wolfgang Niedenzu

Betreuer: Univ.-Prof. Dr. Helmut Ritsch, Institut für Theoretische Physik

Innsbruck, Juni 2012

Zusammenfassung

Die Entwicklung verschiedener Atomkühlverfahren in den letzten Jahrzehnten ebnete den Weg zur Erforschung der Bewegung stark korrelierter Atome in optischen Gittern. Idealisierte »klassische« optische Gitter, die von zwei gegenläufigen Laserstrahlen gebildet werden, sind keiner Rückwirkung der in ihnen gefangenen Atome ausgesetzt. Dies ändert sich, wenn das Licht in einem optischen Hohlraumresonator hoher Güte eingeschlossen ist. In diesen Systemen werden Lichtfelder und die durch sie induzierten Potentiale stark von den eingeschlossenen Teilchen beeinflusst und somit integraler Bestandteil der Dynamik. Diese Rückwirkung erlaubt es, Atome mittels Licht in optischen Resonatoren zu kühlen. Des weiteren lassen sich dadurch effektive nichtlokale Wechselwirkungen zwischen Teilchen realisieren, da jegliche von einem Teilchen verursachte Änderung des elektrischen Feldes von sämtlichen anderen verspürt wird.

Die vorliegende Dissertation fasst meine Forschungsergebnisse zu Systemen kalter Atome in optischen Hohlraumresonatoren zusammen. Sie gliedert sich thematisch in drei Teile, die einem Hintergrundteil sowie den zwei unterschiedlichen studierten Systemen entsprechen. Im ersten Forschungsteil untersuchen wir das Verhalten von ultrakalten Atomen in einem Ringresonator. Dazu werden Konzepte und Methoden, wie sie für die Beschreibung sowohl »klassischer« als auch von Stehwellenresonatoren gebildeter, das heißt »gequantelter«, optischer Gitter angewandt werden, verallgemeinert. Ein wichtiges Resultat dieser Arbeit ist, dass Näherungen, die für die eben genannten Systeme üblicherweise durchgeführt werden, die Dynamik nicht mehr adäquat beschreiben können. Im Speziellen zeigen wir, dass im von uns abgeleiteten mathematischen Modell (ein verallgemeinerter Bose-Hubbard-Hamiltonoperator) Kopplungen zu energetisch höher gelegenen Teilchenzuständen vorkommen, welche die Systemdynamik nachhaltig beeinflussen. Dies hat wichtige Konsequenzen für das Tunnelverhalten, wie wir durch Analyse von Quantensprungtrajektorien zeigen konnten. Quantensprünge des Feldes haben stets signifikante Auswirkungen auf die Teilchenbewegung. Diese konnten wir in einem Grenzfall, in dem sich die Dynamik durch adiabatische Eliminierung der Hohlraummode vereinfachen lässt, vermittels eines einfachen analytischen Modells begründen. Diese quantenmechanische Dynamik führt zu starken nichtlokalen Bewegungskorrelationen und Teilchenverschränkung. Ein besonders überraschendes Ergebnis der Arbeit ist, dass sich die Quantenkorrelationen massiv von ihren klassischen Äquivalenten unterscheiden. Dies kann für zukünftige Experimente, die den Übergang von der Quantenmechanik zur klassischen

Physik untersuchen, von Bedeutung sein.

Im zweiten Forschungsteil untersuchen wir das kollektive Phänomen der Selbstorganisation in optischen Stehwellenresonatoren. Dabei befinden sich die Atome im Lichtfeld eines Lasers und streuen Licht in den Resonator. Oberhalb einer kritischen Laserintensität ordnen sich die Teilchen in einem bestimmten Muster an, welches dem durch ihre eigenen gestreuten Photonen gebildeten Potential entspricht. Sie fangen sich also in ihrer selber errichteten Falle. Numerische Simulationen zeigen, dass Resonatorkühlen diesen Selbstorganisationsprozess auf langen Zeitskalen auszulösen vermag, selbst wenn die ursprüngliche Lichtintensität des einstrahlenden Lasers hierfür nicht ausreichend ist. Wir leiten eine Bewegungsgleichung für die Phasenraumverteilung der Teilchen her, die im Gegensatz zu früheren Arbeiten Fluktuationen explizit berücksichtigt und somit das Verhalten auf langen Zeitskalen vorhersagen kann. Diese nichtlineare Fokker-Planck-Gleichung erlaubt neue Einblicke sowohl in den Selbstorganisations- als auch in den Kühlprozess. Darüber hinaus schlagen wir ein neues effizienteres Kühlverfahren für Moleküle vor, das auf der Beimengung leichterer vorgekühlter Atome beruht. Dies ist von praktischer Bedeutung, da konventionelle Laserkühlverfahren für die meisten Moleküle aufgrund der im Vergleich zu Atomen erhöhten Anzahl an Freiheitsgraden nicht angewendet werden können.

Abstract

The investigation of the motion of strongly correlated atoms in optical lattices became possible owing to the development of various atom cooling schemes during the last decades. Idealised "classical" optical lattices, created by two counter-propagating laser beams, are not subject to any back-action stemming from the confined particles. This behaviour is altered when the light field is enclosed within a high-finesse optical cavity. In such systems the trapped atoms strongly influence the intracavity light field and, consequently, the light-induced forces. Therefore the optical lattice itself becomes an integral part of the dynamics. This back-action is the physical ground for cooling atoms within optical cavities. Furthermore, the interaction of all atoms with a single common cavity mode induces non-local couplings between the particles because any modification of the light field originating from a single particle is experienced by all the others.

The present thesis summarises my research on systems of cold atoms in optical resonators. It is divided into three parts, a background part and two parts devoted to the two different systems studied. In the first research part we investigate the behaviour of ultracold particles in ring resonators. To this end we generalise concepts and methods frequently employed in the investigation of either "classical" optical lattices or "quantised" lattices generated by standing-wave cavities. An important result of this work is, that common approximations for such systems do not provide an accurate description of the dynamics within ring resonators any more. Particularly, we show that couplings to excited particle states appear in the model we have derived (a generalised Bose–Hubbard Hamilton operator), which strongly alter the dynamics. As we could show by analysing quantum jump trajectories, these couplings have important consequences for the tunnelling behaviour of the particles. We could motivate the occurring correlated particle-field jumps by means of a simple analytical model in a limit, where the cavity mode can be adiabatically eliminated from the dynamics. These genuine quantum effects lead to strong non-local motional correlations and entanglement between the atoms. A surprising result of this work is, that the quantum correlations strongly differ from their classical counterparts. This may be applicable in experiments exploring the quantum-classical boundary.

In the second research part of the thesis we investigate the collective phenomenon of self-organisation in optical standing-wave cavities. In this setup the atoms are illuminated by a transverse laser beam and scatter light into the resonator. Above a certain critical threshold laser intensity, the particles order themselves in a specific

pattern. Its form is related to the potential created by the scattered photons. Therefore the atoms are aligned in a trap created by themselves. Numerical simulations reveal that cavity cooling can trigger a self-organisation processes even if the initial light intensity of the irradiating laser is insufficient. We derive an equation of motion for the phase-space density of the particles, which contrary to previous work explicitly takes into account fluctuations, allowing for prediction of the system behaviour on long time scales. This non-linear Fokker–Planck equation offers new insights into the cooling- and the self-organisation process. Furthermore, we propose a new cooling scheme for molecules which is based on the admixture of lighter pre-cooled atoms. This new proposal is of practical relevance because conventional laser cooling schemes are not applicable for molecules due to their plethora of degrees of freedom.

Danksagung

An dieser Stelle möchte ich mich bei allen Personen bedanken, die mich während des Studiums und der Arbeit an dieser Dissertation in unterschiedlichster Art und Weise unterstützt haben. Eine solche Aufzählung kann leider trotz aller Sorgfalt nie vollständig sein und ich bitte all diejenigen, die hier natürlich namentlich erwähnt gehörten aber nicht aufscheinen, um Entschuldigung.

In erster Linie gebührt mein Dank meinem Betreuer Prof. Helmut Ritsch, der mit viel Geduld und physikalischer Intuition meine Arbeit in die richtigen Bahnen zu lenken vermochte. Ungeachtet der zeitlichen Belastung durch zusätzliche administrative Aufgaben am Institut fand er stets die Zeit für Diskussionen und hilfreiche Ratschläge. Seine kollegiale Art und Weise sowie sein stetiges Anliegen, ein hervorragendes Klima in der Arbeitsgruppe zu schaffen und zu erhalten, stellten eine große Motivation für mich dar. Auch danke ich ihm dafür, mir die Teilnahme an verschiedenen internationalen Konferenzen ermöglicht zu haben.

Allen derzeitigen und ehemaligen Mitgliedern unserer Forschungsgruppe – János Asbóth, Erez Boukobza, Claudiu Genes, Tobias Grießer, Sebastian Krämer, Christoph Maschler, Igor Mekhov, Laurin Ostermann, Thomas Salzburger, Kathrin Sandner, Raimar Sandner, Rainer Schulze, Matthias Sonnleitner, András Vukics und Hashem Zoubi – danke ich für die hervorragende Arbeitsatmosphäre sowie für die vielen Diskussionen, sei es nun über physikalische Fragestellungen oder über außeruniversitäre Geschehnisse. Meine Bürokollegen Matthias, Sebastian und Tobias sowie früher Rainer und Thomas wussten und wissen stets für eine gute Stimmung zu sorgen. Bei Hashem, Kathrin und Laurin möchte ich mich für die aufmunternden Worte, wenn es mal nicht so gut lief, bedanken, ebenso bei Tobias für seine große Hilfsbereitschaft. Die Zusammenarbeit mit András, Claudiu, Raimar, Rainer und Tobias hat mir viel Freude bereitet und ich habe dabei auch viel über Physik im Allgemeinen gelernt. Raimar und Sebastian konnten mir dank ihres profunden Linuxwissens einige Male weiterhelfen, wohingegen Matthias äußerst hilfreiche Gnuplot-Kniffe aus dem Ärmel zu zaubern vermag. Mit Matthias und Raimar führte ich einige sehr unterhaltsame abendliche Fußballspiele auf unserer Gruppenkonsole (Danke, Erez!). Diese, wie auch die vielen Wanderungen, die Skiausflüge mit Matthias und Tobias sowie die Raftingtour mit Laurin, Matthias und Sebastian waren stets schöne und willkommene Abwechslungen zum Unialltag. Mit Erez und Laurin verbrachte ich viele vergnügliche Filmeabende, auch verdanke ich ihnen unzählige wertvolle Musikempfehlungen. Bei Erez möchte ich mich besonders für seine Versuche, mir die hebräische Sprache

näherzubringen, bedanken, ich habe die zahlreichen Gelegenheiten zum »Deutsch-Hebräisch Ping-Pong« sehr genossen. תודה רבה על הכל, ארז! Auch danke ich ihm und Hashem für die vielen interessanten und lehrreichen Gespräche über ihre Heimat. Unvergessen bleibt mir auch Rainers Abschiedsständchen am Saxophon als Erez unsere Gruppe wieder verließ. Die gemeinsamen Kaffeepausen boten stets eine Plattform für interessante Diskussionen; Lars Bonnes, Florian Fröwis, Volckmar Nebendahl und Markus Penz waren auch öfters dabei, was stets eine Bereicherung war.

Am Institut gebührt mein Dank unserem Systemadministrator Hans Embacher für die perfekte Wartung unserer Computersysteme sowie unseren Sekretärinnen Lidija Infeld, Nicole Jorda, Birgit Siorpaes, Monika Weiß, Elke Wölflmaier und Manuela Zine für die reibungslose Administration. Bei Prof. Gebhard Grübl möchte ich mich für die grandiosen Bergtouren, die er in den letzten Jahren organisiert hat, bedanken. Nicht unerwähnt bleiben soll auch Steven Bass – seine alljährlichen interdisziplinären AFI-Symposien erlauben seit vielen Jahren faszinierende Einblicke in andere Fachgebiete.

Außerhalb Innsbrucks möchte ich mich besonders bei Prof. Giovanna Morigi bedanken, die mir zwei inspirierende Aufenthalte in ihrer Forschungsgruppe in Barcelona und Saarbrücken ermöglicht hat. Ich danke Christian Arenz, Cecilia Cormick, Gabriele De Chiara, Sònia Fernández-Vidal, Stefan Rist, Stefan Schütz, meinen Saarbrücker Bürokolleginnen Susanne Blum und Katharina Rojan sowie besonders Hessam Habibian für viele interessante und hilfreiche Diskussionen. Bei Hessam möchte ich mich zusätzlich für die vielen Gespräche abseits der Physik und die tolle Zeit in Barcelona und Saarbrücken bedanken. Muchas gracias a Cecilia por su paciencia todas las veces en que tuve que buscar una palabra durante nuestras conversaciones, y por su buen humor. Muchas gracias también a Clara Inés Osorio por todo su apoyo durante los años pasados.

Für ihre großartige Unterstützung seit unserem Studienbeginn vor knapp zehn Jahren möchte ich mich ganz besonders bei meinen Freunden und Kollegen Manfred Mark, Markus Müller und Matthias Sonnleitner bedanken. Umso mehr freute es mich, dass Matthias vor zwei Jahren in unser Büro einzog. Für die schöne Zeit möchte ich mich zusätzlich bei Michael Kugler, Cornelia Lechner und Simon Schallhart bedanken.

Bei Kathrin, Laurin und Matthias bedanke ich mich für das Korrekturlesen einzelner Kapitel dieser Arbeit.

Den größten Dank jedoch verdienen meine Eltern, ohne ihre Unterstützung wäre ein Studium für mich nicht möglich gewesen.

Wolfgang Niedenzu, Juni 2012

Contents

Chapter 1

General introduction and overview

The beginning of the twentieth century was a remarkable period since most of the foundations of modern physics were developed at this time. Max Planck's revolutionary work on black body radiation from 1900 [1.1, 1.2], where he postulated that energy can only be absorbed or emitted in *discrete* portions by oscillators, and Albert Einstein's discussion of the photoelectric effect from 1905 [1.3] are commonly regarded as the birth of quantum mechanics. Paul Dirac's subsequent studies of particle-light interaction in the 1920s and his derivation of the Einstein coefficients for spontaneous and stimulated emission [1.4, 1.5] established the basis for the theory of quantum electrodynamics (QED). Later contributions by Fermi, Dyson, Feynman and others [1.6–1.8] provided a deeper understanding of the interaction of quantised light fields with quantised matter. Moreover, the mathematical formulation of quantum electrodynamics as a field theory could also be applied very successfully to describe the weak and strong forces of particle physics, which are responsible for radioactive decay and describe the interactions within the atomic nucleus, respectively.

On the experimental side, it was as early as 1933 that R. Frisch could confirm Einstein's hypothesis, that absorption and emission of a photon by an atom are associated with a recoil kick on the particle [1.9]. One of the most ground-breaking experimental achievements of the twentieth century was without a doubt the realisation of the laser in 1960 [1.10] following a theoretical proposal from 1958 [1.11]. This invention favoured a vast expansion of research in atomic, molecular and optical physics (AMO). Besides having huge experimental and theoretical impact by themselves, nowadays lasers are an indispensable tool in any quantum optics laboratory around the world and also found their way into our everyday life. They are routinely used for trapping and cooling atoms [1.12–1.14] and also provide a wide range of applications as optical tweezers [1.13], for example in the investigation of DNA strings [1.15] or for the manipulation of large living objects [1.16]. Based upon work by Ashkin on light forces [1.17], Hänsch and Schawlow [1.18] and, independently, Wineland and Dehmelt [1.19], proposed the Doppler cooling scheme in 1975. Since then, a variety of novel schemes like, for example, polarisation-gradient cooling [1.20], allowing for sub-Doppler cooling have been proposed [1.21]. In 1997, the Nobel Prize was awarded to Steven Chu, Claude Cohen-Tannoudji and William D. Phillips for

their contributions to laser cooling and trapping [1.22–1.24].

The possibility of cooling atomic gases allowed for the experimental realisation of Bose–Einstein condensates (BECs) in 1995 [1.25, 1.26], which Eric A. Cornell, Carl E. Wieman and Wolfgang Ketterle were awarded the Nobel Prize for in 2001 [1.27, 1.28]. This particular state of matter has been predicted by Einstein in 1925 [1.29, 1.30] based upon the Bose–Einstein distribution [1.31]. This genuine quantum-mechanical phase is characterised by a macroscopic population of the lowest energy state, where all particles behave like a single matter wave. In the same way as light can show corpuscular behaviour, matter can also show wave properties. The extremely low temperatures in the range of a few hundred nano-Kelvin to a few micro-Kelvin required for the phase transition to happen could not be reached by ordinary laser cooling alone. Indeed, an additional evaporative cooling technique was applied [1.25, 1.26]. Since 1995, Bose–Einstein condensation has been realised experimentally for a variety of atomic species [1.32–1.35].

1.1 Light forces, laser cooling and optical lattices

The general idea of light exerting mechanical forces on matter is not new, already Johannes Kepler suggested the idea of radiation being responsible for the fact that the tail of a comet always points away from the sun in his work *De cometis* from 1619. Let us elaborate on the two radiative forces an atom can experience, the *radiation pressure force* and the *dipole force* [1.36]. Even though they have different names and physical interpretations, it is of note that they both stem from the very same interaction of the atomic dipole with the electric field.

First, let us consider the situation of a two-level atom being illuminated by a plane wave. Every time the atom absorbs a photon from the laser, a subsequent spontaneous emission of one photon into free space follows on a time scale determined by the atomic linewidth. This spontaneous emission process has no distinct direction and hence does not contribute to any net force on average, yet there is a contribution to force fluctuations and therefore to momentum diffusion. That is, for each absorption-spontaneous emission cycle—on average—the momentum of one photon pointing into the propagation direction of the wave is transferred to the atom. This is the dissipative radiation pressure force and it is proportional to the spontaneous emission rate of the two-level atom. Note that absorption-stimulated emission cycles do not contribute to the force as the photon is emitted back into the laser propagation direction.

Things change considerably when the atom is not illuminated by a single plane wave but rather by two counter-propagating laser beams forming a standing wave. In this setup the atom experiences a force proportional to the light intensity gradient, the so-called dipole force. It occurs due to the interaction of the induced atomic

dipole with the laser, hence the name. Contrary to the radiation pressure force caused by absorption-spontaneous emission cycles, the dipole force originates from absorption-*stimulated* emission processes, where the atom absorbs a photon from one beam and subsequently emits one into the counter-propagating beam [1.36]. Hence every such cycle is associated with a momentum transfer of twice the momentum carried by a single photon of a laser beam. The momentum of the field and the particle are changed in this process but the field energy remains constant because both light beams have the same frequency. Thus, photon redistribution in a standing wave is a dispersive process rendering the force conservative. With increasing laser power the dipole force becomes larger, as opposed to the radiation pressure force which is bound by the atomic linewidth, independent of the light intensity [1.36]. We conclude this discussion by noting that the dipole force is of great practical relevance, especially in dipole traps [1.14] and optical lattices [1.37] to mention two important examples.

Let us now briefly explain the basic idea of Doppler cooling. Due to the Doppler effect the frequency of a laser beam appears higher to an atom moving towards the laser and lower when it moves away from it. This can be exploited for cooling using counter-propagating laser beams, which are both appropriately red-detuned with respect to the atomic transition. Let us imagine an atom moving towards one of the detuned lasers. Owing to the Doppler effect, the latter appears in resonance to (and the co-propagating one farer detuned from) the atom and it experiences different radiation pressures from the two beams [1.36]. On average this amounts to a net friction force decelerating the particle. This way the atomic motion can be cooled down to temperatures determined by the atomic linewidth. This limiting temperature is called Doppler limit and is typically of the order of a few hundred micro-Kelvin. The setup involving counter-propagating laser beams has been dubbed optical molasses because the forces resemble the ones for a viscous fluid [1.38].

As mentioned, the dipole force allows for the creation of optical lattices. They have been in the centre of attention since the middle of the 1990s, when Jaksch *et al.* [1.39] showed that a dilute gas of cold atoms trapped within an optical lattice could be mapped to the Bose–Hubbard model, a model originally proposed in the 1960s for the computation of correlations in fermionic systems [1.40]. The great advantage of optical lattices compared to actual solid-state systems is their controllability and the quasi-absence of decoherence on experimental time scales [1.41]. The dipole force and hence the depth of the lattice can easily be varied with the laser intensity and various lattice geometries can be realised with different laser setups [1.41, 1.42]. The quantum phase transition between a Mott insulator and a superfluid state for the Bose–Hubbard model, as predicted in 1989 [1.43], could be demonstrated experimentally with a Bose–Einstein condensate of ultracold atoms in 2002 [1.44]. Since then, optical lattices have been applied very successfully for the realisation of otherwise inaccessible condensed matter and solid-state systems [1.37], especially in one [1.45–1.47] and

two dimensions [1.48]. The idea of simulating a quantum system with the help of another quantum system goes back to Feynman [1.49]. Optical lattices are also an important resource for quantum information and quantum computing [1.50–1.52]. New experimental directions include the investigation of Bose–Fermi mixtures [1.53] or ultracold chemistry [1.54]. Furthermore, ultracold atoms play an important role in quantum metrology [1.55], for example new proposals for more precise atomic clocks are based on optical lattices [1.56].

1.2 Atoms in optical cavities

The last part of this general introduction is devoted to cavity quantum electrodynamics (cavity QED), describing the interaction of quantised particles with the quantised electromagnetic field within an optical resonator. Here, due to the longer interaction times a significant back-action of the particles on the radiation field can be observed. Indeed, in the strong-coupling regime of cavity QED, where the coherent processes are much stronger than their dissipative counterparts, atom and field cannot be treated as independent constituents of a joint system any more—much rather the atom and the field have to be considered as one single entity. This behaviour has been predicted theoretically by Jaynes and Cummings in 1963 [1.57], the predicted vacuum Rabi splitting was experimentally demonstrated in 1992 [1.58]. A few years later, light forces could be observed for the first time in optical resonators [1.59]. An astonishing effect in the strong-coupling regime was demonstrated in 2000, namely the possibility of trapping an atom in the field of a *single* photon [1.60–1.62].

Parallel to the experimental developments in the 1990s, the theoretical proposal of exploiting the dissipation channels of optical resonators as a new resource for particle cooling, called *cavity cooling*, was published by Horak *et al.* in 1997 [1.63]. The theoretical understanding was improved in many subsequent publications [1.64–1.70] and collected in a review paper by Domokos and Ritsch in 2003 [1.71]. The major advantage of the proposed cavity cooling scheme as compared to usual laser cooling schemes—like Doppler cooling—is, that it does not require any closed spontaneous emission-repumping cycle for the particles. Conventional laser cooling schemes cannot be applied to atoms with unfavourable level structures, molecules which have a wide range of rotational or vibrational states [1.72, 1.73] or other polarisable objects like nanoparticles [1.74]. In cavity cooling, the non-perfect mirrors allow for transporting energy and entropy out of the system, independent of the internal structure of the particle as long it is linearly polarisable [1.71]. Spontaneous emission, which is indispensable for all previous laser cooling schemes, is not required as a resource. Basically, one exploits the time lag of the field when reacting to the particle, which amounts to a friction force experienced by the latter [1.71]. The limiting factor for the achievable temperatures is the cavity linewidth, which can be much lower than

the Doppler limit. We close this discussion on cooling by mentioning two important experimental achievements, the successful observation of cavity cooling of a single atom in 2004 [1.75] and the very recent realisation of sub-recoil cooling in 2012 [1.76].

As a generalisation of the Bose–Hubbard model for ultracold atoms in optical lattices [1.39], Maschler and Ritsch [1.77] investigated the case of resonator-generated lattices within a cavity, where all particles interact with each other via the common trapping cavity mode. These effective interactions lead to a non-local correlated motion of distant particles, which is in clear contrast to the behaviour of ultracold atoms in "classical" optical lattices not subject to any back-action from the particles. Furthermore, the phase diagram changes considerably when the light field is enclosed in an optical lattice [1.78–1.82], involving areas of co-existing Mott insulator and superfluid phases. In a closely related application, Mekhov *et al.* showed that the quantum phases of ultracold atoms in classical optical lattices can be determined by analysing the transmission spectra of appropriately placed optical cavities [1.83]. See [1.84] for a recent review.

Predicted in our group in 2002 [1.70] and experimentally demonstrated shortly afterwards in 2003 [1.85], self-organisation of atoms within an optical cavity is a striking example for a collective effect. In this setup the particles are directly illuminated by a laser beam transverse to the cavity axis and scatter light from the laser into the resonator. When the particles are homogeneously distributed, these contributions add up destructively so that the particles do not experience any force. Above a certain critical laser intensity, however, the atoms begin to scatter in phase so that a dipole potential builds up. The more particles are trapped, the deeper the potential gets. The atoms are thus trapped in a potential created by their own scattered light, hence the name self-organisation. When all particles scatter in phase, the intracavity light intensity scales with the square of the particle number, a phenomenon known as superradiance [1.86]. The threshold condition for the laser power was lately confirmed experimentally [1.87].

1.3 Outline of the thesis

This thesis is organised into three parts and contains three published articles and one preprint. A short note at the beginning of each publication indicates the primary contribution of the author of the present thesis to that article.

The first part provides an introduction into cavity QED and the physics of particles in optical lattices. Basic physical models like the Jaynes–Cummings Hamiltonian as well as some mathematical background needed for our research contained in this thesis are presented. The Monte Carlo wave function simulation algorithm is also introduced as we made heavily use of it in the publications found in the second part of the present thesis.

The second part is devoted to ultracold particles in ring resonators and contains a publication, a preprint and additional material to the latter. The first article describes a generalisation of the Bose–Hubbard model to optical lattices generated by a ring resonator. Due to the changed boundary conditions we expected crucial differences to the case of standing-wave cavities studied in [1.77, 1.80]. This is indeed the case, one of the most striking differences emerging from this research was the break-down of a simple lowest-band model. It proved to be non-sufficient for an accurate description of the dynamics because in this approximation the standing-wave lattice is recovered. The coupling of higher bands also causes entanglement and correlations between the particles. The preprint is devoted to these topics, where we employed an optomechanical approach for the case of two particles. Surprisingly, a major difference to the classical case investigated by Gangl *et al.* [1.65, 1.66] could be observed. Whilst classically the particles tend to anti-correlate their motion, quantum-mechanically we have found the opposite behaviour of positive correlations.

The last part, finally, summarises our research on particle self-organisation in optical resonators. It contains two journal articles together with an additional chapter presenting details of the calculations not contained in the publications. In the first article we derive a Fokker–Planck equation for the particle phase-space density. This equation governs the time evolution beyond the mean-field limit on longer time scales where correlations of fluctuations are taken into account as well. In the second article we generalise this idea to an ensemble of different species. We find that adding any extra species always lowers the laser power needed for self-organisation. Additionally, we studied a sympathetic cooling scheme where heavy particles—like molecules—can be efficiently cooled by admixing particles of a lighter species, e.g. atoms, without the need of any direct particle-particle interactions.

Each chapter has its own bibliography, which are all gathered at the end of this thesis, starting on page 153. Inevitably, some references appear there multiple times. This thesis closes with a list of publications and conference contributions of the author.

Part I

Background to cavity QED and optical lattices

Chapter 2

Cold particles in optical cavities

In this chapter we review some basic physical models and concepts of cavity QED (cavity quantum electrodynamics) relevant for our work. In section 2.1 we introduce the fundamental Jaynes–Cummings Hamiltonian, which describes the interaction of a two-level atom with a single mode of the quantised electric field. Resonator-generated optical lattices are introduced in section 2.3. The latter require techniques allowing for the description of so-called open systems, i.e. systems in contact with some environment—leading to dissipation and quantum noise. We present these necessary tools in the intermediate section 2.2. Additionally, we also review the Monte Carlo wave function simulations algorithm, a numerical integration technique for the efficient computation of the time evolution of large systems. Such calculations are ubiquitous in our research and therefore we heavily make use of this algorithm in the present thesis.

2.1 The Jaynes–Cummings model

The interaction of a two-level atom with an isolated quantised light mode has first been investigated by Jaynes and Cummings in 1963 [2.1]. A single light mode can be addressed with the help of an optical cavity, the eigenfrequencies $\omega = n\pi c/L$ ($n \in \mathbb{N}$) of which being separated by the free spectral range $\omega_{\mathrm{fsr}} = \pi c/L$ [2.2]. Here L denotes the cavity length. We assume one of those frequencies to be close to the atomic transition frequency, so that we can neglect all other distant (in frequency space) modes of the cavity, see figure 2.1. This system is omnipresent in the field of quantum optics and lies at the heart of cavity QED. Due to its importance for our research we shall present it here in more detail.

The electric field operator for a single mode reads [2.3]

$$\mathbf{E}(\mathbf{x}) = i\sqrt{\frac{\hbar\omega_{\mathrm{c}}}{2\varepsilon_0 V}}(a - a^\dagger)u(\mathbf{x})\mathbf{e}, \tag{2.1}$$

where V is the mode volume and $u(\mathbf{x})$ the mode function. We have assumed the latter to be real because we will consider the case of sinusoidal mode functions throughout

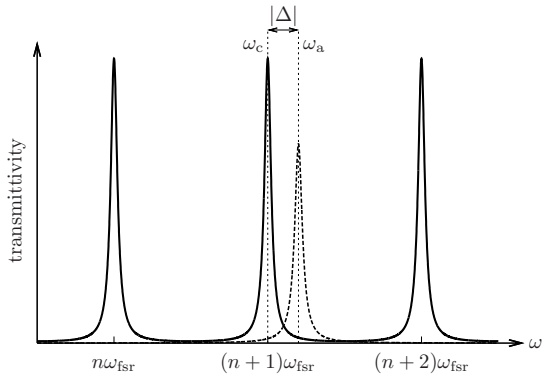

Figure 2.1: Illustration of the frequencies of the system. The cavity is transmissive for certain discrete frequencies which are separated by the free spectral range (solid line). The atomic line (dashed) is close to a single cavity mode and far off-resonant to all the other resonator modes.

this thesis. The polarisation vector is denoted by $\mathbf{e}$ and the cavity frequency by ω_c. Photons are created and annihilated by the bosonic operators $a^\dagger$ and a. Denoting by x the direction along the cavity axis, the fundamental mode of a Fabry–Perot cavity with spherical mirrors is periodic in this direction with Gaussian shape in the two transverse directions near the cavity centre [2.2],

$$u(\mathbf{x}) = \cos(kx) e^{-\frac{y^2+z^2}{w_0^2}}. \tag{2.2}$$

The width of the Gaussian is called mode waist and also appears in the mode volume

$$V = \int_0^L \mathrm{d}x \iint_{\mathbb{R}^2} \mathrm{d}y\,\mathrm{d}z |u(\mathbf{x})|^2 = \frac{\pi}{4} w_0^2 L. \tag{2.3}$$

We assume the two-level atom to be confined along the cavity axis, so that we are left with an effective one-dimensional system. In dipole- and long-wavelength approximation the interaction Hamilton operator reads [2.3]

$$H_\mathrm{int} = -\mathbf{d} \cdot \mathbf{E}(x). \tag{2.4}$$

Expressing the dipole operator $\mathbf{d}$ in the ground- and excited states $|g\rangle$ and $|e\rangle$ of the atom yields

$$H_\mathrm{int} = -i\hbar g(x)(\sigma_+ + \sigma_-)(a - a^\dagger), \tag{2.5}$$

with the coupling strength $g(x) = \sqrt{\frac{\omega_\mathrm{c}}{2\hbar\varepsilon_0 V}}\,\langle g|\mathbf{d}\cdot\mathbf{e}|e\rangle \cos(kx)$, the wave number k and the operators $\sigma_+ := |e\rangle\langle g|$ and $\sigma_- := |g\rangle\langle e|$ describing the excitation and the de-excitation of the atom, respectively. Four different physical processes are contained

in this Hamiltonian, two of them energy-conserving and two non-energy-conserving. The former are

- $\sigma_+ a$—absorption of a photon and excitation of the atom
- $\sigma_- a^\dagger$—emission of a photon and de-excitation of the atom

and the latter

- $\sigma_- a$—absorption of a photon and de-excitation of the atom
- $\sigma_+ a^\dagger$—emission of a photon and excitation of the atom.

The non-energy-conserving terms are usually neglected in the *rotating wave approximation* (RWA). The justification therefor can be seen in an interaction picture with respect to the free evolution

$$H_0 = \hbar\omega_\mathrm{c} a^\dagger a + \hbar\omega_\mathrm{a}\sigma_+\sigma_-. \tag{2.6}$$

Performing this transformation one observes that the energy-conserving terms rotate with the *difference* of the frequencies, whereas the non-energy-conserving terms rotate with the *sum* of them. The RWA consists of neglecting such rapidly oscillating terms [2.3].

Including the centre-of-mass momentum of the atom with mass m, the complete Hamiltonian reads

$$H = \frac{p^2}{2m} + \hbar\omega_\mathrm{a}\sigma_+\sigma_- + \hbar\omega_\mathrm{c} a^\dagger a - i\hbar g(x)(a\sigma_+ - \sigma_- a^\dagger). \tag{2.7}$$

We will, however, ignore the motional degrees of freedom for the moment and the following considerations. First of all, we notice that the Hamiltonian commutes with the excitation operator $N := a^\dagger a + \sigma_+\sigma_-$, i.e. the Hamiltonian only couples states $|g, n\rangle$ (atom in the ground state and n photons in the cavity) with $|e, n-1\rangle$ (atom in the excited state and $n-1$ photons in the cavity). Its ground state is $|g, 0\rangle$. Consequently, the Hamiltonian can be decomposed as $H = \bigoplus_n H_n$, where H_n only acts on the subspace (called manifold in this context) with n excitations, spanned by the vectors $|e, n-1\rangle$ and $|g, n\rangle$. The Hamilton operator H_n can easily be diagonalised within this two-dimensional manifold. Its eigenstates

$$|+, n\rangle = \quad \cos\vartheta_n\,|e, n-1\rangle + \sin\vartheta_n\,|g, n\rangle \tag{2.8a}$$
$$|-, n\rangle = -\sin\vartheta_n\,|e, n-1\rangle + \cos\vartheta_n\,|g, n\rangle \tag{2.8b}$$

are called *dressed states* [2.3]. They are neither atomic nor photonic excitations but combinations of both. This means that the two independent systems—atom and cavity—have been replaced by a single entity—the joint atom-cavity system—due

to the interaction. Defining the detuning $\Delta := \omega_\mathrm{c} - \omega_\mathrm{a}$ and $\Omega_n := \sqrt{\Delta^2 + 4g^2 n}$, the mixing coefficients are found to be

$$\cos\vartheta_n = \sqrt{\frac{\Omega_n - \Delta}{2\Omega_n}} \tag{2.9a}$$

$$\sin\vartheta_n = \sqrt{\frac{\Omega_n + \Delta}{2\Omega_n}}. \tag{2.9b}$$

The corresponding eigenenergies are

$$E_{\pm,n} = -\frac{\hbar\Delta}{2} + \hbar\omega_\mathrm{c} n \pm \frac{\hbar}{2}\Omega_n. \tag{2.10}$$

The two levels within a manifold are separated by the detuning Δ for a non-interacting system, the interaction increases the splitting to Ω_n. At resonance, the energy gap is $\Delta E_n = E_{+,n} - E_{-,n} = 2\hbar g\sqrt{n}$, see figure 2.2. The cavity frequency ω_c determines the energy difference between the manifolds, cf. figure 2.3 for an illustration. The splitting of the (without interaction degenerate) lowest energy manifold at resonance,

$$\Delta E_1 = E_{+,1} - E_{-,1} = 2\hbar g, \tag{2.11}$$

is known as *vacuum Rabi splitting* or *normal mode splitting*. To be visible, the interaction strength needs to be much larger than the atomic and the cavity linewidth (strong-coupling regime). Experimentally, it has first been observed by Thompson *et al.* in 1992 [2.4].

Up to now we have considered an immobile atom, so let us briefly investigate the case of a moving particle. The position-dependent coupling strength causes a corresponding spatial variation of the energy splitting. The Jaynes–Cummings interaction can be treated in second-order time-independent perturbation theory in the dispersive limit $|\Delta| \gg g\sqrt{n}$ to obtain the shifts

$$\Delta E_{g,n} \approx \hbar g^2(x)\frac{n}{\Delta} \tag{2.12a}$$

$$\Delta E_{e,n-1} \approx -\hbar g^2(x)\frac{n}{\Delta} \tag{2.12b}$$

of the bare atom-resonator system for the manifold containing n excitations. For negative detuning, $\Delta < 0$, the levels are repelled whereas in the opposite case $\Delta > 0$ the spatial modulation causes an attraction of the levels. The ground state $|g, 0\rangle$ remains unshifted. See figure 2.4.

2.2 Open systems

The Jaynes–Cummings Hamiltonian describes the idealised situation of a perfectly closed system without losses like spontaneous emission or photons leaking out of the

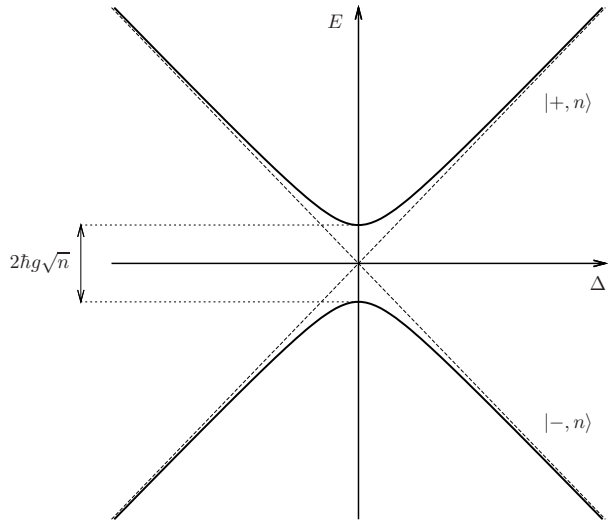

Figure 2.2: Illustration of the avoided crossing for the manifold containing n excitations. The gap increases with increasing excitation number n.

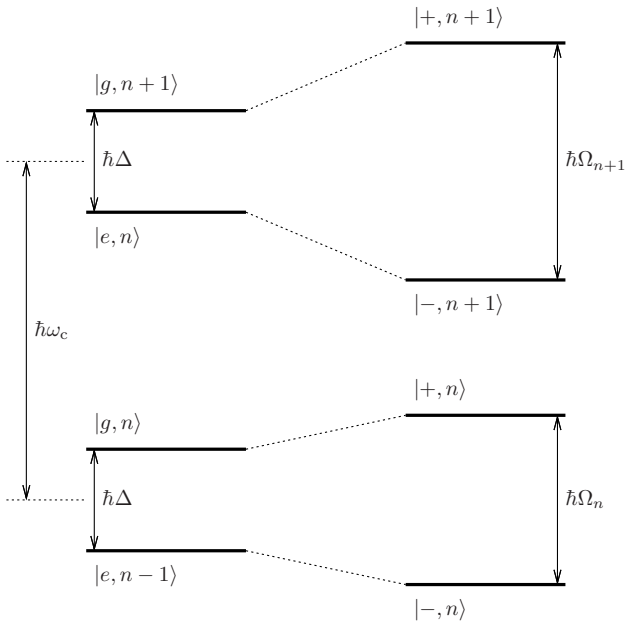

Figure 2.3: Illustration of the energy levels of the bare system (left) and of the dressed states (right) for two manifolds containing n and $n+1$ excitations, respectively. The splitting increases with increasing excitation number n.

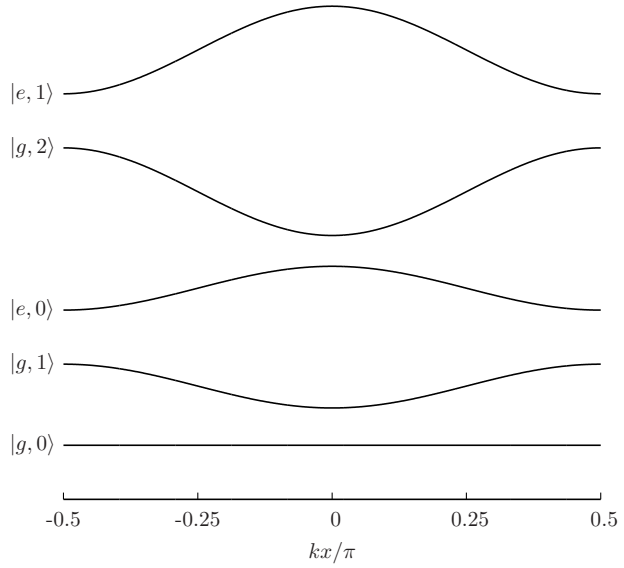

Figure 2.4: Spatial variation of the energy levels for $\Delta < 0$ (off scale). The splitting increases with increasing excitation number n.

resonator. Of course, this assumption is subject to failure when it comes to describing actual experiments—they inevitably always interact with their environment, introducing (quantum) noise to the system of interest. Albeit an unwanted property in many situations (and one strives hard minimising it), it is an absolutely indispensable feature rather than a bug for many other applications. Cavity cooling, for example, requires such a dissipation channel for taking entropy out of the system [2.5–2.7]. Furthermore, damping mechanisms allow for monitoring the system and obtaining information about the atoms and the light confined within the cavity.

The mathematical description of quantum noise can be done in a twofold way—either in the Schrödinger picture for the density matrix or with the help of stochastic Heisenberg–Langevin equations in the Heisenberg picture. Naturally, both formulations are equivalent. The classical analogon would be the Fokker–Planck equation describing the time evolution of the probability density, which is equivalent to a set of stochastic differential equations for the quantities of interest [2.8] (cf. also section 8.1).

2.2.1 Heisenberg–Langevin equations

Let us first describe the influence of a heat bath with many degrees of freedom on a "small" system in the Heisenberg picture. In quantum optics the environment

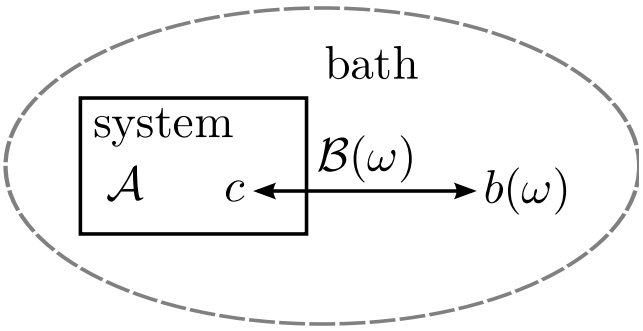

Figure 2.5: Schematic view of the coupling between a system and its surrounding environment. The interaction between the system operator c and the bath operators $b(\omega)$ with strength $\mathcal{B}(\omega)$ is described by the Hamiltonian (2.14b). We are interested in the time evolution of a system operator $\mathcal{A}$.

consists of all modes of the surrounding electromagnetic field. We shall present the derivation following [2.9].

We start from the idealised Hamiltonian

$$H = H_{\text{sys}} + H_{\text{bath}} + H_{\text{int}} \tag{2.13}$$

with

$$H_{\text{bath}} = \hbar \int_{-\infty}^{\infty} \mathrm{d}\omega b^\dagger(\omega) b(\omega) \tag{2.14a}$$

$$H_{\text{int}} = i\hbar \int_{-\infty}^{\infty} \mathrm{d}\omega \mathcal{B}(\omega) \left[b^\dagger(\omega) c - c^\dagger b(\omega) \right]. \tag{2.14b}$$

H_{sys} is a generic Hamiltonian containing variables of the small system of interest only. The operators $b(\omega)$ and $b^\dagger(\omega)$ are bosonic annihilation and creation operators fulfilling the commutation relation

$$\left[b(\omega), b^\dagger(\omega') \right] = \delta(\omega - \omega') \tag{2.15}$$

and c is an operator of the small system mediating the interaction with the environment. Our goal is to find an equation of motion for an arbitrary system operator $\mathcal{A}$. See figure 2.5 for a sketch. To this end we formally integrate the equation for the bath operator $b(\omega)$ and plug in the result into the equation for $\mathcal{A}$. As we will see, quantum noise and damping will be introduced to the latter due to the interaction (2.14b).

The Heisenberg equations of motion derived from the Hamilton operator (2.13) are

$$\dot{b}(\omega) = -i\omega b(\omega) + \mathcal{B}(\omega) c \tag{2.16a}$$

$$\dot{\mathcal{A}} = \frac{1}{i\hbar} [\mathcal{A}, H_{\text{sys}}] + \int \mathrm{d}\omega \mathcal{B}(\omega) \left(b^\dagger(\omega) [\mathcal{A}, c] - [\mathcal{A}, c^\dagger] b(\omega) \right). \tag{2.16b}$$

The formal solution for the bath operator is

$$b(\omega) = b_0(\omega)e^{-i\omega(t-t_0)} + \mathcal{B}(\omega)\int_{t_0}^{t} \mathrm{d}t' e^{-i\omega(t-t')}c(t'). \tag{2.17}$$

Substituting this result into the equation (2.16b) for $\mathcal{A}$ yields

$$\begin{aligned}\dot{\mathcal{A}} = \frac{1}{i\hbar}[\mathcal{A}, H_{\mathrm{sys}}] + \\ + \int \mathrm{d}\omega \mathcal{B}(\omega)\left(e^{i\omega(t-t_0)}b_0^\dagger(\omega)[\mathcal{A}, c] - [\mathcal{A}, c^\dagger]e^{-i\omega(t-t_0)}b_0(\omega)\right) + \\ + \int \mathrm{d}\omega \mathcal{B}^2(\omega)\int_{t_0}^{t}\mathrm{d}t'\left(e^{i\omega(t-t')}c^\dagger(t')[\mathcal{A}, c] - [\mathcal{A}, c^\dagger]e^{-i\omega(t-t')}c(t')\right).\end{aligned} \tag{2.18}$$

At this point we apply the first Markov approximation

$$\mathcal{B}(\omega) = \sqrt{\frac{\kappa}{\pi}}, \tag{2.19}$$

i.e. a frequency-independent coupling to the reservoir. Its most striking consequence is the fact that the resulting equation for $\mathcal{A}$ is now a first order differential equation. This means that the future behaviour of any operator is fully determined by the value of all system operators in the present. Furthermore, we use the representation

$$\int_{-\infty}^{\infty}\mathrm{d}\omega e^{-i\omega(t-t')} = 2\pi\delta(t-t') \tag{2.20a}$$

of the Dirac δ-function and the relation

$$\int_{t_0}^{t}\mathrm{d}t' c(t')\delta(t-t') = \frac{1}{2}c(t). \tag{2.20b}$$

Moreover, we define an "input" field

$$b_{\mathrm{in}}(t) := \frac{1}{\sqrt{2\pi}}\int \mathrm{d}\omega e^{-i\omega(t-t_0)}b_0(\omega) \tag{2.21}$$

satisfying

$$\left[b_{\mathrm{in}}(t), b_{\mathrm{in}}^\dagger(t')\right] = \delta(t-t'). \tag{2.22}$$

Putting everything together we obtain the Heisenberg–Langevin equation

$$\dot{\mathcal{A}} = \frac{1}{i\hbar}[\mathcal{A}, H_{\mathrm{sys}}] - [\mathcal{A}, c^\dagger]\left[\kappa c + \sqrt{2\kappa}\, b_{\mathrm{in}}(t)\right] + \left[\kappa c^\dagger + \sqrt{2\kappa}\, b_{\mathrm{in}}^\dagger(t)\right][\mathcal{A}, c] \tag{2.23}$$

for the system operator $\mathcal{A}$, where the input operators are to be taken as noise terms. Setting $\mathcal{A} = c = a$ as an example, we obtain the well-known quantum Langevin equation

$$\dot{a} = \frac{1}{i\hbar}[a, H_{\mathrm{sys}}] - \kappa a + \sqrt{2\kappa}\, a_{\mathrm{in}}(t) \tag{2.24}$$

for a decaying cavity mode a.

2.2.2 Master equation

The interaction of the small system (e.g. an experimental setup) with the surrounding environment can also be described in the Schrödinger picture. Instead of time-dependent operators like in the Heisenberg picture, one considers a time-dependent density operator ρ_{tot} and static operators. The subscript "tot" refers to the compound setup of the small system together with the bath. Its time evolution is governed by the von Neumann equation

$$\dot{\rho}_{\mathrm{tot}} = \frac{1}{i\hbar}\left[H, \rho_{\mathrm{tot}}\right] \tag{2.25}$$

with an Hamiltonian of the form (2.13). Usually, one is not interested in the evolution of the total density operator but rather in its counterpart ρ describing the small system only. It is obtained by tracing over the bath variables,

$$\rho := \mathrm{Tr}_{\mathrm{bath}}\left(\rho_{\mathrm{tot}}\right). \tag{2.26}$$

In the same way as we have derived an effective equation for an arbitrary system operator $\mathcal{A}$ in the previous section, we now strive to find an evolution equation for ρ. We again follow the line of [2.9] but skip the details of the calculation for brevity and only mention the main steps and ideas. One starts by formally integrating the von Neumann equation (2.25) in the interaction picture with respect to the free evolution $H_0 = H_{\mathrm{sys}} + H_{\mathrm{bath}}$. This solution is plugged back into the evolution equation (2.25) iteratively twice and subsequently differentiated with respect to time yielding an integro-differential equation for ρ_{tot} assuming an initially factorised density operator $\rho_{\mathrm{tot}}(0) = \rho(0) \otimes \rho_{\mathrm{bath}}$. Furthermore, one makes a weak coupling assumption, meaning that the reservoir density operator is not significantly affected by the interaction, in contrast to the system density operator which describes a much smaller (and hence easier to perturb) system. Mathematically, this is expressed by the factorisation assumption

$$\rho_{\mathrm{tot}}(t) \approx \rho(t) \otimes \rho_{\mathrm{bath}} \quad \forall t, \tag{2.27}$$

which results in an integro-differential equation for ρ. As last step one makes the Markov approximation assuming the bath autocorrelation time being much faster than the time scale on which $\rho(t)$ evolves on, to finally end up with a first order differential equation for ρ. For a system-bath interaction like (2.14b) one finds the master equation

$$\dot{\rho} = \frac{1}{i\hbar}\left[H_{\mathrm{sys}}, \rho\right] + \mathcal{L}\rho. \tag{2.28}$$

The last term is called *Liouvillean* and has the Lindblad form [2.10, 2.11]

$$\mathcal{L}\rho = \kappa\left(2c\rho c^{\dagger} - c^{\dagger}c\rho - \rho c^{\dagger}c\right). \tag{2.29}$$

Like for the Heisenberg–Langevin equations, knowledge of the system density operator at present suffices to compute its value at all future times.

We have assumed the surrounding bath to be in its vacuum state when writing down the Liouvillean (2.29), an assumption widely used in quantum optics. This is justified because the number of thermal excitations of modes with optical frequencies ($\omega \sim 400$–$800\,\mathrm{THz}$) at room temperature tends to zero. In situations where this approximation is not adequate, the Liouvillean adopts the form

$$\mathcal{L}\rho = \kappa(\bar{n}+1)\left(2c\rho c^\dagger - c^\dagger c\rho - \rho c^\dagger c\right) + \kappa\bar{n}\left(2c^\dagger\rho c - cc^\dagger\rho - \rho cc^\dagger\right), \tag{2.30}$$

with $\bar{n}$ the mean occupation of the mode with frequency ω. For an environment at temperature T it is determined by the Bose–Einstein distribution [2.12]

$$\bar{n}(\omega, T) = \frac{1}{e^{\frac{\hbar\omega}{k_\mathrm{B}T}} - 1}. \tag{2.31}$$

We shall now very briefly present a numerical method for solving the master equation (2.28) frequently used in our work before coming back to the cavity QED system consisting of a single atom interacting with a single mode—this time including damping.

2.2.3 Monte Carlo wave function simulations

Even though being an equation for the reduced density matrix of the "small" system of interest only, the master equation (2.28) may still be computationally very hard to integrate for more complicated systems. As an example occurring in our work, consider two moving particles interacting with a single cavity mode. The Hilbert space of such a system can easily consist of several thousand dimensions, making it virtually impossible to directly solve the master equation numerically, both in terms of execution time and memory consumption. In such situations the "quantum jump" approach of the Monte Carlo wave function simulation algorithm can be employed. Instead of propagating a large density matrix of dimension $d \times d$, one repeatedly solves the stochastic time evolution for state vectors of dimension $d \times 1$ with a different random number seed for each trajectory [2.13–2.15]. Each trajectory evolves independently from the others so that many of them can be computed in parallel. This renders the algorithm very efficient for execution on high performance computing (HPC) clusters. For large ensembles the mean of all trajectories converges towards the full solution of the master equation. Besides its numerical advantages, the quantum trajectory method is also a powerful tool for unravelling the density matrix dynamics, i.e. to depict the microscopic behaviour of the system [2.16]. A nice example for this is the description of quantum self-organisation found in reference [2.17].

Let us now briefly describe the algorithm [2.3, 2.15]. We consider the master equation

$$\dot{\rho} = \frac{1}{i\hbar}\left[H, \rho\right] + \mathcal{L}\rho \tag{2.32}$$

containing the general Liouvillean

$$\mathcal{L}\rho = \sum_n \left(J_n \rho J_n^\dagger - \frac{1}{2} J_n^\dagger J_n \rho - \frac{1}{2} \rho J_n^\dagger J_n \right). \tag{2.33}$$

The J_n are called jump operators. As an example, the jump operator for a decaying cavity is $J = \sqrt{2\kappa} a$. Introducing the non-Hermitian Hamiltonian

$$H_{\mathrm{nH}} := H - \frac{i\hbar}{2} \sum_n J_n^\dagger J_n \tag{2.34}$$

the master equation (2.32) can be rearranged to

$$\dot{\rho} = \frac{1}{i\hbar} \left(H_{\mathrm{nH}} \rho - \rho H_{\mathrm{nH}}^\dagger \right) + \sum_n J_n \rho J_n^\dagger. \tag{2.35}$$

Its first part will describe damping via a non-unitary time evolution whereas the second part will be responsible for quantum jumps at randomly chosen times according to a special selection criterion.

The Monte Carlo wave function method time step consists of two parts, a non-unitary time step and a possible quantum jump afterwards. The state vector is re-normalised after each time step.

1. **Non-unitary evolution**—The state vector is first evolved for a short time δt according to the Schrödinger equation containing the non-Hermitian Hamiltonian (2.34). In lowest order this gives

$$\left| \psi^1(t+\delta t) \right\rangle = e^{-iH_{\mathrm{nH}}\delta t/\hbar} = \left(1 - \frac{iH_{\mathrm{nH}}\delta t}{\hbar} \right) |\psi(t)\rangle + \mathcal{O}\left(\delta t^2\right). \tag{2.36}$$

   As a consequence of the non-Hermiticity of the Hamiltonian, the norm of $|\psi(t)\rangle$ is not preserved and decreases,

$$\begin{aligned} \left\| \left| \psi^1(t+\delta t) \right\rangle \right\|^2 &= \left\langle \psi(t) \right| \left(1 + \frac{iH_{\mathrm{nH}}^\dagger \delta t}{\hbar} \right) \left(1 - \frac{iH_{\mathrm{nH}}\delta t}{\hbar} \right) \left| \psi(t) \right\rangle = \\ &= 1 - \frac{i\delta t}{\hbar} \left\langle \psi(t) \right| H_{\mathrm{nH}} - H_{\mathrm{nH}}^\dagger \left| \psi(t) \right\rangle + \mathcal{O}\left(\delta t^2\right) \simeq \\ &\simeq 1 - \delta t \sum_n \left\langle \psi(t) \right| J_n^\dagger J_n \left| \psi(t) \right\rangle =: \\ &=: 1 - \sum_n \delta p_n =: 1 - \delta p. \end{aligned} \tag{2.37}$$

2. **Quantum jump**—The second step contains the possibility of a quantum jump. To this end we draw a random number ε uniformly distributed between zero and one and compare it to the loss of the norm δp. We have to distinguish two cases.

- $\varepsilon \geq \delta p$. This will be the more probable case since $\delta p \ll 1$. No quantum jump occurs and the state vector is just re-normalised,

$$|\psi(t+\delta t)\rangle = \frac{|\psi^1(t+\delta t)\rangle}{\sqrt{1-\delta p}}. \tag{2.38}$$

- $\varepsilon < \delta p$. In this case a quantum jump occurs and the new normalised state vector is chosen among the different states $C_n |\psi(t)\rangle$ according to the probability law $\Pi_n = \delta p_n / \delta p$ ($\sum_n \Pi_n = 1$),

$$|\psi(t+\delta t)\rangle = \frac{C_n |\psi(t)\rangle}{\sqrt{\delta p_n / \delta p}}. \tag{2.39}$$

It can be shown that this procedure is on average equivalent to the solution of the master equation [2.15], i.e. that

$$\rho_{\mathrm{MC}}(t) = \frac{1}{N} \sum_{j=1}^{N} |\psi_j(t)\rangle\langle\psi_j(t)| \tag{2.40}$$

converges towards the solution of the master equation (2.32) as the number of trajectories N tends to infinity.

A quantum jump corresponds to the application of a specific jump operator on the stochastic state vector. Quantum jumps can therefore be interpreted as a measurement event, where e.g. a leaked photon is detected outside of the resonator for $J \propto a$. The non-Hermitian Hamiltonian is also called "conditional Hamiltonian" because it describes the system dynamics under the condition that no quantum jump occurs.

The numerical implementation of the algorithm is simple for small systems with few dimensions, for larger systems (like the ones considered in our work) additional considerations have to be made to minimise the usage of computer resources. One very efficient attempt in this direction is the C++QED framework developed by A. Vukics [2.18, 2.19], which presents an ideal basis for the numerical implementation of the quantum systems considered in this thesis.

2.3 Resonator-generated optical lattices

After the mathematical excursus concerning the description of open systems we now return to the model considered in section 2.1 to apply these techniques. In contrast to the presentation there, this time we explicitly take into account resonator losses as well as spontaneous decay of the atom. We will in particular concentrate on a regime where the excited atomic state can be adiabatically eliminated from the dynamics,

leading to an effective model for the external particle degrees of freedom and the resonator mode only. The resulting model is one of the most important fundaments of the work considered in this thesis.

We again consider a single two-level atom coupled to a single mode. Not only do we include dissipation, we also add an external drive of the cavity mode via a laser shining through one of the cavity mirrors. Its pump strength is denoted η. In a frame rotating with the pump laser frequency ω_p the Hamiltonian reads [2.6]

$$H = \frac{p^2}{2m} - \hbar\Delta_\mathrm{c} a^\dagger a - \hbar\Delta_\mathrm{a}\sigma_+\sigma_- - i\hbar g(x)\left(a\sigma_+ - \sigma_- a^\dagger\right) - i\hbar\eta\left(a - a^\dagger\right). \tag{2.41}$$

Here we have introduced the detunings of the cavity and the atom from the laser as $\Delta_\mathrm{c} := \omega_\mathrm{p} - \omega_\mathrm{c}$ and $\Delta_\mathrm{a} = \omega_\mathrm{p} - \omega_\mathrm{a}$, respectively. Denoting by 2κ the decay rate of cavity photons and by γ the polarisation decay rate of the atom, the Liouvillean superoperator reads

$$\mathcal{L}\rho = \kappa\left(2a\rho a^\dagger - a^\dagger a\rho - \rho a^\dagger a\right) + \gamma\left(2\sigma_-\rho\sigma_+ - \sigma_+\sigma_-\rho - \rho\sigma_+\sigma_-\right). \tag{2.42}$$

Note that we have assumed the environment to be in its vacuum state ($T = 0$) as previously discussed. The master equation containing (2.41) and (2.42) is equivalent to the Heisenberg–Langevin equations

$$\dot{a} = (i\Delta_\mathrm{c} - \kappa)a + g(x)\sigma_- + \eta + \xi_a \tag{2.43a}$$

$$\dot{\sigma}_- = (i\Delta_\mathrm{a} - \gamma)a\sigma_- + g(x)a\sigma_z + \xi_\sigma. \tag{2.43b}$$

These are non-linear equations because of the appearing term $a\sigma_z$. The white noise operators ξ_a and ξ_σ fulfil [2.9] (cf. also equation (2.22))

$$\left[\xi_a(t), \xi_a^\dagger(t')\right] = 2\kappa\delta(t - t') \tag{2.44a}$$

$$\left[\xi_\sigma(t), \xi_\sigma^\dagger(t')\right] = 2\gamma\delta(t - t'). \tag{2.44b}$$

We now consider a situation where the excited atomic state is very weakly populated (*low saturation regime*), which can be achieved for either large detuning Δ_a or large decay γ. In this limit we can perform a *bosonisation* of the atomic dipole, i.e. virtually extend the two levels to an infinite ladder as for a bosonic mode [2.7]. This means that the population inversion operator $\sigma_z = |e\rangle\langle e| - |g\rangle\langle g|$ is replaced by its mean value $\langle\sigma_z\rangle$ and the commutator $[\sigma_-, \sigma_+] = -\sigma_z \to -\langle\sigma_z\rangle$ is now a c-number. In principal its value has to be computed self-consistently, but in the low saturation regime it may readily be set to $\langle\sigma_z\rangle = -1$. This way the non-linear correlation $a\sigma_z$ is removed from the Heisenberg–Langevin equation (2.43b) and we obtain a linear set of equations. This regime is particularly interesting for the description of polarisable particles with no significant internal excitations, i.e. in the limit of

vanishing spontaneous decay [2.7]. The excited atomic state can now be adiabatically eliminated from the dynamics. The steady-state value of the polarisation operator is found to be [2.7]

$$\sigma_- = \frac{g(x)a}{i\Delta_\mathrm{a} - \gamma}. \tag{2.45}$$

For the approximation to be valid we require the population of the excited state to remain small,

$$\langle \sigma_+ \sigma_- \rangle = \frac{g^2(x)}{\gamma^2 + \Delta_\mathrm{a}^2} \left\langle a^\dagger a \right\rangle \ll 1. \tag{2.46}$$

For further convenience we define the light shift per photon

$$U_0 := \frac{g_0^2 \Delta_\mathrm{a}}{\gamma^2 + \Delta_\mathrm{a}^2} \tag{2.47}$$

and the incoherent scattering rate

$$\Gamma_0 := \frac{g_0^2 \gamma}{\gamma^2 + \Delta_\mathrm{a}^2}. \tag{2.48}$$

Here the coupling has been chosen to $g(x) = g_0 \cos(kx)$. The new Heisenberg–Langevin equation for the field,

$$\dot{a} = \left(i \left[\Delta_\mathrm{c} - U_0 \cos^2(kx) \right] - \left[\kappa + \Gamma_0 \cos^2(kx) \right] \right) a + \eta + \xi_a, \tag{2.49}$$

clearly demonstrates the dispersive and absorptive effects of the atom. Alternatively, we can also substitute the polarisation (2.45) into the Hamiltonian (2.41) and the Liouvillean (2.42), yielding

$$H_\mathrm{eff} = \frac{p^2}{2m} - \hbar \Delta_\mathrm{c} a^\dagger a + \hbar U_0 a^\dagger a \cos^2(kx) - i\hbar\eta \left(a - a^\dagger \right) \tag{2.50a}$$

and

$$\mathcal{L}_\mathrm{eff} \rho = \left[\kappa + \Gamma_0 \cos^2(kx) \right] \left(2a\rho a^\dagger - a^\dagger a \rho - \rho a^\dagger a \right). \tag{2.50b}$$

In the limit of large detuning, $|\Delta_\mathrm{a}| \gg \gamma$, the particle-induced terms approximately read $U_0 \approx g_0^2/\Delta_\mathrm{a}$ and $\Gamma_0 \approx \gamma g_0^2/\Delta_\mathrm{a}^2$ so that we can safely neglect any effects stemming from spontaneous emission, $\Gamma_0 \ll \kappa$. In this limit the particle mainly acts as a moving refractive index, shifting the cavity resonance frequency according to its position relative to the mirrors.

The Hamilton operator (2.50a) describes a particle moving within a *resonator-generated optical lattice* as the depth $\hbar |U_0| a^\dagger a$ of the periodic potential is now a fluctuating quantum operator instead of a simple c-number. For negative detuning, $\Delta_\mathrm{a} < 0$, the particle is attracted towards the points of maximal light intensity and

hence called a *high-field seeker*. Accordingly, the particle is called a *low-field seeker* in the opposite case of positive detuning, $\Delta_\mathrm{a} > 0$, where the potential wells are located at the points of vanishing light intensity.

The model (2.50) can be regarded as an extension of the theory of optical lattices [2.20–2.22] (cf. also section 3.3) to quantised light fields subject to the back-action induced by the particle. Notably, the Bose–Hubbard model (cf. section 3.2) can be generalised to the quantum potential [2.23–2.27].

2.4 Mechanical effects of light in optical resonators: Forces and cooling

Following the previous considerations we will neglect any effects emerging from spontaneous emission of the atom. The force operator associated with the Hamilton operator (2.50a) reads

$$F = \dot{p} = \frac{1}{i\hbar}\,[p, H_\mathrm{eff}] = -\frac{\mathrm{d}}{\mathrm{d}x} H_\mathrm{eff} = -\hbar U'(x) a^\dagger a, \tag{2.51}$$

where we have defined $U(x) := U_0 \cos^2(kx)$. It is convenient for the following investigation to decompose the force operator (2.51) into its mean value and fluctuations [2.7],

$$F = \langle F \rangle + \delta F. \tag{2.52}$$

The expectation value $\langle F \rangle$ gives rise to a conservative force associated with a potential in steady state as well as to an additional velocity-dependent force, which for properly chosen parameters can become negative (friction). The fluctuations δF (usually called Langevin force), in contrast, do not contribute to any net force. However, they do cause momentum diffusion, i.e. a linear growth of the momentum variance with time. This heating counteracts the friction force and is therefore a limiting factor for the achievable final temperature in steady state.

For an immobile atom the mean steady-state photon number is found from the Heisenberg–Langevin equation (2.49) to be

$$\left\langle a^\dagger a \right\rangle = \frac{\eta^2}{\kappa^2 + \left[\Delta_\mathrm{c} - U(x)\right]^2}. \tag{2.53}$$

Consequently, the mean force is

$$\langle F \rangle = -\frac{\hbar \eta^2 U'(x)}{\kappa^2 + \left[\Delta_\mathrm{c} - U(x)\right]^2}. \tag{2.54}$$

This is the dipole force and it is a result of coherent absorption and stimulated emission processes, where the particle absorbs photons from and emits photons into

the mode [2.7]. More precisely, the atom redistributes photons between the two counter-propagating waves forming the standing-wave lattice. This process is energy conserving and therefore the dipole force is conservative, i.e. it can be obtained from the potential

$$V(x) = -\frac{\hbar\eta^2}{\kappa}\arctan\left(\frac{\Delta_\mathrm{c} - U(x)}{\kappa}\right). \tag{2.55}$$

The dipole force (2.54) shows the expected behaviour of high-field-seeking atoms for red detuning ($U_0 < 0$) and low-field-seeking atoms for blue detuning ($U_0 > 0$).

All these considerations so far hold for non-moving particles. Let us now investigate the case of a slowly moving atom. First of all, we have to elaborate on what "slowly" means in this context. The field cannot react instantaneously to the particle motion, its dynamics is subject to an intrinsic delay determined by the field damping time κ^{-1}. A slow atom is an atom that does not move considerably (compared to a wavelength) on this time scale, i.e. $k|v| \ll \kappa$. This field delay will result in a velocity-dependent force and is the physical ground for cavity cooling. In this limit of slowly moving particles the velocity dependence can be taken into account in a consistent manner by replacing $\mathrm{d}/\mathrm{d}t \to \partial/\partial t + v\partial/\partial x$ and solving the Heisenberg–Langevin equation (2.49) for different orders of the velocity ($a = a_0 + va_1 + \dots$) [2.7]. In such a treatment the external degrees of freedom of the particle are considered classically, which is valid for temperatures (kinetic energy) much larger than the recoil energy, $k_\mathrm{B}T \gg E_\mathrm{R}$. We will come back to this condition later on in section 8.2 where we investigate the Wigner transformation of the master equation to obtain stochastic semiclassical equations of motion.

To first order in the velocity we find [2.6]

$$a_0 = \frac{\eta}{\kappa - i[\Delta_\mathrm{c} - U(x)]} \tag{2.56a}$$

$$a_1 = \frac{-a_0'}{\kappa - i[\Delta_\mathrm{c} - U(x)]}. \tag{2.56b}$$

Inserting these results into the mean force defined in equation (2.52) yields

$$\langle F\rangle = F_0 + vF_1, \tag{2.57}$$

with F_0 the dipole force (2.54) and

$$F_1 = \frac{4\hbar\eta^2\kappa[\Delta_\mathrm{c} - U(x)][U'(x)]^2}{\left(\kappa^2 + [\Delta_\mathrm{c} - U(x)]^2\right)^3}. \tag{2.58}$$

Neglecting localisation effects [2.28] one can consider the position-averaged force $\overline{F}_1$. If it is negative, $\overline{F}_1$ corresponds to friction and in the opposite case to heating of

the particle. We have plotted its behaviour in figure 2.6. In the limit $\Delta_c = -\kappa$ and $\kappa \gg |U_0|$ we find the simple expression [2.28]

$$\overline{F}_1 \approx -\frac{\hbar\eta^2 k^2 U_0^2}{4\kappa^4}. \tag{2.59}$$

Even though this force is independent of the sign of U_0 (and hence Δ_a), negative light shifts are more favourable as they allow for trapping in a generalised three-dimensional model [2.28].

Let us now take into account the fluctuating part of the force (2.52), amounting for momentum diffusion. The general definition of the momentum diffusion coefficient $\mathcal{D}$ is [2.29]

$$\frac{\mathrm{d}}{\mathrm{d}t}\,\mathrm{Var}\,(p(t)) = 2\mathcal{D}. \tag{2.60}$$

It can also be related to the two-time force correlation function[1] [2.29, 2.30],

$$\mathrm{Cov}\,(F(t), F(t')) = \langle F(t)F(t')\rangle - \langle F(t)\rangle\,\langle F(t')\rangle = \mathcal{D}\delta(t-t'), \tag{2.61}$$

which facilitates its evaluation using the fluctuating steady-state solution

$$a(t) = \frac{\eta + \xi_a(t)}{\kappa - i[\Delta_c - U(x)]} \tag{2.62}$$

of (2.49) and the only non-vanishing correlation [2.7]

$$\left\langle \xi_a(t)\xi_a^\dagger(t')\right\rangle = 2\kappa\delta(t-t'). \tag{2.63}$$

In the same parameter regime as employed for the friction we find [2.28]

$$\overline{\mathcal{D}} = \frac{\hbar\kappa}{2}\frac{\hbar\eta^2 k^2 U_0^2}{4\kappa^4} \tag{2.64}$$

and the steady-state temperature

$$k_B T = \frac{\overline{\mathcal{D}}}{\overline{F}_1} = \frac{\hbar\kappa}{2}. \tag{2.65}$$

If the cavity linewidth is smaller than the atomic spontaneous emission rate γ, the final temperature (2.65) can be much lower than the temperatures achievable with Doppler cooling [2.31] (which are limited by γ). Another striking advantage of cavity cooling is, that the cavity itself provides the decay channel. So there is no need for closed spontaneous emission–repumping cycles of the atom. This is particularly useful for the cooling of any kind of polarisable particle, e.g. molecules, for which in many cases such cycles cannot be found [2.32]. We conclude this section by mentioning that cavity cooling of single atoms has been experimentally demonstrated, see for example [2.33].

[1] This expression is directly related to the force fluctuations since $\mathrm{Cov}\,(F(t), F(t')) \equiv \langle \delta F(t)\delta F(t')\rangle$ with $\delta F = F - \langle F\rangle$.

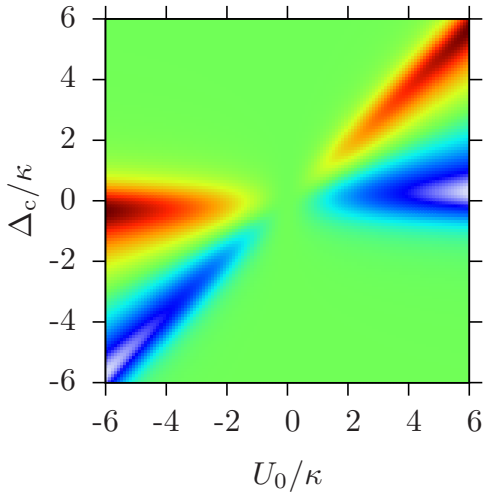

Figure 2.6: Averaged friction force $\overline{F}_1$. The region of red detuning for both, the particle and the cavity, is a cooling regime characterised by a negative force (blue regions).

Chapter 3

Ultracold atoms in optical lattices

In this chapter we present—in condensed form—the basics of lattice physics, of the Bose–Hubbard model and of the theory of optical lattices needed for our work.

3.1 One particle in a periodic potential

For the following considerations we treat the potential as an external, prescribed, quantity and ignore its physical origin. Optical lattices, which are typically generated by two counter-propagating laser beams, are introduced later on in section 3.3.

Let the potential $V(x)$ be periodic with periodicity a such that $V(x+a) = V(x)$. For simplicity we restrict ourselves to a one-dimensional system for the remainder of this chapter. A single particle in such a periodic potential is described by the simple Hamilton operator

$$H = \frac{p^2}{2m} + V(x). \tag{3.1}$$

3.1.1 Bloch functions and Bloch bands

The Hamiltonian (3.1) commutes with the translation operator T_a defined as [3.1]

$$T_a \psi(x) = \psi(x+a). \tag{3.2}$$

Therefore, both operators can be diagonalised simultaneously. We now adopt reference [3.1] for the derivation of the Bloch theorem. Let $\psi(x)$ denote an eigenstate of T_a with eigenvalue $\lambda \in \mathbb{C}$. Consequently, multiple displacements fulfil $T_a^n \psi(x) = \psi(x+na) = \lambda^n \psi(x)$. To avoid $\psi(x)$ to grow without bounds for $x \to \pm\infty$ we require $|\lambda| = 1$. Consequently, the eigenvalue can always be written $\lambda = e^{iqa}$ with $-\pi \leq qa < \pi$ and the eigenfunction $\psi(x)$ has the form

$$\psi(x) = e^{iqx} u(x), \tag{3.3}$$

with $u(x+na) = u(x)$ for $n \in \mathbb{Z}$. This important result is known as Bloch theorem and was first derived by F. Bloch in 1929 [3.2]. The parameter q is called quasi-momentum.

The periodic functions $u(x)$ fulfil the stationary Schrödinger equation

$$\left[\frac{(p+q)^2}{2m} + V(x)\right] u(x) = Eu(x). \tag{3.4}$$

Its spectrum is found to be discrete with eigenvalues $E_n(q)$, where $n \in \mathbb{N}_0$ is denoted band index. The Bloch theorem (3.3) now takes the form

$$\phi_q^{(n)}(x) = e^{iqx} u_q^{(n)}(x), \tag{3.5}$$

where the functions $\phi_q^{(n)}(x)$ are called Bloch functions.

Numerically, the Schrödinger equation (3.4) is most easily solved in Fourier space,

$$u_q^{(n)}(x) = \frac{1}{\sqrt{2\pi}} \sum_{j\in\mathbb{Z}} c_j^{(n,q)} e^{2ikx_j}, \tag{3.6}$$

where the factor two is due to the special choice $V(x) = V_0 \cos^2(kx)$ for the periodic potential. It has been chosen because—as we will see later—optical lattices have this shape. The eigenvalue equation (3.4) then reads

$$\sum_{j'\in\mathbb{Z}} H_{jj'} c_{j'}^{(n,q)} = E_q^{(n)} c_j^{(n,q)} \tag{3.7}$$

with the matrix

$$H_{jj'} = \begin{cases} \left[2j + \frac{q}{\hbar k}\right]^2 E_\mathrm{R} + \frac{V_0}{2} & \text{for } j' = j \\ \frac{V_0}{4} & \text{for } j' = j \pm 1 \\ 0 & \text{otherwise} \end{cases}. \tag{3.8}$$

Here we have defined the recoil energy $E_\mathrm{R} := \hbar^2 k^2 / 2m$. The eigenvalue equation is solved numerically for a finite number of coefficients (typically, around twenty are sufficient). In figures 3.1 and 3.2 we show the band structure computed numerically for different potential depths. It can be seen that the number of bound states, i.e. states for which $E_q^{(n)} < 0$, increases with the potential depth. Without potential the quadratic dispersion of free particles is recovered. For very deep lattices the bandwidth shrinks and the band gap converges towards the harmonic oscillator energy $\Delta E = \hbar\omega$, with the frequency $\omega = \sqrt{4V_0 E_\mathrm{R}}/\hbar$. For very cold—i.e. *ultracold*—particles we can thus restrict ourselves to the lowest Bloch band [3.3]. This will lead to the development of the Bose–Hubbard model treated in section 3.2. There we will also find a very important relation between the bandwidth and particle tunnelling. An example for a Bloch function is plotted in figure 3.3.

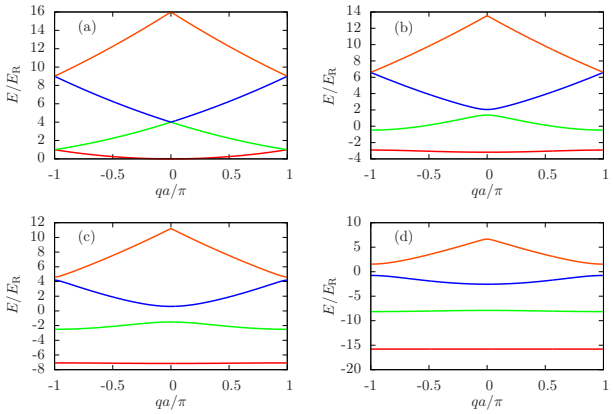

Figure 3.1: Bloch bands for the potential $V(x) = V_0 \cos^2(kx)$ and different potential depths. The lattice constant is $a = \pi/k$. (a) $V_0 = 0$, (b) $V_0 = 5E_R$, (c) $V_0 = 10E_R$ and (d) $V_0 = 20E_R$. Without potential the free dispersion is recovered. The number of bound bands increases with the potential depth, for $V_0 = 20E_R$ the three lowest bands are bound.

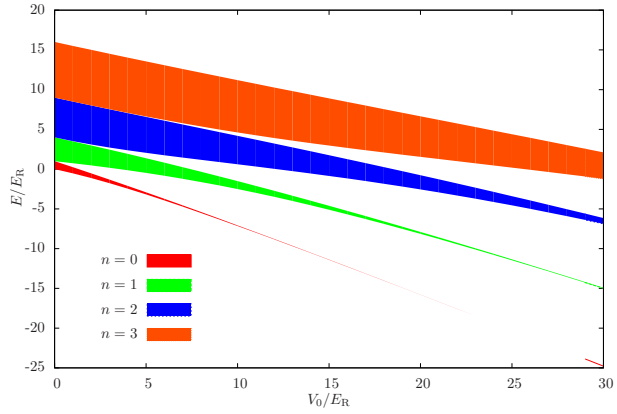

Figure 3.2: Bandwidth of the Bloch bands as a function of the potential depth [3.4]. The transition from the continuum (free particle) to separated bands is clearly visible. For very deep potentials the bandwidth converges towards zero and the spacing between the bands (gap) approaches the oscillator frequency, $\Delta E \to \hbar\omega$ (harmonic oscillator limit).

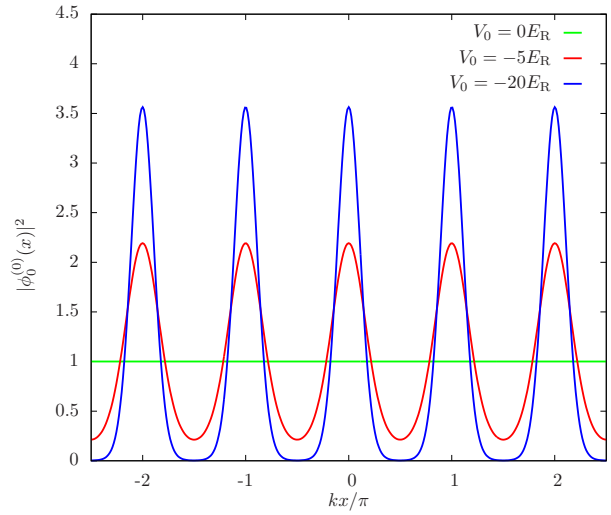

Figure 3.3: Modulus of the (unnormalised) lowest Bloch functions with $n = q = 0$ for different potential depths.

3.1.2 Wannier functions

The Bloch functions are not very suited for the description of localised particles because they are inherently de-localised. However, as they form a complete basis, it is possible to find their right combination to derive a set of functions describing states localised at a certain potential well. These functions were first introduced by G. H. Wannier in 1937 [3.5]. Some twenty years later, W. Kohn investigated their analytical properties [3.6] and proofed that there exists a unique superposition of Bloch functions localised at a potential well with the properties of (i) being real, (ii) having a definite parity (even or odd) with respect to the potential minimum and (iii) falling off exponentially with distance. These functions are known as *maximally localised Wannier functions* or *Wannier–Kohn functions* and shall be treated here in more detail.

Wannier functions are defined as [3.6]

$$w^{(n)}(x) := \sqrt{\frac{a}{2\pi}} \int_{-\pi/a}^{\pi/a} \phi_q^{(n)}(x) \mathrm{d}q. \tag{3.9}$$

From (3.5) we find the shifted Wannier function at $x_j := aj$,

$$w^{(n)}(x - x_j) := \sqrt{\frac{a}{2\pi}} \int_{-\pi/a}^{\pi/a} \phi_q^{(n)}(x) e^{-iqx_j} \mathrm{d}q. \tag{3.10}$$

The Wannier functions (3.10) are orthonormal and fulfil

$$\int_{-\infty}^{\infty} w_n(x - x_j)^* w_m(x - x_{j'}) \mathrm{d}x = \delta_{nm}\delta_{jj'}. \tag{3.11}$$

Multiplying equation (3.10) with $e^{iq'x_j}$ and using

$$\sum_j e^{i(q'-q)x_j} = \frac{2\pi}{a}\delta(q' - q) \tag{3.12}$$

we obtain the back transformation

$$\phi_q^{(n)}(x) = \sqrt{\frac{a}{2\pi}} \sum_j w^{(n)}(x - x_j) e^{iqx_j}. \tag{3.13}$$

Note that the functions (3.10) are not unique because the Bloch functions (3.5) are only defined up to a phase. Maximally localised Wannier functions are obtained if the phases are chosen the following way [3.6]. For even n one has to choose $\phi_q^{(n)}(0) \in \mathbb{R}$ such that $q \mapsto \phi_q^{(n)}(0)$ is an analytic function. This is the case if all Fourier coefficients in equation (3.6) have the same sign. The resulting Wannier function is then real and even around x_j. For the odd Wannier functions $\phi_q^{(n)}(0)$ has to be chosen purely imaginary and the same analyticity condition as for the even states has to be fulfilled. This can be achieved with antisymmetric Fourier coefficients, $c_j^{(n,q)} = -c_{-j}^{(n,q)}$.

The so-found Wannier functions decrease exponentially with distance, i.e. $w^{(n)}(x) \propto \exp(-h_n|x|)$ for large $|x|$ and some $h_n > 0$. This behaviour strongly differs from harmonic oscillator functions which decay $\propto \exp(-x^2/\xi_0^2)$, with the typical oscillator length $\xi_0 = \sqrt{\hbar/m\omega}$. See figure 3.4.

As mentioned earlier it is sufficient to take into account only the lowest Bloch band for ultracold particles. Consequently, we can restrict ourselves to the $n = 0$ Wannier functions for the derivation of the Bose–Hubbard model. In this work we will always mean the maximally localised Wannier functions when referring to "Wannier functions" unless otherwise stated.

3.2 The Bose–Hubbard model

We will now give a short review on the microscopic derivation of the Bose–Hubbard model and its properties. The model has first been introduced in the early 1960s to describe correlations in fermionic systems [3.7]. Its zero temperature phase diagram for a bosonic system was later investigated by Fisher *et al.* in the late 1980s [3.8], depicting a quantum phase transition between a superfluid phase and a Mott-insulator phase. A decade later, Jaksch *et al.* [3.9] proposed a realisation of the Bose–Hubbard model with an ultracold dilute gas of bosonic atoms confined within an optical lattice. The phase transition [3.10] was experimentally demonstrated a couple of years later by Greiner *et al.* [3.11]. See [3.3] for a recent review of the field.

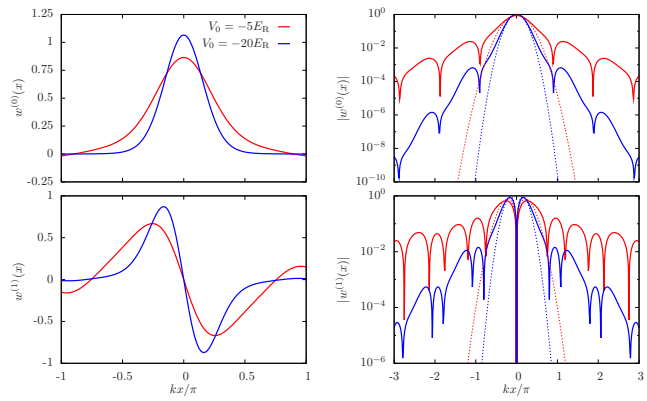

Figure 3.4: Wannier functions for two different potential depths on a linear (left) and on a logarithmic scale (right). The dashed lines are harmonic oscillator functions corresponding to the chosen potential depth. The different decay of the Wannier ($\propto e^{-h_n|x|}$) and oscillator functions ($\propto e^{-(x/\xi_0)^2}$) is clearly visible.

3.2.1 Microscopic derivation

The derivation given here is based upon the work by Jaksch *et al.* [3.9]. Again, our starting point is the single-particle Hamilton operator

$$H_0 = \frac{p^2}{2m} + V_0 \cos^2(kx). \tag{3.14}$$

The corresponding many-body Hamiltonian is obtained within the second quantisation formalism (see, for example, [3.12]) as

$$H = \int \mathrm{d}x\, \Psi^\dagger(x) \left(-\frac{\hbar^2}{2m}\frac{\mathrm{d}^2}{\mathrm{d}x^2} + V_0 \cos^2(kx) + V_\mathrm{T}(x) \right) \Psi(x) + \\ + \frac{1}{2} \iint \mathrm{d}x\, \mathrm{d}x'\, \Psi^\dagger(x)\Psi^\dagger(x')U(x,x')\Psi(x')\Psi(x), \tag{3.15}$$

where we added an external trapping potential $V_\mathrm{T}(x)$ and included two-body interactions $U(x,x')$. In the limit of very low temperatures the most important interactions stem from s-wave collisions which can be described by the pseudo-potential [3.13]

$$U(x,x') = g_\mathrm{1D}\delta(x-x'). \tag{3.16}$$

Its coupling parameter g_1D is a function of the one-dimensional scattering length. The physical meaning of equation (3.16) is that only particles trapped at the very same potential well will effectively interact with each other. We now expand the field

operator $\Psi(x)$ in terms of the previously derived Wannier functions (3.10),

$$\Psi(x) = \sum_{j=1}^{M} \sum_{n=0}^{\infty} w^{(n)}(x - x_j) b_j^n, \tag{3.17}$$

with M the number of lattice sites. The bosonic operators b_j^n ($b_j^{n\dagger}$) destroy (create) a particle at the jth site in the nth Bloch band. As previously mentioned we assume the particles to be very cold, i.e. their energy being well below the excitation gap to the first excited Bloch band. The same has to hold for the mean interaction energy [3.3]. Under these simplifying conditions we readily find the lowest-band Hamiltonian

$$H = \sum_{i,j=1}^{M} J_{ij} b_i^\dagger b_j + \frac{1}{2} \sum_{i,j,k,l=1}^{M} U_{ijkl} b_i^\dagger b_j^\dagger b_k b_l + \sum_{i,j=1}^{M} V_{ij} b_i^\dagger b_j \tag{3.18}$$

with the matrix elements

$$J_{ij} = \int_{-\infty}^{\infty} \mathrm{d}x\, w(x - x_i) \left(-\frac{\hbar^2}{2m} \frac{\mathrm{d}^2}{\mathrm{d}x^2} + V_0 \cos^2(kx) \right) w(x - x_j), \tag{3.19a}$$

$$V_{ij} = \int_{-\infty}^{\infty} \mathrm{d}x\, w(x - x_i) V_\mathrm{T}(x) w(x - x_j) \tag{3.19b}$$

and

$$U_{ijkl} = g_{1\mathrm{D}} \int_{-\infty}^{\infty} \mathrm{d}x\, w(x - x_i) w(x - x_j) w(x - x_k) w(x - x_l). \tag{3.19c}$$

The diagonal terms J_{ii} describe the on-site energies and the off-diagonal terms J_{ij} tunnelling between site i and site j. As shown in [3.14] the next-nearest neighbour hopping matrix elements are at least one order of magnitude smaller than their nearest-neighbour counterparts $J_{i,i+1}$. Hence we restrict ourselves to the latter mechanism and define $J := J_{i,i+1}$. A similar observation holds for the interaction matrix element (3.19c), the on-site term $U := U_{iiii}$, describing the interaction of two particles trapped at the same site, dominates all other non-local combinations. These observations hold for lattices deeper than $V_0 \sim 5E_\mathrm{R}$ [3.14]. The external trapping potential $V_\mathrm{T}(x)$ typically includes several dozen to hundred lattices sites, so that it is justified to approximate it by a constant at each potential well. The matrix element V_{ij} then simplifies to

$$V_{ij} \approx V_\mathrm{T}(x_i) \int \mathrm{d}x\, w(x - x_i) w(x - x_j) = V_\mathrm{T}(x_i) \delta_{ij} =: \varepsilon_i \delta_{ij}. \tag{3.20}$$

Using the considerations above we find the Bose–Hubbard Hamilton operator (omitting a global energy shift)

$$H = J \sum_{\langle i,j \rangle} b_i^\dagger b_j + \frac{U}{2} \sum_i n_i(n_i - 1) + \sum_i \varepsilon_i b_i^\dagger b_i, \tag{3.21}$$

where $\langle i, j\rangle$ denotes the sum over nearest-neighbour sites only. The first term describes hopping (tunnelling) between adjacent wells, the second one two-body interactions and the last one describes a local energy shift due to an external trapping potential. A Fourier transformation of the hopping contribution in (3.21) yields (tight binding)

$$H_{\text{hopping}} = 2J \sum_k \cos(ka) a_k^\dagger a_k. \tag{3.22}$$

The bandwidth of the lowest Bloch band is therefore directly related to the tunnelling matrix element, $\Delta E = 4J$.

3.2.2 Superfluid and Mott-insulator phases

For $\varepsilon_i = 0$ the Bose–Hubbard Hamiltonian (3.21) is subject to a competition between kinetic energy J and interaction energy U. For $J/U \to \infty$ the ground state consists of particles de-localised over the whole lattice and is called superfluid state. The ideal superfluid state for $U = 0$ for N particles in M wells is [3.3]

$$|\text{SF}\rangle = \frac{1}{\sqrt{N!}} \left(\frac{1}{\sqrt{M}} \sum_{j=1}^{M} b_j^\dagger \right)^N |0\rangle\,, \tag{3.23}$$

with the vacuum state $|0\rangle = |0, \ldots, 0\rangle$ denoting an empty lattice. The state (3.23) exhibits large on-site particle number fluctuations and long-range off-diagonal coherences, where $\left\langle b_i^\dagger b_j \right\rangle$ decreases polynomially with $|i - j|$. For increasing U tunnelling is hindered by repelling interactions. For commensurate filling the ground state for $J/U \to 0$ is a Mott insulator state with $\bar{n} = N/M$ particles per site [3.3],

$$|\text{MI}\rangle = \prod_{j=1}^{M} |\bar{n}\rangle_j\,. \tag{3.24}$$

This states shows no number fluctuations and its off-diagonal elements decay exponentially. For $N/M \notin \mathbb{N}$ the perfect Mott insulator is not the ground state, a small fraction remains superfluid even for $J/U \to 0$ [3.3].

3.3 Optical lattices

Up to now we have ignored the physical origin of the lattice and have considered it to be an external prescribed quantity. Let us now elucidate the background of optical lattices, which are typically created by two counter-propagating laser beams. Actually, we have already encountered their quantised version in equation (2.50a) in section 2.3. The physical ground of the force is again the AC-Stark shift (cf.

equation (2.12)) stemming from the coherent absorption and stimulated emission of photons. The mathematics is very similar to the derivation presented in section 2.1. We start from the Hamiltonian [3.15]

$$H = \frac{p^2}{2m} + \hbar\omega_\mathrm{a}\sigma_+\sigma_- - \mathbf{d}\cdot\mathbf{E}(x) \tag{3.25}$$

in dipole approximation. Here x and p denote the particle's centre-of-mass position and momentum operator, respectively, m its mass and ω_a the transition frequency between the ground state $|g\rangle$ and an excited state $|e\rangle$. The atomic raising and lowering operators are defined as $\sigma_+ = |e\rangle\langle g|$ and $\sigma_- = |g\rangle\langle e|$, respectively. The electric field $\mathbf{E}(x) = E_\mathrm{l}(x)\cos(\omega_\mathrm{l}t)\mathbf{e}$ is created by two counter-propagating laser beams of frequency ω_l and $\mathbf{e}$ is the polarisation vector. Due to the odd parity of the dipole operator $\mathbf{d}$, the particle-field interaction can be expressed as

$$\begin{aligned} H_\mathrm{int} &= -\mathbf{d}\cdot\mathbf{E}(x) = \\ &= -\frac{\hbar\Omega(x)}{2}\left(\sigma_+ e^{-i\omega_\mathrm{l}t} + \sigma_- e^{-i\omega_\mathrm{l}t}\right) - \frac{\hbar\Omega^\dagger(x)}{2}\left(\sigma_+ e^{i\omega_\mathrm{l}t} + \sigma_- e^{i\omega_\mathrm{l}t}\right) \end{aligned} \tag{3.26}$$

with the Rabi frequency $\Omega(x) := E_\mathrm{l}(x)\,\langle e|\mathbf{d}\cdot\mathbf{e}|g\rangle\,/\hbar$. The terms in the first parenthesis of the Hamiltonian (3.26) correspond to absorption of a laser photon and excitation (first part) or de-excitation (second part) of the atom, respectively. The second parenthesis describes the reverse processes with emission of a photon. The two non-energy-conserving processes can be neglected within the following rotating wave approximation. We transform the Hamiltonian (3.26) into an interaction picture with respect to $H_0 = \hbar\omega_\mathrm{a}\sigma_+\sigma_-$,

$$\begin{aligned} H_\mathrm{I} = -\frac{\hbar\Omega(x)}{2}\left(\sigma_+ e^{-i(\omega_\mathrm{l}-\omega_\mathrm{a})t} + \sigma_- e^{-i(\omega_\mathrm{l}+\omega_\mathrm{a})t}\right) - \\ - \frac{\hbar\Omega^\dagger(x)}{2}\left(\sigma_+ e^{i(\omega_\mathrm{l}+\omega_\mathrm{a})t} + \sigma_- e^{i(\omega_\mathrm{l}-\omega_\mathrm{a})t}\right). \end{aligned} \tag{3.27}$$

For $\omega_\mathrm{l} \approx \omega_\mathrm{a}$ two of the terms oscillate very rapidly with frequency $\omega \approx 2\omega_\mathrm{l}$. The non-resonant terms can be neglected with respect to the near-resonant ones in the rotating wave approximation [3.16]. Performing another transformation into a frame rotating with the laser frequency ω_l to get rid of the explicit time dependence, we obtain the final Hamiltonian

$$H = -\hbar\delta\sigma_+\sigma_- - \frac{\hbar\Omega(x)}{2}\sigma_+ - \frac{\hbar\Omega^\dagger(x)}{2}\sigma_-, \tag{3.28}$$

with the detuning $\delta := \omega_\mathrm{l} - \omega_\mathrm{a}$. Its eigenvalues are

$$E = -\frac{\hbar\delta}{2} \pm \frac{\hbar}{2}\sqrt{\delta^2 + |\Omega(x)|^2}. \tag{3.29}$$

For large detuning, $|\delta| \gg |\Omega|$, the population of the excited state remains very small.[1] An expansion of the eigenvalues yields

$$E \approx -\frac{\hbar\delta}{2} \pm \frac{\hbar\delta}{2}\left(1 + \frac{1}{2}\frac{|\Omega(x)|^2}{\delta^2}\right). \tag{3.30}$$

This is the AC-Stark shift and it amounts to a spatially varying potential [3.14]

$$V(x) = \frac{\hbar|\Omega(x)|^2}{4\delta} \tag{3.31}$$

for ground-state atoms. As for the quantum case treated in section 2.3 we find for red detuning $\delta < 0$ that the atom is dragged towards the points of maximal light intensity, whereas in the opposite, blue-detuned, case the atom is repelled from these points and attracted towards the points of vanishing light intensity.

3.4 Spontaneous emission

The potential (3.31) originates from the conservative part of the atom-light interaction, called dipole force. A second, non-conservative force (called Langevin force) stemming from spontaneous emission has not been taken into account yet. Its physical origin is the process of an atom absorbing a photon from the laser followed by a *spontaneous* emission of a photon into free space. Every time this happens the atom experiences a recoil kick into the opposite direction. On average, these kicks do no contribute to any net force (all directions are equally probable) but rather to momentum diffusion (heating). The spontaneous emission rate Γ due to incoherent scattering by the particle can be estimated by the atomic decay rate γ times the occupation probability of the excited state [3.14]. For $|\delta| \gg |\Omega|$ this rate is given by

$$\Gamma(x) = \frac{\gamma|\Omega(x)|^2}{4(\delta^2 + \gamma^2)}. \tag{3.32}$$

For large detuning $|\delta| \gg |\Omega|, \gamma$ this rate scales like $\Gamma \sim \delta^{-2}$ and can thus safely be neglected in comparison to the potential scaling as $V \sim \delta^{-1}$. Of course, this is the same result (semiclassical analogon) as the one obtained in section 2.3 for a quantised light field. The scattering rate can also be derived in a more systematic way, e.g. with the help of a stochastic Schrödinger equation or the master equation [3.18], cf. also section 2.3.

Let us evaluate the scattering rate (3.32) for a deeply trapped particle where a harmonic oscillator approximation of the lowest Wannier function is possible.

[1] The saturation parameter obtained from the optical Bloch equations is $s = |\Omega(x)|^2/2\delta^2$ [3.17].

Calculating the effective spontaneous emission rate for the state

$$\psi(x) = \frac{1}{\pi^{1/4}\sqrt{\xi_0}} \exp\left(-\frac{1}{2}\frac{(x-x_0)^2}{\xi_0^2}\right) \tag{3.33}$$

in a red detuned lattice ($\delta < 0 \Rightarrow x_0 = 0$) yields

$$\Gamma_{\mathrm{red}} \approx \frac{\gamma\Omega_0^2}{4\delta^2}\left(1 - \frac{\omega_{\mathrm{R}}}{\omega}\right) \approx \frac{V_0}{\hbar|\delta|}\gamma. \tag{3.34}$$

For blue detuning ($\delta > 0 \Rightarrow x_0 = \pi/2k$) we find

$$\Gamma_{\mathrm{blue}} \approx \frac{\omega}{4\delta}\gamma. \tag{3.35}$$

Here we have used the definitions $\Omega(x) = \Omega_0 \cos(kx)$, $V_0 = \hbar\Omega_0^2/4|\delta|$, the recoil frequency $\omega_{\mathrm{R}} = E_{\mathrm{R}}/\hbar = \hbar k^2/2m$ and the oscillator frequency $\omega = \sqrt{4V_0 E_{\mathrm{R}}}/\hbar$. The effective spontaneous scattering rate in blue-detuned lattices is smaller than for their red-detuned counterparts with the same $|\delta|$ [3.14],

$$\frac{\Gamma_{\mathrm{red}}}{\Gamma_{\mathrm{blue}}} = \frac{\hbar\omega}{E_{\mathrm{R}}} > 1. \tag{3.36}$$

For typical experiments the time scales defined by Γ are of the order of minutes compared to typical experimental time scales of the order of seconds [3.14]. Therefore spontaneous emission does not play an important role for such experiments. To provide some experimental numbers [3.19], for a red-detuned $\lambda_{\mathrm{l}} = 1064.5\,\mathrm{nm}$ ($\omega_{\mathrm{l}} = 2\pi \times 281.6\,\mathrm{THz}$) laser trapping Cesium atoms via the $6^2S_{1/2}$ to $6^2P_{3/2}$ transition with $\omega_{\mathrm{a}} = 2\pi \times 351.7\,\mathrm{THz}$ and a linewidth $\gamma = 2\pi \times 5.2\,\mathrm{MHz}$ in a potential of depth $V_0 = 20E_{\mathrm{R}}$, with $\omega_{\mathrm{R}} = 2\pi \times 1.3\,\mathrm{kHz}$, the spontaneous emission rate is $\Gamma = 1.2 \times 10^{-2}\,\mathrm{s}^{-1}$.

Recently, however, the problem of heating of bosons in optical lattices has raised growing interest. See, for example, references [3.20, 3.21] for two recent publications in this direction.

Part II

Ultracold particles in ring resonators

Chapter 4

Background to particles in ring resonators

4.1 Introduction

So far we have only considered linear standing-wave resonators in this thesis. They are characterised by a large free spectral range and thus allow for the isolation of a single non-degenerate mode of the electric field [4.1]. In our research on ultracold atoms, however, we have focused on a different geometry, namely on ring resonators. In the simplest case such a ring resonator can be realised with the help of three mirrors, in lieu of only two like for a linear Fabry–Perot cavity. The most striking difference of ring resonators compared to the latter is the existence of degenerate modes [4.2]. Although it is still possible to address a single frequency owing to the large free spectral range, this frequency is now associated with two different running wave modes $u(x) \propto \exp(\pm ikx)$, one travelling clockwise and the other one anti-clockwise along the cavity axis. The boundary conditions within a Fabry–Perot cavity with perfectly conducting mirrors require that the electric field vanishes on the mirror surfaces [4.3]. For ring resonators this boundary condition does not apply, which offers an additional degree of freedom to the system, the *phase* of the intracavity light field. This has the important consequence that the resonator-generated lattice (similar to the one derived in section 2.3 for a standing-wave resonator) does not only exhibits an operator-valued depth, but also an operator-valued phase. That is, both, the lattice depth and its phase, depend on the quantum state of both intracavity fields. This is a major difference to the linear resonator and has important physical implications. Owing to these freedoms the system is translation invariant, meaning that the total momentum of the atoms and all the light fields (including the pump and loss fields) is conserved. Hence, no momentum is absorbed by the mirrors, contrary to Fabry–Perot resonators [4.2].

All these properties of ring cavities offer new possibilities for cavity cooling of polarisable particles. Studies of the ring resonator [4.2, 4.4] and, more general, of arbitrary multimode cavities [4.2, 4.5, 4.6], in the semiclassical limit revealed, for example, reduced cooling times as compared to single-mode setups in linear resonators. Systems of cold particles within ring resonators have also been realised experimentally, see, for example [4.7, 4.8].

For ultracold particles the semiclassical treatment becomes inadequate[1] and the full quantum nature of the particles must be taken into account. One method to reduce the complicated Hamiltonian is to generalise the Bose–Hubbard model [4.10] to resonator-generated lattices. Maschler and Ritsch presented such a model in 2005 [4.11] and showed that—within some limitations—the approximations required for the derivation of the "classical" Bose–Hubbard model remained valid. For example, the lowest-band approximation also holds for quantised lattices. Furthermore, it is still justified to consider nearest-neighbour hopping only due to the fast decaying matrix elements for jumps over larger distances. However, the cavity mode mediates non-local interactions between all particles at all sites, leading to effective non-locally correlated two-particle hopping processes as demonstrated in [4.11]. Further phenomena as well as the implications of the particle back-action on the field and hence on the phase diagram have been extensively studied, notably in the groups of Lewenstein, Morigi and Ritsch [4.12–4.16]. Since this description proofed to be very successful we strived to apply this formalism also to ring resonators. On this way we encountered several a priori unexpected results such as the break-down of a simple lowest-band model (see the publication in chapter 5 for details). This is because additional physical processes which couple different Bloch bands appear in the Hamiltonian. Such processes are not present in linear cavities, or, more precisely, can safely be ignored due to the small magnitudes of the associated matrix elements. These dynamical couplings to higher bands are a crucial feature of ring-resonator-generated optical lattices, causing non-local position and momentum correlations, particle entanglement and squeezing. These phenomena are studied in the preprint in chapter 6.

4.2 Derivation of the Hamiltonian

The lattice Hamiltonian for linearly polarisable particles can readily be derived following the line of section 2.3. For convenience we perform a transformation of the mode functions and consider the standing waves $u_\mathrm{s}(x) = \sin(kx)$ and $u_\mathrm{c}(x) = \cos(kx)$ instead of the two counter-propagating waves. Both modes interact with the particle via a Jaynes–Cummings interaction so that the Hamiltonian including the pump terms reads

$$H = \frac{p^2}{2m} - \hbar\Delta_\mathrm{c} \sum_{j=\mathrm{s,c}} a_j^\dagger a_j - \hbar\Delta_\mathrm{a}\sigma_+\sigma_- - \\ - i\hbar g_0 \sum_{j=\mathrm{s,c}} u_j(x) \left(a_j\sigma_+ - \sigma_- a_j^\dagger\right) - i\hbar \sum_{j=\mathrm{s,c}} \eta_j \left(a_j - a_j^\dagger\right). \quad (4.1)$$

[1] The semiclassical approximation is limited to temperatures much larger than the recoil energy [4.9].

We note that symmetric pumping of the two counter-propagating modes results in an effective pump of the cosine mode; the sine mode is driven for an appropriate phase shift between the two pump lasers. As previously done for the standing-wave resonator, we consider the parameter regime of large detuning between the pump laser and the atomic transition frequency. This allows for a bosonisation of the atomic dipole and an adiabatic elimination of the atom from the dynamics [4.2]. Following [4.2] we find the polarisation

$$\sigma_- = \frac{g_0 \sum_{j=\mathrm{s,c}} u_j(x) a_j}{i\Delta_\mathrm{a} - \gamma} \tag{4.2}$$

and the effective Hamiltonian

$$H = \frac{p^2}{2m} - \hbar\Delta_\mathrm{c} \sum_{j=\mathrm{s,c}} a_j^\dagger a_j + \hbar U_0 \mathcal{E}^\dagger(x)\mathcal{E}(x) - i\hbar \sum_{j=\mathrm{s,c}} \eta_j \left(a_j - a_j^\dagger\right) \tag{4.3}$$

with the dimensionless electric field

$$\mathcal{E}(x) := \sum_{j=\mathrm{s,c}} u_j(x) a_j. \tag{4.4}$$

Explicitly, the particle-field interaction term reads

$$\mathcal{E}^\dagger(x)\mathcal{E}(x) = a_\mathrm{c}^\dagger a_\mathrm{c} \cos^2(kx) + a_\mathrm{s}^\dagger a_\mathrm{s} \sin^2(kx) + \left(a_\mathrm{c}^\dagger a_\mathrm{s} + a_\mathrm{s}^\dagger a_\mathrm{c}\right) \sin(kx)\cos(kx). \tag{4.5}$$

The first two terms describe the well-known quantum potentials created by the two standing-wave modes. The last term does not exist for linear resonators and describes the coherent particle-mediated redistribution of photons between the two standing-wave modes. It is this term which gives rise to the previously mentioned coupling between the various Bloch bands. This can easily be seen as follows. Suppose one of the two modes to be strongly pumped so that the particle is trapped in a minimum of the optical lattice. The term $\sin(kx)\cos(kx) \equiv \frac{1}{2}\sin(2kx)$ is asymmetric with respect to these potential wells. Hence it will not give any contribution when only considering the lowest band Wannier functions. Localised particle states of different parity, however, are coupled through this operator.

Chapter 5

Publication

Physical Review A **82**, 043605 (2010)

Microscopic dynamics of ultracold particles in a ring-cavity optical lattice[†]

Wolfgang Niedenzu[1], Rainer Schulze[1,2], András Vukics[1], and Helmut Ritsch[1]

[1] *Institut für Theoretische Physik, Universität Innsbruck, Technikerstraße 25, A-6020 Innsbruck, Austria*
[2] *Institut für Ionenphysik und Angewandte Physik, Universität Innsbruck, Technikerstraße 25, A-6020 Innsbruck, Austria*

The quantum dynamics of particles optically trapped in a symmetrically pumped high-Q ring cavity exhibits much richer physics than for a standing-wave resonator. In addition to modifying the lattice depth, light scattering by the particles shifts and reshapes the trapping potential. We calculate the corresponding changes in tunneling amplitudes and damping by an effective bipotential (two-level) model for the particle motion. As a crude truncation of the Bose-Hubbard model, expansion to the lowest band decouples particle and field dynamics. Only including excitations to higher bands can capture this essential additional physics and correctly describe decoherence, damping, and long-range correlations of the particle dynamics. The validity limits of the analytic models are confirmed by quantum Monte Carlo wave-function simulations, which exhibit correlated particle-field quantum jumps as unambiguous quantum signature of the system dynamics.

URL: `http://link.aps.org/doi/10.1103/PhysRevA.82.043605`
DOI: 10.1103/PhysRevA.82.043605
PACS: 37.30.+i, 05.30.Jp, 37.10.Vz, 42.50.Wk

[†] The author of the present thesis performed all the calculations in this publication. R. S. implemented the classical simulations and, together with A. V., acted as a discussion partner on all other aspects of the work.

5.1 Introduction

In the past decade the theoretical and experimental study of ultracold quantum gases in optical potentials has seen tremendous progress and growth [5.1–5.3]. Optical lattices generated by spatially periodic laser fields can be routinely loaded with atoms very close to $T = 0$ with different filling factors and including multiple species [5.4]. Using magnetic fields or extra lasers the local interactions between the particles can be controlled providing for a versatile test ground of many-particle quantum phenomena. In most of these cases the backaction of the particles on the trapping and control fields is so small that the forces are well described by prescribed external potentials. Nevertheless for large lattices this backaction cannot be ignored and couples particle and field dynamics [5.5]. This coupled dynamics gets a particularly important new dimension when the light fields generating the potentials are enclosed in optical resonators [5.6] and the field amplitudes thus constitute separate dynamical quantum variables. Following initial theoretical studies [5.7] recent experiments now opened this new dimension by loading Bose-Einstein condensates (BECs) into optical resonators of high finesse [5.8–5.10]. Due to the large number of atoms the so-called strong-coupling limit of cavity QED was surpassed by several orders of magnitude reaching new parameter regimes of cavity QED and nonlinear quantum dynamics [5.9, 5.11, 5.12].

From a theoretical point of view, a dynamic lattice potential with quantum properties creates a wealth of new phenomena like atom-field entanglement, long-range interactions, and phononlike excitations with controllable properties. In particular, if several field modes are involved as in a ring cavity, new phenomena related to long-range (phonon-type) interactions of solid-state physics should become accessible for thorough tests in cold-atom setups. As a striking example, translation invariance and momentum conservation of the combined atom-field system induce pair correlations in the momentum space of the particles. Similarly, even small momenta transferred from atoms to the field should lead to measurable optical phase shifts [5.13], which might give a direct handle to observe the onset of superfluidity of the atoms or construct ultrasensitive acceleration detectors with BECs.

Of course, these new quantum degrees of freedom strongly increase the mathematical complexity of the theoretical model. As a first consequence the fairly simple, and for free-space optical lattices very successful, description of the system properties in terms of a single-band Bose-Hubbard model [5.1] cannot be directly applied in the case of dynamic potentials of varying depth and position. For standing-wave cavities an effective description in terms of self-consistent effective parameters has already been developed [5.14–5.16]. It will be a central goal of this work to develop improved approximative model descriptions for ring resonators and to study the limits, where a generalized version of the Bose-Hubbard model can still be applied to understand key features of the underlying physics.

Initially, setups of atoms in ring cavities were mainly considered to generalize and test cavity cooling of a wide class of polarizable particles, where no alternative laser cooling schemes exist. A ring geometry offers a wider capture range, faster cooling times [5.6], as well as lower temperatures [5.17], including even the idea of stopping and cooling a fast molecular beam [5.18]. An ultimate goal here is the development of an all-optical route to a BEC of polarizable point objects replacing evaporative cooling by cavity cooling which involves no particle loss. More recently, an alternative research direction studies quantum dynamics of atomic ensembles of very low temperature stored within a ring-cavity optical lattice [5.19, 5.20]. As discussed in early theoretical work [5.21, 5.22], controlling phase and amplitude of both pump fields of the ring cavity, which was verified in various experiments [5.19, 5.23], gives great flexibility in controlling position and depth of the generated optical potential as well as the mode properties of lattice beams [5.24]. In the limiting case of a single-side pump one also recovers the model of the collective atomic recoil laser (CARL) [5.25, 5.26]. First experiments using a single-side pump were already performed [5.20]. So far, the theoretical descriptions of BECs in ring cavities were mainly based on a Gross-Pitaevskii description of the atoms [5.20, 5.27, 5.28] and a coherent-state approximation for the cavity modes.

As for ultracold atomic gases in general the theoretical focus now shifts toward new quantum phases of degenerate gases near $T = 0$ [5.7, 5.14, 5.15, 5.29, 5.30], where mean-field approximations have to be abandoned. Interestingly, for the case of a single-mode standing-wave cavity it was possible to derive an effective Bose-Hubbard-type model which still proved valid for a dynamical quantized field creating the optical potential. This could capture important aspects of the dynamics and predict surprising modifications of the corresponding phase diagram [5.14–5.16]. As expected this dynamics in general invokes particle-field entanglement and nonlinear optics as well [5.31, 5.32]. Here we investigate in which cases an extension of the Bose-Hubbard model for a ring-resonator-generated optical lattice is feasible. This is complicated by the fact that not only the lattice depth but also the lattice position are now fluctuating quantum variables. Thus already the definition of the proper Wannier basis functions is hard.

The article is organized as follows: We start with a tutorial review of the classical point-particle motion in ring-cavity-generated optical potentials and the presentation of the general atom-field Hamiltonian in Sec. 5.2. In the following Sec. 5.3 we concentrate on the weak-coupling case, where only a single or a few excitations are generated in the unpumped mode and adiabatic effective potentials for the atomic motion can be derived on elimination of the mode dynamics. Here the cavity dynamics modifies tunneling and induces damping of nonlocal coherence. Subsequently, in Sec. 5.4 we set out to derive an effective Bose-Hubbard-type model. Interestingly we miss central physical effects if we use the standard single-band approximation. Actually, central properties of ring-resonator-generated lattices appear in a two-

band expansion presented in Sec. 5.4.3, where tunneling is accompanied by photon scattering and jumps to the higher band. Finally, in Sec. 5.5 we compare an effective multiband model with numerical simulations of the coupled atom-field dynamics in full momentum space.

5.2 One polarizable point particle in a ring resonator

Let us first exhibit some essential physical properties of particle motion in ring cavities by considering a single linearly polarizable point particle moving inside a symmetrically driven ring resonator, cf. Fig. 5.1. The two counter-propagating modes with wave number k are pumped with amplitudes $\eta_\pm$ and decay at a rate κ. The pump frequency is detuned by $\Delta_\mathrm{c} = \omega_\mathrm{pump} - \omega_\mathrm{cavity}$ with respect to the bare cavity resonance. Symmetric pumping, i.e., $\eta_+ = \eta_-$, generates a standing-wave field with spatial dependence $\propto \cos(kx)$ in the empty cavity. The second orthogonal field mode with spatial dependence $\propto \sin(kx)$ thus will not be excited by the pump [5.13], but it still cannot be ignored for the dynamics. Note that physical differences between a standing-wave resonator and a ring resonator have been investigated before, e.g., in Ref. [5.33]. At this point for simplicity we assume sufficient transverse localization of the particle so we can restrict ourselves to an effective one-dimensional description along the resonator axis.

5.2.1 Classical and semiclassical description

Before turning to the quantum model we shall briefly review the corresponding classical field equations [5.6, 5.22] to obtain a first qualitative insight into the underlying dynamical principles of the system. These classical equations of motion for the two driven and damped amplitudes of the counterpropagating modes coupled by a polarizable point particle read [5.22]

$$\dot{\alpha}_\pm = \Big[i(\Delta_\mathrm{c} - U_0) - \kappa - \Gamma_0\Big]\alpha_\pm - (\Gamma_0 + iU_0)\alpha_\mp e^{\mp 2ikx} + \eta_\pm. \tag{5.1}$$

The central parameters U_0, which denotes the frequency shift of the mode induced by the particle and Γ_0, which gives the particle-induced extra loss of the mode, are directly related to the real and imaginary parts of the particle's linear susceptibility [5.34, 5.35]. These parameters also play a central role in the light forces determining the equations of motion for the particle [5.6]

$$F_\mathrm{dip} = -4\hbar k U_0 \,\mathrm{Im}\left(\alpha_+^* \alpha_- e^{-2ikx}\right) \tag{5.2a}$$

$$F_\mathrm{rp} = 2\hbar k \Gamma_0 \left(|\alpha_+|^2 - |\alpha_-|^2\right), \tag{5.2b}$$

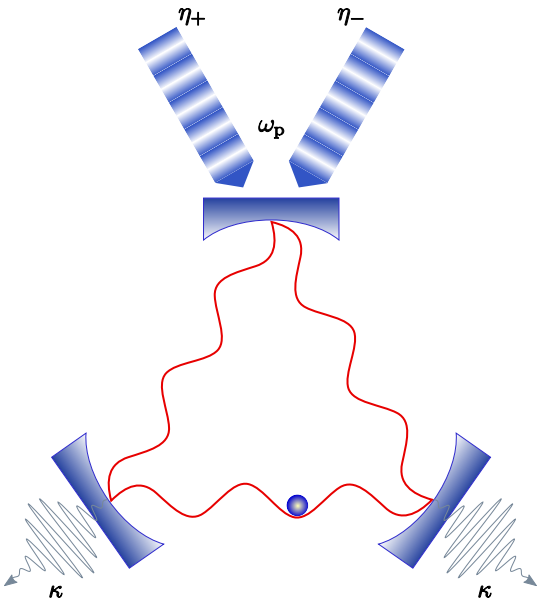

Figure 5.1: (Color online) Sketch of the system: One polarizable particle in a symmetrically driven ring cavity (pumping fields η_+ and η_-). The resonator loss is characterized by the decay rate κ.

where (5.2a) is the dipole force and (5.2b) the radiation-pressure force. We see that U_0 gives the optical light shift and Γ_0 the photon scattering rate per photon in the mode. The dipole force can be derived from a potential proportional to the intracavity intensity and is—in a quantum picture—associated with the coherent redistribution of photons between the two modes. Depending on $\operatorname{sgn} U_0$ the particles are trapped either at the intensity minima ($U_0 > 0$, "low-field seekers") or at the intensity maxima ($U_0 < 0$, "high-field seekers"). As we will focus on the dispersive, far-detuned limit where $\Gamma_0 \ll |U_0|$, we will neglect the radiation-pressure force (5.2b) and scattering loss in the following. Nevertheless, photons leak out of the resonator irreversibly and carry away momentum of the particle, which generates a nonconservative dynamics, including friction and diffusion of particle motion [5.22]. The fluctuations in the photon numbers inducing diffusion (heating) then limit the final steady-state temperature [5.36] of the particle. Computation of this friction coefficient stemming from the dipole force indicates a cooling regime for $U_0 < 0$ and $\Delta_c < 0$ [5.6, 5.22]. We will therefore concentrate on this parameter regime for the rest of this work.

We show a typical result of the combined particle-field equations in Fig. 5.2. An initially fast moving particle slows down while moving along the resonator axis before eventually getting trapped and oscillating around a potential minimum. This

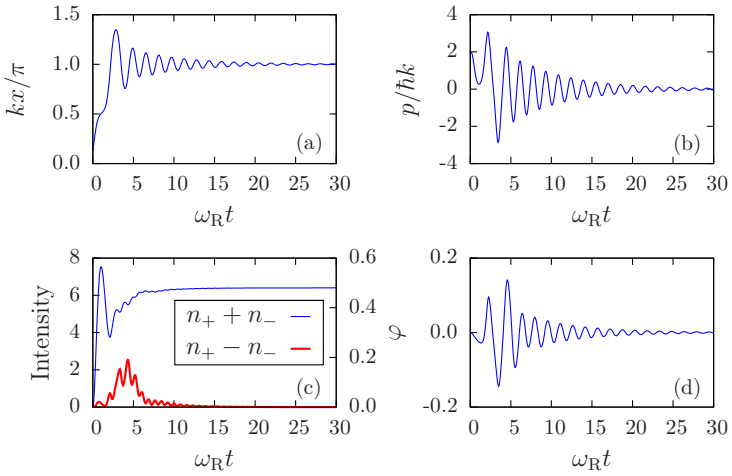

Figure 5.2: (Color online) Particle motion in a ring cavity as solution of Eqs. (5.1) and (5.2). The particle moves along the cavity axis and eventually gets trapped. (a) Position, (b) momentum, (c) intensities split into symmetric (left y-axis) and antisymmetric (right y-axis) parts, and (d) phase shift from an initially $\cos^2(kx)$-shaped potential. Parameters: $\Delta_c = -2.6\omega_R$, $\kappa = \omega_R$, $U_0 = -0.3\omega_R$, and $\eta_+ = \eta_- = 4\omega_R$.

is reflected clearly in the field dynamics as well since symmetric pumping of the counter-propagating running waves corresponds to a pumped [$\propto \cos(kx)$] and an unpumped [$\propto \sin(kx)$] standing wave. A moving particle will scatter light from the cosine to the sine mode so that the resulting superimposed fields correspond to a shifted cosine mode. Hence also the resulting optical potential $\propto \cos^2(kx)$ gets shifted due to excitations of the sine mode as long as the particle moves. This can be clearly seen in Figs. 5.2(c) and 5.2(d). In the classical limit a particle at rest will scatter no more light into the sine mode and we obtain a pure cosine field in the resonator. In quantum mechanics the uncertainty relation will prevent this and quantum fluctuations of the particle position and momentum will couple the two modes even at zero temperature [5.17].

5.2.2 Quantum description

Let us now turn to a quantum description of the particle motion and the field modes. For convenience, we use a basis of $\{\cos(x), \sin(x)\}$ mode functions rather than the propagating wave modes $\{\exp(\pm ikx)\}$. This facilitates a straightforward comparison with the case of the standing-wave resonator by putting the coupling to the sine mode to zero and also allows for a better separation of the classical part of the field amplitude in the cosine mode. The corresponding Hamiltonian for symmetric

pumping thus reads:

$$H = \frac{p^2}{2m} + \hbar U_0 \left[a_\mathrm{c}^\dagger a_\mathrm{c} \cos^2(kx) + a_\mathrm{s}^\dagger a_\mathrm{s} \sin^2(kx) \right] + \\ + \frac{\hbar U_0}{2} \left(a_\mathrm{c}^\dagger a_\mathrm{s} + a_\mathrm{s}^\dagger a_\mathrm{c} \right) \sin(2kx) - \\ - \hbar \Delta_\mathrm{c} \left(a_\mathrm{c}^\dagger a_\mathrm{c} + a_\mathrm{s}^\dagger a_\mathrm{s} \right) - i\hbar\eta_\mathrm{c} \left(a_\mathrm{c} - a_\mathrm{c}^\dagger \right). \quad (5.3)$$

While the first line contains the optical potentials induced by the two field modes independently, the second line describes the particle-position-dependent coherent scattering of photons between the two modes. The third line contains the free-field evolution for both modes as well as the pumping of the cosine mode.

Let us first look at the corresponding Heisenberg equations for the particle momentum,

$$\dot{p} = \hbar k U_0 \left(a_\mathrm{c}^\dagger a_\mathrm{c} - a_\mathrm{s}^\dagger a_\mathrm{s} \right) \sin(2kx) - \\ - \hbar k U_0 \left(a_\mathrm{c}^\dagger a_\mathrm{s} + a_\mathrm{s}^\dagger a_\mathrm{c} \right) \cos(2kx), \quad (5.4a)$$

and for the mode amplitudes (dropping the input noise operators),

$$\dot{a}_\mathrm{c} = \left\{ i \left[\Delta_\mathrm{c} - U_0 \cos^2(kx) \right] - \kappa \right\} a_\mathrm{c} - \frac{iU_0}{2} \sin(2kx) a_\mathrm{s} + \eta_\mathrm{c} \quad (5.4b)$$

$$\dot{a}_\mathrm{s} = \left\{ i \left[\Delta_\mathrm{c} - U_0 \sin^2(kx) \right] - \kappa \right\} a_\mathrm{s} - \frac{iU_0}{2} \sin(2kx) a_\mathrm{c}. \quad (5.4c)$$

The first line of equation (5.4a) describes a force which solely depends on the photon numbers in the modes whereas the second line is phasedependent and stems from the interference terms of the two modes of the intracavity electric field. In the special case of only one mode (e.g., setting $a_\mathrm{s} = 0$) we recover the case of a standing-wave resonator. Small field amplitudes in the sine mode then simply induce a phase-dependent force on the particle while small deviations of the particle position from $x = 0$ determine the phase of the sine-mode field.

In the Schrödinger picture the time evolution of the density matrix ρ of the coupled system is determined by the master equation

$$\dot{\rho} = \frac{1}{i\hbar} [H, \rho] + \mathcal{L}_\mathrm{c}\rho + \mathcal{L}_\mathrm{s}\rho, \quad (5.5)$$

where the Liouvillean superoperator describing photon losses is given by [5.37]

$$\mathcal{L}_i \rho = \kappa \left(2a_i \rho a_i^\dagger - a_i^\dagger a_i \rho - \rho a_i^\dagger a_i \right), \; i \in \{\mathrm{c}, \mathrm{s}\}. \quad (5.6)$$

In general the field damping time will be shorter than the time scale of particle motion so the fields will reach a particle-dependent quasi-stationary state. For strong coherent pumping of the cosine mode one thus can approximate a_c by a coherent field of amplitude α_c and only treat the sine mode quantum mechanically. In the limit of very deep optical potentials, where particles are trapped near $x \approx 0$, this leads to the equations [5.17]

$$\dot{p} = 2\hbar k U_0 \left(|\alpha_\mathrm{c}|^2 - a_\mathrm{s}^\dagger a_\mathrm{s}\right) kx - \hbar k U_0 \left(\alpha_\mathrm{c}^* a_\mathrm{s} + \alpha_\mathrm{c} a_\mathrm{s}^\dagger\right) \tag{5.7a}$$

$$\dot{a}_\mathrm{s} = \left(i\Delta_\mathrm{c} - \kappa\right) a_\mathrm{s} - i\alpha_\mathrm{c} U_0 kx, \tag{5.7b}$$

which are well known in optomechanics. In the opposite limit of a very weak potential and an initially flat particle distribution ($k = 0$) the $\sin(2kx)$ term will only amount to scattering to particle waves with $p = \pm 2\hbar k$ [5.38], where again a simple coupled-oscillator model can be applied. In this work we will concentrate on the general case where the particles are weakly trapped in the optical potential but still can tunnel between adjacent sites. This should finally lead to a Bose-Hubbard-type description with new types of long-range interactions.

5.3 Effective potentials and dynamics in the weak-coupling limit

As the general quantum dynamics is too complex for a direct solution we have to resort to interesting limiting cases. In this section we first work out the cavity-induced corrections to the particle dynamics in a classical potential. As outlined above the particles moving in the cavity field will scatter light between the modes and thus change the depth and shape of the optical potential. If the adjustment time of the field, i.e., the cavity decay, is faster than the typical particle motion, one can still expect to be able to define an effective potential for the particle. These cavity losses, from another viewpoint, can also be seen as a continuous measurement of the particle dynamics [5.39] which modifies the system dynamics via measurement backaction [5.40]. In the following we try to address these new key aspects in the strong-damping and weak-coupling limit, where they give only small corrections.

In a cavity the optical potential felt by the the particle is no longer conservative and constant as fluctuations in the field amplitude (quantum jumps) lead to momentum diffusion and dephasing of the wave function. This behavior is generic for a quantum system coupled to an open system. For free-space optical lattices the most important part of the decoherence stems from spontaneous photon scattering from the trap field to free space. However, for typical operating conditions far off any resonance, decoherence times are of the order of minutes rendering the light fields to constitute conservative classical potentials [5.2]. In a resonator-generated potential one has a

second important contribution to decoherence via cavity decay. For sufficient atom-field coupling, the corresponding decoherence times can be quite short. Actually, one recovers the free-space conservative-field limit in the case of a very bad, "infinitely" fast decaying cavity together with a very strong pump and weak coupling, where the particles cannot induce any changes to the field dynamics.

In the following, we calculate corrections to this limit in the bad-cavity case via adiabatic elimination of the field dynamics. We first demonstrate semiclassically in secular approximation within the Schrödinger picture that the field always relaxes to a very low-excited state for properly chosen parameters. This allows us to derive an effective potential for the coherent particle dynamics. Still, the field dynamics induces dephasing as can be clearly observed on the decay of coherent tunneling oscillations due to photon scattering. In the following we will study this dephasing and derive an estimate for this decay rate.

5.3.1 Low-excitation limit in the Schrödinger picture

As seen from the Heisenberg equations (5.4) for the field modes the sine mode will only be populated by photons scattered in by the particles from the strongly pumped cosine mode. On the other hand, the driven cosine mode will be highly occupied and close to a coherent state $|\alpha_\mathrm{c}\rangle$ with $|\alpha_\mathrm{c}| \gg 1$. This generates an optical potential of depth $V_0 = \hbar|U_0||\alpha_\mathrm{c}|^2$ forming a periodic optical lattice. In the limit of small $|\alpha_\mathrm{c}||U_0|/|\Delta_\mathrm{c}|$ we find only a very small field corresponding to at most one photon in the second mode. The wave function of the total system thus can be well approximated by the sum of a zero-photon and a one-photon component in the sine mode and a coherent state in the cosine mode. Neglecting higher sine-mode photon numbers as well as constant terms an effective approximate Hamiltonian in this limit thus can be conveniently written as

$$H = \left(\frac{p^2}{2m} + \hbar U_0|\alpha_\mathrm{c}|^2\cos^2(kx)\right) - \hbar\left(\Delta_\mathrm{c} - U_0\sin^2(kx)\right)\tilde{\sigma}^+\tilde{\sigma}^- + \\ + \frac{\hbar U_0}{2}\sin(2kx)\left(\alpha_\mathrm{c}^*\tilde{\sigma}^- + \alpha_\mathrm{c}\tilde{\sigma}^+\right), \quad (5.8)$$

where we have introduced the (photonic) raising and lowering operators $\tilde{\sigma}^+ := |1\rangle\langle 0|$ and $\tilde{\sigma}^- \equiv (\tilde{\sigma}^+)^\dagger = |0\rangle\langle 1|$. For simplicity and without loss of generality we choose the pump phase in a way that $\mathrm{Im}\,\alpha_\mathrm{c} = 0$ in the following. The rather familiar-looking Hamiltonian (5.8) now exactly corresponds to a two-level particle moving in an optical potential, whose internal degrees of freedom are interacting with a classical spatially varying light field. Note that while the two states here physically describe zero or one photon in the sine mode and not actual internal particle excitations, the mathematics is the same as for an internal atomic excitation. Actually, in the past

decades numerous ways to treat this generic laser-cooling Hamiltonian in different approximations have been developed.

Here we will follow the well-established *dressed-states* approach, based on the possibility to analytically diagonalize the Hamiltonian for any fixed particle position x and determine the corresponding adiabatic field states. Hence x and p are treated as classical variables [5.41]. Alternatively, it would be also possible to directly solve the optical Bloch equations. Both methods start from a semiclassical approximation of the external particle variables. However, as shown in Refs. [5.42, 5.43] there exists a corresponding consistent quantum-mechanical interpretation of the dressed-states picture. Here we will follow both approaches. The semiclassical approximation allows to obtain analytical results for the effective potential, which will give significant qualitative insight to the expected system dynamics and the latter treatment allows for an estimate of the effective motional decoherence and damping rates.

Diagonalization in the semiclassical limit yields the eigenvalues (the "adiabatic potentials" [5.44])

$$V_{\pm}(x) = \hbar U_0 \left(|\alpha_\mathrm{c}|^2 - \frac{1}{2}\right) \cos^2(kx) - \frac{\hbar(\Delta_\mathrm{c} - U_0)}{2} \pm \frac{\hbar\Omega(x)}{2} \tag{5.9}$$

and the corresponding normalized eigenvectors

$$|x;+\rangle = \quad \cos\vartheta\,|0\rangle + \sin\vartheta\,|1\rangle \tag{5.10a}$$

$$|x;-\rangle = -\sin\vartheta\,|0\rangle + \cos\vartheta\,|1\rangle\,, \tag{5.10b}$$

where we have defined

$$\Delta(x) := \Delta_\mathrm{c} - U_0 \sin^2(kx) \tag{5.11a}$$

$$\Omega(x) := \sqrt{\Delta^2(x) + U_0^2 |\alpha_\mathrm{c}|^2 \sin^2(2kx)} \tag{5.11b}$$

$$\sin\vartheta(x) := \mathrm{sgn}\left(U_0 \alpha_\mathrm{c} \sin(2kx)\right) \sqrt{\frac{\Omega(x) - \Delta(x)}{2\Omega(x)}} \tag{5.11c}$$

$$\cos\vartheta(x) := \sqrt{\frac{\Omega(x) + \Delta(x)}{2\Omega(x)}}. \tag{5.11d}$$

For $|U_0||\alpha_\mathrm{c}| \ll |\Delta_\mathrm{c}|$ the state $|x;-\rangle$ contains only a very small amount of the one-photon state (it is thus a "quasidark state" [5.44]) since in leading order

$$\cos^2\vartheta(x) \simeq \frac{|\alpha_\mathrm{c}|^2}{4} \frac{U_0^2}{\Delta_\mathrm{c}^2} \sin^2(2kx) \tag{5.12a}$$

$$\sin^2\vartheta(x) \simeq 1 - \frac{|\alpha_\mathrm{c}|^2}{4} \frac{U_0^2}{\Delta_\mathrm{c}^2} \sin^2(2kx). \tag{5.12b}$$

The equations of motion for the two populations (in secular approximation which is valid for well-resolved lines, i.e., $\Omega(x) \gg \kappa \Rightarrow |\Delta_\mathrm{c}| \gg \kappa$) read [5.41, 5.45]

$$\dot{\Pi}_+ = -\Gamma_+^\mathrm{eff}\Pi_+ + \Gamma_-^\mathrm{eff}\Pi_- \tag{5.13a}$$

$$\dot{\Pi}_- = -\Gamma_-^\mathrm{eff}\Pi_- + \Gamma_+^\mathrm{eff}\Pi_+, \tag{5.13b}$$

with the position-dependent effective rates

$$\Gamma_+^\mathrm{eff}(x) = 2\kappa \sin^4\vartheta(x) \tag{5.14a}$$

$$\Gamma_-^\mathrm{eff}(x) = 2\kappa \cos^4\vartheta(x). \tag{5.14b}$$

Its steady-state solution reads

$$\Pi_+ = \frac{\Gamma_-^\mathrm{eff}}{\Gamma_+^\mathrm{eff}+\Gamma_-^\mathrm{eff}} \simeq \frac{\Gamma_-^\mathrm{eff}}{\Gamma_+^\mathrm{eff}} = \left(\frac{\Omega+\Delta}{\Omega-\Delta}\right)^2 \tag{5.15a}$$

$$\Pi_- = \frac{\Gamma_+^\mathrm{eff}}{\Gamma_+^\mathrm{eff}+\Gamma_-^\mathrm{eff}} \simeq 1 - \frac{\Gamma_-^\mathrm{eff}}{\Gamma_+^\mathrm{eff}} = 1 - \left(\frac{\Omega+\Delta}{\Omega-\Delta}\right)^2. \tag{5.15b}$$

This state is reached within a time determined by the population decay rate $\Gamma_\mathrm{pop} = 2\kappa(\sin^4\vartheta + \cos^4\vartheta)$. Since $\Gamma_-^\mathrm{eff} \ll \Gamma_+^\mathrm{eff}$ the field will always end up in the local $|x;-\rangle$ state provided that $\omega_\mathrm{R} \ll \Gamma_\mathrm{pop}$. The low-excitation approximation is thus well justified. For $U_0/\Delta_\mathrm{c} \ll 1$ the steady-state populations (5.15) reduce to

$$\Pi_+ \simeq \frac{|\alpha_\mathrm{c}|^4}{16}\frac{U_0^4}{\Delta_\mathrm{c}^4}\sin^4(2kx) \tag{5.16a}$$

$$\Pi_- \simeq 1 - \frac{|\alpha_\mathrm{c}|^4}{16}\frac{U_0^4}{\Delta_\mathrm{c}^4}\sin^4(2kx). \tag{5.16b}$$

A small photon number in the sine mode is thus consistent with the approximation $\Pi_- \simeq 1$ as the photon number scales with $U_0^2/\Delta_\mathrm{c}^2$ and the population with $U_0^4/\Delta_\mathrm{c}^4$. Hence, in steady state the effective potential reads

$$\langle V(x)\rangle \simeq \hbar U_0 |\alpha_\mathrm{c}|^2 \cos^2(kx) + \frac{|\alpha_\mathrm{c}|^2}{4}\frac{\hbar U_0^2}{\Delta_\mathrm{c}}\sin^2(2kx). \tag{5.17}$$

This is of course the same result as obtained for optical lattice potentials (AC Stark shift) [5.2]. There the potential is found to be $V(x) = \hbar|\Omega(x)|^2/4\delta$, where $\Omega(x)$ is the Rabi frequency and δ the detuning of the two-level system with respect to the driving laser. Setting $\Omega(x) := U_0\alpha_\mathrm{c}\sin(2kx)$ and $\delta := \Delta_\mathrm{c}$ the second part of equation (5.17) is recovered. The first part is just some additional classical potential which in our case does not affect the "internal" variables of the particle.

Let us now treat the problem in a closely related quantum-mechanical way. To this end we apply the unitary transformation

$$U = \begin{pmatrix} \cos\vartheta & \sin\vartheta \\ -\sin\vartheta & \cos\vartheta \end{pmatrix} \tag{5.18}$$

on the Hamiltonian (5.8). Assuming adiabaticity (non adiabatic off-diagonal terms much smaller than the difference between the adiabatic eigenvalues [5.42]), the resulting Hamiltonian in the adiabatic basis $\{|+\rangle, |-\rangle\}$ reads [5.42]

$$H_{\mathrm{ad}} = \left(\frac{p^2}{2m} + \hbar U_0 \left(|\alpha_{\mathrm{c}}|^2 - \frac{1}{2} \right) \cos^2(kx) \right) + \frac{\hbar\Omega(x)}{2} \Big(|+\rangle\langle+| - |-\rangle\langle-| \Big). \tag{5.19}$$

The eigenstates of (5.19) are

$$\left| \Psi^{\pm}_{n,q} \right\rangle = \left| \phi^{n,\pm}_q \right\rangle |\pm\rangle \,, \tag{5.20}$$

where $\left| \phi^{n,\pm}_q \right\rangle$ denotes the Bloch state with quasi momentum q for the nth energy band of the two adiabatic potentials $V_{\pm}(x)$ defined in (5.9). Looking again at the rate equations stemming from the master equation including photon decay one finds the effective decay rates [5.46]

$$\Gamma^{+}_{n,q} = 2\kappa \left\langle \phi^{n,+}_q \middle| \sin^2\vartheta \middle| \phi^{n,+}_q \right\rangle \tag{5.21a}$$

$$\Gamma^{-}_{n,q} = 2\kappa \left\langle \phi^{n,-}_q \middle| \cos^2\vartheta \middle| \phi^{n,-}_q \right\rangle . \tag{5.21b}$$

The dynamics described by the corresponding rate equations is shown in Fig. 5.3. Again, as in the semiclassical case we have $\Gamma^{+}_{n,q} \gg \Gamma^{-}_{n,q}$, and only the subspace belonging to $|-\rangle$ will be significantly populated in steady state. Therefore the adiabatic potential $V_{-}(x)$ can be treated as an effective potential for the particle motion as long as the incoherent processes within this subspace are sufficiently small [5.2]. Decoherence manifests itself as finite lifetime of the Bloch states within this potential, leading to a damping of the particle motion. This can be understood in the following way: Localized particles within the lattice are described by coherent superpositions of Bloch states [5.47]. If these coherences get lost due to a finite life time of the Bloch states, the particles can no longer coherently move through the lattice and experience an additional friction force. We estimate the effective rate to be

$$\Gamma \sim \max_q \Gamma^{-}_{0,q} \simeq 2\kappa \frac{|\alpha_{\mathrm{c}}|^2 U_0^2}{4\Delta_{\mathrm{c}}^2} \max_q \left\langle \phi^0_q \middle| \sin^2(2kx) \middle| \phi^0_q \right\rangle , \tag{5.22}$$

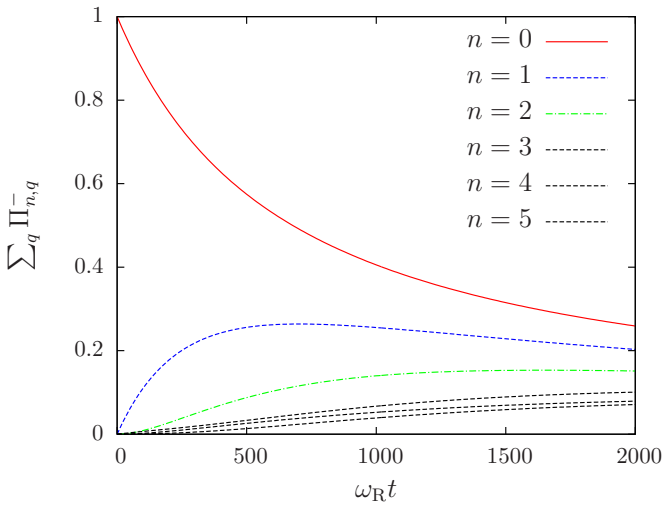

Figure 5.3: (Color online) Time evolution of the band populations stemming from the rate equations in the basis (5.20) containing the rates (5.21). The potential depth is $V_0 = 25E_R$ and thus the first three bands are bound. We have assumed a double-well potential hence each band consists of two Bloch states with different quasi momenta. The initial state was $\Pi^-_{0,-1} = \Pi^-_{0,0} = 0.5$. There is no significant population transfer to the subspace belonging to the $|+\rangle$ adiabatic eigenstate, whereas the population distribution within the $|-\rangle$ subspace changes, the particle is heated. Parameters: $U_0 = -\omega_R$, $\alpha_c = 5$, $\Delta_c = -500\omega_R$, and $\kappa = 100\omega_R$.

which in a very crude approximation gives

$$\Gamma \lesssim 2\kappa \frac{|\alpha_c|^2 U_0^2}{4\Delta_c^2} = \frac{|V_0|}{2} \frac{|U_0|\kappa}{\Delta_c^2}. \tag{5.23}$$

This rate has to be compared to the tunneling time T, which is determined by the inverse bandwidth of the lowest Bloch band. A high Q factor requires

$$\Gamma T \leq 2\kappa T \frac{|\alpha_c|^2 U_0^2}{4\Delta_c^2} \overset{!}{\ll} 1. \tag{5.24}$$

5.3.2 Effective potential via adiabatic elimination in the Heisenberg picture

As a second alternative approach we will directly work in the Heisenberg picture. In contrast to the previous section, where we applied a two-level approximation for the field, we consider the full mode operator a here. Its equation of motion apart from

the vacuum input noise operator reads

$$\dot{a} = (i\Delta(x) - \kappa)a - i\eta(x), \tag{5.25}$$

where we have defined

$$\eta(x) := \frac{\alpha_c U_0}{2} \sin(2kx). \tag{5.26}$$

Its formal steady-state solution reads

$$a = \frac{-i\eta(x)}{\kappa - i\Delta(x)}. \tag{5.27}$$

Hence one obtains the photon number

$$a^\dagger a = \frac{|\eta(x)|^2}{\kappa^2 + \Delta^2(x)} \simeq \frac{|\alpha_c|^2}{4} \frac{U_0^2}{\kappa^2 + \Delta_c^2} \sin^2(2kx), \tag{5.28}$$

where the latter is valid in the limit $U_0/\Delta_c \ll 1$. For $|\Delta_c| \gg \kappa$ it converges to the result (5.12a) obtained previously in the Schrödinger picture in secular approximation. The scattered coherent field $|\alpha(x)\rangle$ with amplitude (5.27) coincides with the steady-state solution $|x;-\rangle$ of the rate equations (5.13) in the same limit up to a phase depending on the (arbitrary) global phase of the eigenstates $|x;\pm\rangle$. Note that without the secular approximation κ also appears in the steady-state solution of the rate equations and thus in the photon number and the effective potential. The steady-state solution then can contain coherent superpositions of $|x;+\rangle$ and $|x;-\rangle$ as the states are not well enough separated.

The effective potential for the particle thus reads

$$\begin{aligned} V_{\text{eff}}(x) = \hbar U_0 |\alpha_c|^2 \cos^2(kx) + \frac{\hbar\Delta(x)|\eta(x)|^2}{\kappa^2 + \Delta^2(x)} \simeq \\ \simeq \hbar U_0 |\alpha_c|^2 \left(\cos^2(kx) + \frac{1}{4} \frac{\Delta_c U_0}{\Delta_c^2 + \kappa^2} \sin^2(2kx) \right), \end{aligned} \tag{5.29}$$

which equals the adiabatic potential $V_-(x)$ in the aforementioned approximation.

Now we can proceed exactly as before and estimate the particle's motion damping rate via the rates between the Bloch states,

$$\begin{aligned} \Gamma_{\text{eff}} \sim \max_q 2\kappa \left\langle \phi_q^{0,\text{eff}} \middle| \frac{|\eta(x)|^2}{\kappa^2 + \Delta^2(x)} \middle| \phi_q^{0,\text{eff}} \right\rangle \simeq \\ \simeq 2\kappa \frac{|\alpha_c|^2}{4} \frac{U_0^2}{\Delta_c^2 + \kappa^2} \max_q \left\langle \phi_q^{0,\text{eff}} \middle| \sin^2(2kx) \middle| \phi_q^{0,\text{eff}} \right\rangle. \end{aligned} \tag{5.30}$$

We have plotted this rate in Fig. 5.4 and the effective potential in Fig. 5.5. Figure 5.6 shows the particle motion for different parameters. The adiabatic elimination of the

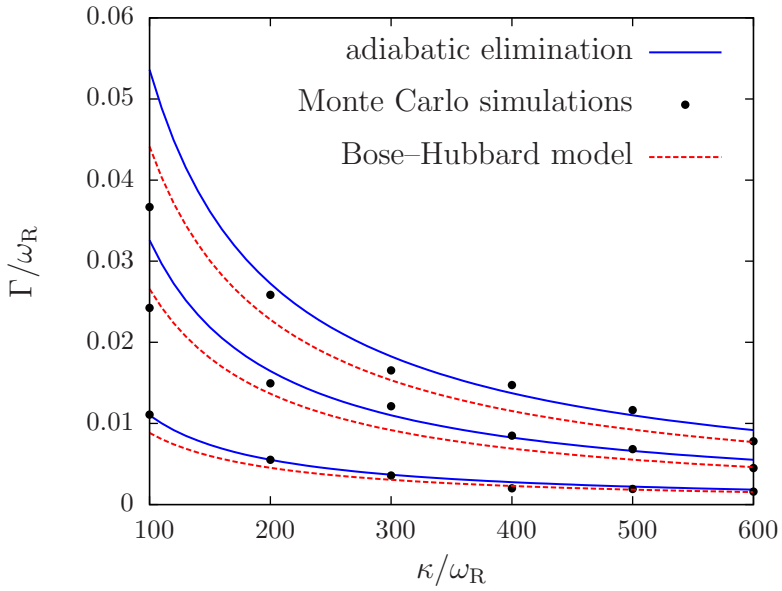

Figure 5.4: (Color online) Damping coefficient Γ stemming from the adiabatic elimination (solid lines), from Monte Carlo wave-function simulations (dots, cf. Sec. 5.5, model (ii)) and computed with the two-band Bose-Hubbard model (dashed lines) presented in Sec. 5.4.3. The statistical error from the MCWFs is of the order of the point size. From bottom to top: $U_0 = (-1, -3, -5)\omega_\mathrm{R}$. The other parameters are $\alpha_\mathrm{c} = \sqrt{12\omega_\mathrm{R}/|U_0|}$ and $\Delta_\mathrm{c} = U_0 - \kappa$.

field dynamics results in a loss of information about the system and a broadening of the effective potential wells for the particles (cf. Fig. 5.5). Physically, this can be interpreted as a mixture of a shift of the cosine-squared potential to the left as well as to the right. These shifts originate from the single-photon field of undetermined phase in the sine mode. A similar situation occurs in transversally pumped standing-wave resonators [5.48], where for a given cavity-field phase every even potential well gets deepened (leading to selforganization of the particles) and for the opposite phase every odd well is deeper. After adiabatic elimination of the field the mixture of both effects can be observed which deepens the whole lattice. Note that the effect of different atoms in the same state adds up coherently here, so even a tiny single-particle effect could have dramatic consequences for a superfluid many-particle state in the lattice.

In principle the model could also be applied to the case of a BEC of N particles in the same motional state. In this case the backaction effect on the potential would be strongly enhanced and modifications of tunneling will lead to significant changes of the collective nonlinear dynamics of a corresponding mean-field model. We will, however, not pursue this route any further here and rather turn to a description in

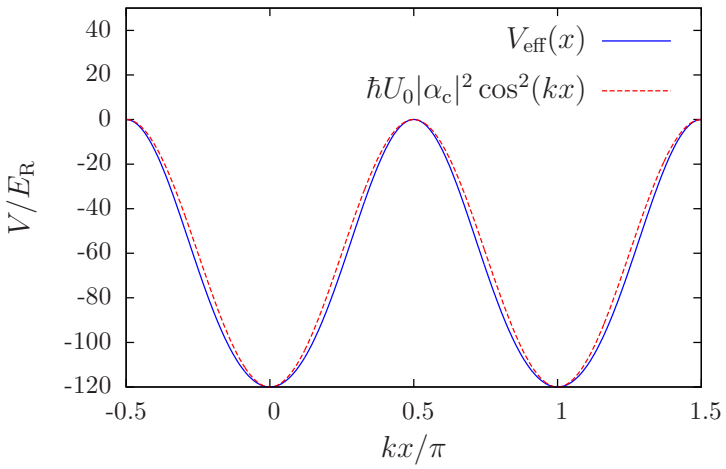

Figure 5.5: (Color online) Effective potential $V_{\mathrm{eff}}(x)$ compared to the unperturbed potential $V(x) = \hbar U_0|\alpha_c|^2\cos^2(kx)$. At $kx = n\pi/2$ ($n \in \mathbb{Z}$) the two potentials agree as for these points the coupling to the mode vanishes. Parameters: $U_0 = -50\omega_R$, $\alpha_c = \sqrt{2.4}$, $\Delta_c = -150\omega_R$, and $\kappa = 100\omega_R$.

terms of localized basis function in the spirit of a Bose-Hubbard model.

5.4 Bose-Hubbard model for a ring-cavity potential

The many-body version of the single-particle Hamiltonian (5.3) is conveniently obtained through a second-quantization formalism. With $\Psi(x)$ denoting the bosonic particle field operator, the corresponding Hamilton operator reads

$$H = \int \mathrm{d}x\, \Psi^\dagger(x) H_1 \Psi(x) - \hbar\Delta_c \left(a_c^\dagger a_c + a_s^\dagger a_s\right) - \\ - i\hbar\eta_c \left(a_c - a_c^\dagger\right) + \frac{g_{1D}}{2}\int \mathrm{d}x\, \Psi^\dagger(x)\Psi^\dagger(x)\Psi(x)\Psi(x), \quad (5.31)$$

with

$$H_1 = \frac{p^2}{2m} + \hbar U_0 \left(a_c^\dagger a_c - a_s^\dagger a_s\right)\cos^2(kx) + \\ + \hbar U_0 a_s^\dagger a_s + \frac{\hbar U_0}{2}(a_c^\dagger a_s + a_s^\dagger a_c)\sin(2kx). \quad (5.32)$$

The two-body interaction at very low temperatures (s-wave scattering) is modeled by a short-range pseudopotential containing the scattering length [5.49]. As our central goal is to study the implications of the quantized potential, we will, however,

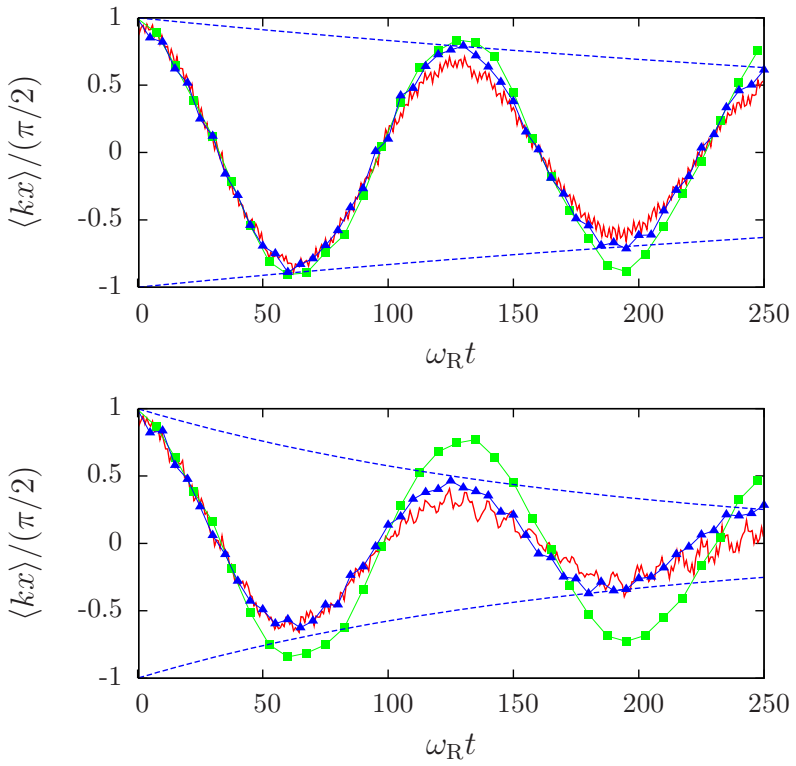

Figure 5.6: (Color online) Particle motion simulated with three different models [cf. models (i)-(iii) in Sec. 5.5]. [Red (solid line without additional points] Solution of the complete ring resonator with both dynamical modes. [Green (squares)] Solution setting the coupling to the unpumped mode to zero, i.e. a standing-wave lattice formed by the pumped mode. [Blue (triangles)] Solution of the model (5.8), where the pumped mode has been set to a static coherent state. The blue (dashed) envelope is the exponential decay predicted in equation (5.30). As the photon number in the pumped mode is high (and thus the fluctuations small), most of the damping originates from fluctuations in the unpumped mode. Tunneling is slightly enhanced compared to the standing-wave lattice, which is consistent with the shape of the effective potential: A broader potential results in slightly larger hopping matrix elements. However, stronger damping can be observed whenever tunneling gets enhanced as the coupling to the unpumped mode increases. Ensemble averages over 100 Monte Carlo wave-function trajectories. Parameters: $U_0 = -\omega_R$, $\alpha_c = \sqrt{12}$, $\Delta_c = U_0 - \kappa$, and $\kappa = 600\omega_R$ (upper plot) and $\kappa = 200\omega_R$ (lower plot), respectively.

neglect any direct particle-particle interaction for the moment. It can be reintroduced later by effective on-site interactions in the corresponding generalized Bose-Hubbard model.

In order to obtain a Bose-Hubbard description of the particle dynamics, the standard procedure is to expand the field operators appearing in (5.31) using a suitable set of localized Wannier functions which can be obtained from Bloch eigenfunctions of the single-particle Hamiltonian [5.47]. In the limit of particle energies well below the trap frequency $\omega_{\mathrm{T}} = \sqrt{4V_0 E_{\mathrm{R}}}/\hbar$ (V_0 is the potential depth), the expansion may be even restricted to the lowest Bloch band [5.1, 5.2]. In many cases, this approximation is very good and thus the consideration of higher bands is not necessary—even in the presence of any direct particle-particle interaction. Although one has to take extra care in choosing the correct Wannier basis, to some extent this procedure can still be applied when the optical lattice is generated not by a classically described coherent light field but rather by a quantized standing-wave mode of an optical resonator [5.14–5.16, 5.50]. As long as the photon-number uncertainty is much less than the average photon number, a self-consistent average potential depth can be chosen to calculate suitable particle basis states for the expansion of the field operator. The relevant parameters like tunneling- and on-site energies then only weakly depend on the photon-number fluctuations in the mode. Note that this procedure gets doubtful or even inapplicable if the cavity damping rate gets comparable with the time scale of particle motion, or when only few photons are present in the field mode generating the potential.

Naturally, one is tempted to try an analogous approach for the ring-cavity lattice formed by two quantized light modes as a first step. In the case of symmetric pump, only the cosine mode is excited in the empty cavity, and thus we can start with a Wannier basis involving only the lowest band of the highly excited cosine-mode potential. Interestingly, we find that within this ansatz a restriction of the particle dynamics to the lowest band immediately implies a complete decoupling of the sine mode from the dynamics. The ring resonator then behaves exactly as a standing-wave cavity because the possibility of a lattice displacement is neglected by this ansatz. In principle, one needs to consider displaced Wannier functions, which is not an obvious task: Treating the displacement δx as a self-consistent c-number (in the spirit of the afore discussed self-consistent potential depth) would result in a vanishing displacement for all times, if it was zero initially. This obviously does not reproduce the scattering of photons into the unpumped mode. On the other hand, differently displaced Wannier functions—which would take into account that the Hamiltonian modifies the lattice—are not orthogonal and hence do not form a suitable basis for a lattice model. One way to overcome this problem by taking into account higher Bloch bands will be presented in Sec. 5.4.2, where we show, that the corresponding cooperative tunneling and scattering processes are needed for a correct physical modeling of the dynamics.

5.4.1 Single-band model

As just discussed, in a first attempt we restrict the particle dynamics in the Hamiltonian (5.31) to the lowest Bloch band in the potential generated solely by the strongly pumped cosine mode. The field operator is thus approximated by

$$\Psi(x) \simeq \sum_i w_0(x - x_i) b_i, \tag{5.33}$$

where the bosonic operators $b_i^{(\dagger)}$ destroy (create) a particle at the ith lattice site and $w_0(x - x_i) =: w_i^0(x)$ denotes the zeroth-band Wannier function localized there. The expanded Hamilton operator (5.31) then reads

$$\begin{aligned} H = \sum_{i,j} E_{ij} b_i^\dagger b_j + \hbar U_0 \left(a_\mathrm{c}^\dagger a_\mathrm{c} - a_\mathrm{s}^\dagger a_\mathrm{s}\right) \sum_{i,j} J_{ij} b_i^\dagger b_j + \\ + \hbar U_0 N a_\mathrm{s}^\dagger a_\mathrm{s} + \frac{\hbar U_0}{2} \left(a_\mathrm{c}^\dagger a_\mathrm{s} + a_\mathrm{c} a_\mathrm{s}^\dagger\right) \sum_{i,j} \tilde{J}_{ij} b_i^\dagger b_j - \\ - \hbar \Delta_\mathrm{c} \left(a_\mathrm{c}^\dagger a_\mathrm{c} + a_\mathrm{s}^\dagger a_\mathrm{s}\right) - i\hbar\eta_\mathrm{c} \left(a_\mathrm{c} - a_\mathrm{c}^\dagger\right), \end{aligned} \tag{5.34}$$

where we have defined the matrix elements

$$E_{ij} := \left\langle w_i^0, \frac{p^2}{2m} w_j^0 \right\rangle \tag{5.35a}$$

$$J_{ij} := \left\langle w_i^0, \cos^2(kx) w_j^0 \right\rangle \tag{5.35b}$$

$$\tilde{J}_{ij} := \left\langle w_i^0, \sin(2kx) w_j^0 \right\rangle. \tag{5.35c}$$

As the next-nearest neighbor matrix elements are at least one order of magnitude smaller than their nearest-neighbor counterparts, we keep only the latter. Looking closely at the above expressions, the most interesting point to note is that $\tilde{J}_{ik} = 0 \; \forall i, k$ due to symmetry. This can easily be seen analytically: The product $w_0(x - x_i) w_0(x - x_j)$ is symmetric about the point $(x_i + x_j)/2$ and has compact support due to the exponential localization of the Wannier functions. The function $\sin(2kx)$, on the other hand, is an odd function with respect to the extrema of the potential. The integrand appearing when evaluating the scalar product (5.35c) is thus an odd function and therefore the integral over $\mathbb{R}$ vanishes. Hence the Bose-Hubbard-type Hamiltonian reads

$$\begin{aligned} H = E_0 N + EB + \left[\hbar U_0 \left(a_\mathrm{c}^\dagger a_\mathrm{c} - a_\mathrm{s}^\dagger a_\mathrm{s}\right)\right] (J_0 N + JB) + \\ + \hbar U_0 N a_\mathrm{s}^\dagger a_\mathrm{s} - \hbar \Delta_\mathrm{c} \left(a_\mathrm{c}^\dagger a_\mathrm{c} + a_\mathrm{s}^\dagger a_\mathrm{s}\right) - i\hbar\eta_\mathrm{c} \left(a_\mathrm{c} - a_\mathrm{c}^\dagger\right), \end{aligned} \tag{5.36}$$

where we have defined the particle number operator N and the hopping operator $B := \sum_i (b_i^\dagger b_{i+1} + b_{i+1}^\dagger b_i)$. E_0, J_0 (E, J) denote the on-site (nearest-neighbor off-site) matrix elements (5.35).

Note the lack of terms accounting for scattering into the sine mode in this Hamiltonian. The unpumped mode thus completely decouples from the system dynamics and simply decays to its vacuum state. Hence there will be no difference to the standing-wave cavity case after this decay. Mathematically, this can be seen by explicitly writing the Heisenberg equations for the sine mode,

$$\dot{a}_\mathrm{s} = \left(i\left(\Delta_\mathrm{c} + U_0\left((J_0 - 1)N + JB\right)\right) - \kappa\right) a_\mathrm{s} \tag{5.37a}$$

$$\dot{a_\mathrm{s}^\dagger a_\mathrm{s}} = -2\kappa a_\mathrm{s}^\dagger a_\mathrm{s}. \tag{5.37b}$$

In the bad-cavity limit, when the field relaxes almost instantaneously to its steady-state value, both quantities vanish. To capture more of the physics of the ring resonator, higher bands need to be included. This will be done in Sec. 5.4.2.

As the single-mode model has been extensively treated in previous literature, we will not discuss this much further. But is this result a bug or a feature? Mathematically, the decoupling of the sine mode originates from the even symmetry of the lowest-band Wannier functions, which we used as our basis. Physically, one could argue that tunneling between sites within a band does not invoke any force or momentum transfer and thus introduces no coupling or scattering to the empty sine mode. Hence the model can be at least self-consistent for a superfluid phase strictly limited to a single band. Of course, adding on-site interactions already destroys this argument as these are connected to changes of the local wave functions which amounts to the appearance of higher-band contributions. These will couple to the sine mode as seen in the numerical examples in Sec. 5.2 and the appearance of sine photons thus would herald the breakdown of zeroth-band superfluidity.

5.4.2 Multiband model

In order to incorporate excitations of the unpumped mode we have to allow for tunneling events from one site to a neighboring site with a simultaneous generation of a photon in the sine mode. This means that the final particle wave function is shifted with respect to the unperturbed basis: As the Wannier states corresponding to the cosine potential form an orthogonal basis set, mathematically this amounts, of course, to the admixture of higher-band Bloch functions in the dynamics. One might at this point be tempted to state that the zeroth-band motion will thus largely decouple from the unpumped sine mode whenever the excitation energy to the next band is sufficiently large. However, one has to be more careful here. Actually, the lowest-band approximation in the cosine potential does not necessarily coincide with the lowest-band approximation for the ring cavity. During the time evolution the

potential can get shifted relative to the unperturbed potential generated by the pump field. Hence, despite possessing contributions from higher-band wave functions, the particle can still have an energy corresponding to the lowest band as its wave function is simply a shifted lowest-band Wannier state.

Mathematically, one can estimate such contributions by expanding the lowest-band Wannier functions of a shifted lattice in the Wannier functions (including higher bands) of the original one, which, as said, form a complete basis set. We see, that to lowest order only the first antisymmetric band significantly contributes. This can be easily checked. If $w_0(x - x_i)$ is the lowest-band Wannier function localized at the ith lattice site of the unperturbed lattice, the Taylor expansion of a slightly shifted Wannier function to lowest order in the shift δx reads

$$w_0(x - x_i - \delta x) \simeq w_0(x - x_i) - \delta x\, w_0'(x - x_i). \tag{5.38}$$

The first derivative of the ground-state Wannier function is antisymmetric and thus the first band gets involved.

Let us therefore develop an improved version of the previously derived Bose-Hubbard model, which includes the important new physics originating from the ring-cavity geometry. To this end, we reconsider the original Hamiltonian (5.3) and assume a sufficiently strong coherent field α_c in the cosine mode so that its quantum properties can be ignored and only the sine mode needs a description by an operator a. The Hamiltonian thus reads

$$H = \frac{p^2}{2m} + \hbar U_0 \left(|\alpha_\mathrm{c}|^2 - a^\dagger a\right) \cos^2(kx) - \\ - \hbar \left(\Delta_\mathrm{c} - U_0\right) a^\dagger a + \frac{\hbar U_0}{2} \sin(2kx) \left(\alpha_\mathrm{c}^* a + \alpha_\mathrm{c} a^\dagger\right). \tag{5.39}$$

For very low photon numbers in the sine mode, we can neglect its contribution proportional to $a^\dagger a$ to the potential depth and get:

$$V(x) = \hbar U_0 \left(|\alpha_\mathrm{c}|^2 - a^\dagger a\right) \cos^2(kx) \simeq \hbar U_0 |\alpha_\mathrm{c}|^2 \cos^2(kx). \tag{5.40}$$

This Hamiltonian is closely related to an optomechanical coupling as used in Ref. [5.17], but here we have a periodic trapping potential for the particle motion. During the dynamics, the classical periodic potential is modified through the scattering term. A photon in the sine mode essentially leads to a broadening of the effective potential, which lowers the ground state energy and modifies the tunnel coupling to neighboring sites.

From a physics point of view, the dynamics induced by this Hamiltonian in several aspects resembles the case of particle motion in a standing-wave light field across a high-finesse resonator [5.31, 5.48], where a self-organization of the particles in two

possible patterns filling every second lattice site can occur. Position-dependent light scattering modifies the optical potential so the occupied sites deepen. The difference to our system is the symmetry of the scattering term, which here is antisymmetric with respect to the extrema of the classical potential. So instead of resulting in a state-dependent deepening of the lattice, the scattered light shifts the position of the lattice sites with respect to the classical potential. In a Bloch expansion with respect to the classical potential this shift amounts to contributions of higher bands like any interaction term would do.

To obtain a lattice model we expand the field operator to

$$\Psi(x) = \sum_i \sum_n b_i^n w_i^n(x), \tag{5.41}$$

where b_i^n destroys a particle in the nth band at the ith well and w_i^n denotes the corresponding Wannier function. Neglecting any direct particle-particle interaction, we obtain the second-quantized version of the Hamiltonian (5.39),

$$H = \sum_{n,m} \sum_{i,j} E_{ij}^{nm} b_i^{n\dagger} b_j^m - \hbar \left(\Delta_\mathrm{c} - \hat{N} U_0\right) a^\dagger a + \\ + \frac{\hbar U_0}{2} \sum_{n<m} \left(\tilde{J}^{nm} \tilde{T}^{nm} + \sum_{i \neq j} \tilde{J}'^{nm}_{ij} \tilde{B}_{ij}^{nm} \right) \left(\alpha_\mathrm{c}^* a + \alpha_\mathrm{c} a^\dagger\right), \tag{5.42}$$

where we have defined the operators

$$\hat{N} := \sum_n \sum_i b_i^{n\dagger} b_i^n \equiv N id \tag{5.43a}$$

$$\tilde{T}^{nm} := \sum_i \left(b_i^{n\dagger} b_i^m + b_i^{m\dagger} b_i^n \right) \tag{5.43b}$$

$$\tilde{B}_{ij}^{nm} := b_i^{n\dagger} b_j^m + b_j^{m\dagger} b_i^n. \tag{5.43c}$$

$\hat{N}$ is the number operator and proportional to the identity operator id as the total number of particles is conserved. $\tilde{T}^{nm}$ describes transitions between two bands within one well, whereas $\tilde{B}_{ij}^{nm}$ accounts for hopping between two wells together with a change of the band. The corresponding matrix elements read

$$E_{ij}^{nm} := \left\langle w_i^n, \left(\frac{p^2}{2m} + \hbar U_0 |\alpha_\mathrm{c}|^2 \cos^2(kx) \right) w_j^m \right\rangle \tag{5.44a}$$

$$\tilde{J}^{nm} := \langle w_i^n, \sin(2kx) w_i^m \rangle \tag{5.44b}$$

$$\tilde{J}'^{nm}_{ij} := \left\langle w_i^n, \sin(2kx) w_j^m \right\rangle. \tag{5.44c}$$

Note that in-well transitions between bands without photon exchange are prohibited as $E_{ii}^{nm} = 0 \; \forall n \neq m$.

5.4.3 Two-band lattice model

The Hamiltonian (5.42) is still complex and hard to solve completely. Hence, we will first try to highlight the basic physics of particle motion and lattice shifts in an as-simple-as-necessary model and restrict the particle motion to two bands. As pointed out earlier, to lowest order the first excited band gets coupled. It will be the superpositions of odd- and even parity eigenstates within one well which scatter a coherent field into the sine mode with non-vanishing amplitude $\langle a \rangle$. Keeping only the on-site and nearest-neighbor matrix elements and defining $E^n := E^{nn}_{ii}$, $\tilde{J} := \tilde{J}^{01}$ and $\tilde{J}' := \tilde{J}'^{01}_{i,i+1}$ the Hamiltonian reads

$$H = \sum_{\substack{n=0,1 \\ i}} E^n b_i^{n\dagger} b_i^n + \sum_{\substack{n,m=0,1 \\ \langle i,j \rangle}} E^{nm}_{i,j} b_i^{n\dagger} b_j^m + \\ + \frac{\hbar U_0}{2} \left(\tilde{J}\tilde{T} + \sum_{\langle i,j \rangle} \tilde{J}' \tilde{B}_{ij} \right) \left(\alpha_\mathrm{c}^* a + \alpha_\mathrm{c} a^\dagger \right) - \hbar \left(\Delta_\mathrm{c} - \hat{N} U_0 \right) a^\dagger a. \quad (5.45)$$

$\tilde{T} := \tilde{T}^{01}$ and $\tilde{B} := \tilde{B}^{01}_{i,i+1}$ describe on-site (off-site) parity changes.

Here we make a short remark concerning very deep potentials. There the hierarchy

$$|\tilde{J}| \gg |E^1| \gg |E^0| \sim |\tilde{J}'| \gg |E^{01}_{i,i+1}| \quad (5.46)$$

holds. Hence, tunneling happens preferably via excitation to the first band and subsequent tunneling within this band (see also Figs. 5.7 and 5.13). However, one has to be conscious that a too-large effective coupling strength invalidates the two-band model as even higher bands need to be taken into account. See Fig. 5.10 for a situation where the two-band model fails whereas the three-band version allows for reproducing the results of the full Monte Carlo simulations (cf. Sec. 5.5).

Most of the new physics involving tunneling with light scattering and hopping between bands can be already seen in a truncated two-site version of the model. Labeling the two sites by indices l and r for left and right, the Heisenberg equation of motion for the field then explicitly reads (neglecting the input noise operator)

$$\dot{a} = \left(i \left(\Delta_\mathrm{c} - N U_0 \right) - \kappa \right) a - i \frac{\alpha_\mathrm{c} U_0}{2} \left(\tilde{J}\tilde{T} + \tilde{J}'\tilde{B} \right) \quad (5.47)$$

and its steady-state solution

$$a_\mathrm{ss} = \frac{-i \frac{\alpha_\mathrm{c} U_0}{2} \left(\tilde{J}\tilde{T} + \tilde{J}'\tilde{B} \right)}{\kappa - i \left(\Delta_\mathrm{c} - N U_0 \right)}. \quad (5.48a)$$

For the photon number one obtains

$$\left(a^\dagger a \right)_\mathrm{ss} = \frac{\frac{|\alpha_\mathrm{c}|^2 U_0^2}{4} \left(\tilde{J}\tilde{T} + \tilde{J}'\tilde{B} \right)^2}{\kappa^2 + \left(\Delta_\mathrm{c} - N U_0 \right)^2} \simeq \frac{|\alpha_\mathrm{c}|^2}{4} \frac{U_0^2}{\Delta_\mathrm{c}^2 + \kappa^2} \left(\tilde{J}\tilde{T} + \tilde{J}'\tilde{B} \right)^2, \quad (5.48b)$$

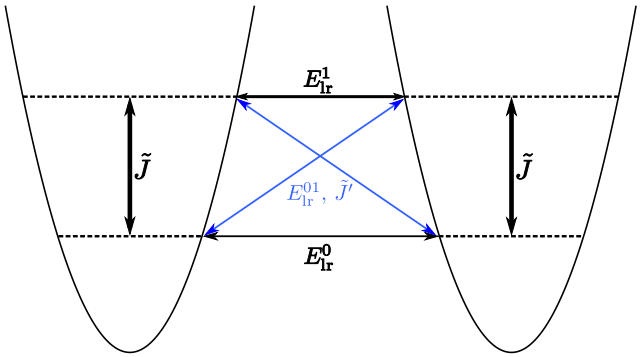

Figure 5.7: (Color online) Schematic view of some processes appearing in the Hamiltonian (5.45) for two chosen lattice sites. The width of the arrows corresponds to the amplitude of the process, i.e., the magnitude of the matrix elements (5.44).

where the latter is valid for $|U_0| \ll |\Delta_\mathrm{c}|$.

For large resonator damping constants κ, where the particle dynamics follows the field adiabatically, the localized states within one band radiate a field with zero amplitude,

$$\langle w_i^n | a_\mathrm{ss} | w_i^n \rangle = 0 \ \forall i, n \tag{5.49}$$

but non-vanishing photon number. Indeed, for one particle, the photon number is the same for all four localized basis states,

$$\Big\langle \psi \Big| (\tilde{J}\tilde{T} + \tilde{J}'\tilde{B})^2 \Big| \psi \Big\rangle = \tilde{J}^2 + \tilde{J}'^2 \ \forall\, |\psi\rangle \in \Big\{ \, |w_i^n\rangle \, \Big| \, i \in \{\mathrm{l}, \mathrm{r}\}, \ n \in \{0, 1\} \Big\}. \tag{5.50}$$

As pointed out before, the ground state will always have a non-negligible contribution of the first band. Therefore it is convenient to switch to the basis of even and odd localized states,

$$\Big| \psi^\pm_{\mathrm{l,r}} \Big\rangle := \frac{1}{\sqrt{2}} \Big(\Big| w^0_{\mathrm{l,r}} \Big\rangle \pm \Big| w^1_{\mathrm{l,r}} \Big\rangle \Big) \tag{5.51}$$

which radiate an approximately coherent field $|\pm\alpha\rangle$ with amplitude

$$\alpha = \frac{-i \frac{\alpha_\mathrm{c} U_0}{2} \tilde{J}}{\kappa - i \left(\Delta_\mathrm{c} - N U_0 \right)} \tag{5.52}$$

into the resonator. Strictly speaking, this is valid only as long $\tilde{J}^2 \gg \tilde{J}'^2$. However, this does not bring about any further restriction on the potential depth $V_0 = \hbar |U_0| |\alpha_\mathrm{c}|^2$ since already for $V_0 = 5 E_\mathrm{R}$ (for shallower potentials, the localized Wannier states cannot be properly defined [5.2]) the squared matrix elements already differ by three orders of magnitude, $\tilde{J}'^2 / \tilde{J}^2 \sim 0.002$. This difference gets much more pronounced for deeper and deeper lattices. We can thus safely assume $\tilde{J}^2 + \tilde{J}'^2 \simeq \tilde{J}^2$.

The basis decomposition of an arbitrary particle state in one well reads

$$\sqrt{1-|\varepsilon|^2}\left|w_i^0\right\rangle + \varepsilon\left|w_i^1\right\rangle = \frac{\sqrt{1-|\varepsilon|^2}+\varepsilon}{\sqrt{2}}\left|\psi_i^+\right\rangle + \frac{\sqrt{1-|\varepsilon|^2}-\varepsilon}{\sqrt{2}}\left|\psi_i^-\right\rangle. \tag{5.53}$$

The vanishing field amplitude for a particle in a parity eigenstate ($|\varepsilon| \in \{0,1\}$) can thus be explained as a consequence of destructive interference: The two components of the particle state radiate a field $|\alpha\rangle$ and a field $|-\alpha\rangle$, respectively. The resulting field state described by the reduced density matrix $\rho \propto |\alpha\rangle\langle\alpha| + |-\alpha\rangle\langle-\alpha|$ has a vanishing amplitude expectation value but a non vanishing photon-number expectation value, cf. the broadened adiabatic potential derived in Sec. 5.3 which can be explained as an average effect of the two shifts.

The jump operator $\sqrt{2\kappa}a$ can act as a parity-switch operator: Suppose the particle being in the lowest band of the left well prior to the jump,

$$|\psi\rangle \propto \left|\psi_\mathrm{l}^+\right\rangle|\alpha\rangle + \left|\psi_\mathrm{l}^-\right\rangle|-\alpha\rangle. \tag{5.54a}$$

Directly after the jump, the system state reads

$$a\,|\psi\rangle \propto \left|\psi_\mathrm{l}^+\right\rangle|\alpha\rangle - \left|\psi_\mathrm{l}^-\right\rangle|-\alpha\rangle, \tag{5.54b}$$

which corresponds to the antisymmetric particle state ($\varepsilon = 1$ above). Figures 5.11, 5.12, and 5.13 show single Monte Carlo trajectories depicting this behavior. More generally, quantum jumps result in a loss of the coherences in the system state [5.48]: During the coherent evolution the composed system state reads

$$\begin{aligned}|\psi_t\rangle = c_\mathrm{l}^+(t)\left|\psi_\mathrm{l}^+\right\rangle|\alpha\rangle + c_\mathrm{l}^-(t)\left|\psi_\mathrm{l}^-\right\rangle|-\alpha\rangle + \\ + c_\mathrm{r}^+(t)\left|\psi_\mathrm{r}^+\right\rangle|\alpha\rangle + c_\mathrm{r}^-(t)\,|\psi_\mathrm{r}^-\rangle\,|-\alpha\rangle.\end{aligned} \tag{5.55a}$$

Acting with the jump operator $\propto a$ on this state causes two phase shifts destroying the coherences:

$$\begin{aligned}a\,|\psi_t\rangle \propto c_\mathrm{l}^+(t)\left|\psi_\mathrm{l}^+\right\rangle|\alpha\rangle - c_\mathrm{l}^-(t)\left|\psi_\mathrm{l}^-\right\rangle|-\alpha\rangle + \\ + c_\mathrm{r}^+(t)\left|\psi_\mathrm{r}^+\right\rangle|\alpha\rangle - c_\mathrm{r}^-(t)\,|\psi_\mathrm{r}^-\rangle\,|-\alpha\rangle.\end{aligned} \tag{5.55b}$$

For the ensemble average over many quantum trajectories this effects leads to dephasing and thus to a damping of the tunneling oscillations.

5.5 Comparison with full Monte Carlo wave-function simulations

So far our treatment relied on a series of analytic approximations which allowed us to predict a wealth of new physical phenomena. To get a first check on the validity

and the prediction power of these models we compare them to "full" numerical simulations of the single-particle dynamics in a ring resonator. They are carried out in a momentum- and photon-number basis truncated at sufficiently high numbers to include all the relevant physics. In addition to a quantitative check for the analytic approximations these simulations also give nice qualitative insights into the microscopic origins of the observed phenomena. These simulations with at least three independent quantum degrees of freedom are generally very expensive in computer memory and time. They were performed using a Monte Carlo wave-function simulation algorithm as implemented in the locally developed C++QED framework [5.51][1], which is highly optimized for efficient memory handling and time-evolution speed. For technical reasons we swapped the role of the the two modes in the simulations, the sine mode is thus pumped and therefore the two potential wells (periodic boundary conditions) are located at $kx = \pm\pi/2$.

We performed Monte Carlo simulations of three different systems:

(i) the full ring resonator as described by the Hamilton operator (5.3),

(ii) the reduced system with the pumped mode set to a coherent state described by the Hamiltonian (5.39) [without the approximation (5.40)],

and, for comparison,

(iii) the pumped standing-wave resonator.

Additionally, we performed as well a series of Monte Carlo simulations of

(iv) the Bose-Hubbard model (5.45) to demonstrate the effects of quantum jumps on the particle parity. However, for the time evolution of the density matrix this much lower-dimensional model was alternatively solved by directly integrating the full master equation.

In order to reobtain the (approximately) same potential depth in the full system (i) we set $\eta_{\mathrm{c}} = |\alpha_{\mathrm{c}}|\sqrt{\kappa^2 + (\Delta_{\mathrm{c}} - U_0)^2}$. In all simulations, the particle was initially in a Gaussian state (momentum-space simulations) or in the lowest Wannier state (lattice model), respectively, localized in the right well. Note that due to the periodic boundary conditions, tunneling is enhanced by a factor of 2 in all numerical simulations. For comparison, we have taken this into account in the Bose-Hubbard model as well and have doubled all hopping matrix elements.

In Fig. 5.8 the standing-wave lattice is compared to the ring resonator. Although the unpumped mode is hardly populated—$\left\langle a^\dagger a \right\rangle \sim 1.4 \times 10^{-5}$—its impact on the

[1] The latest—and strongly improved with respect to the previous one described in Ref. [5.51]—release of the framework (version 2) can be downloaded from the project's homepage `www.uibk.ac.at/th-physik/qo/research/cppqed.html` or directly at `www.cppqed.sourceforge.net`.

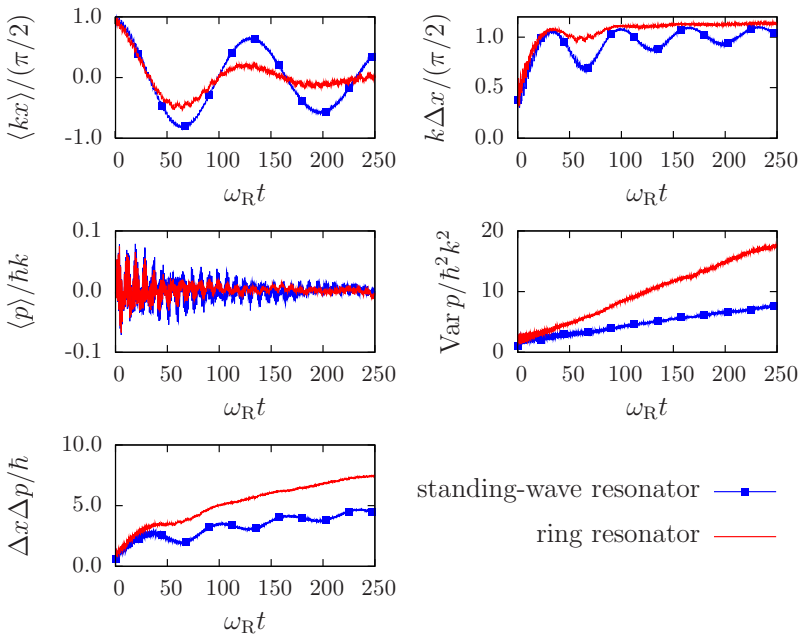

Figure 5.8: (Color online) Comparison of the standing-wave resonator [model (iii)] and the ring resonator [model (i)] for one particle. Ensemble average over 250 trajectories. Parameters: $U_0 = -3\omega_\mathrm{R}$, $\alpha_\mathrm{c} = 2$, $\Delta_\mathrm{c} = U_0 - \kappa$, and $\kappa = 400\omega_\mathrm{R}$.

particle is well pronounced. We see a significantly faster decay of coherent tunneling due to the presence of the second mode as source of decoherence. One might also recognize a slightly faster tunneling time due to the modified effective potential but this would require a much larger ensemble to be quantitatively checked. Here the validity condition for the approximation (5.40) is very well fulfilled. Note that for the parameters used in the figure the average photon number in the pumped mode generating the optical potential was only 4, which, however, still proves enough for the classical (coherent state) approximation for this mode amplitude to give qualitatively similar results. As particle motion is based essentially on tunneling in the low temperature limit, scattering to the unpumped mode can be viewed as an effective friction mechanism in the model.

Figure 5.9 shows the particle hopping between two sites computed from all four aforementioned models. The reduced system (ii) is indeed a good approximation for sufficiently large $|\alpha_\mathrm{c}|$. Since the effective coupling is not too large the two-band Bose-Hubbard model can remarkably well reproduce the results. However, as the coupling increases the two-band approximation turns out to be too restrictive. Including higher bands in such cases becomes absolutely necessary. Such a situation is depicted in Fig. 5.10, where taking into account the second excited band allows for reproducing

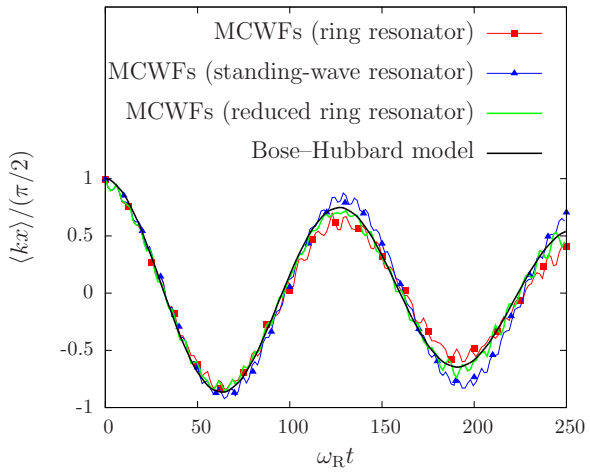

Figure 5.9: (Color online) Average position of the particle computed with the four models described in Sec. 5.5. For the Bose-Hubbard model the population imbalance $\langle N_{\mathrm{r}}\rangle - \langle N_{\mathrm{l}}\rangle$ has been plotted. Ensemble average over 100 trajectories. Parameters: $U_0 = -\omega_{\mathrm{R}}$, $\alpha_{\mathrm{c}} = \sqrt{12}$, $\Delta_{\mathrm{c}} = U_0 - \kappa$, and $\kappa = 400\omega_{\mathrm{R}}$.

the predictions of model (ii).

Looking at the microscopic origin of the dephasing and decoherence, the crucial effect of quantum jumps on these can be seen in Figs. 5.11, 5.12, and 5.13. The parity swaps predicted in Eqs. (5.54) can be nicely seen and the different tunneling time scales corresponding to the two bands are clearly visible. As the jump times have a strong random contribution, the source of dephasing thus gets very obvious. Actually, a related mechanism might also occur in free-space optical lattices if collisions invoke higher bands in the particle dynamics. Note that transitions between the bands visible in changes of the tunnel oscillation frequency are also accompanied by jumps in the photon number, which provides for real-time monitoring of the band populations.

Finally, we demonstrate that the Bose-Hubbard model can capture a great deal of the underlying physics if several bands are included. This is depicted in Fig. 5.14 which exhibits a significant excitation of the first excited band in steady state. This is consistent with the full simulations above, where a similar heating to higher bands can be observed, cf. Fig. 5.8.

5.6 Conclusions

We have developed several approximative analytical models to describe the dynamics of a quantum particle in an optical lattice which is generated by counter propagating fields in a high-Q ring resonator. A standard single-band description in terms

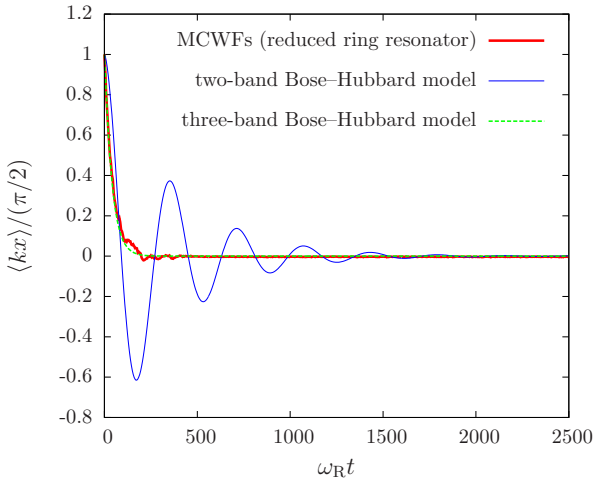

Figure 5.10: (Color online) Average position of the particle computed with Monte Carlo simulations (ensemble average over 150 trajectories) of the reduced model (ii) and with the two- and three-band lattice models. The two-band version fails, whereas the inclusion of the next band reproduces the correct behavior. Parameters: $U_0 = -2\omega_R$, $\alpha_c = \sqrt{12.5}$, $\Delta_c = U_0 - \kappa$, and $\kappa = 10\omega_R$.

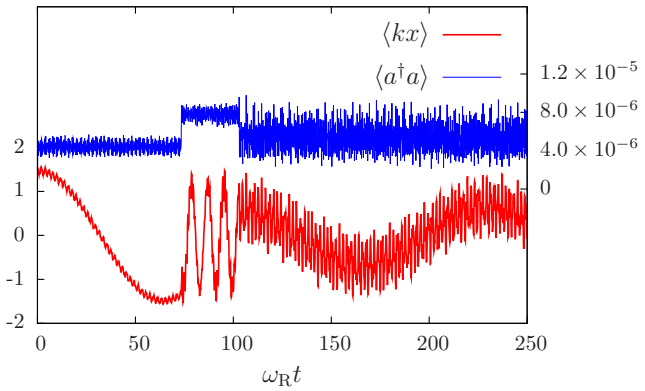

Figure 5.11: (Color online) Sample trajectory of the reduced model (ii) showing the position expectation value $\langle kx \rangle$ (left y-axis, lower curve) and $\langle a^\dagger a \rangle$ (right y-axis, upper curve). The two quantum jumps occurring at $\omega_R t \sim 70$ and $\omega_R t \sim 100$ are clearly visible: The photon number in the mode and the occupied band of the particle are changed simultaneously as seen from the sudden change of the oscillation frequency and amplitude between the potential wells. Here even higher bands are excited. After the fast oscillation between the wells the particle gets trapped again, but in a higher excited state, as can be seen from the higher amplitude. The photon-number variance is much more pronounced. Parameters: $U_0 = -2\omega_R$, $\alpha_c = \sqrt{6}$, $\Delta_c = U_0 - \kappa$, and $\kappa = 500\omega_R$.

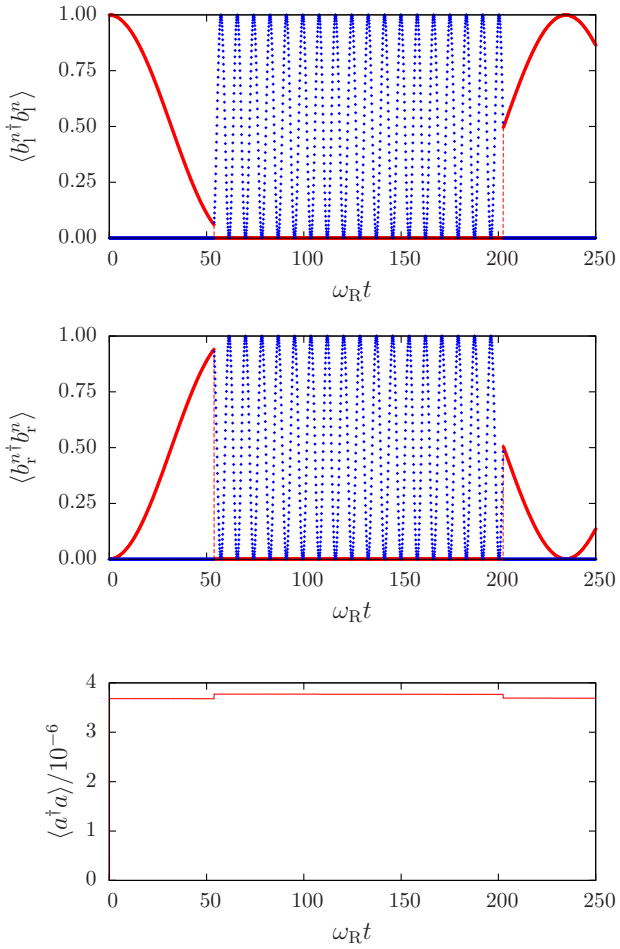

Figure 5.12: (Color online) Single Monte Carlo trajectory of the two-band Bose-Hubbard model for a shallow potential ($V_0 = 12E_{\mathrm{R}}$) and two wells. [Red solid line (blue dots)] Expectation value of the particle number in the zeroth (first) band within each well. Quantum jumps in the photon number can indeed trigger parity changes of the particle as sketched in the text [Eqs (5.54)]. The different tunneling time scales for the two bands can be seen. This trajectory can be regarded as a Bose-Hubbard equivalent to Fig. 5.11; the parameters are the same as described in the caption.

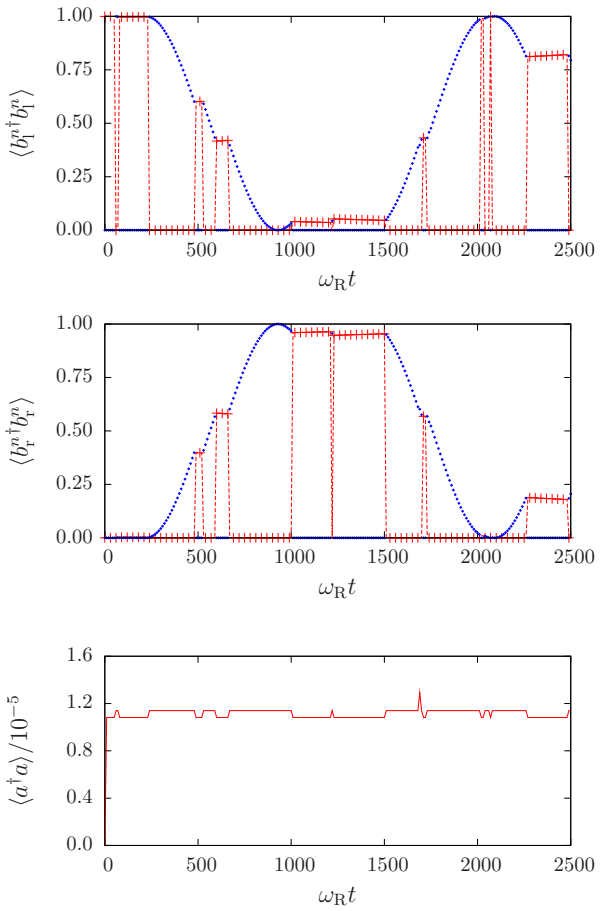

Figure 5.13: (Color online) Single Monte Carlo trajectory of the two-band Bose-Hubbard model for a very deep potential ($V_0 = 50E_R$) and two wells. [Red crosses (blue dots)] Expectation value of the particle number in the zeroth (first) band within each well. As zeroth-band tunneling is neglectable on the simulated time scale, the population within this band does not change considerably (horizontal lines). Only the first-band tunneling has a significant effect and subsequently modifies the zeroth-band distribution within the two lattice sites. Parameters: $U_0 = -2\omega_R$, $\kappa = 500\omega_R$, $\alpha_c = 5$, and $\Delta_c = U_0 - \kappa$.

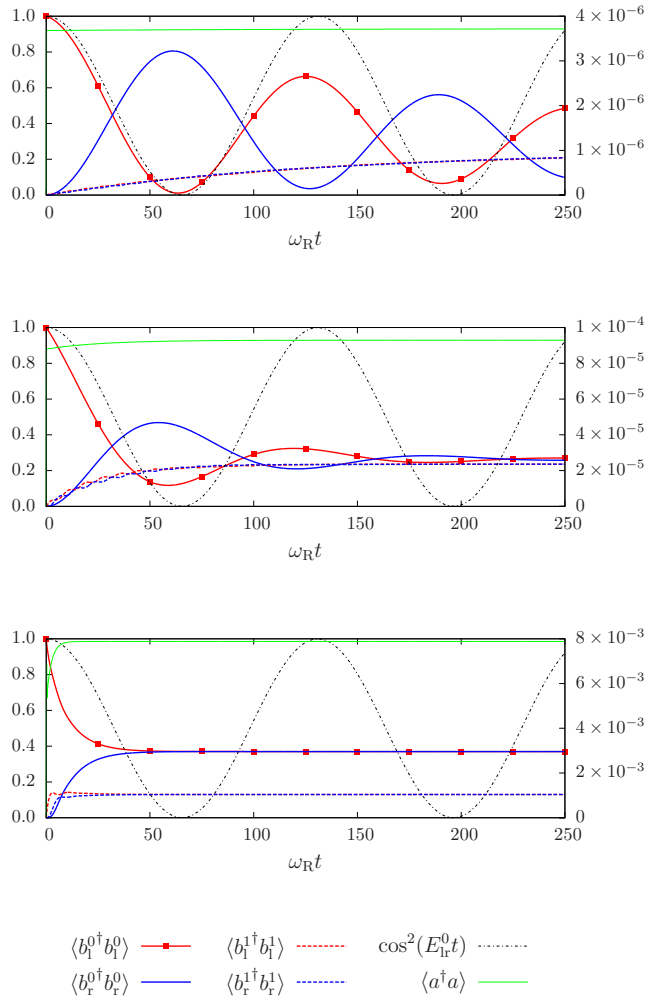

Figure 5.14: (Color online) Population evolution from the Bose-Hubbard-like lattice model for a fixed potential depth $V_0 = 12E_R$. The different time scales for the two bands are clearly visible. The particle was initially in the lowest band and located in the left well. The black dash-dotted line shows the tunneling Rabi oscillation for the lowest band without any coupling to the mode, i.e. $H = E_{lr}^0 b_l^{0\dagger} b_r^0 + \text{H. c.}$, for comparison. (Left y-axis) Populations; (right y-axis) photon number. As the parameters are similar to the ones used in figure 5.6, these plots give a microscopic band interpretation of the particle motion presented there. Parameters: $U_0 = -2\omega_R$, $\alpha_c = \sqrt{6}$, $\Delta_c = U_0 - \kappa$, and $\kappa = (500, 100, 10)\omega_R$ from top to bottom.

of Bloch or Wannier functions calculated from the unperturbed optical potential predicts frictionless tunneling motion of the particles and long-range coherence of the corresponding wave function. However, this approximation misses most of the essential physics. Already a perturbative inclusion of the first excited band reveals particle hopping between bands and sites accompanied by photon scattering into empty field modes as a key mechanism to provide for a realistic description of the dynamics. Even for very small photon scattering rates it leads to dephasing of tunnel oscillations and decoherence of the wave function. This will strongly diminish coherent transport together with heating of particle motion. In the perturbative approach it essentially leads to a modified effective potential shape and a phase-decay term. Note that this term, although being much smaller in a free-space-lattice setup, will finally also pose limits on obtainable coherence lengths and acceleration sensitivity in large free-space optical lattices. Microscopically, dephasing can be traced back to the strongly band (energy) dependent tunneling times, so even very small contributions of different bands lead to significant time shifts of tunnel oscillations. The corresponding approximative models which we developed will give a basis for future many-body generalizations of the model involving short- and long-range interactions between different particles. The interactions mediated by the scattered photons play a very similar role as phonons in real solid-state systems and thus can be a useful handle to shape and study long-range interactions in cold-atom optical lattices. As the photons scattered by different particles into the same mode even at long distances will interfere, they can lead to nonlocal momentum-space pairing of particle motion. The interaction will also help to establish long-range order, which will be particularly the case for the transverse-pump case, where no *a-priori* order is prescribed by the field modes and the atoms can self-arrange in a supersolid with diagonal and off-diagonal order.

In addition to modifying the dynamics and steady state of the particles, the scattering modes also provide for a basis for a real-time monitoring system of the particles to study the transition between different quantum phases or quantum models of transport in lattices with destruction of the system. This would require including direct local interactions in addition, which should be possible at least in the few-band limit of the model. As we centrally only need polarizable point particles, corresponding effects could as well be observed with molecules or even nanoparticles which are optically trapable.

Acknowledgments

This work has been supported by the Austrian Science Fund FWF through projects P20391 and F4013. We thank Tobias Grießer, Matthias Sonnleitner and Hashem Zoubi for helpful discussions.

Chapter 6

Preprint

arXiv:1205.6596 [quant-ph] (2012)

Quantum-correlated motion and heralded entanglement of distant optomechanically coupled objects[†]

Wolfgang Niedenzu, Raimar M. Sandner, Claudiu Genes and Helmut Ritsch

Institut für Theoretische Physik, Universität Innsbruck,
Technikerstraße 25, 6020 Innsbruck, Austria

The motion of two distant trapped particles or mechanical oscillators can be strongly coupled by light modes in a high finesse optical resonator. In a two mode ring cavity geometry, trapping, cooling and coupling is implemented by the same modes. While the cosine mode provides for trapping, the sine mode facilitates ground state cooling and mediates non-local interactions. For classical point particles the centre-of-mass mode is strongly damped and the individual momenta get anti-correlated. Surprisingly, quantum fluctuations induce the opposite effect of positively-correlated particle motion, which close to zero temperature generates entanglement. The non-classical correlations and entanglement are dissipation-induced and particularly strong after detection of a scattered photon in the sine mode. This allows for heralded entanglement by post-selection. Entanglement is concurrent with squeezing of the particle distance and relative momenta while the centre-of-mass observables acquires larger uncertainties.

URL: `http://arxiv.org/abs/1205.6596`
PACS: 37.30.+i, 03.65.Ud

[†]The author of the present thesis performed all the calculations in this publication. R. M. S. assisted in the implementation of the numerical simulations and, together with C. G., acted as a discussion partner on all other aspects of the work.

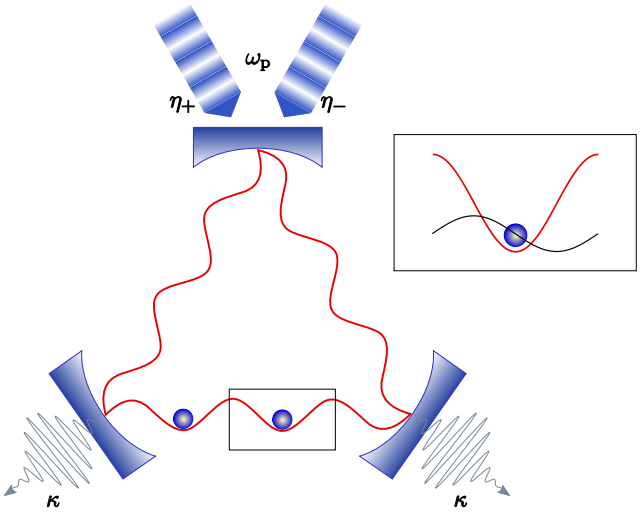

Figure 6.1: (Colour on-line) Sketch of the system. The pumped standing-wave mode (red) traps the particles, the second orthogonal one (black) mediates an effective interaction between them.

6.1 Introduction

The past decades have seen tremendous success in the implementation of control schemes for the motional state of matter via light fields either in free space or in optical cavities. A diversity of examples exist where the quantum regime of motion has been reached. The masses span many orders of magnitude, from the microscopic atomic size systems such as atoms in optical cavities [6.1–6.4] and laser-cooled ions in ion traps [6.5] to the macroscopic level with cavity-embedded membranes [6.6], mirrors [6.7] or levitated dielectric nano-particles [6.8].

A common interaction Hamiltonian that well approximates many quantum light-matter interfaces is quadrature-quadrature coupling [6.9]; more specifically, the displacement of the mechanics is coupled directly to a quadrature of the high-Q optical field mode that can be then used as an observable for indirect position detection. Adding a second mechanical system coupled to the field then allows one to engineer an effective two particle mechanical coupling by eliminating the mediating light mode. Here we find pulsed regime entanglement, non-classical momentum correlations and heralded entanglement triggered by photon detection. Recently, an expansion to quadratic coupling has been proposed [6.10] and the investigation of dissipation-induced [6.11, 6.12], noise-induced [6.13] and remote entanglement [6.14, 6.15] has been of great interest, including a scheme for sensitive force measurements [6.16] and entanglement of macroscopic oscillators [6.17].

Here we show that all this can be implemented in a system consisting of two

particles strongly trapped in the cosine mode of a ring cavity, where the two-particle interaction is carried by sideband photons in the sine mode. For deep trapping it yields the typical optomechanical Hamiltonian [6.18]. We start our presentation with a brief review of this result extended to two particles. We then analyse single quantum trajectories depicting strong correlations and entanglement. A subsequent investigation of momentum correlations reveals classically forbidden positive values in steady state, even in the absence of entanglement. The steady state shows a strong delocalisation of the centre-of-mass independent of the particle separation. We also show how to generate entanglement either in a pulsed regime or heralded by the detection of photons. Analytical calculations are carried out in the regime of strong particle confinement and matched to the more generally valid numerical simulations with good agreement. Finally, the occurrence of correlations in the system is explained in a simple adiabatic model.

6.2 Optomechanical dynamics of two particles in a ring cavity

We study two small polarisable particles confined within a symmetrically-pumped ring resonator, see fig. 6.1. Symmetric pumping results in a standing-wave optical potential with spatial dependence $\cos^2(kx)$ [6.18, 6.19]. The cosine mode is strongly pumped and approximated by a highly excited coherent state $|\alpha_\mathrm{c}\rangle$ with $|\alpha_\mathrm{c}| \gg 1$ (and without loss of generality $\alpha_\mathrm{c} \in \mathbb{R}$). The particles scatter photons into the unpumped orthogonal sine mode. This setup can be generally described by the Hamiltonian [6.18, 6.19]

$$H = \sum_{i=1}^{2} \left[\frac{p_i^2}{2m} + \hbar U_0 \alpha_\mathrm{c}^2 \cos^2(kx_i) + \hbar U_0 a^\dagger a \sin^2(kx_i) \right] + \\ + \frac{\hbar U_0 \alpha_\mathrm{c}}{2} \left(a + a^\dagger \right) \sum_{i=1}^{2} \sin(2kx_i) - \hbar \Delta_\mathrm{c} a^\dagger a. \quad (6.1)$$

Here, a denotes the annihilation operator of the quantum-mechanical sine mode, $U_0 < 0$ the optical potential depth per photon, x_i and p_i the particles' centre-of-mass position and momentum operators, respectively, and m the particle mass. The pump is detuned by $\Delta_\mathrm{c} := \omega_\mathrm{p} - \omega_\mathrm{c}$ from the bare cavity resonance frequency ω_c. To avoid instabilities we restrict ourselves to red detuned lasers ($\Delta_\mathrm{c} < 0$) for which a cooling regime exists [6.20]. The sine mode is only weakly populated by scattering such that $\left\langle a^\dagger a \right\rangle$ is negligible compared to α_c^2 [6.18]. Damping of the cavity mode is taken into account by the Liouvillean $\mathcal{L}\rho = \kappa \left(2a\rho a^\dagger - a^\dagger a \rho - \rho a^\dagger a \right)$ [6.21] in the master

equation

$$\dot{\rho} = \frac{1}{\mathrm{i}\hbar}\left[H, \rho\right] + \mathcal{L}\rho. \tag{6.2}$$

In the limit of tightly trapped particles, when it is justified to keep only the first and second order terms in the expansion of the trigonometric factors, the Hamiltonian (6.1) can be mapped onto the optomechanical model [6.18]

$$H = \sum_{i=1}^{2} \hbar\omega b_i^\dagger b_i - \hbar\Delta_\mathrm{c} a^\dagger a + \hbar g \sum_{i=1}^{2} (b_i + b_i^\dagger)(a + a^\dagger) \tag{6.3}$$

with $\omega := \sqrt{4\hbar|U_0|\alpha_\mathrm{c}^2 E_\mathrm{R}}/\hbar$, $g := U_0\alpha_\mathrm{c}k\xi_0/\sqrt{2}$, the recoil energy $E_\mathrm{R} \equiv \hbar\omega_\mathrm{R} := \hbar^2k^2/2m$ and the oscillator length $\xi_0 := \sqrt{\hbar/m\omega}$. The scaling of the latter suggests that the Lamb–Dicke regime $k\xi_0 \ll 1$ may also be reached for very heavy particles in shallower traps. As we do not consider any direct particle-particle interactions, the Hamiltonian (6.3) is also valid for particles not confined in the same, but rather in distant sites within the resonator.

Interestingly, the Hamiltonian (6.3) applies to a whole class of systems. A few well-studied realisations are (i) a cavity with vibrating end mirrors where the mirror-light field is always linear and governed mainly by the cavity length and the zero point motion of the mechanics [6.22, 6.23], (ii) two light membranes inside a cavity field positioned at the maximum slope of the field amplitude where the coupling depends on the reflective properties of the membranes and is increased with decreasing mass [6.24] and (iii) very light nano-sized dielectric spheres held inside the cavity field either by an external trapping light mode or by means of optical tweezers [6.8].

6.3 Single trajectory treatment

To get some first insight into the dynamics, let us solve eq. (6.2) numerically for some typical parameters. The direct solution of the master equation (6.2) is computationally very demanding owing to the large Hilbert space of the joint particles-field system. Therefore we resort to Monte Carlo wave function simulations [6.25], in which the system is coherently evolved between so-called "quantum jumps". These jumps correspond to a photon detected at the resonator output [6.25]. Besides the more favourable usage of computer resources, single trajectories also provide additional insight into the microscopic processes in the system. The simulations were efficiently implemented with the freely available[1] C++QED framework [6.26, 6.27] and performed in a joint momentum- and Fock basis.

A typical trajectory is shown in fig. 6.2, where the blue arrows indicate the times at which jumps occur. Initially, the particles were prepared in the ground state of

[1] `http://cppqed.sourceforge.net`

two separated potential wells and owing to the deep potential tunnelling is strongly suppressed. The momentum correlation coefficient $\mathcal{C}_p$ for the two particles is defined as

$$\mathcal{C}_p := \frac{\mathrm{Cov}(p_1, p_2)}{\Delta p_1 \Delta p_2} = \frac{\langle p_1 p_2 \rangle - \langle p_1 \rangle \langle p_2 \rangle}{\Delta p_1 \Delta p_2}, \tag{6.4}$$

where $\mathcal{C}_p = 1$ means perfect correlation and $\mathcal{C}_p = -1$ perfect anti-correlation of the motion. Quantum jumps by photodetection trigger strong correlations and entanglement between the particles due to the cavity-mediated interaction. The logarithmic negativity [6.28] already after the first jump approaches the value for a maximally entangled Bell state and the correlation reaches a value of $\mathcal{C}_p \approx 0.5$. The emerging state corresponds to a superposition of two particles moving to the right and two particles moving to the left such that the centre-of-mass momentum remains zero. As we will see later this behaviour is caused by excitation of a single particle into the first excited state within the trap. Beginning with the second jump the system is subject to fast oscillations which are of the order of the trap frequency. Note that only the field is dissipative in our model and induces quantum jumps. However, the particles respond to the sudden changes of the field in a correlated way.

Interestingly, while entanglement is quite pronounced on single trajectories, it remains small on average, see also fig. 6.3, where we have depicted the initial and final momentum distribution. The averaged steady-state logarithmic negativity is $\mathcal{E}_\mathcal{N} \sim 10^{-3}$.

6.4 Non-classical momentum correlations

We now examine the momentum correlations in more detail. Classical simulations reveal much stronger damping of the centre-of-mass motion than of the relative motion. Hence the particles become anti-correlated [6.1, 6.20, 6.29], see fig. 6.4. Surprisingly, the quantum simulations of the ring resonator system yield the opposite result. On average, initially uncorrelated particles become positively correlated due to the cavity input noise. This effect is visible in the steady-state density matrix presented in fig. 6.3. There, the momentum distribution is elongated into the first quadrant, which is a signature of positive correlations. Note that quantum mechanics allows pure states with positive correlations, but still zero average centre-of-mass motion with large uncertainty. The time evolution of the momentum correlation coefficient is depicted in fig. 6.5. We observe smaller correlations around the cooling sideband $\Delta_\mathrm{c} = -\omega$ as compared to the other chosen detuning $\Delta_\mathrm{c} = -\kappa$. For comparison, we also present the results of simulations containing the quadratic optomechanical Hamiltonian (6.3). The latter yields accurate results provided that the position spread remains small compared to a wavelength, $k\Delta x \ll 1$. This is fulfilled for operation near the cooling sideband, but not for $\Delta_\mathrm{c} = -\kappa$. Positive correlations of the particle

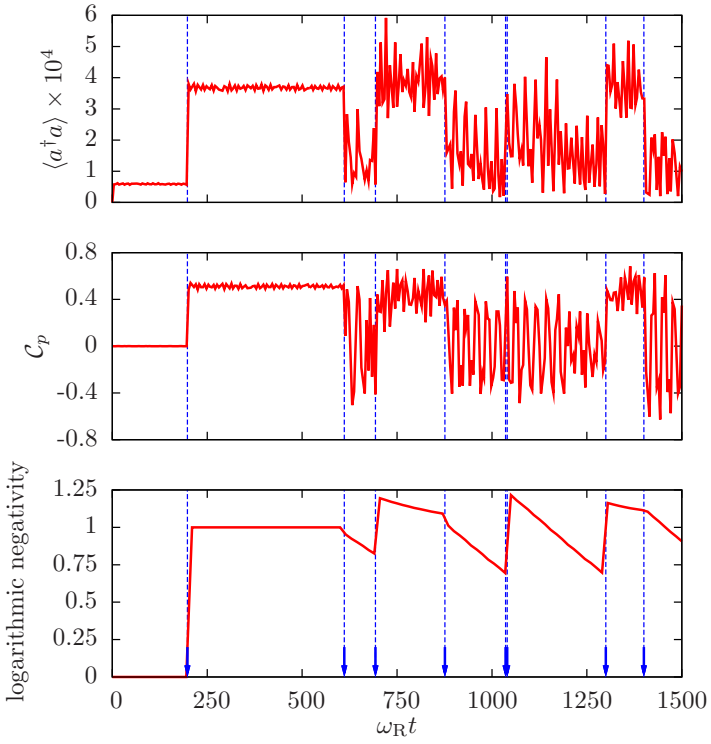

Figure 6.2: (Colour on-line) Photon number, momentum correlation and entanglement for a single trajectory. The dashed vertical lines indicate quantum jumps. Parameters: $\alpha_c = 150$, $U_0 = -\frac{1}{\alpha_c}\omega_R$, $\Delta_c = -\kappa$ and $\kappa = 10\omega_R$.

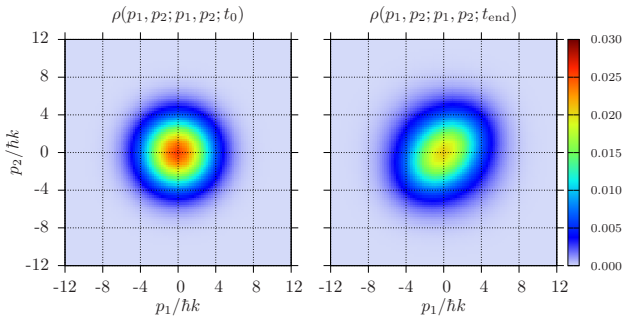

Figure 6.3: (Colour on-line) Diagonal elements of the two-particle reduced density matrix in momentum space, initially (left) and in steady state (right). Ensemble average of 5000 trajectories. Same parameters as in fig. 6.2.

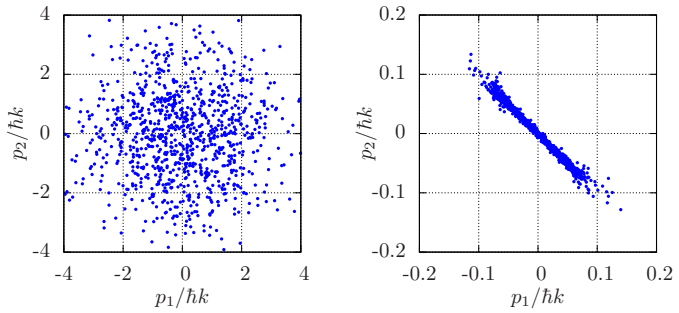

Figure 6.4: (Colour on-line) Classical simulations [6.20] for 1000 initial conditions. Left: Initial condition, right: Distribution at $\omega_{\mathrm{R}} t = 3000$. The particles become anti-correlated and cooled. Same parameters as in fig. 6.2.

motion can also be observed in much shallower potentials where the particles are barely trapped and both light modes are treated quantum-mechanically [6.30].

6.5 Heralded entanglement

In the dynamics correlations and entanglement are generated by quantum jumps induced by photon count events. Hence they are particularly strong immediately after a jump. In real experiments it is generally not possible to exactly keep track of each emitted photon due to the detector efficiency, i.e. one cannot exactly follow a certain quantum trajectory. Hence, the system always evolves into a mixed state and if a photon is observed (measured) outside of the resonator, it is impossible to determine whether it was the first, the second and so on. Naturally, the question arises whether effects observed on single trajectories (like entanglement) "survive" this averaging and can still be expected to be observable after jumps. Every time a photon is detected, the mixed state inside the resonator is projected into the state

$$\rho_{\mathrm{j}} := \frac{a\rho a^\dagger}{\mathrm{Tr}\,(a\rho a^\dagger)}, \tag{6.5}$$

where ρ is the density matrix evolved according to the master equation (6.2). Interestingly, the momentum correlation coefficient (6.4) is nearly constant ($\mathcal{C}_p \approx 0.5$ for $\Delta_{\mathrm{c}} = -\kappa$ and $\mathcal{C}_p \approx 0.3$ on the cooling sideband, respectively), regardless of the time the jump occurred at, see also fig. 6.6. The logarithmic negativity is smaller than on single trajectories, but still prominent with a value $\mathcal{E}_{\mathcal{N}} \sim 0.2$ for our parameters and a jump in steady state.

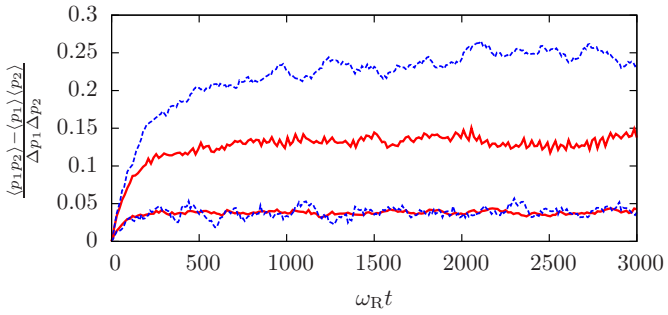

Figure 6.5: (Colour on-line) Red solid lines: Momentum correlation coefficient obtained from the master equation containing (6.1) for $\Delta_c = -\kappa$ (upper curve) and $\Delta_c = -\omega$ (lower curve). Blue dashed lines: Result of the oscillator approximation (6.3) (600 trajectories). The other parameters are the same as in fig. 6.2.

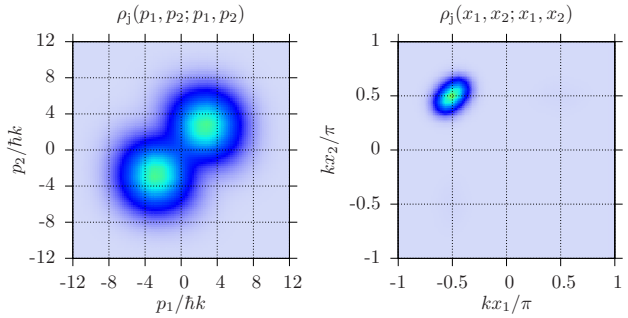

Figure 6.6: (Colour on-line) Diagonal elements of the reduced two-particle conditional density matrix (6.5) after a photon detection in steady state. Particle correlations as well as entanglement become much more pronounced compared to the density matrix shown in fig. 6.3. Same parameters and colour code as there.

The conditional density matrix (6.5) is closely related to the field autocorrelation function [6.21]

$$g^{(2)}(0) = \frac{\left\langle a^\dagger a^\dagger a a \right\rangle}{\langle a^\dagger a\rangle^2} \equiv \frac{\left\langle a^\dagger a \right\rangle_{\rho_j}}{\langle a^\dagger a\rangle_\rho}. \tag{6.6}$$

It has the very intuitive interpretation as the ratio between the photon number after and prior to a jump in steady state [6.31]. For our parameters it indicates photon bunching close to a thermal (chaotic) state (for which $g^{(2)}(0) = 2$). This is consistent with the picture of the mode being incoherently populated through particle noise—perfectly localised particles do not scatter. Hence the field expectation vanishes and only its variance gives a contribution.

6.6 Covariance matrix analysis for deep potentials

As we concentrate on deeply trapped particles we now make an approach widely used in the field of optomechanics. The Hamiltonian (6.3) is quadratic in the bosonic operators so that an initially Gaussian state remains Gaussian throughout the time evolution. Gaussian states are completely defined by a displacement vector and a covariance matrix $V_{ij} := \frac{1}{2}\left[\mathrm{Cov}(\xi_i, \xi_j) + \mathrm{Cov}(\xi_j, \xi_i)\right]$, with $\xi := (\tilde{x}_1, \tilde{p}_1, \tilde{x}_2, \tilde{p}_2, X, P)$, $\tilde{x}_i := x_i/\xi_0 = (b_i + b_i^\dagger)/\sqrt{2}$, $\tilde{p}_i := p_i\xi_0/\hbar = (b_i - b_i^\dagger)/(\mathrm{i}\sqrt{2})$ and the field quadratures X and P [6.32]. As shown in [6.9], the time evolution of V is determined by the equation (its steady-state version is called Lyapunov equation)

$$\dot{V}(t) = AV(t) + V(t)A^T + B, \tag{6.7}$$

where A and B are the drift- and diffusion matrices appearing in stochastic Heisenberg–Langevin equations equivalent to the master equation [6.9]. The steady-state solution of (6.7) for the covariances is $\mathrm{Cov}(\tilde{p}_1, \tilde{p}_2) = \mathrm{Var}(\tilde{p}_i) - 1/2$ and $\mathrm{Cov}(\tilde{x}_1, \tilde{x}_2) = \mathrm{Var}(\tilde{x}_i) - 1/2$ (both particles behave the same way). It only exists in the cooling regime $\Delta_\mathrm{c} < 0$ since the momentum variance is only positive for red detuning. The momentum covariance is also genuinely positive. For $\mathcal{C}_p$ we find the simple (g-independent) expression

$$\mathcal{C}_p = \frac{\kappa^2 + (\Delta_\mathrm{c} + \omega)^2}{\kappa^2 + (\Delta_\mathrm{c} - \omega)^2} > 0, \tag{6.8}$$

which is precisely the ratio of the Stokes- (Γ_-, heating) and anti-Stokes (Γ_+, cooling) scattering rates found when adiabatically eliminating the cavity field [6.9]. These rates $\Gamma_\pm = \frac{g^2\kappa}{\kappa^2 + (\Delta_\mathrm{c} \pm \omega)^2}$ also define the time scale $\tau \sim (\Gamma_+ - \Gamma_-)^{-1}$ on which the steady state is reached.

$\mathcal{C}_p$ has a minimum at $\Delta_\mathrm{c} = -\sqrt{\kappa^2 + \omega^2}$ and approaches unity for $|\Delta_\mathrm{c}| \to \infty$ and $\Delta_\mathrm{c} \to 0^-$. From the form of the steady-state covariance matrix we can deduce that steady-state entanglement between the particles can only occur if $\mathrm{Cov}(\tilde{x}_1, \tilde{x}_2) < 0$, which implies squeezing of the position variable. This is a direct consequence of the entanglement criterion derived in [6.33]. See fig. 6.7 for an example of the Lyapunov time evolution. For such deep potentials we restricted ourselves to Monte Carlo simulations of the master equation containing the Hamiltonian (6.3). Again, the C++QED framework provides a helpful basis for their numerical implementation as it also supports the simulation of coupled oscillators.

The steady-state covariance matrix reveals strong correlations between the particles and the field quadratures, making it intuitively clear that the reduced conditional density matrix for the particles strongly differs from its steady-state counterpart. Each photon detection highly influences the joint state of particles and cavity field. We show both density matrices in fig. 6.7. The logarithmic negativity for the

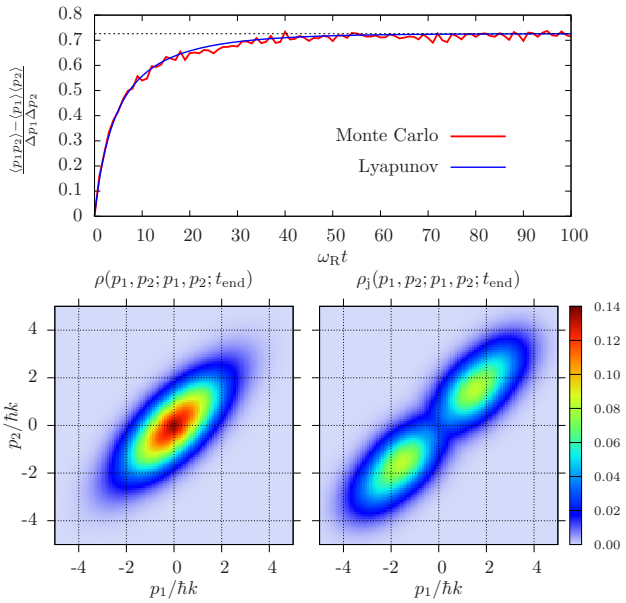

Figure 6.7: (Colour on-line) Upper plot: Momentum correlation obtained from Monte Carlo simulations in the Lamb–Dicke limit for $k\xi_0 = 0.1$ (red, ensemble of 500 trajectories) and solution of eq. (6.7) (blue). The position correlation is likewise pronounced. Lower plots: Diagonal elements of the reduced particle density matrix in steady state (left) and of the reduced conditional density matrix (6.5) (right). Parameters: $\omega = 200\omega_R$, $g = 5\omega_R$, $\kappa = 100\omega_R$ and $\Delta_c = -20\omega_R$.

conditional density matrix is $\mathcal{E}_{\mathcal{N}} \approx 0.25$ and $\mathcal{C}_p$ is found to be $\mathcal{C}_p \approx 0.9$. Due to the particles-field correlations in steady state the conditional density matrix (6.5) does not describe a Gaussian state. Indeed, it reveals a double-peak structure.

6.7 Transient entanglement

Quantum jumps project the states out of equilibria. Similar non-equilibrium dynamics can be studied by starting from a prescribed initial condition as e.g. an uncorrelated product state. We now move to investigate the transient regime, where light pulses can be used to generate build-up of motional correlations in the system. While we are free to explore any regime numerically, the problem can be analytically treated only in the adiabatic case where the cavity mode can be eliminated from the dynamics, i.e. when $g \ll \kappa$ or $g \ll |\Delta_c \pm \omega|$ [6.9]. We verify, however, that the optimal entanglement regime is indeed around the point analytically tackled. In this limit the tripartite system can be reduced to a quadrature-quadrature coupled mechanical bipartition that exhibits quantum-mechanical correlations and entanglement. We

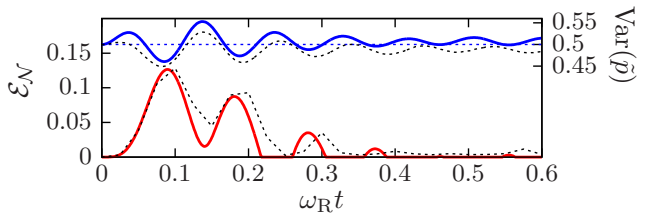

Figure 6.8: (Colour on-line) Transient entanglement (lower red curve) and momentum variance (upper blue curve) as obtained from the Lyapunov equation. Black dashed lines: Solution of the master equation for the ring resonator (2000 trajectories), for comparison. Parameters: $\omega = 30\omega_R$, $g = 5\omega_R$, $\kappa = 5\omega_R$ and $\Delta_c = -(\omega - \kappa)$.

skip the cumbersome adiabatic elimination process for brevity and only note, that the effective particle-particle interaction is determined by the parameter

$$\Upsilon = -\left(\frac{\Delta_c - \omega}{\kappa}\Gamma_- + \frac{\Delta_c + \omega}{\kappa}\Gamma_+\right). \tag{6.9}$$

One can see in fig. 6.8 an example of the time evolution of entanglement. Tailoring the cavity driving laser pulse to match the half-period of the particle-particle state swap process can then lead to a strongly entangled state.

6.8 Microscopic interpretation of dynamics and quantum jumps

Our effective optomechanical Hamiltonian (6.3) is formally similar to a model describing the microscopic dynamics of self-organisation of particles in a cavity field [6.34]. The behaviour of single trajectories there can be explained with the help of an adiabatic model. In this section we generalise that specific method to the master equation containing the quadratic Hamiltonian (6.3).

For a model in the spirit of [6.34] we diagonalise the scattering operator $\sum_i (b_i + b_i^\dagger)$ to obtain the new particle basis $\{|e_i\rangle\}$ containing bright (eigenvalue $\lambda_i \neq 0$, they always appear with both signs ± 1) and dark ($\lambda_i = 0$) states. Ignoring terms stemming from the oscillator energies for the moment, the bright states radiate a field $|\lambda_i \alpha\rangle$ with $\alpha := -ig/(\kappa - i\Delta_c)$. The crucial assumption now is adiabaticity (cavity decay assumed to define the fastest time scale), i.e. we assume each particle state $|e_i\rangle$ to be correlated with its associated unperturbed field state to find the approximated joint particle-field stochastic state vector

$$|\psi(t)\rangle = \sum_j c_j(t)\,|e_j\rangle\,|\lambda_j \alpha\rangle\,. \tag{6.10}$$

The coefficients $c_i(t)$ are determined by the effective conditional Monte Carlo time evolution generated by the non-Hermitian Hamiltonian (abbreviating $|i\rangle := |e_i\rangle$)

$$H_{\mathrm{nH}} := \hbar\omega \sum_{ij} \langle i| \sum_k b_k^\dagger b_k |j\rangle |i\rangle\langle j| - \mathrm{i}\hbar\kappa \sum_i |\lambda_i\alpha|^2 |i\rangle\langle i| \tag{6.11}$$

for the particles only. Its Hermitian part contains the oscillator energies expressed in the scattering basis and couples the constituents of the latter.

From the form of the state vector (6.10) one can conclude what happens if a photon is detected. Applying the jump operator $\propto a$ on the internal state (6.10) at time t_j yields $a|\psi(t_\mathrm{j})\rangle \propto \sum_i c_i(t_\mathrm{j})\lambda_i |e_i\rangle |\lambda_i\alpha\rangle$. Hence, all information about the dark contributions are erased and the relative phases between the bright states change sign (as for each λ_i there exists also an eigenvalue $-\lambda_i$). Since $|\lambda_i\alpha|^2 \ll 1$ the reduced density matrix for the particles directly after a jump mainly contains the pure state $|\psi_\mathrm{p}\rangle \propto \sum_j c_j(t)\lambda_j |e_j\rangle$ (during the time evolution the particle state reads $|\psi_\mathrm{p}\rangle \approx \sum_j c_j(t)|e_j\rangle$). Inserting the coefficients for a state describing two particles in the ground state, the first jump excites one of them and the photon number increases by a factor of three. The resulting particles state $|\psi_\mathrm{p}\rangle \approx \frac{1}{\sqrt{2}}(|\psi_0\psi_1\rangle + |\psi_1\psi_0\rangle)$ is entangled with $\mathcal{E}_\mathcal{N} = 1$ and correlated with $\mathcal{C}_p = 1/2$. Beginning with the second jump, fast oscillations with a frequency determined by ω build up, see fig. 6.9. The same qualitative behaviour can also be observed in the "full" trajectory shown in fig. 6.2, even though there are some important differences, e.g. the photon number after the first jump. They are due to the fact that the quadratic expansion (6.3) is not very accurate and that the adiabatic approximation is doubtful for the parameters employed there. It is also possible to generalise (6.11) to two wells by including a tunnelling rate, the latter giving rise to slow enveloping oscillations.

6.9 Conclusion and outlook

Starting from two particles in a ring resonator, our conclusions are quite general. We have proposed a tripartite optomechanical system with two identical oscillators that can be correlated via the mediation of a photon field and the interaction amplified by the cavity confinement. The Gaussian evolution of the reduced mechanical bipartition has been followed both numerically and analytically, while non-Gaussian effects owing to the deviation from the bilinear Hamiltonian have been investigated numerically. The non-intuitive and classically forbidden positive momentum correlations are a main result of the paper, and are interpreted as strong delocalisations (superpositions) of the centre-of-mass independent of the particle separation and thus of the extension of the effective system; this suggests possible use of the setup to test the quantum-classical boundary. Transient entanglement as shown here can also be exploited in a pulsed regime where light pulses can drive the mechanical bipartition into a strongly entangled state.

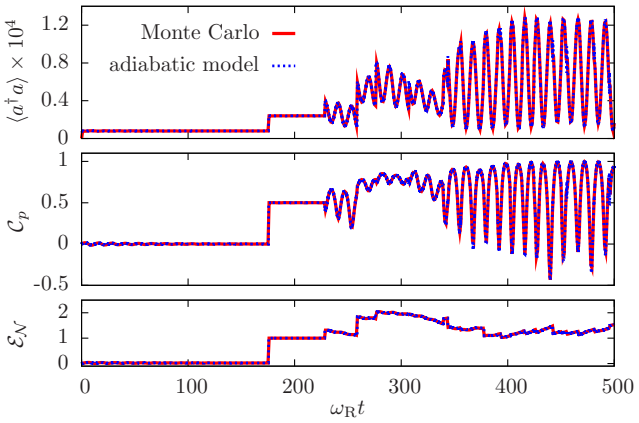

Figure 6.9: (Colour on-line) Comparison of a single Monte Carlo trajectory containing (6.3) (red) and its reconstruction with the model (6.11) (blue), both curves coincide. The parameters $\omega = 0.25\omega_\mathrm{R}$, $g = \omega_\mathrm{R}$, $\kappa = 500\omega_\mathrm{R}$ and $\Delta_\mathrm{c} = -10\omega_\mathrm{R}$ have been chosen for illustration purposes so that a resolution of the fast oscillations is possible.

Acknowledgments

This work has been supported by the Austrian Science Fund FWF through projects P20391 and F4013 and by the EU-ITN CCQED project. We would like to thank Cecilia Cormick, Tobias Grießer, Sebastian Krämer and András Vukics for helpful discussions and Hans Embacher for technical support.

Chapter 7

Additional material

In this chapter we provide some additional calculations to the preceding publication (chapter 6). We present the adiabatic elimination of the field using the projection technique. This elimination leads to an effective master equation for the particles, containing the Stokes and anti-Stokes sidebands as heating and cooling channels. This way more insight into the physical processes involved in the dynamics is provided. Afterwards, we summarise a general recipe on how to transform a quadratic master equation into an equation for the covariance matrix, which is very helpful for the computation of the time evolution of Gaussian states. Finally, we briefly review some entanglement criteria and—for comparison—the "full" solution without adiabatic elimination of the field.

7.1 Adiabatic elimination of the field

In the publication we consider the master equation

$$\dot{\rho} = \frac{1}{i\hbar}\left[H, \rho\right] + \mathcal{L}\rho \tag{7.1}$$

containing the quadratic Hamiltonian

$$H = \sum_i \hbar\omega b_i^\dagger b_i - \hbar\Delta_\mathrm{c} a^\dagger a + \hbar g \sum_i (b_i + b_i^\dagger)(a + a^\dagger) \tag{7.2}$$

and the Liouvillean

$$\mathcal{L}\rho = \kappa\left(2a\rho a^\dagger - a^\dagger a\rho - \rho a^\dagger a\right). \tag{7.3}$$

Assuming, that the field evolution defines the fastest time scale, $g \ll \kappa$ or $g \ll |\Delta_\mathrm{c} \pm \omega|$, the field may be adiabatically eliminated from the dynamics. We perform this adiabatic elimination with the projection technique and very closely follow the line of [7.1, 7.2]. As for every adiabatic elimination process, the crucial assumption is a separation of time scales.

It is convenient for the following calculations to consider the master equation (7.1) in an interaction picture with respect to the free evolution

$$H_0 = \sum_i \hbar\omega b_i^\dagger b_i - \hbar\Delta_\mathrm{c} a^\dagger a. \tag{7.4}$$

To this end we apply the unitary transformation

$$U(t) = \exp\left[-i\left(\omega \sum_j b_j^\dagger b_j - \Delta_\mathrm{c} a^\dagger a\right) t\right] \tag{7.5}$$

on the Hamiltonian (7.2) to obtain its representation

$$H_\mathrm{int}(t) = U^{-1}(t) H U(t) - i\hbar U^{-1}(t) \frac{\partial U(t)}{\partial t} \tag{7.6}$$

in the interaction picture. Explicitly, this time-dependent Hamilton operator reads

$$H_\mathrm{int}(t) = \hbar g \sum_j \left(b_j e^{-i\omega t} + b_j^\dagger e^{i\omega t}\right)\left(a e^{i\Delta_\mathrm{c} t} + a^\dagger e^{-i\Delta_\mathrm{c} t}\right). \tag{7.7}$$

Let us remark that the following derivation is very similar to the derivation of the general master equation presented in section 2.2.2. There we have considered a small system, e.g. an experimental setup, interacting with a large surrounding heat bath. Here, the resonator mode corresponds to this bath.

The master equation for the joint particles-field density matrix ρ_tot reads

$$\dot{\rho}_\mathrm{tot} = \frac{1}{i\hbar}\left[H_\mathrm{int}(t), \rho_\mathrm{tot}\right] + \mathcal{L}\rho_\mathrm{tot}. \tag{7.8}$$

The aforementioned separation of time scales allows for the approximation

$$\rho_\mathrm{tot} \simeq \rho_\mathrm{c}^0 \otimes \rho \tag{7.9}$$

for times $t > |\Delta|^{-1}$. The appearing reduced density matrix $\rho := \mathrm{Tr}_\mathrm{c}(\rho_\mathrm{tot})$ is for the particles only and $\rho_\mathrm{c}^0 = |0\rangle\langle 0|$ is the steady state of the shifted resonator modes [7.1]. The effective master equation for the particles after the adiabatic elimination of the field has the generic form

$$\dot{\rho} = \mathcal{L}_\mathrm{ad}\rho, \tag{7.10}$$

where the Liouvillean is found to be [7.1]

$$\mathcal{L}_\mathrm{ad}\rho = -\frac{1}{\hbar^2}\int_0^\infty \mathrm{d}\tau\, \mathrm{Tr}_\mathrm{c}\left(\left[H_\mathrm{int}(t), e^{\mathcal{L}\tau}\left[H_\mathrm{int}(t-\tau), \rho_\mathrm{c}^0 \otimes \rho\right]\right]\right) \tag{7.11}$$

in second order perturbation theory (cf. also section 2.2.2). Defining the abbreviations

$G(t) := \sum_j \left(b_j e^{-i\omega t} + b_j^\dagger e^{i\omega t}\right)$ and $F(t) := a e^{i\Delta_c t} + a^\dagger e^{-i\Delta_c t}$, the partial trace is

$$\begin{aligned}
&- \mathrm{Tr_c}\left(\left[H_{\mathrm{int}}(t), e^{\mathcal{L}\tau}\left[H_{\mathrm{int}}(t-\tau), \rho_c^0 \otimes \rho\right]\right]\right) = \\
&\quad = -g^2 \,\mathrm{Tr_c}\left(\left[G(t)F(t), e^{\mathcal{L}\tau}\left[G(t-\tau)F(t-\tau), \rho_c^0 \otimes \rho\right]\right]\right) = \\
&\quad = -g^2 \,\mathrm{Tr_c}\left(G(t)F(t)e^{\mathcal{L}\tau}G(t-\tau)F(t-\tau)\rho_c^0 \otimes \rho\right) + \\
&\qquad + g^2 \,\mathrm{Tr_c}\left(G(t)F(t)e^{\mathcal{L}\tau}\rho_c^0 \otimes \rho G(t-\tau)F(t-\tau)\right) + \\
&\qquad + g^2 \,\mathrm{Tr_c}\left(e^{\mathcal{L}\tau}G(t-\tau)F(t-\tau)G(t)F(t)\rho_c^0 \otimes \rho\right) - \\
&\qquad - g^2 \,\mathrm{Tr_c}\left(e^{\mathcal{L}\tau}\rho_c^0 \otimes \rho G(t-\tau)F(t-\tau)G(t)F(t)\right).
\end{aligned} \tag{7.12}$$

Finally, we find

$$\begin{aligned}
&- \mathrm{Tr_c}\left(\left[H_{\mathrm{int}}(t), e^{\mathcal{L}\tau}\left[H_{\mathrm{int}}(t-\tau), \rho_c^0 \otimes \rho\right]\right]\right) = \\
&\qquad = e^{-(\kappa+i\Delta_c)\tau}\left[G(t), \rho G(t-\tau)\right] + e^{-(\kappa-i\Delta_c)\tau}\left[G(t-\tau)\rho, G(t)\right],
\end{aligned} \tag{7.13}$$

where we used that only terms of the form $\mathrm{Tr_c}(aa^\dagger\rho_c^0)$ give a contribution. Hence, the Liouvillean (7.11) reads

$$\begin{aligned}
\mathcal{L}_{\mathrm{ad}}\rho = g^2 \sum_{jk} \int_0^\infty \mathrm{d}\tau e^{-(\kappa+i\Delta_c)\tau} \times \\
\times \left[b_k e^{-i\omega t} + b_k^\dagger e^{i\omega t}, \rho\left(b_j e^{-i\omega(t-\tau)} + b_j^\dagger e^{i\omega(t-\tau)}\right)\right] + \mathrm{H.c.}
\end{aligned} \tag{7.14}$$

Evaluation of the integral yields

$$\mathcal{L}_{\mathrm{ad}}\rho = g^2 \sum_{jk}\left[b_k e^{-i\omega t} + b_k^\dagger e^{i\omega t}, \rho\left(\frac{b_j e^{-i\omega t}}{\kappa + i(\Delta_c - \omega)} + \frac{b_j^\dagger e^{i\omega t}}{\kappa + i(\Delta_c + \omega)}\right)\right] + \mathrm{H.c.} \tag{7.15}$$

Upon a transformation back into the original frame, this equation reads

$$\begin{aligned}
\mathcal{L}_{\mathrm{ad}}\rho &= \hbar \sum_{jk}\left[b_k + b_k^\dagger, \rho\left(u_- b_j + u_+ b_j^\dagger\right)\right] + \mathrm{H.c.} = \\
&= \hbar \sum_{jk}\left\{\left(b_k + b_k^\dagger\right)\rho\left(u_- b_j + u_+ b_j^\dagger\right) - \rho\left(u_- b_j + u_+ b_j^\dagger\right)\left(b_k + b_k^\dagger\right)\right\} + \mathrm{H.c.},
\end{aligned} \tag{7.16}$$

with the abbreviations

$$u_\pm := \frac{g^2}{\kappa + i(\Delta_c \pm \omega)} \equiv \frac{g^2\kappa - ig^2(\Delta_c \pm \omega)}{\kappa^2 + (\Delta_c \pm \omega)^2}. \tag{7.17}$$

This equation should be equivalent to an effective master equation (cf. equation (7.10))

$$\dot{\rho} = \mathcal{L}_{\mathrm{ad}}\rho = \frac{1}{i\hbar}\left[H_{\mathrm{eff}}, \rho\right] + \mathcal{L}_{\mathrm{eff}}\rho. \tag{7.18}$$

To find the corresponding effective Hamiltonian and Liouvillean we make use of the identity [7.1]

$$-\left(\rho A + \mathrm{H.c.}\right) = \frac{1}{i}\left[\frac{i}{2}\left(A - A^\dagger\right), \rho\right] - \left\{\frac{1}{2}\left(A + A^\dagger\right), \rho\right\}_+. \tag{7.19}$$

Inserting $A = \left(u_- b_j + u_+ b_j^\dagger\right)\left(b_k + b_k^\dagger\right)$ we find the effective Hamiltonian (adding the free evolution)

$$H_{\mathrm{eff}} = \sum_k \hbar\omega b_k^\dagger b_k + \sum_{jk} \frac{i\hbar}{2}\left[\left(u_- b_j + u_+ b_j^\dagger\right)\left(b_k + b_k^\dagger\right) - \left(b_k + b_k^\dagger\right)\left(u_-^* b_j^\dagger + u_+^* b_j\right)\right] \tag{7.20}$$

and the effective Liouvillean

$$\begin{aligned}\mathcal{L}_{\mathrm{eff}}\rho = &\sum_{jk}\frac{1}{2}\left[2\left(b_k + b_k^\dagger\right)\rho\left(u_- b_j + u_+ b_j^\dagger\right) - \left\{\left(u_- b_j + u_+ b_j^\dagger\right)\left(b_k + b_k^\dagger\right), \rho\right\}_+\right] + \\ &+ \sum_{jk}\frac{1}{2}\left[2\left(u_-^* b_j^\dagger + u_+^* b_j\right)\rho\left(b_k + b_k^\dagger\right) - \left\{\left(b_k + b_k^\dagger\right)\left(u_-^* b_j^\dagger + u_+^* b_j\right), \rho\right\}_+\right].\end{aligned} \tag{7.21}$$

In rotating-wave approximation (for $\omega \gg \Gamma_\pm$ [7.1], cf. also sections 2.1 and 3.3) the latter may be written as a sum of two correlated decay channels,

$$\mathcal{L}_{\mathrm{eff}}\rho = \Gamma_+ \mathcal{D}\left[\sum_i b_i\right](\rho) + \Gamma_- \mathcal{D}\left[\sum_i b_i^\dagger\right](\rho) \tag{7.22}$$

with $\mathcal{D}[A](\rho) := 2A\rho A^\dagger - A^\dagger A\rho - \rho A^\dagger A$. The effective rates for correlated decay (anti-Stokes) and heating (Stokes) are given by

$$\Gamma_\pm := \mathrm{Re}(u_\pm) = \frac{g^2\kappa}{\kappa^2 + (\Delta_\mathrm{c} \pm \omega)^2}. \tag{7.23}$$

Defining

$$\Gamma_+ =: \gamma(\bar{n} + 1) \quad \text{and} \quad \Gamma_- =: \gamma\bar{n} \tag{7.24}$$

one finds

$$\gamma = \Gamma_+ - \Gamma_- \quad \text{and} \quad \bar{n} = \frac{1}{2}\left(\frac{\Gamma_+ + \Gamma_-}{\Gamma_+ - \Gamma_-} - 1\right). \tag{7.25}$$

For $\Delta_\mathrm{c} < 0$ cooling is stronger than heating, $\Gamma_+ - \Gamma_- > 0$. We will therefore restrict ourselves to this parameter regime.

7.2 Lyapunov equation

The master equation (7.1) is equivalent to stochastic Heisenberg–Langevin equations (see also sections 2.2.1 and 2.2.2). For quadratic Hamiltonians these stochastic equations are fully determined by a drift- and a diffusion matrix. These matrices can easily be found [7.1] from the generic master equation

$$\dot{\rho} = \frac{1}{i\hbar}\left[\boldsymbol{\xi}^T M \boldsymbol{\xi}, \rho\right] + \sum_i \Gamma_i \mathcal{D}\left[L_i^T \boldsymbol{\xi}\right](\rho) \tag{7.26}$$

as

$$A = 2\sigma[M + \mathrm{Im}(\Gamma)] \quad \text{and} \quad B = 2\sigma\,\mathrm{Re}(\Gamma)\sigma^T, \tag{7.27}$$

with

$$\Gamma_{mn} := \sum_i \Gamma_i L_{i,m}^* L_{i,n} \tag{7.28}$$

and $\boldsymbol{\xi} := (x_1, p_1, \ldots, x_n, p_n)^T$. Furthermore, $\sigma := \bigoplus_i J$, with J being the symplectic matrix $J := \left(\begin{smallmatrix} 0 & 1 \\ -1 & 0 \end{smallmatrix}\right)$. Note that the position and momentum operators have to be provided in their dimensionless form (quadratures) such that their general commutator adopts the form $[\xi_j, \xi_k] = i\sigma_{jk}$.

Quadratic Hamilton operators as in equation (7.26) preserve the Gaussian nature of an initially Gaussian state. In this context, Gaussian states are states with a Gaussian-shaped Wigner function [7.3]. We skip a discussion of the latter at this point and rather refer to section 8.1, where we will re-encounter the Wigner function in a somewhat more general context. Gaussian states include a variety of important states, notably coherent-, squeezed- and thermal states [7.3]. The striking feature of Gaussian states is, that they are fully determined by the covariance matrix

$$V_{ij} := \frac{1}{2}\left[\mathrm{Cov}(\xi_i, \xi_j) + \mathrm{Cov}(\xi_j, \xi_i)\right] \tag{7.29}$$

and a displacement vector $\mathbf{d} = \langle \boldsymbol{\xi} \rangle$ [7.3]. All higher moments of a Gaussian state can be expressed through these quantities. It is therefore unnecessary to integrate the full master equation for Gaussian initial conditions. Rather, the former can be reduced to two ordinary differential equation systems for the covariance matrix and the displacement vector.

According to reference [7.1] the time evolution of the displacement vector determined by the master equation (7.26) is given by

$$\frac{\mathrm{d}}{\mathrm{d}t}\mathbf{d}(t) = A\mathbf{d}(t). \tag{7.30}$$

The corresponding equation for the covariance matrix is [7.1]

$$\frac{\mathrm{d}}{\mathrm{d}t}V = AV(t) + V(t)A^T + B. \tag{7.31}$$

The steady-state version of this equation is called Lyapunov equation in literature. We will, however, also refer to equation (7.31) as (time-dependent) Lyapunov equation for convenience.

The drift and diffusion matrices corresponding to the master equation (7.18) containing the effective Hamiltonian (7.20) and Liouvillean (7.22) explicitly read

$$A = \begin{pmatrix} 0 & \omega & 0 & 0 \\ 2\Upsilon - \omega & -2\gamma & 2\Upsilon & -2\gamma \\ 0 & 0 & 0 & \omega \\ 2\Upsilon & -2\gamma & 2\Upsilon - \omega & -2\gamma \end{pmatrix} \tag{7.32a}$$

and

$$B = \begin{pmatrix} \Gamma_+ + \Gamma_- & 0 & \Gamma_+ + \Gamma_- & 0 \\ 0 & \Gamma_+ + \Gamma_- & 0 & \Gamma_+ + \Gamma_- \\ \Gamma_+ + \Gamma_- & 0 & \Gamma_+ + \Gamma_- & 0 \\ 0 & \Gamma_+ + \Gamma_- & 0 & \Gamma_+ + \Gamma_- \end{pmatrix}, \tag{7.32b}$$

where we have defined $\gamma := \Gamma_+ - \Gamma_-$ and

$$\Upsilon := -\left(\frac{\Delta_\mathrm{c} - \omega}{\kappa} \Gamma_- + \frac{\Delta_\mathrm{c} + \omega}{\kappa} \Gamma_+ \right). \tag{7.33}$$

These matrices are equivalent to

$$A = \begin{pmatrix} \gamma & \omega & \gamma & 0 \\ 2\Upsilon - \omega & -\gamma & 2\Upsilon & -\gamma \\ \gamma & 0 & \gamma & \omega \\ 2\Upsilon & -\gamma & 2\Upsilon - \omega & -\gamma \end{pmatrix} - \gamma \begin{pmatrix} 1 & 0 & 1 & 0 \\ 0 & 1 & 0 & 1 \\ 1 & 0 & 1 & 0 \\ 0 & 1 & 0 & 1 \end{pmatrix} \tag{7.34a}$$

and

$$B = \gamma(2\bar{n} + 1) \begin{pmatrix} 1 & 0 & 1 & 0 \\ 0 & 1 & 0 & 1 \\ 1 & 0 & 1 & 0 \\ 0 & 1 & 0 & 1 \end{pmatrix} \tag{7.34b}$$

with $\bar{n}$ defined in equation (7.25).

The Lyapunov equation can easily be integrated numerically to obtain $V(t)$. In order to find the steady-state covariance matrix fulfilling $AV + VA^T = -B$ analytically, one has to be a little bit careful. As the mechanical oscillators do not decay, two eigenvalues of the drift matrix have zero real part and thus give rise to undamped solutions and hence hinder finding the steady-state solution directly. We circumvent this problem by introducing some Brownian noise to the particle momenta and by taking the limit of zero additional noise afterwards. We have checked numerically that the so-found steady state solution agrees with the numerical

time-integrated solution. Because Brownian noise cannot be formulated in Lindblad form [7.2] we manually add it to the drift and diffusion matrices (7.32) as

$$A \mapsto A + \begin{pmatrix} 0 & 0 & 0 & 0 \\ 0 & -\gamma_\mathrm{B} & 0 & 0 \\ 0 & 0 & 0 & 0 \\ 0 & 0 & 0 & -\gamma_\mathrm{B} \end{pmatrix} \quad \text{and} \quad B \mapsto B + \begin{pmatrix} 0 & 0 & 0 & 0 \\ 0 & \gamma_\mathrm{B} & 0 & 0 \\ 0 & 0 & 0 & 0 \\ 0 & 0 & 0 & \gamma_\mathrm{B} \end{pmatrix}. \tag{7.35}$$

The steady-state covariance matrix then reads

$$\lim_{\gamma_\mathrm{B}\to 0} V = \begin{pmatrix} a & c & a-\frac{1}{2} & c \\ c & b & c & b-\frac{1}{2} \\ a-\frac{1}{2} & c & a & c \\ c & b-\frac{1}{2} & c & b \end{pmatrix} \tag{7.36}$$

with

$$a := \frac{4(\Gamma_+ - \Gamma_-)^2(\Gamma_+ + \Gamma_-) - (3\Gamma_+ - \Gamma_-)\Upsilon\omega + \Gamma_+\omega^2}{-2(\Gamma_+ - \Gamma_-)(4\Upsilon - \omega)\omega} \tag{7.37a}$$

$$b := \frac{\Upsilon(\Gamma_+ + \Gamma_-) - \omega\Gamma_+}{-2\omega(\Gamma_+ - \Gamma_-)} \tag{7.37b}$$

$$c := -\frac{\Gamma_+ + \Gamma_-}{2\omega}. \tag{7.37c}$$

The momentum correlation coefficient (6.4) is found to be

$$\mathcal{C}_p = \frac{(\Gamma_+ + \Gamma_-)\Upsilon - \Gamma_-\omega}{(\Gamma_+ + \Gamma_-)\Upsilon - \Gamma_+\omega}. \tag{7.38}$$

The position and momentum correlations are positive for $a, b \geq 1/2$, i.e. for all non-squeezed states. If either x or p are squeezed the corresponding correlation becomes negative. The momentum correlation coefficient (7.38) has a minimum at $\Delta_\mathrm{c} = -\kappa$ and approaches unity for $\Delta_\mathrm{c} \to -\infty$.

7.3 Entanglement criteria for Gaussian states

Here we just briefly summarise two important theorems concerning the entanglement of bipartite Gaussian states. For their respective proofs we refer to the original publications.

A necessary and sufficient criterion for inseparability of a bipartite Gaussian state is violation of the inequality [7.4]

$$\det A \det B + \left(\frac{1}{4} - |\det C|\right)^2 - \mathrm{Tr}\left(AJCJBJC^TJ\right) \geq \frac{1}{4}\left(\det A + \det B\right), \tag{7.39}$$

where the covariance matrix has been written in the block form $V := \left(\begin{smallmatrix} A & C \\ C^T & B \end{smallmatrix}\right)$.

The logarithmic negativity [7.5] of a bipartite Gaussian state can easily be computed from its covariance matrix (7.29). To this end we need to calculate the symplectic eigenvalues c_i of V^{T_B}. They can easily be obtained from the eigenvalues $\pm i c_i$ of $\Omega^{-1}\Lambda V \Lambda$, with the mirror reflection matrix $\Lambda := \mathrm{diag}(1,1,1,-1)$ and $\Omega := J \oplus J$, with J being the symplectic matrix $J := \left(\begin{smallmatrix} 0 & 1 \\ -1 & 0 \end{smallmatrix}\right)$. The logarithmic negativity is then $\mathcal{E}_{\mathcal{N}} = F(c_1) + F(c_2)$ with F defined as [7.5]

$$F(c) = \begin{cases} 0 & c \geq \frac{1}{2} \\ -\log_2(2c) & c < \frac{1}{2} \end{cases}. \tag{7.40}$$

7.4 Steady-state solution without adiabatic elimination

The procedure of section 7.2 can of course also be applied to the joint particles-field system (7.1) without adiabatically eliminating the cavity field. In this case the full drift and diffusion matrices defined in equation (7.27) read

$$A = \begin{pmatrix} 0 & \omega & 0 & 0 & 0 & 0 \\ -\omega & -\gamma_{\mathrm{B}} & 0 & 0 & -2g & 0 \\ 0 & 0 & 0 & \omega & 0 & 0 \\ 0 & 0 & -\omega & -\gamma_{\mathrm{B}} & -2g & 0 \\ 0 & 0 & 0 & 0 & -\kappa & -\Delta_{\mathrm{c}} \\ -2g & 0 & -2g & 0 & \Delta_{\mathrm{c}} & -\kappa \end{pmatrix} \tag{7.41}$$

and

$$B = \begin{pmatrix} 0 & 0 & 0 & 0 & 0 & 0 \\ 0 & \gamma_{\mathrm{B}} & 0 & 0 & 0 & 0 \\ 0 & 0 & 0 & 0 & 0 & 0 \\ 0 & 0 & 0 & \gamma_{\mathrm{B}} & 0 & 0 \\ 0 & 0 & 0 & 0 & \kappa & 0 \\ 0 & 0 & 0 & 0 & 0 & \kappa \end{pmatrix}. \tag{7.42}$$

Using the same method (addition of Brownian noise) as in section 7.2, the steady-state covariance matrix is found to be

$$\lim_{\gamma_{\mathrm{B}} \to 0} V = \begin{pmatrix} a & 0 & a - \frac{1}{2} & 0 & c & -\frac{\kappa}{\Delta_{\mathrm{c}}} c \\ 0 & b & 0 & b - \frac{1}{2} & 0 & -\frac{g}{2\Delta_{\mathrm{c}}} \\ a - \frac{1}{2} & 0 & a & 0 & c & -\frac{\kappa}{\Delta_{\mathrm{c}}} c \\ 0 & b - \frac{1}{2} & 0 & b & 0 & -\frac{g}{2\Delta_{\mathrm{c}}} \\ c & 0 & c & 0 & d & f \\ -\frac{\kappa}{\Delta_{\mathrm{c}}} c & -\frac{g}{2\Delta_{\mathrm{c}}} & -\frac{\kappa}{\Delta_{\mathrm{c}}} c & -\frac{g}{2\Delta_{\mathrm{c}}} & f & e \end{pmatrix} \tag{7.43}$$

with

$$a := \frac{8g^2\Delta_\mathrm{c}(2\Delta_\mathrm{c}-\omega)-(\kappa^2+\Delta_\mathrm{c}^2)(\kappa^2+(\Delta_\mathrm{c}-\omega)^2)}{8\Delta_\mathrm{c}(8g^2\Delta_\mathrm{c}+(\kappa^2+\Delta_\mathrm{c}^2)\omega)} \tag{7.44a}$$

$$b := -\frac{\kappa^2+(\Delta_\mathrm{c}-\omega)^2}{8\Delta_\mathrm{c}\omega} \tag{7.44b}$$

$$c := -\frac{g}{2}\frac{\kappa^2+\Delta_\mathrm{c}^2}{8g^2\Delta_\mathrm{c}+(\kappa^2+\Delta_\mathrm{c}^2)\omega} \tag{7.44c}$$

$$d := \frac{4g^2\Delta_\mathrm{c}+(\kappa^2+\Delta_\mathrm{c}^2)\omega}{2(8g^2\Delta_\mathrm{c}+(\kappa^2+\Delta_\mathrm{c}^2)\omega)} \tag{7.44d}$$

$$e := \frac{g^2(8\Delta_\mathrm{c}^2-4\kappa^2)+\Delta_\mathrm{c}(\kappa^2+\Delta_\mathrm{c}^2)\omega}{2\Delta_\mathrm{c}(8g^2\Delta_\mathrm{c}+(\kappa^2+\Delta_\mathrm{c}^2)\omega)} \tag{7.44e}$$

$$f := \frac{2g^2\kappa}{8g^2\Delta_\mathrm{c}+(\kappa^2+\Delta_\mathrm{c}^2)\omega}. \tag{7.44f}$$

This steady-state solution describes a physical state in the cooling regime ($\Delta_\mathrm{c} < 0$) only, in the opposite case of positive detuning the momentum variance would become negative. The steady-state momentum covariance explicitly reads

$$\mathrm{Cov}(p_1,p_2) = \mathrm{Var}(p_i) - \frac{1}{2} = -\frac{\kappa^2+(\Delta_\mathrm{c}+\omega)^2}{8\Delta_\mathrm{c}\omega} \tag{7.45}$$

and is thus also genuinely positive. The momentum correlation coefficient adopts the particularly simple form

$$\mathcal{C}_p = 1 + \frac{4\Delta_\mathrm{c}\omega}{\kappa^2+(\Delta_\mathrm{c}-\omega)^2} = \frac{\kappa^2+(\Delta_\mathrm{c}+\omega)^2}{\kappa^2+(\Delta_\mathrm{c}-\omega)^2} \equiv \frac{\Gamma_-}{\Gamma_+}. \tag{7.46}$$

Note that this coefficient is independent of the coupling strength g, but of course it is zero if the coupling is set to zero from the beginning.

Due to the positiveness of the momentum covariance, entanglement between the particles can only occur if $\mathrm{Cov}(x_1,x_2) < 0$ and thus for a squeezed state in the position variable (as a negative position covariance implies $\mathrm{Var}(x_i) < 1/2$). This is a direct consequence of the separability criterion (7.39). The state described by the covariance matrix (7.43) is always separable for positive position correlations. An entangled state might exist if the latter become negative.

We conclude this chapter by noting that within the adiabatic elimination the cross-covariances $\mathrm{Cov}(x_i,p_j)$ do not vanish in steady state as in the full model. However, the rotating-wave approximation in the effective Liouvillean is only valid for $\omega \gg \Gamma_\pm$ [7.1], hence these terms are very small.

Part III

Self-organisation of cold particles in optical resonators

Chapter 8

Background to self-organisation

In this chapter we review the semiclassical approximation used in the remainder of this thesis and present a short introduction into particle self-organisation in optical cavities.

The principal idea of the semiclassical theory is to convert the complicated and high-dimensional master equation for the density matrix into a partial differential equation (PDE) for an equivalent c-number quasi-probability distribution, in our case this will be the Wigner function. Upon an approximation this PDE can be transformed into a Fokker–Planck equation (FPE), which itself can be transformed into a system of stochastic differential equations (SDEs). These SDEs can efficiently be numerically integrated in parallel on a high performance computing cluster.

8.1 Wigner function, Fokker–Planck equation and stochastic differential equations

Historically, there were many attempts to introduce a classical phase-space probability density distribution into quantum mechanics. The first goes back to 1932, when E. Wigner proposed the function (provided here in its one-dimensional version) [8.1]

$$W(x,p) = \frac{1}{2\pi\hbar}\int_{-\infty}^{\infty} \mathrm{d}\xi\, \exp\left(-\frac{i}{\hbar}p\xi\right)\left\langle x+\frac{1}{2}\xi\middle|\rho\middle|x-\frac{1}{2}\xi\right\rangle, \tag{8.1}$$

which is nowadays known as Wigner function. It fulfils some desired requirements of a genuine probability distribution, notably its marginal distributions for position or momentum, i.e. $W(x)$ and $W(p)$, are obtained by integrating (8.1) with respect to the other variable. However, there is one important property which forbids its probability density interpretation—it can become negative. As an example, the Wigner function of Fock states (except the vacuum state) adopts negative values. For this reason the Wigner function is called a *quasi-probability distribution function*.

The time-evolution equation for the Wigner function can be obtained from its definition (8.1). As an important example, consider the von Neumann equation

$$\dot{\rho} = \frac{1}{i\hbar}\,[H,\rho] \tag{8.2}$$

with the Hamiltonian

$$H = \frac{p^2}{2m} + V(x) \tag{8.3}$$

describing a single particle moving in some potential. It translates into the partial differential equation [8.2]

$$\left(\frac{\partial}{\partial t} + \frac{p}{m}\frac{\partial}{\partial x} - \frac{\mathrm{d}V(x)}{\mathrm{d}x}\frac{\partial}{\partial p}\right) W(x,p,t) = \\ = \sum_{l=1}^{\infty} \frac{(-1)^l(\hbar/2)^{2l}}{(2l+1)!}\frac{\mathrm{d}^{2l+1}V(x)}{\mathrm{d}x^{2l+1}}\frac{\partial^{2l+1}}{\partial p^{2l+1}}W(x,p,t) \tag{8.4}$$

containing all derivatives of the potential. If, however, the potential is at most harmonic, the classical Liouville equation

$$\left(\frac{\partial}{\partial t} + \frac{p}{m}\frac{\partial}{\partial x} - \frac{\mathrm{d}V(x)}{\mathrm{d}x}\frac{\partial}{\partial p}\right) W(x,p,t) = 0 \tag{8.5}$$

is recovered. PDEs containing higher order derivatives than second cannot be transformed into a set of corresponding stochastic differential equations and therefore lack the classical probability density interpretation. Another possible problem arises in systems for which the PDE is a Fokker–Planck equation (i.e. containing only second order derivatives)—but with negative diffusion matrix, leading to the very same interpretation problems as discussed above. In such situations one may consider different quasi-probability distribution functions, e.g. the Glauber–Sudarshan P-distribution or the Husimi–Kano Q-distribution [8.2]. However, for our systems considered here the Wigner function formalism is still very suited.

How does one transform an arbitrary master equation, possibly containing a Liouvillean superoperator, into an equation for the Wigner function? As shown in [8.3] one can derive so-called operator correspondences for this purpose,

$$x\rho \mapsto \left(x + \frac{i\hbar}{2}\frac{\partial}{\partial p}\right) W(x,p), \qquad \rho x \mapsto \left(x - \frac{i\hbar}{2}\frac{\partial}{\partial p}\right) W(x,p), \tag{8.6a}$$

$$p\rho \mapsto \left(p - \frac{i\hbar}{2}\frac{\partial}{\partial x}\right) W(x,p), \qquad \rho p \mapsto \left(p + \frac{i\hbar}{2}\frac{\partial}{\partial x}\right) W(x,p), \tag{8.6b}$$

$$a\rho \mapsto \left(\alpha + \frac{1}{2}\frac{\partial}{\partial \alpha^*}\right) W(x,p), \qquad \rho a \mapsto \left(\alpha - \frac{1}{2}\frac{\partial}{\partial \alpha^*}\right) W(x,p), \tag{8.6c}$$

$$a^\dagger\rho \mapsto \left(\alpha^* - \frac{1}{2}\frac{\partial}{\partial \alpha}\right) W(x,p), \qquad \rho a^\dagger \mapsto \left(\alpha^* + \frac{1}{2}\frac{\partial}{\partial \alpha}\right) W(x,p). \tag{8.6d}$$

We conclude this section with the recipe on how to transform a general Fokker–Planck equation into a set of stochastic differential equations. A general FPE has

the generic form

$$\frac{\partial}{\partial t}F(\mathbf{x},t) = -\sum_{i=1}^{N}\frac{\partial}{\partial x_i}\Big[A_i(\mathbf{x},t)F(\mathbf{x},t)\Big] + \frac{1}{2}\sum_{i,j=1}^{N}\frac{\partial^2}{\partial x_i \partial x_j}\Big[B_{ij}(\mathbf{x},t)F(\mathbf{x},t)\Big], \quad (8.7)$$

with the drift vector $\mathbf{A}(\mathbf{x},t)$ and the diffusion matrix $B(\mathbf{x},t)$. Provided that the latter is positive semidefinite the FPE (8.7) is equivalent to the Itō SDE system [8.4]

$$\mathrm{d}\mathbf{x}(t) = \mathbf{A}(\mathbf{x},t)\,\mathrm{d}t + V(\mathbf{x},t)\,\mathrm{d}\mathbf{W} \quad (8.8)$$

with $B = VV^T$ and the Wiener processes $\mathbf{W} = (W_1,\ldots,W_N)^T$ [8.5].

8.2 Introduction to self-organisation

The phenomenon of self-organising systems can be observed in many fields of science. Some examples are the flocking behaviour of birds [8.6] in biology, supramolecular chemistry [8.7] and the sandpile as a generic example of self-organised criticality [8.8] in physics. Notably, this rather generic mechanism can also be found in a simple cavity QED setup we are about to present.

Contrary to all situations discussed so far in the present thesis the cavity mode is not driven by an external pump but the particles are directly illuminated by a transverse laser and scatter pump photons into the resonator mode. The contributions from the different particles interfere and—depending on the particle positions—may add up constructively. Above a certain critical laser power the scattered light creates a sufficiently deep potential into which more and more particles are dragged. These additional trapped particles in turn now also scatter in phase, thus amplifying the intracavity light field and consequently deepening the potential. The particles are trapped by their own scattered light field, thus the name "self-organisation". As we will see, there are two equivalent particle patterns maximising Bragg scattering. In two dimensions, they resemble a chessboard where either only the black or only the white squares are populated. The first theoretical investigation of this phenomenon was presented by Domokos and Ritsch in 2002 [8.9]. An experimental confirmation by Black *et al.* followed shortly afterwards in 2003 [8.10].

For the mathematical description of transversally pumped particles within an optical cavity we combine the Hamiltonians (2.41) of section 2.3 and (3.28) of section 3.3,

$$H = \frac{p^2}{2m} - \hbar\Delta_{\mathrm{c}}a^\dagger a - \hbar\Delta_{\mathrm{a}}\sigma_+\sigma_- - i\hbar g(x)(a\sigma_+ - \sigma_- a^\dagger) - i\hbar\zeta(y)(\sigma_- - \sigma_+). \quad (8.9)$$

Here $\zeta(y)$ denotes the effective atom pump strength, x the direction along the cavity axis and y the transverse direction. After an adiabatic elimination of the excited

state as presented in section 2.3, and a generalisation to N particles we find

$$H = \sum_{i=1}^{N} \left[\frac{p_{x,i}^2 + p_{y,i}^2}{2m} + \hbar U_0 a^\dagger a \sin^2(kx_i) + \hbar \frac{\eta^2}{U_0} \cos^2(ky_i) \right] + \\ + \sum_{i=1}^{N} \hbar\eta (a + a^\dagger) \sin(kx_i) \cos(ky_i) - \hbar\Delta_\mathrm{c} a^\dagger a. \quad (8.10)$$

Here we have used $g(x) = g_0 \sin(kx)$, $\zeta(y) = \zeta_0 \cos(ky)$, $U_0 := g_0^2/\Delta_\mathrm{a}$ and $\eta := g_0\zeta_0/\Delta_\mathrm{a}$. Note that we have ignored spontaneous emission as previously discussed in section 2.3. The master equation describing the system contains the Hamiltonian (8.10) and the Liouvillean $\mathcal{L}\rho = \kappa \left(2a\rho a^\dagger - a^\dagger a \rho - \rho a^\dagger a \right)$. We now have all ingredients needed for the derivation of the time evolution equation for the Wigner function. The potential terms are not second order in x and y, the resulting PDE will therefore contain an infinite amount of derivatives and needs to be truncated to a Fokker–Planck equation (the FPE is only exact for Gaussian processes [8.11]). This step is justified under the following conditions [8.12, 8.13]. First of all, absorption or emission of a photon should not affect the Wigner function considerably. This is the case if the photon momentum $\hbar k$ is small compared to the momentum width Δp of the Wigner function. The latter is related to the gas temperature, making the condition equivalent to the requirement for the gas temperature to be much larger than the recoil energy, $k_\mathrm{B}T \gg E_\mathrm{R}$. The second condition is that the field is close to a coherent state with an average photon number larger than one. This makes the second order derivative $\partial_\alpha \partial_{\alpha^*}$ negligible compared to $|\alpha|^2$ allowing for the neglection of a third-order derivative term $\partial_\alpha \partial_{\alpha^*} \partial_p$. Applying the operator correspondences (8.6), the FPE in the semiclassical limit reads

$$\frac{\partial}{\partial t} W = \left[-i \left(\Delta_\mathrm{c} - U_0 \sum_j \sin^2(kx_j) \right) \left(\frac{\partial}{\partial \alpha} \alpha - \frac{\partial}{\partial \alpha^*} \alpha^* \right) \right] W \\ + \left[i\eta \sum_j \sin(kx_j) \cos(ky_j) \left(\frac{\partial}{\partial \alpha} - \frac{\partial}{\partial \alpha^*} \right) \right] W + \\ + \left[\kappa \left(\frac{\partial}{\partial \alpha} \alpha + \frac{\partial}{\partial \alpha^*} \alpha^* + \frac{\partial^2}{\partial \alpha \partial \alpha^*} \right) \right] W + \\ + \left[-\sum_j \frac{p_{x,j}}{m} \frac{\partial}{\partial x_j} + \sum_j \frac{\partial V(\alpha, \alpha^*, x_j, y_j)}{\partial x_j} \frac{\partial}{\partial p_{x,j}} \right] W + \\ + \left[-\sum_j \frac{p_{y,j}}{m} \frac{\partial}{\partial y_j} + \sum_j \frac{\partial V(\alpha, \alpha^*, x_j, y_j)}{\partial y_j} \frac{\partial}{\partial p_{y,j}} \right] W, \quad (8.11)$$

with the single-particle potential

$$V(\alpha,\alpha^*,x,y) = \hbar U_0|\alpha|^2\sin^2(kx)+\hbar\eta(\alpha+\alpha^*)\sin(kx)\cos(ky)+\hbar\frac{\eta^2}{U_0}\cos^2(ky). \quad (8.12)$$

The Wigner function W depends on all particle positions and momenta as well as on the cavity field, $W(x_1,y_1,\ldots,x_N,y_N,p_{x,1},p_{y,1},\ldots,p_{x,N},p_{y,N},\alpha,\alpha^*)$. The first two lines of the FPE (8.11) describe the coherent evolution of the field mode, containing the particles as effective refractive index (first line) and as effective pump through scattering from the pump laser (second line). The third line contains damping and diffusion terms for the mode. Finally, the last two lines describe the coherent particle motion along (fourth line) and transversal (fifth line) to the cavity. There is no explicit momentum diffusion contained in this Fokker–Planck equation, only the mode is lossy. This is a direct consequence of the neglection of spontaneous emission—the additional noise terms appearing in the momentum and field equations would be proportional to the incoherent scattering rate Γ_0 (2.48) defined in section 2.3 [8.14]. However, the mode mediates interactions between the particles, which (for appropriate detuning Δ_c) leads to a friction force and momentum diffusion causing a finite steady-state temperature.

The corresponding system of stochastic differential equations according to equation (8.8) is

$$\mathrm{d}x_j = \frac{p_{x,j}}{m}\,\mathrm{d}t \quad (8.13a)$$

$$\mathrm{d}y_j = \frac{p_{y,j}}{m}\,\mathrm{d}t \quad (8.13b)$$

$$\mathrm{d}p_{x,j} = -\frac{\partial V(\alpha,\alpha^*,x_j,y_j)}{\partial x_j}\,\mathrm{d}t \quad (8.13c)$$

$$\mathrm{d}p_{y,j} = -\frac{\partial V(\alpha,\alpha^*,x_j,y_j)}{\partial y_j}\,\mathrm{d}t \quad (8.13d)$$

$$\begin{aligned}\mathrm{d}\alpha = &\left[i\left(\Delta_c - U_0\sum_j \sin^2(kx_j)\right)-\kappa\right]\alpha\,\mathrm{d}t- \\ &- i\eta\sum_j \sin(kx_j)\cos(ky_j)\,\mathrm{d}t + \sqrt{\frac{\kappa}{2}}\,(\mathrm{d}W_1 + i\,\mathrm{d}W_2)\,.\end{aligned} \quad (8.13e)$$

These SDEs are called semiclassical equations of motion. The particle and field operators have been replaced by classical variables but the noise terms are of quantum-mechanical origin, hence the name. In principle, the stochastic equations (8.13) have to be interpreted in the Itō sense. However, as the diffusion is constant, the corresponding Stratonovich equations are readily obtained and do not contain any corrections to the drift terms [8.5]. This would not be the case when considering spontaneous emission where the diffusion terms are position- and field-dependent [8.14].

The equation (8.13e) for the field now makes clear what we have expressed in words at the beginning of this section. The collective scattering term sums up particle contributions $\sin(kx_j)\cos(ky_j)$, which vary from $+1$ to -1 like on a checkerboard pattern with spacing $\Delta x = \Delta y = \lambda = 2\pi/k$. For a homogeneous distribution on the x–y plane, the sum over these scattered fields averages out. If, however, the pump power is increased and the particle density higher at points where $\sin(kx)\cos(ky) = +1$ (denoted "even" sites), their contributions sum up constructively amounting for an increasing intracavity field and thus potential. More precisely, the even lattice sites become deeper and therefore attract more and warmer particles, which now constructively contribute to the sum in equation (8.13e). The odd sites become shallower as the even ones deepen. The very same mechanism of course also holds for the odd sites being populated, both self-organisation patterns are completely equivalent and one is chosen at random in each realisation. This is an example for spontaneous symmetry breaking. See figure 8.1 for an illustration and a numerical example. If all particles are confined in either the odd or the even sites, the field is effectively pumped with strength ηN and the intensity $|\alpha|^2$ scales with N^2. This is known as the superradiance effect [8.14] and is an undoubtful signature for a cooperative mechanism involving all particles. Since the mode is dissipative, it is eligible for transporting energy and entropy out of the cavity. This allows for cooperative cooling for correctly chosen parameters. The minimal final temperature possible below threshold is then solely determined by a cavity parameter, the linewidth κ. Experimentally, such cooperative effects have been demonstrated e.g. in the group of Vuletić [8.10, 8.15, 8.16]. More details can be found in the publication in the next chapter.

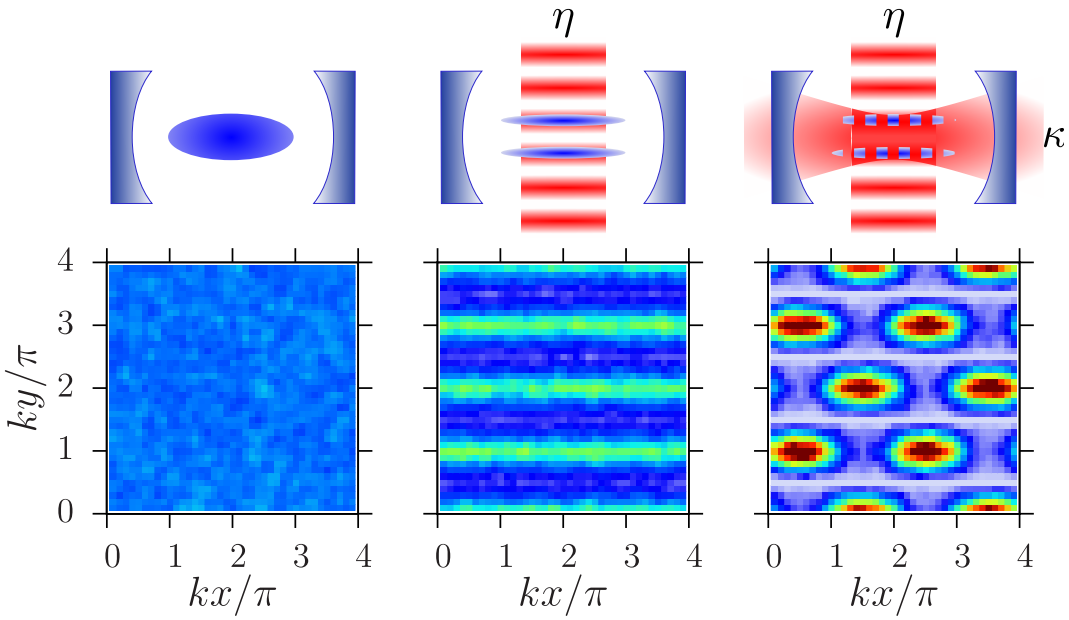

Figure 8.1: Illustration of the self-organisation process (upper plots) and a single trajectory of the stochastic differential equations (8.13) for $N = 50000$ particles (lower plots). Initially, without pump laser, the atoms are homogeneously distributed (left). After the laser is switched on, the particles organise in its standing wave (middle). Finally, the particles self-organise in the potential created by their own scattered light (right).

Chapter 9

Publication

EPL (Europhysics Letters) **96**, 43001 (2011)

Kinetic theory of cavity cooling and self-organisation of a cold gas[†]

W. Niedenzu, T. Grießer and H. Ritsch

Institut für Theoretische Physik, Universität Innsbruck - Technikerstraße 25, 6020 Innsbruck, Austria, EU

We study spatial self-organisation and dynamical phase-space compression of a dilute cold gas of laser-illuminated polarisable particles in an optical resonator. Deriving a non-linear Fokker–Planck equation for the particles' phase-space density allows us to treat arbitrarily large ensembles in the far-detuning limit and explicitly calculate friction forces, momentum diffusion and steady-state temperatures. In addition, we calculate the self-organisation threshold in a self-consistent analytic form. For a homogeneous ensemble below threshold the cooling rate for fixed laser power is largely independent of the particle number. Cooling leads to a q-Gaussian velocity distribution with a steady-state temperature determined by the cavity linewidth. Numerical simulations using large ensembles of particles confirm the analytical threshold condition for the appearance of an ordered state, where the particles are trapped in a periodic pattern and can be cooled to temperatures close to a single vibrational excitation.

URL: `http://iopscience.iop.org/0295-5075/96/4/43001`
DOI: 10.1209/0295-5075/96/43001
PACS: 37.30.+i, 37.10.-x, 51.10.+y

[†]The primary contribution of the author of the present thesis to this publication was the implementation and the analysis of the numerical simulations. All analytical results were calculated in collaboration with T. G., where each author individually performed the calculations, except of the distribution function above threshold which was obtained by T. G.

9.1 Introduction

A dilute cold gas of polarisable particles can be manipulated in a controlled way using the light forces induced by a sufficiently strong laser far off any internal optical resonance [9.1]. For a free-space laser setup this force generates a conservative optical potential for the particles with a depth proportional to the local light intensity. As the forces are generated via photon redistribution among different spatial directions, the particles in turn alter the field distribution and act essentially as a spatially varying refractive index. While this backaction can safely be ignored in standard optical traps [9.2], it was shown to have a significant effect if the light fields are confined within an optical resonator enhancing the effective particle-light interaction [9.3].

For transverse illumination a threshold pump intensity where this coupled particle-field dynamics can lead to spatial self-ordering of the particles into a regular pattern—resembling very closely a phase transition—was theoretically predicted and experimentally confirmed [9.4–9.6]. Due to cavity losses this dynamics is dissipative and thus can constitute a new cooling mechanism for a very general class of polarisable objects [9.7, 9.8]. Extensive simulations using fairly large numbers of particles with large detunings predict that already with current molecular sources and cavity technology a useful phase-space compression could be achieved [9.9]. However, particle-based simulations cannot be applied to sufficiently large particle numbers and laser powers for the whole parameter range of interest. As an alternative, a Vlasov-equation-based approach [9.10] for the particles' phase-space distribution provides a description for arbitrarily large ensembles, but excludes correlations important on longer time scales. In this work we adopt methods from plasma kinetic theory to generalise the Vlasov model to include correlations, leading to a non-linear Fokker–Planck equation for the statistically averaged phase-space distribution, which includes friction and diffusion and allows to predict cooling time scales and the unique steady-state distribution.

9.2 Semiclassical equations of motion

We consider N polarisable particles moving along the axis of a lossy standing-wave resonator assuming strong transversal confinement. The particles are off-resonantly illuminated by a transverse standing-wave pump laser and scatter light, whose phase is determined by the particle positions, into the cavity. The quantum master equation describing this system can be transformed into a partial differential equation for the Wigner function [9.11]. Truncating this equation at second-order derivatives (semiclassical limit) yields a Fokker–Planck equation, which for positive Wigner functions—excluding all non-classical states [9.12]—is equivalent to the Itō stochastic differential equation (SDE) system

$$\mathrm{d}x_j = v_j \,\mathrm{d}t \tag{9.1a}$$

$$\mathrm{d}v_j = -\frac{1}{m}\frac{\partial U(x_j,\alpha)}{\partial x_j}\,\mathrm{d}t \tag{9.1b}$$

$$\mathrm{d}\alpha = \left[\mathrm{i}\left(\Delta_\mathrm{c} - U_0\sum_{j=1}^{N}\sin^2(kx_j)\right) - \kappa\right]\alpha\,\mathrm{d}t - \\ - \mathrm{i}\eta\sum_{j=1}^{N}\sin(kx_j)\,\mathrm{d}t + \sqrt{\frac{\kappa}{2}}\left(\mathrm{d}W_1 + \mathrm{i}\,\mathrm{d}W_2\right), \tag{9.1c}$$

with the single-particle potential

$$U(x,\alpha) = \hbar U_0|\alpha|^2\sin^2(kx) + \hbar\eta(\alpha+\alpha^*)\sin(kx). \tag{9.2}$$

Each particle has the mass m; x_j and v_j denote the centre-of-mass position and velocity of the jth particle, respectively. U_0 is the light shift per photon and κ the cavity decay rate; the associated input noise is taken into account by the two Wiener processes $\mathrm{d}W_1$ and $\mathrm{d}W_2$. Here we have neglected momentum diffusion caused by spontaneous emission, which is valid for large ensembles and large detunings [9.8]. The transverse laser standing wave gives an effective position-dependent pump of magnitude η of the field mode α with wave number k. This laser is detuned by $\Delta_\mathrm{c} = \omega_\mathrm{p} - \omega_\mathrm{c}$ from the bare cavity resonance frequency. We will focus on the weak-coupling limit $N|U_0| \ll |\Delta_\mathrm{c}| \sim \kappa$ throughout this paper. Refer to fig. 9.1 for a schematic view of the system.

We used the scheme proposed in [9.13, 9.14] for the direct numerical integration of the SDE system (9.1). However, for analytical predictions and the description of very large ensembles, a continuous phase-space description as described below proves far more suitable.

9.3 Continuous description, instability threshold

The semiclassical SDEs (9.1) are equivalent to the Klimontovich equation [9.15]

$$\frac{\partial f_\mathrm{K}}{\partial t} + v\frac{\partial f_\mathrm{K}}{\partial x} - \frac{1}{m}\frac{\partial U}{\partial x}\frac{\partial f_\mathrm{K}}{\partial v} = 0 \tag{9.3}$$

together with an evolution equation for the field mode α obtained replacing the sums in eq. (9.1c) by the integrals $N\iint \bullet f_\mathrm{K}(x,v,t)\mathrm{d}x\mathrm{d}v$. $f_\mathrm{K}(x,v,t)$ is the so-called Klimontovich or "exact" distribution function with initial condition

$$f_\mathrm{K}(x,v,0) = \frac{1}{N}\sum_{j=1}^{N}\delta(x - x_j(0))\delta(v - v_j(0)). \tag{9.4}$$

As this function is highly irregular, the above reformulation has no computational merit by itself, but provides an ideal starting point for a statistical treatment. To

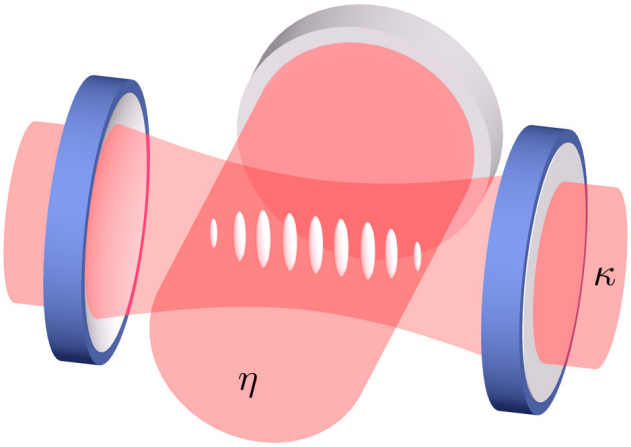

Figure 9.1: (Colour on-line) An ensemble of particles is illuminated by a transverse standing-wave laser and scatters light into the resonator (effective pump strength η). Above a threshold pump intensity the particles self-organise in a periodic pattern. Cavity losses are characterised by the decay rate κ.

this end we decompose every quantity (f_{K}, α and U) into its smooth mean value and fluctuations,

$$f_{\mathrm{K}}(x,v,t) =: \langle f(x,v,t)\rangle + \delta f(x,v,t), \tag{9.5}$$

with $\langle \delta f(x,v,t)\rangle = 0$. The statistical average $\langle \bullet \rangle$ is over an ensemble of similar initial conditions $\{(x_j(0), v_j(0))\}$ and $\alpha(0)$, as well as over the realisations of the white noise process mimicking the input noise for the cavity field.

For the smooth ensemble-averaged Klimontovich distribution, called *one-particle distribution function*, we then find

$$\frac{\partial \langle f\rangle}{\partial t} + v\frac{\partial \langle f\rangle}{\partial x} - \frac{1}{m}\frac{\partial \langle U\rangle}{\partial x}\frac{\partial \langle f\rangle}{\partial v} = \left\langle \frac{\partial \delta U}{\partial x}\frac{\partial \delta f}{\partial v}\right\rangle. \tag{9.6}$$

Neglecting all correlations in eq. (9.6) leads to the Vlasov equation, which becomes exact in the limit $N \to \infty$ [9.10].

The Vlasov equation together with the equation for $\langle\alpha\rangle$ possesses an infinite number of possible spatially homogeneous stationary solutions with zero cavity field, of which, however, not all are necessarily stable against perturbations. Indeed, for any (dimensionless) symmetric velocity distribution $g(v/v_{\mathrm{T}}) := Lv_{\mathrm{T}}\langle f(v)\rangle$ and $\delta := \Delta_{\mathrm{c}} - NU_0/2 < 0$ we find, that if

$$\frac{N\eta^2}{k_{\mathrm{B}}T}\,\mathrm{vp}\int_{-\infty}^{\infty}\frac{g'(\xi)}{-2\xi}\mathrm{d}\xi > \frac{\delta^2+\kappa^2}{\hbar|\delta|}, \tag{9.7}$$

where vp denotes the Cauchy principal value, perturbations trigger a self-organisation process. Here we have defined the thermal velocity $v_\mathrm{T}^2 := 2k_\mathrm{B}T/m$; L is the cavity length. For a Gaussian distribution the integral evaluates to one. The relation (9.7) has been derived by methods presented in [9.10]. There it was shown that the threshold can be computed from the zeros of the dispersion relation ($\mathrm{Re}(s) > 0$)

$$D(s) = (s+\kappa)^2 + \delta^2 - \mathrm{i}\hbar k\delta \frac{NL\eta^2}{2m} \int_{-\infty}^{\infty} \left(\frac{\partial_v \langle f \rangle}{s + \mathrm{i}kv} - \frac{\partial_v \langle f \rangle}{s - \mathrm{i}kv} \right) \mathrm{d}v. \tag{9.8}$$

9.4 Kinetic equation for the velocity distribution in the non-organised phase

Let us now return to eq. (9.6), which for weak spatial inhomogeneity—as expected below the instability threshold (9.7)—approximately reads

$$\frac{\partial \langle f \rangle}{\partial t} \approx \overline{\left\langle \frac{\partial \delta U}{\partial x} \frac{\partial \delta f}{\partial v} \right\rangle}, \tag{9.9}$$

where the overbar denotes the spatial average. The right-hand-side correlation function can be computed using established methods from plasma physics as in [9.15] when the fluctuations evolve on a much faster time scale than the average values, which are considered "frozen". This is justified as long as the system remains far from instability. After some lengthy calculations, which we omit here for the sake of compactness, we obtain (for symmetric distributions) the non-linear Fokker–Planck equation

$$\frac{\partial}{\partial t} \langle F \rangle + \frac{\partial}{\partial v} \Big(A[\langle F \rangle] \langle F \rangle \Big) = \frac{\partial}{\partial v} \left(B[\langle F \rangle] \frac{\partial}{\partial v} \langle F \rangle \right) \tag{9.10}$$

for the velocity distribution $\langle F(v,t) \rangle := L \langle f(v,t) \rangle$, with the coefficients

$$A[\langle F \rangle] := \frac{2\hbar k\delta\kappa\eta^2}{m} \frac{kv}{|D(\mathrm{i}kv)|^2} \tag{9.11a}$$

$$B[\langle F \rangle] := \frac{\hbar^2 k^2 \eta^2 \kappa}{2m^2} \frac{\kappa^2 + \delta^2 + k^2 v^2}{|D(\mathrm{i}kv)|^2}. \tag{9.11b}$$

This equation, which describes the sub-threshold gas dynamics, is one of the central analytical results of this work. Note that the coefficients functionally depend on $\langle F \rangle$ through the dispersion relation $D(\mathrm{i}\omega) := \lim_{\varepsilon \downarrow 0} D(\varepsilon + \mathrm{i}\omega)$. A and B represent the deterministic part of the equations and the field noise, respectively. All cavity-mediated long-range particle interactions are encoded in the dispersion relation. Note that very far below threshold the full dispersion relation (9.8) reduces to $D(\mathrm{i}kv) \simeq (\mathrm{i}kv + \kappa)^2 + \delta^2$, which corresponds to the N independent-particles case.

9.5 Equilibrium distribution and temperature

Normalisable steady-state solutions of eq. (9.10) exist only for negative detuning $\delta < 0$, where light scattering is accompanied by kinetic-energy extraction from the motion. For positive detuning the particles are heated. Interestingly, we obtain the non-thermal q-Gaussian velocity distribution function (also known as Tsallis distribution and closely related to Student's t-distribution) [9.16, 9.17]

$$\langle F(v)\rangle \propto \left(1-(1-q)\frac{mv^2}{2k_{\mathrm{B}}T}\right)^{\frac{1}{1-q}}, \tag{9.12}$$

with $q := 1+\omega_{\mathrm{R}}/|\delta|$ and the recoil frequency $\omega_{\mathrm{R}} := \hbar k^2/2m$. We have defined an effective "temperature" parameter

$$k_{\mathrm{B}}T = \hbar\frac{\kappa^2+\delta^2}{4|\delta|} = \frac{\hbar\kappa}{2}. \tag{9.13}$$

The latter minimum value of T appears for $\delta = -\kappa$. The parameter $|\delta|/\omega_{\mathrm{R}}$ determines the shape of the distribution and gives rise to further restrictions. Normalisable solutions exist for $|\delta| > \omega_{\mathrm{R}}/2$, the second moment (kinetic energy) only for $|\delta| > 3\omega_{\mathrm{R}}/2$. The case $|\delta| = \omega_{\mathrm{R}}$ corresponds to a Lorentzian distribution. For $|\delta|/\omega_{\mathrm{R}} \to \infty$, i.e. $q \to 1$, the distribution (9.12) converges to a Gaussian distribution with kinetic temperature $k_{\mathrm{B}}T_{\mathrm{kin}} := m\langle v^2\rangle$ given by the parameter $k_{\mathrm{B}}T$ defined in eq. (9.13), which justifies the choice of "temperature" above. Refer to fig. 9.2 for an example of prominent q-Gaussian behaviour ($q = 1.4$). Tsallis distributions have already been observed experimentally in dissipative optical lattices [9.18].

Of course the distribution (9.12) can be unstable and in fact is, if

$$\sqrt{N}\eta > \sqrt{N}\eta_{\mathrm{c}} := \frac{\kappa^2+\delta^2}{2|\delta|}\sqrt{\frac{2}{3-q}} \overset{\delta=-\kappa}{=} \kappa\sqrt{\frac{2}{3-q}}, \tag{9.14}$$

which can be seen by inserting the q-Gaussian into (9.7). For a Gaussian and $\delta = -\kappa$ this criterion may be reformulated as

$$N|U_0|V_{\mathrm{opt}} > \hbar\kappa^2, \tag{9.15}$$

where V_{opt} is the optical potential depth created by the pump laser. If the condition (9.14) is satisfied, we conclude that there exists no spatially homogeneous steady state at all and consequently we expect the system to organise. The possibility of attaining such an inhomogeneous equilibrium even though the uniform distribution (9.12) is stable cannot be ruled out mathematically but seems unlikely on physical grounds. These expectations are confirmed by all our numerical simulations of eqs. (9.1).

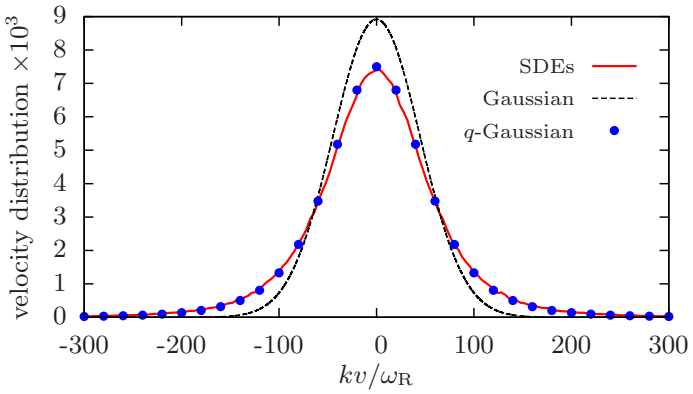

Figure 9.2: (Colour on-line) Normalised q-Gaussian velocity distribution for $\delta = -2.5\omega_R$ obtained by integrating the semiclassical equations (9.1) up to $\omega_R t = 5N$ (solid line) compared to the theoretically predicted q-Gaussian (9.12) (circles). The Gaussian (dashed line) is plotted for the temperature (9.13). The kinetic temperature differs considerably from eq. (9.13), $k_B T_{kin} = 2.5 k_B T$. Parameters: $N = 5000$, $NU_0 = -0.1\omega_R$, $\sqrt{N}\eta = 1800\omega_R$, $\kappa = 100\omega_R$ and $\Delta_c = -2.55\omega_R$. Ensemble average over 25 initial conditions and 10 realisations of the white noise process.

Based on these considerations we predict the occurrence of dissipation-induced self-organisation if the self-consistent relation (9.14) is fulfilled. That is, any initially stable, unorganised distribution will loose kinetic energy (cavity cooling) and eventually self-organise. Contrary to the self-organisation process of an initially unstable state, which is abrupt and accompanied by strong heating, dissipation-induced self-organisation is characterised by a much slower buildup of the photon number and monotonous cooling.

9.6 Self-organised phase

Above threshold the mathematics becomes more complex due to the inhomogeneous spatial distribution. However, using action-angle variables [9.19, 9.20], we can still derive a Fokker–Planck equation similar to eq. (9.10) [9.21]. In the limit of deep trapping, where a harmonic approximation for the potential becomes valid, the steady-state solution for the strongly organised phase is a thermal distribution with a kinetic temperature depending on the linewidth κ and the trap frequency ω_0,

$$k_B T_{kin} = \hbar \frac{\kappa^2 + \delta^2 + 4\omega_0^2}{4|\delta|}. \tag{9.16}$$

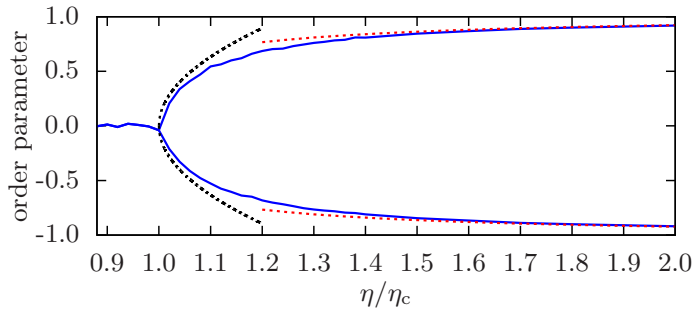

Figure 9.3: (Colour on-line) Order parameter (9.18) as function of the pump strength obtained from eqs. (9.1) in the long-time limit ($\omega_R t = 50N$). The red dashed line is given by eq. (9.19), the black dashed line around the critical point corresponds to eq. (9.21). Parameters: $N = 1000$, $NU_0 = -\omega_R$, $\kappa = 100\omega_R$, $\Delta_c = NU_0/2 - \kappa$ (i.e. $\delta = -\kappa$) and $k_B T_0 = 110 E_R$. Ensemble average of 20 (away of the critical point) and 60 (around the critical point) noise trajectories, respectively, for one initial condition.

The trap frequency is $\omega_0^2 = 4\eta\omega_R \langle |\operatorname{Re}\alpha_\infty| \rangle$ and can be approximated by

$$\omega_0^2 \simeq \sqrt{N}\eta\omega_R \left(\frac{\eta}{\eta_c} + \sqrt{\frac{\eta^2}{\eta_c^2} - 1} \right) \sim N \tag{9.17}$$

in the far-detuned regime where $|\delta| \gg \omega_R$; η_c is the self-consistent critical value defined in eq. (9.14). As the temperature depends explicitly on the laser power, higher pump strengths result in deeper trapped ensembles with increased kinetic energy. Note that this system has the interesting property that the more particles we add, the deeper the optical potential gets as is the case for self-gravitating systems [9.22].

The order parameter

$$\Theta := \lim_{t\to\infty} \iint \sin(kx) \langle f(x,v,t) \rangle \, \mathrm{d}x\mathrm{d}v \tag{9.18}$$

is an adequate measure of particle localisation in equilibrium as it is zero for a completely homogeneous distribution and plus/minus one for the perfectly self-organised phase (i.e. δ-peaks), the sign depends on whether the odd- or even wells are populated [9.6]. In fig 9.3 we depict its behaviour as a function of the pump strength. Initially, the particles were spatially homogeneously distributed with a (stable) Gaussian velocity distribution; self-organisation sets in because of the cavity cooling effect. Hence the branching point is given by the self-consistent threshold (9.14).

For the strongly organised phase, where the distribution function is a thermal state with temperature (9.16), the order parameter reads (in harmonic oscillator

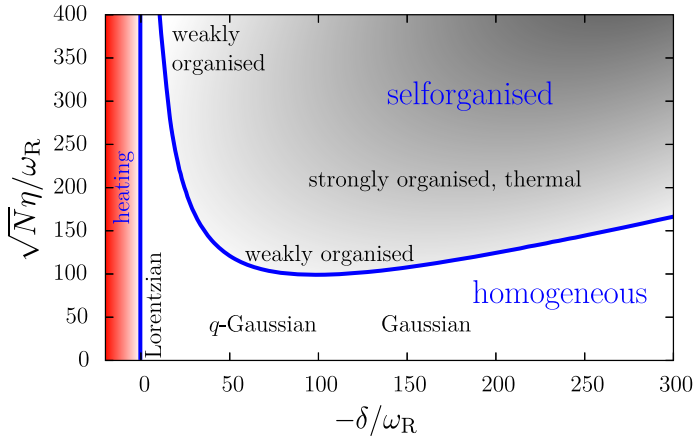

Figure 9.4: (Colour on-line) Schematic view of the phase diagram in the weak-coupling limit ($N|U_0| \ll \kappa$) for $\kappa = 100\omega_R$. Equilibrium solutions exist only for $\delta < -\omega_R/2$, the Lorentzian corresponds to the case $|\delta| = \omega_R$. For large values of the detuning $|\delta|$, strongly organised equilibria exist already for pump strengths slightly above the critical value, cf. also fig. (9.3).

approximation)

$$\Theta = \pm\left(1 - \frac{k_B T_{kin}}{\hbar\omega_0^2}\omega_R\right). \tag{9.19}$$

Its maximum value is limited by the detuning and the recoil frequency, $\Theta \to \pm(1 - \omega_R/|\delta|)$ for $\eta \to \infty$. This corresponds to a Gaussian spatial distribution with width $k^2(\Delta x)^2 = 2\omega_R/|\delta|$. Let us also briefly investigate the opposite limit of pump strengths slightly above threshold. Solving the self-consistency equation

$$\mathrm{Re}\,\langle\alpha\rangle_\infty = \frac{-N\eta|\delta|}{\kappa^2 + \delta^2}\Theta \tag{9.20}$$

perturbatively around the critical point for a thermal state yields

$$\Theta \simeq \pm 2\sqrt{\frac{\eta}{\eta_c} - 1} \tag{9.21}$$

and thus a critical exponent of 1/2, as already predicted in [9.6].

The self-consistent phase diagram including cavity cooling is sketched in fig. 9.4. For small $|\delta|/\omega_R$ the ensemble will always remain weakly organised (i.e. a small spatial modulation on top of a homogeneous background) above threshold as the necessary prerequisites for a strongly organised equilibrium—and hence the validity of eq. (9.16)—cannot be fulfilled.

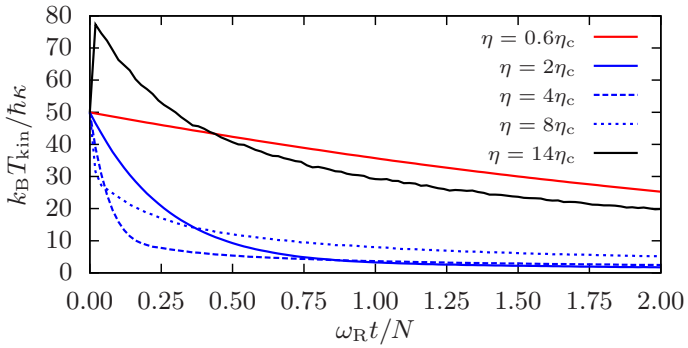

Figure 9.5: (Colour on-line) Kinetic temperature for $N = 500$ and different pump strengths. Parameters: $\kappa = 100\omega_R$ and $\delta = -\kappa$. The initial instability threshold is at $\eta = 10\eta_c$. Ensemble average over 5 initial conditions with 5 noise trajectories.

9.7 Cooling time

Let us take a closer look at the cooling time τ, i.e. the time characteristic for the kinetic-energy equilibrisation. First we treat the case of a fixed ensemble size and variable pump strength. The drift term $A + \partial_v B$ in the non-linear Fokker–Planck equation (9.10)—scaling as $\sim \eta^2/\omega_R$—might suggest the conclusion that the larger the pump strength the shorter the cooling time. However, numerical simulations (cf. fig. 9.5) prove this expectation to be somewhat misleading. The reason therefor is the onset of self-organisation which occurs as soon as the momentary distribution becomes unstable according to eq. (9.7). Particle trapping is a hindrance to optimal cooling in a twofold way. Firstly, with its appearance kinetic energy is dissipated at a significantly lower rate because a part of the laser power is utilised for the buildup of the potential and consequently is not available for cooling. Secondly, the lowest achievable temperature increases with the pump strength, cf. eq. (9.16). The situation is worst for initially unstable ensembles since the particles are heated before being cooled. Hence it is a plausible requirement that self-organisation has to be avoided to realise the optimal cooling time. Accordingly, as a rule of thumb we may state that the latter is achieved for a laser power which renders the desired gas temperature critical. Hence the optimal cooling time is estimated from eq. (9.10) to be

$$\tau_{opt} \approx \frac{k v_{T_0}}{4\sqrt{\pi}\kappa^2} N \tag{9.22}$$

assuming a Gaussian and $\delta = -\kappa$ for simplicity. This estimate is valid for $k v_{T_0} \gg \kappa$, where T_0 is the initial temperature.

For a fixed η, all ensembles composed of $N < N_c$ particles experience in a

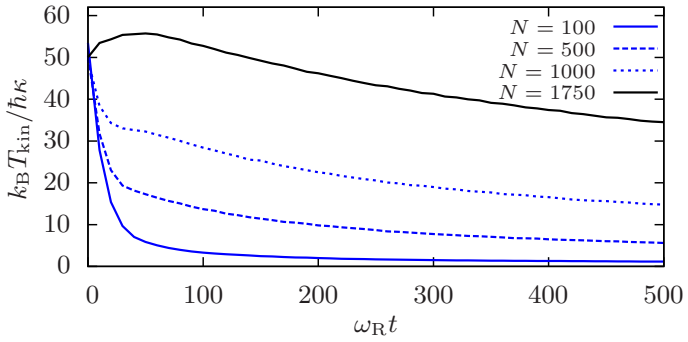

Figure 9.6: (Colour on-line) Kinetic temperature for fixed pump strength and $N = \{100, 500, 1000, 1750\}$, from bottom to top. Parameters: $\eta = 28\omega_R$, $\kappa = 100\omega_R$ and $\delta = -\kappa$. The self-consistent threshold (9.14) is surpassed for all curves; the ensemble with $N = 1750$ is initially unstable. Ensemble average over 25 ($N = 100$) and 8 (higher particle numbers) initial conditions, respectively, and 5 noise trajectories.

good approximation the same cooling time $\tau \sim \omega_R/\eta^2$ for reaching the minimal temperature (9.13). N_c is the critical particle number rendering the given η critical. Note however, that this time scale is suboptimal for all ensemble sizes except $N = N_c$. The scaling with N for fixed laser power is more favourable as for standard cavity cooling [9.23]. Refer to fig. 9.6. For initially stable ensembles the cooling rate is approximately the same until the instability point is reached.

Let us briefly mention another aspect of the scaling of the Fokker–Planck equation (9.10) particularly useful for numerical simulations. Fixing $\sqrt{N}\eta$ for different particle numbers yields a cooling time $\tau \sim N/\omega_R$. Numerical simulations of the semiclassical equations (9.1) confirm this result, cf. figs. 9.7 and 9.8. There we have depicted the temperature evolution for the pump strength being a fixed fraction of the critical value η_c for two different particle numbers, i.e. $\sqrt{N_1}\eta_1 = \sqrt{N_2}\eta_2$. In fig. 9.8 the threshold (9.7) is surpassed during the time evolution.

In order to verify the Fokker–Planck equation (9.10), we consider the equation

$$\frac{\mathrm{d}}{\mathrm{d}t} k_B T_{kin} = -2m \int_{-\infty}^{\infty} v \left(-A \langle F \rangle + B \frac{\partial}{\partial v} \langle F \rangle \right) \mathrm{d}v. \tag{9.23}$$

for the kinetic temperature $k_B T_{kin} := m \langle v^2 \rangle$ and close it by assuming $\langle F(v,t) \rangle$ to be a Gaussian velocity distribution with temperature $k_B T_{kin}$ for all times. This assumption is well justified for large detunings $|\delta| \gg \omega_R$ and its predicted temperature reproduces the results obtained from the SDEs (9.1) quite well, cf. fig. 9.7. The main difference between the curves stems from the relatively small particle numbers in

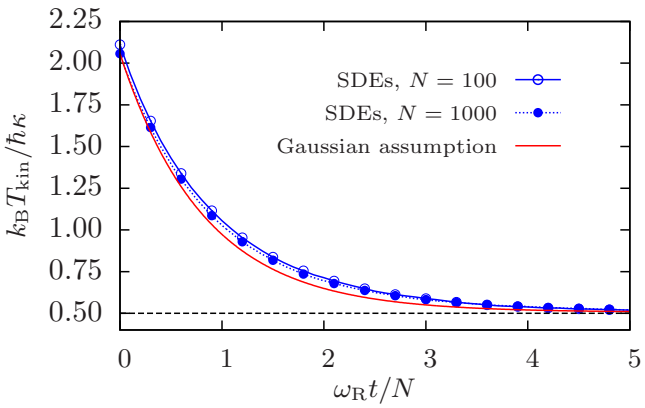

Figure 9.7: (Colour on-line) Comparison of the kinetic temperature obtained from the SDEs (9.1) and as solution of eq. (9.23) for two different particle numbers and constant $\sqrt{N}\eta$. As expected, both ensembles evolve on a time scale $\sim N/\omega_R$. Parameters: $NU_0 = -0.01\omega_R$, $\kappa = 100\omega_R$, $\Delta_c = NU_0/2 - \kappa$ (i.e. $\delta = -\kappa$) and $\sqrt{N}\eta = 80\omega_R \equiv 0.8\sqrt{N}\eta_c$. Ensemble average of 50 ($N = 100$) and 2 ($N = 1000$) initial conditions, respectively, and 50 realisations of the white noise process.

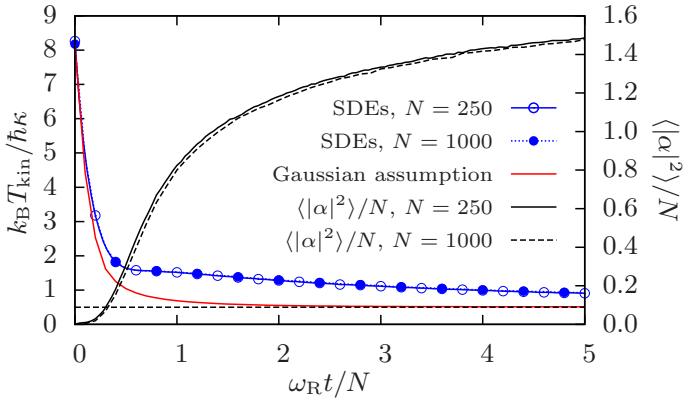

Figure 9.8: (Colour on-line) Temperature evolution above the self-consistent threshold (9.14). The homogeneous distribution is stable until the relation (9.7) is satisfied. This also limits the validity of eq. (9.23). Parameters: $NU_0 = -\omega_R$, $\kappa = 100\omega_R$, $\Delta_c = NU_0/2 - \kappa$ (i.e. $\delta = -\kappa$) and $\sqrt{N}\eta = 200\omega_R \equiv 2\sqrt{N}\eta_c$. As $\sqrt{N}\eta = \text{const.}$, the photon number scales only $\sim N$ and not $\sim N^2$ (superradiance effect). Furthermore, the equilibrium temperature is the same for both ensembles. The simulations were performed up to $\omega_R t = 40N$ and revealed a temperature $k_B T_{kin} \approx 0.57\kappa$, which agrees very well with the theoretical prediction (9.16). Ensemble average of 50 ($N = 250$) and 25 ($N = 1000$) initial conditions, respectively, and 10 realisations of the white noise process.

combination with pump values close to threshold, where the hypothesis of separated time scales used to derive eq. (9.10) is no longer valid due to long-lived fluctuations.

Of course, a thorough investigation of the validity of eq. (9.10) would require a numerical integration thereof. However, in steady state, all results of numerical simulations of the SDE system (9.1) were found to be in excellent agreement with the predictions of the kinetic theory, both, below (e.g. fig. 9.2) and above (e.g. fig. 9.8) threshold.

9.8 Conclusion and outlook

Collective light scattering from a dilute gas of cold particles into a high-Q resonator mode under suitable conditions leads to friction forces and cooling of particle motion even below the self-organisation threshold. In contrast to standard cavity cooling the friction force below threshold only weakly depends on the particle number and leads to fast internal thermalisation towards a q-Gaussian velocity distribution of particles with average kinetic energy determined by the cavity linewidth only. Thus this constitutes a viable method for cooling very large ensembles of particles with sufficient polarisability independent of the need for a cyclic optical transition as well as a way to implement evaporative cooling for low densities, where no direct collisions occur.

As only the polarisability and mass of a particle enter, one can easily envisage a combination of many species within the cavity to commonly interact with the same pump and cavity fields as a generalised form of sympathetic cooling without the need of direct interparticle interactions. The corresponding non-linear equation replacing the Fokker–Planck equation (9.10) will then be of Balescu–Lenard type, cf. [9.21] and references therein.

Acknowledgements

This work has been supported by the Austrian Science Fund FWF through projects P20391 and F4013. We would like to thank J. Asbóth, H. Habibian, G. Morigi and M. Sonnleitner for helpful discussions.

Chapter 10

Additional material

In this chapter we present some of the cumbersome calculations required for the derivation of the results presented in the preceding publication in chapter 9. We concentrate ourselves on three main points, (i) the threshold condition for self-organisation, (ii) the evaluation of the correlation function and (iii) the computation of the trap frequency.

10.1 Threshold condition

In this section we derive the threshold condition (critical pump strength) above which a thermal and spatially homogeneous distribution becomes unstable. To this end we linearise the Vlasov equation [10.1] for the phase-space distribution function $f(x,v,t)$,

$$\frac{\partial f(x,v,t)}{\partial t} + v\frac{\partial f(x,v,t)}{\partial x} - \frac{1}{m}\frac{\mathrm{d}U(x)}{\mathrm{d}x}\frac{\partial f(x,v,t)}{\partial v} = 0, \tag{10.1}$$

around $f(x,v,t) = f_0(v) + \delta f(x,v,t)$ and $\alpha(t) = \alpha_0 + \delta\alpha(t)$ and obtain

$$\frac{\partial \delta f(x,v,t)}{\partial t} + v\frac{\partial \delta f(x,v,t)}{\partial x} = \frac{1}{m}\frac{\mathrm{d}U(x)}{\mathrm{d}x}\frac{\partial f_0(v)}{\partial v}. \tag{10.2}$$

Note that for the spatially homogeneous distribution $\alpha_0 = 0$. As shown in the publication the potential experienced by the particles reads

$$U(x) = \hbar U_0 |\alpha|^2 \sin^2(kx) + \hbar\eta(\alpha + \alpha^*)\sin(kx) \tag{10.3}$$

and the equation of motion for the cavity field is

$$\frac{\mathrm{d}}{\mathrm{d}t}\delta\alpha(t) = (i\delta - \kappa)\delta\alpha(t) - iN\eta\int_{-\infty}^{\infty}\mathrm{d}v\int_0^L \mathrm{d}x\sin(kx)\delta f(x,v,t). \tag{10.4}$$

Here we have defined

$$\delta := \Delta_\mathrm{c} - NU_0\frac{1}{Lv_\mathrm{T}^2\sqrt{\pi}}\int_{-\infty}^{\infty}\mathrm{d}v e^{-\left(\frac{v}{v_\mathrm{T}}\right)^2}\int_0^L \mathrm{d}x\sin^2(kx) = \Delta_\mathrm{c} - \frac{NU_0}{2}, \tag{10.5}$$

the thermal velocity $v_\mathrm{T} := \sqrt{2k_\mathrm{B}T/m}$ and the cavity length L (periodic boundary conditions). As discussed in chapter 9 we neglect the first part of the potential in the following.

An expansion of the density perturbation (with respect to a spatially homogeneous distribution) in its Fourier series

$$\delta f(x,v,t) = \sum_{n\in\mathbb{Z}} \delta\varphi_n e^{inkx} \tag{10.6}$$

yields the linearised equations of motion (the other density modes are not coupled to the potential)

$$\frac{\partial}{\partial t}\delta\varphi_{\pm1} \pm ikv\delta\varphi_{\pm1} = \frac{\hbar k\eta}{2m}(\delta\alpha + \delta\alpha^*)f_0' \tag{10.7a}$$

$$\frac{\mathrm{d}}{\mathrm{d}t}\delta\alpha = (i\delta-\kappa)\delta\alpha - \frac{NL\eta}{2}\int_{-\infty}^{\infty}\mathrm{d}v\,[\delta\varphi_1 - \delta\varphi_{-1}] \tag{10.7b}$$

$$\frac{\mathrm{d}}{\mathrm{d}t}\delta\alpha^* = (-i\delta-\kappa)\delta\alpha^* + \frac{NL\eta}{2}\int_{-\infty}^{\infty}\mathrm{d}v\,[\delta\varphi_1 - \delta\varphi_{-1}] \tag{10.7c}$$

with $f_0' := \partial_v f_0(v)$. Inserting the ansatz $\delta\varphi_n = \delta\varphi_n^0 e^{st}$, $\delta\alpha = \delta\alpha^0 e^{st}$ and $\delta\alpha^* = \delta\beta^0 e^{st}$ with $s = \gamma + i\omega \in \mathbb{C}$ $(\gamma,\omega\in\mathbb{R})$ into these equations yields an algebraic system of equations of the form

$$M\begin{pmatrix}\delta\alpha^0\\ \delta\beta^0\end{pmatrix} = \begin{pmatrix}0\\0\end{pmatrix} \tag{10.8}$$

for the field, where $M\in\mathbb{C}^{2\times2}$. The determinant of M—denominated "dispersion relation" [10.1]—must vanish to allow for non-trivial solutions. It reads

$$D(s) := (s+\kappa)^2 + \delta^2 - i\delta\frac{\hbar kN\eta^2 L}{2m}\int_{-\infty}^{\infty}\mathrm{d}v\left(\frac{f_0'}{s+ikv} - \frac{f_0'}{s-ikv}\right). \tag{10.9}$$

The integrals appearing in the dispersion relation can readily be evaluated in the limit[1] $\gamma\to0^+$ by applying the Sokhotsky–Plemelj theorem

$$\lim_{\varepsilon\downarrow0}\frac{1}{x\pm i\varepsilon} = \mathrm{vp}\frac{1}{x} \mp i\pi\delta(x), \tag{10.10}$$

where vp denotes the Cauchy principal value. We find

$$D(s) = (s+\kappa)^2 + \delta^2 - \hbar\delta\frac{NL\eta^2}{2m}\int_{-\infty}^{\infty}\mathrm{d}v\left(\frac{f_0'}{v+\frac{\mathrm{Im}\,s}{k} - i\frac{\mathrm{Re}\,s}{k}} + \frac{f_0'}{v-\frac{\mathrm{Im}\,s}{k} + i\frac{\mathrm{Re}\,s}{k}}\right) \tag{10.11}$$

[1] The exponential growth rate γ vanishes at the threshold where a spatially homogenous distribution becomes unstable [10.1].

and hence

$$\lim_{\operatorname{Re} s\downarrow 0} D(s) = (i \operatorname{Im} s + \kappa)^2 + \delta^2 - \\ - \hbar\delta \frac{NL\eta^2}{2m} \left[\operatorname{vp} \int_{-\infty}^{\infty} \mathrm{d}v \frac{f_0'(v)}{v + \frac{\operatorname{Im} s}{k}} + i\pi f_0' \left(-\frac{\operatorname{Im} s}{k} \right) \right] - \\ - \hbar\delta \frac{NL\eta^2}{2m} \left[\operatorname{vp} \int_{-\infty}^{\infty} \mathrm{d}v \frac{f_0'(v)}{v - \frac{\operatorname{Im} s}{k}} - i\pi f_0' \left(\frac{\operatorname{Im} s}{k} \right) \right]. \quad (10.12)$$

The real and imaginary parts of this expression read

$$\lim_{\operatorname{Re} s\downarrow 0} \operatorname{Re} D(s) = -(\operatorname{Im} s)^2 + \delta^2 + \kappa^2 - \\ - \hbar\delta \frac{NL\eta^2}{2m} \left[\operatorname{vp} \int_{-\infty}^{\infty} \mathrm{d}v \frac{f_0'(v)}{v + \frac{\operatorname{Im} s}{k}} + \operatorname{vp} \int_{-\infty}^{\infty} \mathrm{d}v \frac{f_0'(v)}{v - \frac{\operatorname{Im} s}{k}} \right] \quad (10.13a)$$

and

$$\lim_{\operatorname{Re} s\downarrow 0} \operatorname{Im} D(s) = 2\kappa \operatorname{Im} s - \hbar\delta \frac{NL\eta^2}{2m} \pi \left[f_0' \left(-\frac{\operatorname{Im} s}{k} \right) - f_0' \left(\frac{\operatorname{Im} s}{k} \right) \right]. \quad (10.13b)$$

The phase-space distribution function $f_0(v)$ still contains the contribution stemming from the spatially homogeneous distribution. Therefore we define the associated velocity distribution

$$f_0(v) =: \frac{1}{L} F(v). \quad (10.14)$$

Assuming $F(v)$ being monotonically decreasing from zero (which holds for all distributions of interest, e.g. Gaussian and Lorentzian), i.e.

$$F'(-|v|) \geq F'(|v|), \quad (10.15)$$

the only solution of $\operatorname{Im} D(s) = 0$ for $\delta < 0$ is $\operatorname{Im} s = 0$. Inserting this result into equation (10.13a) yields the threshold condition

$$N\eta_{\mathrm{c}}^2 \operatorname{vp} \int_{-\infty}^{\infty} \mathrm{d}v \frac{F'(v)}{-2v} = \frac{\delta^2 + \kappa^2}{\hbar|\delta|} \frac{k_{\mathrm{B}}T}{v_{\mathrm{T}}^2}. \quad (10.16)$$

Here we used $m/2 = k_{\mathrm{B}}T/v_{\mathrm{T}}^2$. For the Gaussian—or Boltzmann—velocity distribution $F(v) = \pi^{-1/2} v_{\mathrm{T}}^{-1} e^{-(v/v_{\mathrm{T}})^2}$ the integral evaluates to $1/v_{\mathrm{T}}^2$ and we obtain

$$\sqrt{N}\eta_{\mathrm{c}} = \sqrt{\frac{\delta^2 + \kappa^2}{\hbar|\delta|} k_{\mathrm{B}}T}. \quad (10.17)$$

10.2 Drift and diffusion coefficients below threshold

10.2.1 Preliminary considerations

In the publication we found the general equation of motion

$$\frac{\partial\langle f\rangle}{\partial t} = \frac{1}{m}\frac{\partial}{\partial v}\overline{\left\langle \frac{\mathrm{d}\delta U}{\mathrm{d}x}\delta f\right\rangle}. \tag{10.18}$$

Upon a Fourier transformation of the field and the distribution function the appearing correlation function reads

$$\begin{aligned}\frac{1}{m}\overline{\left\langle \frac{\mathrm{d}\delta U}{\mathrm{d}x}\delta f\right\rangle} &= \frac{\hbar k\eta}{2m}\sum_{n,n'=\pm1}\langle(\delta\alpha+\delta\alpha^*)\delta\varphi_{n'}\rangle\,\frac{1}{L}\int_0^L e^{ikx(n+n')}\mathrm{d}x = \\ &= \frac{\hbar k\eta}{2m}\sum_{n,n'=\pm1}\langle(\delta\alpha+\delta\alpha^*)\delta\varphi_{n'}\rangle\,\delta_{n,-n'} = \\ &= \frac{\hbar k\eta}{2m}\sum_{n=\pm1}\langle(\delta\alpha+\delta\alpha^*)\delta\varphi_{-n}\rangle = \\ &= \frac{\hbar k\eta}{m}\,\mathrm{Re}\,\langle(\delta\alpha+\delta\alpha^*)\delta\varphi_1\rangle\,. \end{aligned} \tag{10.19}$$

10.2.2 Calculation of the friction and diffusion coefficients

The equation of motion for the field fluctuations is

$$\frac{\mathrm{d}}{\mathrm{d}t}\delta\alpha = (i\delta-\kappa)\delta\alpha - \frac{NL\eta}{2}\int_{-\infty}^{\infty}\mathrm{d}v\,[\delta\varphi_1-\delta\varphi_{-1}] + \sqrt{\kappa}\,\xi \tag{10.20}$$

and the Fourier components of the density fluctuations fulfil the linearised Vlasov equation [10.1]

$$\frac{\partial}{\partial t}\delta\varphi_n + ikvn\delta\varphi_n = \frac{\hbar k\eta}{2m}(\delta\alpha+\delta\alpha^*)\frac{\partial}{\partial v}\langle f\rangle\,. \tag{10.21}$$

We perform a Laplace transformation

$$\delta\hat{\varphi}_n(s) := \int_0^\infty \delta\varphi_n(t)e^{-st}\mathrm{d}t \tag{10.22}$$

to obtain

$$\delta\hat{\varphi}_n(s) = \frac{\delta\varphi_n(0)}{s+ikvn} + \frac{\hbar k\eta}{2m}\frac{\langle f'\rangle}{s+ikvn}\left[\delta\hat{\alpha}(s)+\delta\hat{\alpha}^*(s)\right] \tag{10.23}$$

and (ignoring the cavity input noise for the beginning)

$$\delta\hat{\alpha}(s)+\delta\hat{\alpha}^*(s) = \frac{i\delta\eta}{D(s)}I(s). \tag{10.24}$$

Here we have defined

$$I(s) := NL \int_{-\infty}^{\infty} \mathrm{d}v \left(\frac{\delta\varphi_1(0)}{s + ikv} - \frac{\delta\varphi_{-1}(0)}{s - ikv} \right) \tag{10.25}$$

and the dispersion relation (cf. also equation (10.9))

$$D(s) = (s + \kappa)^2 + \delta^2 - i\delta \frac{\hbar k N \eta^2 L}{2m} \int_{-\infty}^{\infty} \mathrm{d}v \left(\frac{\partial_v \langle f \rangle}{s + ikv} - \frac{\partial_v \langle f \rangle}{s - ikv} \right). \tag{10.26}$$

Note the important relation

$$D(s^*) = D^*(s). \tag{10.27}$$

The initial distribution fluctuations can be expressed with the help of the Klimontovich distribution [10.2] (cf. also equation (9.4)),

$$\delta f(x, v, 0) = f_{\mathrm{K}}(x, v, 0) - \langle f(x, v, 0) \rangle = \frac{1}{N} \sum_l \delta(x - x_{l0}) \delta(v - v_{l0}) - \langle f(x, v, 0) \rangle . \tag{10.28}$$

Its Fourier components are

$$\delta\varphi_n(0) = \frac{1}{NL} \sum_l \delta(v - v_{l0}) e^{-ikx_{l0}n} - \langle f(0) \rangle \, \delta_{n,0}. \tag{10.29}$$

The last term gives no contribution as we are solely interested in $n = \pm 1 \neq 0$. Hence, equation (10.25) evaluates to

$$I(s) = \sum_l \left(\frac{e^{-ikx_{l0}}}{s + ikv_{l0}} - \frac{e^{ikx_{l0}}}{s - ikv_{l0}} \right). \tag{10.30}$$

We now transform the equations back into t-space by applying the relation

$$\frac{1}{2\pi i} \int \mathrm{d}s \, e^{st} \bullet \to \sum_{s_k} \mathrm{Res} \, \bullet|_{s_k} \, e^{s_k t}, \tag{10.31}$$

where $\{s_k\}$ are the poles of the function being Laplace transformed. Note that the poles of $D(s)$ have negative real part (i.e. $\langle f \rangle$ is Vlasov-stable) and thus their contributions vanish for $t \to \infty$ [10.1]. For the particles we find from (10.23)

$$\delta\varphi_n(t) =: \delta\varphi_n^1(t) + \delta\varphi_n^2(t), \tag{10.32}$$

with

$$\delta\varphi_n^1(t) := \frac{1}{NL} \sum_l \delta(v - v_{l0}) e^{-ikn(x_{l0} + vt)} \tag{10.33a}$$

and

$$\delta\varphi_n^2(t) := ic\langle f'\rangle \sum_l \frac{1}{ik}\frac{e^{-ikx_{l0}}}{v_{l0}-vn}\left\{\frac{e^{-ikvnt}}{D(-ikvn)} - \frac{e^{-ikv_{l0}t}}{D(-ikv_{l0})}\right\} + \\ + ic\langle f'\rangle \sum_l \frac{1}{ik}\frac{e^{ikx_{l0}}}{v_{l0}+vn}\left\{\frac{e^{-ikvnt}}{D(-ikvn)} - \frac{e^{ikv_{l0}t}}{D(ikv_{l0})}\right\}. \quad (10.33b)$$

Here we have defined

$$c := \frac{\hbar k\eta}{2m}\delta\eta. \quad (10.34)$$

It is easy to check that the symmetry condition $\left(\delta\varphi_1^{1,2}\right)^* \equiv \delta\varphi_{-1}^{1,2}$ for the Fourier coefficients is still fulfilled. Analogous, the field transformed back into the time domain reads

$$\delta\alpha(t) + \delta\alpha^*(t) = i\delta\eta 2i\sum_j \beta_j(t) = -2\delta\eta\sum_j \beta_j(t) \quad (10.35)$$

with

$$\beta_j(t) := \mathrm{Im}\left(\frac{e^{-ik(x_{j0}+v_{j0}t)}}{D\left(-ikv_{j0}\right)}\right). \quad (10.36)$$

In order to find the evolution equation (10.18) for $\langle f\rangle$ we need to calculate the correlation function (10.19) for large times (the fluctuations are assumed to evolve much faster than the mean values as detailed in the preciding publication, cf. also [10.2]). To this end it is convenient to define

$$\mathcal{C} := \lim_{t\to\infty}\frac{1}{m}\overline{\left\langle\frac{\mathrm{d}\delta U}{\mathrm{d}x}\delta f\right\rangle} = \frac{\hbar k\eta}{m}\,\mathrm{Re}\,\langle(\delta\alpha+\delta\alpha^*)\delta\varphi_1\rangle =: \mathcal{C}_1+\mathcal{C}_2, \quad (10.37)$$

where $\mathcal{C}_1$ and $\mathcal{C}_2$ correspond to the two contributions (10.32). They contain expressions of the form

$$\left\langle(\delta\alpha+\delta\alpha^*)\delta\varphi_n^i\right\rangle = -2\delta\eta\left\langle\sum_i \beta_i(t)\delta\varphi_1^i(t)\right\rangle. \quad (10.38)$$

Hence we have to evaluate

$$\left\langle\sum_i \beta_i(t)\delta\varphi_1(t)\right\rangle =: C_1+C_2, \quad (10.39)$$

where the average is defined as

$$\langle\bullet\rangle = \prod_i\int \mathrm{d}x_{i0}\int \mathrm{d}v_{i0}\,\langle f(v_{i0})\rangle\,\bullet\,. \quad (10.40)$$

Evaluation of these integrals (the details can be found in section 10.2.3) for

$$C_1 := \frac{1}{NL}\left\langle \sum_j \beta_j(t) \sum_l \delta(v - v_{l0}) e^{-ikx_{l0}} \right\rangle e^{-ikvt} \tag{10.41}$$

yields

$$C_1 = \frac{i}{2}\langle f(v)\rangle \frac{1}{D(ikv)} \equiv \frac{i}{2}\langle f(v)\rangle \frac{D(-ikv)}{|D(ikv)|^2}. \tag{10.42}$$

Hence, the first part of the correlation function $\mathcal{C}$ defined in equation (10.37) reads

$$\begin{aligned}
\mathcal{C}_1 &= \frac{\hbar k\eta}{m} \operatorname{Re}\left\langle (\delta\alpha + \delta\alpha^*)\delta\varphi_1^1 \right\rangle = \\
&= \frac{\hbar k\eta}{m}(-2\eta\delta) \operatorname{Re} C_1 = \\
&= \frac{\hbar k\delta\eta^2}{m}\langle f(v)\rangle \frac{1}{|D(ikv)|^2} \operatorname{Im}\left[D(-ikv)\right] = \\
&= \frac{\hbar k\delta\eta^2}{m}\frac{\langle f(v)\rangle}{|D(ikv)|^2}\left\{-2\kappa kv - \frac{\hbar\delta N\eta^2 L\pi}{2m}\left[\langle f'(v)\rangle - \langle f'(-v)\rangle\right]\right\}.
\end{aligned} \tag{10.43}$$

Here we have used that the imaginary part of the dispersion relation for $s = \gamma + i\omega$ reads (cf. equation (10.13b))

$$\begin{aligned}
\lim_{\operatorname{Re} s \downarrow 0} \operatorname{Im}(D(s)) &= 2\kappa \operatorname{Im} s - \frac{\hbar\delta N\eta^2 L\pi}{2m}\left[\left\langle f'\left(-\frac{\operatorname{Im} s}{k}\right)\right\rangle - \left\langle f'\left(\frac{\operatorname{Im} s}{k}\right)\right\rangle\right] = \\
&= 2\kappa\omega - \frac{\hbar\delta N\eta^2 L\pi}{2m}\left[\left\langle f'\left(-\frac{\omega}{k}\right)\right\rangle - \left\langle f'\left(\frac{\omega}{k}\right)\right\rangle\right].
\end{aligned} \tag{10.44}$$

Now we have to compute the second part of the correlation function which contains C_2. After some lengthy calculation (the details are again presented in the following section 10.2.3) we find

$$\operatorname{Re}\left\langle (\delta\alpha + \delta\alpha^*)\delta\varphi_1^2 \right\rangle = \frac{\hbar\delta^2 k\eta^3}{2m}\langle f'\rangle \frac{NL\pi}{k}\left[\frac{\langle f(-v)\rangle}{|D(ikv)|^2} + \frac{\langle f(v)\rangle}{|D(ikv)|^2}\right] \tag{10.45}$$

and thus

$$\begin{aligned}
\mathcal{C}_2 &= \frac{\hbar k\eta}{m} \operatorname{Re}\left\langle (\delta\alpha + \delta\alpha^*)\delta\varphi_1^2 \right\rangle = \\
&= \frac{\hbar^2\delta^2 k\eta^4 NL\pi}{2m^2}\langle f'(v)\rangle \frac{1}{|D(ikv)|^2}\left[\langle f(v)\rangle + \langle f(-v)\rangle\right].
\end{aligned} \tag{10.46}$$

Hence the correlation function reads

$$\mathcal{C} = \frac{-2\hbar\delta\kappa\eta^2k^2v}{m}\frac{\langle f(v)\rangle}{|D(ikv)|^2} - \\ - \frac{\hbar^2\delta^2k\eta^4NL\pi}{2m^2}\frac{\langle f(v)\rangle}{|D(ikv)|^2}\left[\langle f'(v)\rangle - \langle f'(-v)\rangle\right] + \\ + \frac{\hbar^2\delta^2k\eta^4NL\pi}{2m^2}\frac{\langle f'(v)\rangle}{|D(ikv)|^2}\left[\langle f(v)\rangle + \langle f(-v)\rangle\right]. \quad (10.47)$$

For symmetric distributions, $\langle f(-v)\rangle = \langle f(v)\rangle \Rightarrow \langle f'(-v)\rangle = -\langle f'(v)\rangle$, this result simplifies considerably to

$$\mathcal{C} = \frac{-2\hbar k\delta\kappa\eta^2}{m}\frac{kv}{|D(ikv)|^2}\langle f(v)\rangle. \quad (10.48)$$

So far we have ignored any contribution stemming from the random input noise. Including it yields an additional term

$$\delta\hat{\alpha}_2(s) + \delta\hat{\alpha}_2^*(s) = \frac{s+\kappa+i\delta}{D(s)}\sqrt{\kappa}\,\hat{\xi}(s) + \frac{s+\kappa-i\delta}{D(s)}\sqrt{\kappa}\,\hat{\xi}^*(s) \quad (10.49)$$

for the field in equation (10.24). Using the Fourier representation of the white noise process,

$$\xi(t) = \frac{1}{2\pi}\int_{-\infty}^{\infty}\tilde{\xi}(\omega)e^{i\omega t}\mathrm{d}\omega, \quad (10.50)$$

with $\left\langle\tilde{\xi}(\omega)\tilde{\xi}^*(\omega')\right\rangle = 2\pi\delta(\omega-\omega')$ [10.3], we find the representation

$$\hat{\xi}(s) = \frac{1}{2\pi}\int_{-\infty}^{\infty}\xi(\omega)\frac{1}{s-i\omega}\mathrm{d}\omega. \quad (10.51)$$

The back-transformation of equation (10.49) into t-space reads

$$\delta\alpha_2(t) + \delta\alpha_2^*(t) = \\ = \frac{\sqrt{\kappa}}{2\pi}\int_{-\infty}^{\infty}\left(\frac{i\omega+\kappa+i\delta}{D(i\omega)}\tilde{\xi}(\omega)e^{i\omega t} + \frac{-i\omega+\kappa-i\delta}{D(-i\omega)}\tilde{\xi}^*(\omega)e^{-i\omega t}\right)\mathrm{d}\omega. \quad (10.52)$$

The particle mode (10.32) gets an additional contribution

$$\delta\hat{\varphi}_n^3(s) := \frac{\hbar k\eta}{2m}\frac{\langle f'\rangle}{s+ikvn}\left[\delta\hat{\alpha}_2(s) + \delta\hat{\alpha}_2^*(s)\right] \quad (10.53)$$

due to the cavity input noise. Transformed back to t-space using equations (10.51) and (10.31), this contribution evaluates to

$$\begin{aligned}\delta\varphi_n^3(t) = &\frac{\hbar k\eta|n|}{2m}\left\langle f'\right\rangle\frac{\sqrt{\kappa}}{2\pi}\int_{-\infty}^{\infty}\mathrm{d}\omega\xi(\omega)\frac{i\omega+\kappa+i\delta}{D(i\omega)(i\omega+ikvn)}e^{i\omega t}+\\ &+\frac{\hbar k\eta}{2m}\left\langle f'\right\rangle\frac{\sqrt{\kappa}}{2\pi}\int_{-\infty}^{\infty}\mathrm{d}\omega\xi(\omega)\frac{-ikv+\kappa+i\delta}{D(-ikvn)(-ikv-i\omega)}e^{-ikvnt}+\\ &+\frac{\hbar k\eta}{2m}\left\langle f'\right\rangle\frac{\sqrt{\kappa}}{2\pi}\int_{-\infty}^{\infty}\mathrm{d}\omega\xi^*(\omega)\frac{-i\omega+\kappa-i\delta}{D(-i\omega)(-i\omega+ikvn)}e^{-i\omega t}+\\ &+\frac{\hbar k\eta}{2m}\left\langle f'\right\rangle\frac{\sqrt{\kappa}}{2\pi}\int_{-\infty}^{\infty}\mathrm{d}\omega\xi^*(\omega)\frac{-ikv+\kappa-i\delta}{D(-ikvn)(-ikv+i\omega)}e^{-ikvnt}. \qquad (10.54)\end{aligned}$$

Again, we have ignored the poles of the dispersion relation as they give rise to exponentially damped contributions and we are only interested in the long-time behaviour on the time scale of the fluctuations. The expression (10.54) introduces an additional contribution

$$C_3 := \left\langle(\delta\alpha_2(t)+\delta\hat{\alpha}_2^*(t))\delta\varphi_n^3(t)\right\rangle \qquad (10.55)$$

to the correlation function (10.37). We find (the details can be found in the following section 10.2.3)

$$\begin{aligned}C_3 &= \frac{\hbar k\eta\kappa}{2m}\left\langle f'\right\rangle\frac{i}{2\pi}\left(-i\pi\frac{|ikvn+\kappa+i\delta|^2}{|D(ikvn)|^2}-i\pi\frac{|ikvn+\kappa-i\delta|^2}{|D(ikvn)|^2}\right)=\\ &= \frac{\hbar k\eta\kappa}{2m}\left\langle f'\right\rangle\frac{\kappa^2+\delta^2+k^2v^2n^2}{|D(ikvn)|^2}. \qquad (10.56)\end{aligned}$$

This expression allows us to evaluate the additional part $\mathcal{C}_3$ of the correlation function $\mathcal{C}$ defined in equation (10.37),

$$\mathcal{C}_3 = \frac{\hbar k\eta}{m}\,\mathrm{Re}(C_3) = \frac{\hbar^2k^2\eta^2\kappa}{2m^2}\frac{\kappa^2+\delta^2+k^2v^2}{|D(ikv)|^2}\left\langle f'\right\rangle. \qquad (10.57)$$

Summarising, the evolution equation (10.18) for $\langle f(v,t)\rangle$ reads

$$\frac{\partial}{\partial t}\left\langle f(v,t)\right\rangle + \frac{\partial}{\partial v}\left(A[\langle f\rangle]\left\langle f(v,t)\right\rangle\right) = \frac{\partial}{\partial v}\left(B[\langle f\rangle]\frac{\partial}{\partial v}\left\langle f(v,t)\right\rangle\right), \qquad (10.58)$$

with the coefficients

$$A[\langle f\rangle] := \frac{2\hbar k\delta\kappa\eta^2}{m}\frac{kv}{|D(ikv)|^2} \qquad (10.59a)$$

$$B[\langle f\rangle] := \frac{\hbar^2k^2\eta^2\kappa}{2m^2}\frac{\kappa^2+\delta^2+k^2v^2}{|D(ikv)|^2}. \qquad (10.59b)$$

Note that (10.58) is a non-linear equation since these coefficients depend on the phase-space distribution function through the dispersion relation

$$\operatorname{Re} D(ikv) = -k^2v^2 + \delta^2 + \kappa^2 + \hbar\delta\frac{NL\eta^2}{m}\operatorname{vp}\int_{-\infty}^{\infty}\mathrm{d}v'\frac{v'\partial_{v'}\langle f(v')\rangle}{v^2 - v'^2} \tag{10.60a}$$

$$\operatorname{Im} D(ikv) = 2\kappa kv + \hbar\delta\frac{NL\eta^2}{m}\pi\frac{\partial\langle f(v)\rangle}{\partial v}. \tag{10.60b}$$

Recasting the equation of motion (10.58) into the standard Fokker–Planck form yields

$$\frac{\partial}{\partial t}\langle f(v,t)\rangle = -\frac{\partial}{\partial v}\Big(\Big[A[\langle f\rangle] + \partial_v B[\langle f\rangle]\Big]\langle f(v,t)\rangle\Big) + \frac{1}{2}\frac{\partial^2}{\partial v^2}\Big(\Big[2B[\langle f\rangle]\Big]\langle f(v,t)\rangle\Big). \tag{10.61}$$

10.2.3 Evaluation of the correlation integrals

First contribution

Let us first evaluate C_1, which is defined as

$$C_1 := \frac{1}{NL}\left\langle\sum_j \beta_j(t)\sum_l \delta(v - v_{l0})e^{-ikx_{l0}}\right\rangle e^{-ikvt}. \tag{10.62}$$

Inserting equation (10.36) yields

$$C_1 = \frac{e^{-ikvt}}{2iNL}\left\langle\sum_j\left\{\frac{e^{-ik(x_{j0}+v_{j0}t)}}{D\left(-ikv_{j0}\right)} - \frac{e^{ik(x_{j0}+v_{j0}t)}}{D\left(ikv_{j0}\right)}\right\}\sum_l \delta(v - v_{l0})e^{-ikx_{l0}}\right\rangle. \tag{10.63}$$

Assuming initially uncorrelated particles, we have

$$\left\langle e^{-ikx_{l0}}e^{-ik'x_{j0}}g(v_{l0})h(v_{j0})\right\rangle = L\delta_{lj}\delta_{k,-k'}\int_{-\infty}^{\infty}\mathrm{d}v_{l0}\,\langle f(v_{l0})\rangle\, g(v_{l0})h(v_{l0}). \tag{10.64}$$

Applying this to our problem yields two terms, one proportional to $\delta_{k,k}$ and one $\propto \delta_{k,-k}$. The latter gives no contribution. Hence we find

$$C_1 = -\frac{e^{-ikvt}}{2iNL}L\sum_l\int_{-\infty}^{\infty}\mathrm{d}v_{l0}\,\langle f(v_{l0})\rangle\,\frac{e^{ikv_{l0}t}}{D\left(ikv_{l0}\right)}\delta(v - v_{l0}). \tag{10.65}$$

Since v_{l0} is only a dummy variable of integration the same integral appears N times and we obtain

$$C_1 = \frac{i}{2}\langle f(v)\rangle\,\frac{D\left(-ikv\right)}{\left|D\left(ikv\right)\right|^2}. \tag{10.66}$$

Here we have made use of the property (10.27) of the dispersion relation.

Second contribution

For C_2 the same arguments apply. Moreover, all integrals must be interpreted as Cauchy principal value integrals to give them a proper meaning. We also can immediately omit parts of the integral that are imaginary because only $\mathrm{Re}(C_2)$ is needed at the end. Let us elaborate on this. We have to evaluate

$$\begin{aligned} C_2 &= \lim_{t\to\infty} \left\langle \sum_j \beta_j(t)\delta\varphi_1^2(t) \right\rangle = \\ &= \lim_{t\to\infty} \frac{1}{2i} \left\langle \sum_j \left\{ \frac{e^{-ik(x_{j0}+v_{j0}t)}}{D\left(-ikv_{j0}\right)} - \frac{e^{ik(x_{j0}+v_{j0}t)}}{D\left(ikv_{j0}\right)} \right\} \delta\varphi_1^2(t) \right\rangle, \end{aligned} \tag{10.67}$$

with, from equation (10.33b),

$$\begin{aligned} \delta\varphi_1^2(t) := ic\left\langle f'\right\rangle \sum_l \frac{1}{ik}\frac{e^{-ikx_{l0}}}{v_{l0}-v} \left\{ \frac{e^{-ikvt}}{D(-ikv)} - \frac{e^{-ikv_{l0}t}}{D(-ikv_{l0})} \right\} + \\ + ic\left\langle f'\right\rangle \sum_i \frac{1}{ik}\frac{e^{ikx_{l0}}}{v_{l0}+v} \left\{ \frac{e^{-ikvt}}{D(-ikv)} - \frac{e^{ikv_{l0}t}}{D(ikv_{l0})} \right\}. \end{aligned} \tag{10.68}$$

By inserting this expression into the equation for C_2 and by using equation (10.64) we find

$$\begin{aligned} C_2 = \frac{icNL}{2}\left\langle f'\right\rangle \mathrm{vp}\int_{-\infty}^{\infty} \mathrm{d}v' \frac{e^{ikv't}}{D\left(ikv'\right)} \frac{1}{kv'-kv} \left\{ \frac{e^{-ikvt}}{D(-ikv)} - \frac{e^{-ikv't}}{D(-ikv')} \right\} - \\ - \frac{icNL}{2}\left\langle f'\right\rangle \mathrm{vp}\int_{-\infty}^{\infty} \mathrm{d}v' \frac{e^{-ikv't}}{D\left(-ikv'\right)} \frac{1}{kv'+kv} \left\{ \frac{e^{-ikvt}}{D(-ikv)} + \frac{e^{ikv't}}{D(ikv')} \right\} \end{aligned} \tag{10.69}$$

and further

$$\begin{aligned} C_2 = \frac{icNL}{2}\left\langle f'\right\rangle \frac{e^{-ikvt}}{D(-ikv)} \mathrm{vp}\int_{-\infty}^{\infty} \mathrm{d}v' \left\langle f(v')\right\rangle \frac{e^{ikv't}}{D\left(ikv'\right)\left(kv'-kv\right)} - \\ - \frac{icNL}{2}\left\langle f'\right\rangle \mathrm{vp}\int_{-\infty}^{\infty} \mathrm{d}v' \left\langle f(v')\right\rangle \frac{1}{\left|D\left(ikv'\right)\right|^2}\frac{1}{kv'-kv} - \\ - \frac{icNL}{2}\left\langle f'\right\rangle \frac{e^{-ikvt}}{D(-ikv)} \mathrm{vp}\int_{-\infty}^{\infty} \mathrm{d}v' \left\langle f(v')\right\rangle \frac{e^{-ikv't}}{D\left(-ikv'\right)\left(kv'+kv\right)} + \\ + \frac{icNL}{2}\left\langle f'\right\rangle \mathrm{vp}\int_{-\infty}^{\infty} \mathrm{d}v' \left\langle f(v')\right\rangle \frac{1}{\left|D\left(ikv'\right)\right|^2}\frac{1}{kv'+kv}. \end{aligned} \tag{10.70}$$

The second and the fourth line can be ignored as they give a purely imaginary contribution and we are only interested in the real part. The remaining integrals are

evaluated using the residual theorem (noting again that the poles of the dispersion relation do not contribute to the integral in the limit $t \to \infty$) and give

$$C_2 = -\frac{cNL\pi}{2k} \langle f' \rangle \frac{1}{|D(ikv)|^2} \left(\langle f(v) \rangle + \langle f(-v) \rangle \right). \tag{10.71}$$

Hence we obtain the required correlation function

$$\begin{aligned} \mathrm{Re} \left\langle (\delta\alpha + \delta\alpha^*) \delta\varphi_1^2 \right\rangle &= -2\delta\eta \,\mathrm{Re}\, C_2 = \\ &= \frac{\hbar\delta^2\eta^3 NL\pi}{2m} \langle f' \rangle \frac{1}{|D(ikv)|^2} \left(\langle f(v) \rangle + \langle f(-v) \rangle \right). \end{aligned} \tag{10.72}$$

Contribution from the noise

By inserting the field (10.52) and the particle mode (10.54) into the correlation function (10.55) and by making use of the correlation properties of the white noise process [10.3] we find

$$\begin{aligned} C_3 = &\frac{\hbar k\eta\kappa}{2m} \frac{\langle f' \rangle}{2\pi} \,\mathrm{vp} \int_{-\infty}^{\infty} \mathrm{d}\omega \frac{i\omega + \kappa + i\delta}{D(i\omega)} \frac{-i\omega + \kappa - i\delta}{D(-i\omega)(-i\omega + ikvn)} + \\ &+ \frac{\hbar k\eta\kappa}{2m} \frac{\langle f' \rangle}{2\pi} \,\mathrm{vp} \int_{-\infty}^{\infty} \mathrm{d}\omega \frac{i\omega + \kappa + i\delta}{D(i\omega)} e^{i\omega t} \frac{-ikv + \kappa - i\delta}{D(-ikvn)(-ikv + i\omega)} e^{-ikvnt} + \\ &+ \frac{\hbar k\eta\kappa}{2m} \frac{\langle f' \rangle}{2\pi} \,\mathrm{vp} \int_{-\infty}^{\infty} \mathrm{d}\omega \frac{-i\omega + \kappa - i\delta}{D(-i\omega)} \frac{i\omega + \kappa + i\delta}{D(i\omega)(i\omega + ikvn)} + \\ &+ \frac{\hbar k\eta\kappa}{2m} \frac{\langle f' \rangle}{2\pi} \,\mathrm{vp} \int_{-\infty}^{\infty} \mathrm{d}\omega \frac{-i\omega + \kappa - i\delta}{D(-i\omega)} e^{-i\omega t} \frac{-ikv + \kappa + i\delta}{D(-ikvn)(-ikv - i\omega)} e^{-ikvnt}, \end{aligned} \tag{10.73}$$

where vp denotes the Cauchy principal value. Rearranging yields

$$\begin{aligned} C_3 = &\frac{\hbar k\eta\kappa}{2m} \frac{\langle f' \rangle}{2\pi} \,\mathrm{vp} \int_{-\infty}^{\infty} \mathrm{d}\omega \frac{\kappa^2 + (\omega + \delta)^2}{|D(i\omega)|^2} \frac{i}{\omega - kvn} + \\ &+ \frac{\hbar k\eta\kappa}{2m} \frac{\langle f' \rangle}{2\pi} i \frac{-ikv + \kappa - i\delta}{D(-ikvn)} e^{-ikvnt} \,\mathrm{vp} \int_{-\infty}^{\infty} \mathrm{d}\omega \frac{i\omega + \kappa + i\delta}{D(i\omega)(kv - \omega)} e^{i\omega t} + \\ &+ \frac{\hbar k\eta\kappa}{2m} \frac{\langle f' \rangle}{2\pi} \,\mathrm{vp} \int_{-\infty}^{\infty} \mathrm{d}\omega \frac{\kappa^2 + (\omega + \delta)^2}{|D(i\omega)|^2} \frac{-i}{\omega + kvn} + \\ &+ \frac{\hbar k\eta\kappa}{2m} \frac{\langle f' \rangle}{2\pi} i \frac{-ikv + \kappa + i\delta}{D(-ikvn)} e^{-ikvnt} \,\mathrm{vp} \int_{-\infty}^{\infty} \mathrm{d}\omega \frac{-i\omega + \kappa - i\delta}{D(-i\omega)(kv + \omega)} e^{-i\omega t}. \end{aligned} \tag{10.74}$$

As before we can ignore the first and the third line because they are purely imaginary and only the real part of C_3 is needed. The remaining integrals are again computed

using the residual theorem and give

$$C_3 = \frac{\hbar k\eta\kappa}{2m}\langle f'\rangle \frac{i}{2\pi}\left(-i\pi\frac{|ikvn+\kappa+i\delta|^2}{|D(ikvn)|^2} - i\pi\frac{|ikvn+\kappa-i\delta|^2}{|D(ikvn)|^2}\right) = \\ = \frac{\hbar k\eta\kappa}{2m}\langle f'\rangle \frac{\kappa^2+\delta^2+k^2v^2}{|D(ikvn)|^2}. \tag{10.75}$$

10.3 Trap frequency and critical exponent

In the publication in chapter 9 we found the trap frequency $\omega_0^2 = 4\eta\omega_\mathrm{R}\,\mathrm{Re}\,\alpha$ in steady state. To evaluate it self-consistently we compute $\mathrm{Re}\,\alpha$ from $\dot{\alpha}=0$ and find

$$\mathrm{Re}\,\alpha = \frac{-N\eta|\delta|}{\kappa^2+\delta^2}\Theta \tag{10.76}$$

with $\Theta := \langle\sin(kx)\rangle = \int f(x)\sin(kx)\mathrm{d}x$. As pointed out in the publication the particle distribution is thermal above steady state so that in harmonic oscillator approximation we have

$$f(x) \propto \exp\left(-\frac{U(x)}{k_\mathrm{B}T}\right) = \exp\left(-\frac{2\hbar\eta\,\mathrm{Re}\,\alpha\left[-1+\frac{1}{2}\left(kx-\frac{3\pi}{2}\right)^2\right]}{k_\mathrm{B}T}\right). \tag{10.77}$$

Hence the order parameter Θ evaluates to

$$\Theta = \int\left[-1+\frac{1}{2}\left(kx-\frac{3\pi}{2}\right)^2\right]f(x)\mathrm{d}x = -1+\frac{k_\mathrm{B}T}{4\hbar\eta\,\mathrm{Re}\,\alpha} \equiv -1+\frac{k_\mathrm{B}T}{\hbar\omega_0^2}\omega_\mathrm{R}. \tag{10.78}$$

Inserting this expression into equation (10.76) yields

$$\mathrm{Re}\,\alpha = \frac{N\eta|\delta|}{\kappa^2+\delta^2}\left(1-\frac{k_\mathrm{B}T}{\hbar\omega_0^2}\omega_\mathrm{R}\right) = \\ = \frac{N\eta|\delta|}{\kappa^2+\delta^2}\left(1-\frac{\kappa^2+\delta^2+4\omega_0^2}{4|\delta|\omega_0^2}\omega_\mathrm{R}\right) = \\ = \frac{\sqrt{N}}{2}\frac{\eta}{\eta_\mathrm{c}}\left(1-\frac{\omega_\mathrm{R}}{|\delta|}-\frac{\sqrt{N}\eta_\mathrm{c}}{2\omega_0^2}\omega_\mathrm{R}\right), \tag{10.79}$$

where we have used the steady-state temperature

$$k_\mathrm{B}T = \hbar\frac{\kappa^2+\delta^2+4\omega_0^2}{4|\delta|} \tag{10.80}$$

and the critical pump strength

$$\sqrt{N}\eta_\mathrm{c} = \frac{\kappa^2 + \delta^2}{2|\delta|}. \tag{10.81}$$

The latter is valid for $\omega_\mathrm{R}/|\delta| \ll 1$, therefore we set $1 - \omega_\mathrm{R}/|\delta| \simeq 1$ in (10.79). Replacing $\mathrm{Re}\,\alpha = \omega_0^2/4\eta\omega_\mathrm{R}$ we find

$$\omega_0^2 = 2\sqrt{N}\eta\omega_\mathrm{R}\frac{\eta}{\eta_\mathrm{c}}\left(1 - \frac{\sqrt{N}\eta_\mathrm{c}}{2\omega_0^2}\omega_\mathrm{R}\right) \tag{10.82}$$

and thus

$$\omega_0^2 = \sqrt{N}\eta\omega_\mathrm{R}\left(\frac{\eta}{\eta_\mathrm{c}} \pm \sqrt{\frac{\eta^2}{\eta_\mathrm{c}^2} - 1}\right). \tag{10.83}$$

As the solution is valid for the strongly organised phase where $\eta \gg \eta_\mathrm{c}$, only the "+"-sign needs to be kept.

For the critical exponent one principally makes the same steps as before with the phase space distribution

$$f(x,v) = \exp\left(-\frac{\frac{mv^2}{2} + 2\hbar\eta\,\mathrm{Re}\,\alpha\sin(kx)}{k_\mathrm{B}T}\right), \tag{10.84}$$

which is expanded up to $\mathcal{O}\left([\mathrm{Re}\,\alpha]^3\right)$. One finds

$$\Theta \simeq 2\sqrt{\frac{\eta}{\eta_\mathrm{c}} - 1} \tag{10.85}$$

and thus a critical exponent of 1/2.

Chapter 11

Publication

New Journal of Physics **14**, 053031 (2012)

Cooperative self-organization and sympathetic cooling of a multispecies gas in a cavity[†]

Tobias Grießer, Wolfgang Niedenzu and Helmut Ritsch

Institut für Theoretische Physik, Universität Innsbruck, Technikerstraße 25, 6020 Innsbruck, Austria

We study the dynamics of a multispecies mixture of laser-illuminated polarizable particles moving inside an optical resonator. Above a certain pump threshold the collective enhanced scattering of laser light into the cavity induces a phase transition from a homogeneous spatial distribution to a common crystalline order. We analytically show that adding particles of any mass and temperature always strictly lowers the minimum pump power required for self-ordering and trapping. This allows to capture and trap new species of atoms, molecules or even polarizable nanoparticles in combination with proven examples, for which a high phase-space density is readily available. Cooperative light scattering mediates effective energy exchange and thus sympathetic cooling between different species without the need of direct collisional interaction. The predicted ordering thresholds and cooling timescales are in range of current technology for particles with a wide range of mass, polarizability and initial temperature.

URL: `http://iopscience.iop.org/1367-2630/14/5/053031`
DOI: 10.1088/1367-2630/14/5/053031
PACS: 42.25.Fx, 37.10.De, 42.25.Ja

[†]The primary contribution of the author of the present thesis to this publication was the implementation and the analysis of the numerical simulations. He also contributed to the analytical calculations and acted as a discussion partner on all other aspects of the work. T. G. performed the majority of the analytical calculations.

11.1 Introduction

Laser light induced forces are routinely used to manipulate polarizable particles from atoms and molecules [11.1] to larger objects such as nanoparticles, micro beads or even protozoae [11.2]. Laser trapping and cooling, however, is limited to a finite class of atomic species, very few kinds of molecules [11.3] or isolated vibration modes of nanomechanical objects [11.4]. Cooling requires specific setups with specifically chosen laser frequencies and configurations for any species, so that their number only slowly increases with time [11.5].

In principle, self-organization and cooling by coherent light-scattering in cavities gives a general alternative to trap and cool any kind of polarizable particles within an optical resonator [11.6–11.8]. In practice, however, the required phase-space densities and laser intensities have so far only been achieved for atomic ensembles [11.9–11.11], where theoretical expectations of fast sub-Doppler cooling were even surpassed [11.12], but the required phase-space density to achieve self-ordering and trapping has not been reached for molecules or nanoparticles [11.7, 11.13].

As solution we propose to put ensembles of different species simultaneously into the same optical resonator. We predict that under suitable conditions all species are simultaneously trapped and cooled using only a single laser frequency and optical resonator. Our central claim is that the simultaneous presence of any additional species always increases the collective light scattering and improves trapping and cooling. As a particularly interesting case we study a mixture of a dense atomic ensemble with a smaller ensemble of heavier molecules or nanoparticles. Even when it is impossible to reach the self-organization threshold for the latter alone, combined trapping and sympathetic cooling can be readily achieved in cooperation with the atoms. Due to the nonlocal interaction the different particles might even be located at different regions within the cavity. This setup opens up a novel way of simultaneous multispecies trapping and cooling without the need of a tailored laser configuration for each species. This can be improved further, using several cavity modes simultaneously [11.7].

11.2 Model

Consider a dilute classical gas consisting of S kinds of N_s polarizable point particles of mass m_s within the overlap region of a high-Q optical resonator and a standing-wave pump laser tuned close to resonance with a cavity mode (figure 11.1). The particles scatter light into and out of the cavity mode and the resulting interference pattern creates dynamical optical potentials guiding the particle motion. For simplicity we approximate pump and cavity field in the interaction region by plane standing waves and consider motion along the cavity axis only. This suffices to describe the

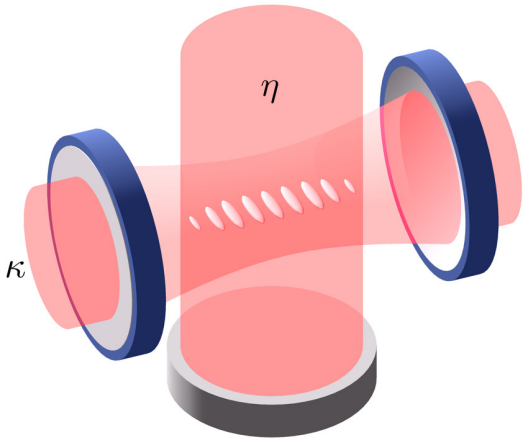

Figure 11.1: Ensembles of particles within a cavity illuminated transversely by a standing wave laser resonant with the cavity. Above threshold the particles order in regular tubes optimizing Bragg scattering into the mode.

essential physics of self-organization and cooling [11.9, 11.14, 11.15]. A practical experimental implementation can be envisaged by confining the particles by two crossed standing-wave pump lasers into a lattice of one-dimensional (1D) tubes along the cavity axis [11.8, 11.16]. Extension to 3D motion and field geometries are straightforward and are expected to induce only minor quantitative changes [11.15]. In terms of the effective pump amplitudes η_s, the light shifts per photon $U_{0,s}$, and the semi-classical cavity mode amplitude a, the optical potentials along the cavity axis are given by [11.14]

$$\Phi_s(x, a, a^*) = \hbar\eta_s\,(a + a^*)\sin(kx) + \hbar U_{0,s}|a|^2\sin^2(kx), \tag{11.1}$$

which lead to the one-body Hamiltonian functions $H_s(x, p, a, a^*) = \frac{p^2}{2m_s} + \Phi_s(x, a, a^*)$, determining the dynamics of an individual particle belonging to the sth species through the canonical equations of motion [11.17]. H_s depends parametrically on the cavity field amplitude a, which in turn is driven by the light scattered collectively by all the particles and by white noise ξ, modeling vacuum fluctuations. As detailed in refs. [11.18, 11.19], for a statistical treatment of the dynamics it is convenient to redefine the state of the particles of the sth species $\{x_{j_s}(t), p_{j_s}(t)\}$ in terms of the Klimontovich distribution [11.20]

$$f^s_{\mathrm{K}}(x, p, t) := \frac{1}{N_s}\sum_{j_s=1}^{N_s}\delta(x - x_{j_s}(t))\delta(p - p_{j_s}(t)). \tag{11.2}$$

Then the mode amplitude evolves according to

$$\dot{a} = (i\Delta_\mathrm{c} - \kappa)a - \frac{i}{\hbar}\sum_{s=1}^{S} N_s \int \frac{\partial H_s}{\partial a^*} f_\mathrm{K}^s(x,p,t)\mathrm{d}x\mathrm{d}p + \sqrt{\kappa}\xi, \tag{11.3}$$

where κ denotes the cavity decay rate and $\Delta_\mathrm{c} = \omega_\mathrm{p} - \omega_\mathrm{c}$ the detuning between pump- and cavity frequency. We decompose the Klimontovich distribution according to $f_\mathrm{K}^s(x,p,t) = f_s(x,p,t) + \delta f_s(x,p,t)$, where $f_s(x,p,t) := \langle f_\mathrm{K}^s(x,p,t)\rangle$, averaged over an ensemble of suitable initial conditions and the realizations of the white noise, is called one-body distribution function. Note that $f_s(x,p,t)\mathrm{d}x\mathrm{d}p$ is equal to the expected fraction of particles of the sth species in a phase space volume $\mathrm{d}x\mathrm{d}p$ around the point (x,p) at time t and the average over its fluctuations vanishes, $\langle \delta f_s(x,p,t)\rangle \equiv 0$. Likewise we decompose the mode amplitude into $a = \alpha + \delta a$, where $\alpha = \langle a\rangle$. The one-body distribution function exactly satisfies

$$\frac{\partial f_s}{\partial t} + \frac{p}{m_s}\frac{\partial f_s}{\partial x} - \frac{\partial \langle \Phi_s\rangle}{\partial x}\frac{\partial f_s}{\partial p} = \left\langle \frac{\partial \delta\Phi_s}{\partial x}\frac{\partial \delta f_s}{\partial p}\right\rangle, \tag{11.4}$$

in which predominantly the rhs describes statistical correlations. For $N_s \to \infty$ these tend to zero and we recover the Vlasov (or mean-field) kinetic theory. There, $\langle \Phi_s(x,a,a^*)\rangle$ is replaced by $\Phi_s(x,\alpha,\alpha^*)$ and the rhs of (11.4) is set to zero, such that spatially homogeneous particle distributions scatter no light into the mode and constitute an equilibrium state at zero cavity field [11.19].

11.3 Multispecies self-organization threshold

Following [11.19], the multispecies self-organization threshold is obtained as the boundary of dynamical stability of spatially uniform distributions in case of negative effective detuning $\delta := \Delta_\mathrm{c} - \frac{1}{2}\sum_s N_s U_{0,s} < 0$, by an analysis of the linearized Vlasov equation [11.21]. For convenience we rescale the uniform equilibrium distributions as $f_{0,s}(p) = (L m_s v_s)^{-1} G_s\left(\frac{p}{m_s v_s}\right)$ in terms of a typical velocity v_s and the cavity length L. Assuming a strictly monotonous decrease in $|p|$, as fulfilled by all relevant distributions (e.g. Gaussian, Bose–Einstein, q-Gaussian, etc.), a given set of spatially homogeneous distributions is unstable if and only if

$$\sum_{s=1}^{S} \frac{N_s \eta_s^2}{k_\mathrm{B} T_s}\left(\mathrm{P}\int_{-\infty}^{\infty} \frac{-1}{2u}\frac{\mathrm{d}G_s}{\mathrm{d}u}\mathrm{d}u\right) > \frac{\kappa^2+\delta^2}{\hbar|\delta|}, \tag{11.5}$$

with $k_\mathrm{B}T_s = m_s v_s^2/2$ and P the Cauchy principal value. For thermal (i.e. Gaussian) momentum distributions the integral in (11.5) is unity and the threshold condition assumes the simple form

$$\sum_{s=1}^{S} \frac{N_s \eta_s^2}{k_\mathrm{B} T_s} > \frac{\kappa^2+\delta^2}{\hbar|\delta|}. \tag{11.6}$$

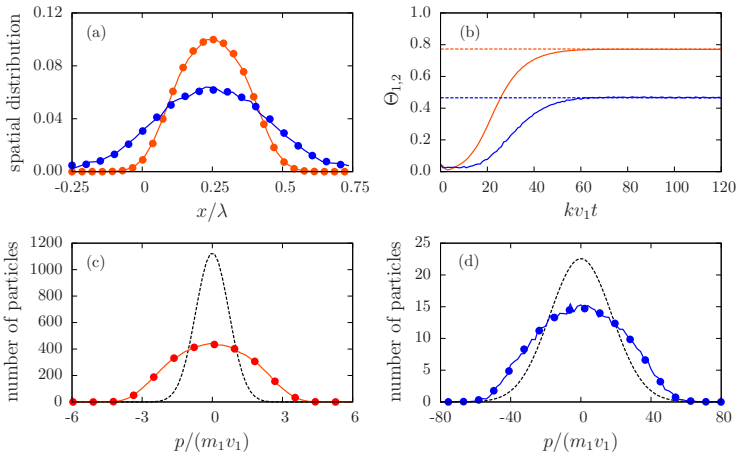

Figure 11.2: Concurrent self-organization of two species, initialized above the combined threshold. Species one (orange) is initialized well above, species two (blue) far below its proper threshold. (a) Final position distributions (periodic boundary conditions). (c,d) Initial (dashed) and self-organized (solid) momentum distributions obtained from numerical stochastic particle simulations (stochastic differential equations, SDEs) [11.18]. Circles: theoretical predictions obtained from Vlasov kinetic theory assuming the adiabatic invariance of the action variables (11.9) as in [11.22]. (b) Growth of the order parameters $\Theta_s = |\int f_s \sin(kx)\mathrm{d}x\mathrm{d}p|$ to predicted values. Parameters: $N_1 = 10^4$, $N_2 = 500$, $m_2 = 10m_1$, $k_\mathrm{B}T_1 = 10^4\hbar\kappa$, $k_\mathrm{B}T_2 = 2.5 \times 10^5\hbar\kappa$, $\eta_1 = 2.4\kappa$, $\eta_2 = 27.4\kappa$ and recoil frequency $\omega_\mathrm{R} = 10^{-2}\kappa$.

This threshold formula is one of the central results of the present work. Above threshold, density perturbations and the electric field amplitude grow exponentially and evolve, if the light shift is not too large, i.e. $N_s|U_{0,s}|\left(1+\sum_{s'\neq s}\frac{N_{s'}\eta_{s'}}{N_s\eta_s}\right) \lesssim |\delta|$ for all species, towards an ordered quasi-stationary state (figure 11.2) with growth exponent $\gamma > 0$ fulfilling

$$(\gamma+\kappa)^2+\delta^2 = \sum_{s=1}^{S}\frac{N_s\eta_s^2\hbar\delta}{2k_\mathrm{B}T_s}\int_{-\infty}^{\infty}\frac{u\mathrm{d}G_s/\mathrm{d}u}{(\gamma/kv_s)^2+u^2}\mathrm{d}u. \tag{11.7}$$

Note that, while the rhs of equations (11.5) and (11.6) only depends on cavity parameters, all terms in the sum on the lhs are manifestly positive and proportional to the pump intensity. This has the important consequence that inserting any extra particle species into the cavity will lower the power needed to start the self-organization process, regardless of temperature or polarizability of the added particles. Note that we neglect absorbtion of the pump beam, consistent with our assumption of a dilute and optically thin gas. At higher temperatures, where $(kv_s)^2 \gg \kappa^2+\delta^2$,

the field amplitude's growth rate is, from (11.7), given by

$$\gamma = -\kappa + \left(\sum_{s=1}^{S} \frac{\hbar|\delta|}{k_{\mathrm{B}} T_s} N_s \eta_s^2 - \delta^2 \right)^{1/2}. \tag{11.8}$$

We thus find strong sympathetic enhancement, i.e. the field grows faster the more species contribute such that the required power and time needed for self-organization is lowered by combining several species.

11.4 Long-term dynamics and equilibrium

For a large but finite number of particles, the Vlasov kinetic theory, which neglects all dynamical correlations, provides an accurate description on a time scale essentially fixed by the solution of equation (11.7). The long-term evolution of the system and in particular its statistical equilibrium state are, on the other hand, governed by precisely these correlations [11.18]. In this section we shall deal with this stage of the time evolution in the limit of weak coupling, i.e. $\sum N_s |U_{0,s}| \ll |\Delta_{\mathrm{c}}|$, where we can neglect the terms $\hbar U_{0,s} |a|^2 \sin^2(kx)$ in the optical potentials (11.1), rendering them linear functions of the mode amplitude. We perform, for each species separately, a canonical transformation of variables $(x, p) \to (I_s, \theta_s)$. Here, I_s denotes the one-body action based on the ensemble-averaged Hamiltonian function $\langle H_s(x, p, a, a^*) \rangle \equiv H_s(x, p, \alpha, \alpha^*)$,

$$I_s = \pm \frac{1}{2\pi} \oint \sqrt{2 m_s \left[\langle H_s \rangle - \langle \Phi_s(x') \rangle \right]} \mathrm{d}x' \tag{11.9}$$

and θ_s its canonically conjugate angle variable

$$\theta_s = \frac{\partial S_s}{\partial I_s}, \tag{11.10}$$

obtained from the generating function $S_s = \pm \int^x \sqrt{2 m_s \left[\langle H_s \rangle - \langle \Phi_s(x') \rangle \right]} \mathrm{d}x'$. The reason for doing this is that at the end of the initial, mean-field governed dynamics, the one-particle distributions depend on (x, p) solely through the ensemble-averaged one-body Hamiltonian functions and thus on the actions alone. From that point onwards, they are slowly modified by the dynamical correlations in such a way that the system evolves towards statistical equilibrium in a sequence of mean-field steady states [11.23]

$$f_s(x, p, t) \simeq f_s(I_s, t). \tag{11.11}$$

After a lengthy calculation in theses new variables, the system's long-term evolution can be cast into a set of coupled nonlinear Fokker–Planck equations

$$\frac{\partial f_s}{\partial t} = \frac{\partial}{\partial I_s} \left(A_s f_s + B_s \frac{\partial f_s}{\partial I_s} + \sum_{r=1}^{S} C[f_s, f_r] \right) \tag{11.12}$$

for the distributions. The quasi-stationary ensemble-averaged mode amplitude is determined by the implicit equation

$$\alpha = \frac{2\pi}{\Delta_c + i\kappa} \sum_{s=1}^{S} N_s \eta_s \int f_s(I_s) g_{0,s}(I_s, \alpha) \mathrm{d}I_s, \tag{11.13}$$

wherein

$$g_{n,s}(I_s, \alpha) := \frac{1}{2\pi} \int_0^{2\pi} \sin(kx) e^{-in\theta_s} \mathrm{d}\theta_s. \tag{11.14}$$

The rhs of equation (11.12), describing the redistribution of particles among the orbits, consists of two contributions originating from fluctuations and decay of the mode amplitude

$$A_s[f_s] = -4\hbar\Delta_c \kappa\omega_s \sum_{n=-\infty}^{\infty} \frac{n^2\eta_s^2 |g_{n,s}|^2}{|D(in\omega_s)|^2} \tag{11.15}$$

$$B_s[f_s] = \hbar^2\kappa \sum_{n=-\infty}^{\infty} \frac{n^2\eta_s^2 |g_{n,s}|^2}{|D(in\omega_s)|^2} \left(\kappa^2 + \Delta_c^2 + n^2\omega_s^2\right) \tag{11.16}$$

and a generalized Balescu-Lenard operator [11.24–11.26]

$$C[f_s, f_r] = \sum_{n,m=-\infty}^{\infty} \int w_{nm}(I_s, I_r') \left(n \frac{\partial f_s}{\partial I_s} f_r' - m \frac{\partial f_r}{\partial I_r'} f_s \right) \mathrm{d}I_r', \tag{11.17}$$

where

$$w_{nm}(I_s, I_r') := 8\pi^2\hbar^2\Delta_c^2 N_r \frac{\eta_s^2 |g_{n,s}|^2 \eta_r^2 |g_{m,r}'|^2}{|D(in\omega_s)||D(im\omega_r')|} n\delta\left(n\omega_s - m\omega_r'\right). \tag{11.18}$$

Here, $\omega_s(I_s) = \partial \langle H_s \rangle / \partial I_s$ is the nonlinear orbital frequency and a prime denotes the function at $I_r = I_r'$. For spatially uniform ensembles $I_s \to p/k$ and the expressions for A_s and B_s given in [11.18] are recovered. $D(i\omega)$, here called the dielectric function, is given by

$$D(i\omega) = (i\omega + \kappa)^2 + \Delta_c^2 - 4\pi\hbar\Delta_c \sum_{s=1}^{S} \sum_{n=-\infty}^{\infty} N_s \eta_s^2 \int \frac{\partial f_s}{\partial I_s} \frac{n|g_{n,s}|^2}{\omega + n\omega_s - i0} \mathrm{d}I_s \tag{11.19}$$

and characterizes the system's collective response. Let us remark that the coupled kinetic equations (11.12) constitute another central result of our present work. In their derivation we assumed that the particle distribution functions $f_s(I_s, t)$ are always strongly Vlasov stable. This assumption breaks down close to the self-organization threshold and thus (11.12) is valid only away from the transition point. The interaction contained in the Balescu-Lenard collision operator (11.17) quantifies the energy and momentum exchange between particles of like and different species and

involves orbits I_r, I_s with $n\omega_r = m\omega_s$. In mechanics such orbits with commensurable frequencies are called resonant. The origin of the energy exchange term (11.17) lies in the scattering of laser light into the cavity by a first particle and subsequent backscattering into the laser mode by a second, resonant particle. This is in effect a pair collision albeit entirely nonlocal. The appearance of the dielectric function also reveals that the remaining particles participate collectively as a medium in that process. These quasi-collisions can be used for efficient sympathetic cooling as demonstrated below. The source of the remaining terms in (11.12) involves only single scattering events and subsequent loss through the cavity mirrors. It is worth remarking that the quasi-collision operator (11.17) vanishes for thermal distributions with equal temperatures, and thus the quasi-collisions tend to establish global thermal equilibrium.

Stable equilibria of (11.12) exist only for $\Delta_\mathrm{c} < 0$. Below threshold they are homogeneous with vanishing field and, independent of the number of species, q-Gaussian momentum distributions

$$f_{s,\mathrm{eq}}(p) \propto \exp_{q_s}\left(\frac{-p^2}{2m_s k_\mathrm{B} T}\right), \tag{11.20}$$

where

$$k_\mathrm{B} T := \hbar \frac{\kappa^2 + \Delta_\mathrm{c}^2}{4|\Delta_\mathrm{c}|} \tag{11.21}$$

and

$$\exp_q(u) = \Big[1 + (1-q)u\Big]^{\frac{1}{1-q}} \tag{11.22}$$

is the q-exponential with parameter $q_s = 1 + \omega_{\mathrm{R},s}/|\Delta_\mathrm{c}|$. For $q_s \to 1$ the distribution becomes an ordinary Gaussian. The recoil frequencies are given by $\omega_{\mathrm{R},s} := \hbar k^2/2m_s$ and $k_\mathrm{B} T$ denotes a "thermal" energy with a minimum of $\hbar\kappa/2$ for $\Delta_\mathrm{c} = -\kappa$. The reason for the fact that the equilibrium state of a given species is unaffected by the presence of others is the vanishing of interspecies scattering $C[f_{s,\mathrm{eq}}, f_{r,\mathrm{eq}}] \equiv 0$.

Sufficiently far above threshold the ordered equilibria are well approximated by Maxwell-Boltzmann distributions

$$f_{s,\mathrm{eq}}(x,p) \propto \exp\left(\frac{-H_s}{k_\mathrm{B} T^s_\mathrm{kin}}\right), \tag{11.23}$$

with kinetic temperatures

$$k_\mathrm{B} T^s_\mathrm{kin} := \frac{\langle p^2 \rangle}{m_s} = k_\mathrm{B} T + \frac{\hbar\omega_{0,s}^2}{|\Delta_\mathrm{c}|} \tag{11.24}$$

and trap frequencies $\omega_{0,s}^2 = 4\eta_s \omega_{\mathrm{R},s} |\mathrm{Re}\,\alpha|$ proportional to the cavity field generated commonly by all species. Therefore, unlike below threshold, the equilibrium of a given

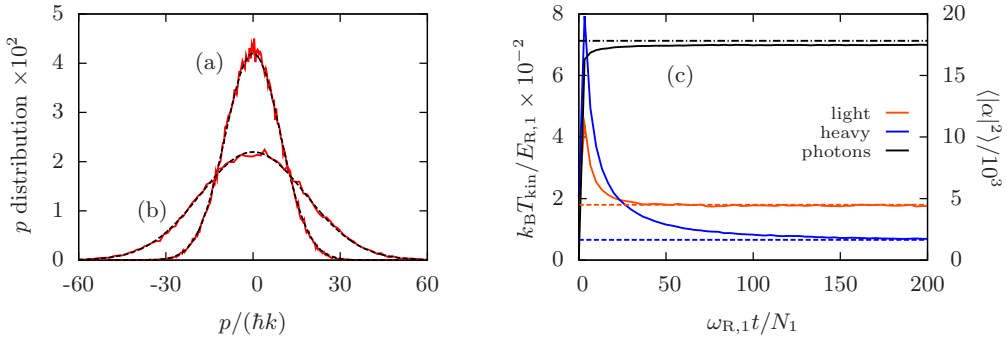

Figure 11.3: Self-organized steady-state momentum distributions of (a) species one and (b) species two with $m_2 = 10m_1$. (c) Kinetic temperatures and the photon number. Dashed lines: theoretical predictions. Dash-dotted line: maximally possible photon number. Parameters: $N_1 = 300$, $N_2 = 200$, $\sqrt{N_1}\eta_1 = \sqrt{N_2}\eta_2 = 600\omega_R$, $\kappa = 100\omega_R$, $\delta = -\kappa$ and $E_{R,1} = \hbar\omega_R$.

species is affected by the presence of the others. Figure 11.3 shows the formation and properties of a two-species self-organized steady state. The initial increase of the kinetic energy originates from the fast growth of the cavity intensity due to instability and is followed by cooling in the trapped state.

11.5 Sympathetic cooling

Most interestingly, the energy exchange between different sorts of particles reduces the cooling time for any species in the presence of another via collisionless sympathetic cooling. At this point it is necessary to clarify the notion of *cooling*. We shall associate with cooling a reduction of the extension of the sth species in one-body phase space. As the quantity $\langle J_s \rangle := \int J_s f_s(I_s) \mathrm{d}I_s$, with $J_s = I_s$ for transient and $J_s = I_s/2$ for trapped orbits, provides a measure of this extension, cooling therefore corresponds to a decrease of $\langle J_s \rangle$.[1] We clearly see that a light species of particles not only assists in trapping heavy particles via self-ordering, but also speeds up cooling. Numerical simulations exhibit an increase of the occupied phase space volume during initial self-trapping if the system starts above threshold (11.5) and there is only a small energy exchange between deeply trapped ensembles if the resonance condition in (11.18) is not satisfied. However, efficient sympathetic cooling can be achieved in any case by initializing the system below threshold, such that interspecies scattering

[1] Let it be remarked that also the Bohr–Sommerfeld correspondence principle between integer multiples of $\hbar$ of the action variable and quantum mechanical energy eigenstates suggests this definition.

can remove energy from the first species. This process continues efficiently until the point of joint self-organization is reached and the lighter particles are trapped. These then provide a continuously deepening potential for the the heavy species, which subsequently gets trapped as well. This process is shown in figure 11.4. For carefully chosen parameters, such that the trap frequencies of the species roughly coincide and thus allow for quasi-collisions even in the self-organized regime, the sympathetic cooling effect persists in principle also above threshold.

Finally, the energy flow per particle from species two to species one, $\dot{Q}_{21}$, for two spatially homogeneous ensembles can, from equation (11.17), be estimated as

$$\dot{Q}_{21} \simeq \frac{2N_1\eta_2^2\eta_1^2\hbar\Delta_\mathrm{c}^2}{(\kappa^2+\Delta_\mathrm{c}^2)^2}\sqrt{\frac{m_1}{m_2}}\sqrt{\frac{\pi\hbar\omega_{\mathrm{R},2}}{k_\mathrm{B}T_1}}\left[1-\frac{T_2}{T_1}\right]\left[1+\frac{m_1T_2}{m_2T_1}\right]^{-\frac{3}{2}}. \tag{11.25}$$

Here we assume that the first species is already cold, i.e. $2k_\mathrm{B}T_1/\hbar\kappa \ll \kappa/\omega_\mathrm{R}$, and far from instability. It is maximal if $\Delta_\mathrm{c} = -\kappa$.

11.6 Conclusions

In summary we have shown that if the self-organization threshold can be reached with a certain species, any species can be added and will be trapped and cooled as well. The final temperatures are only limited by the resonator linewidth and, importantly, the cooling time of a given species can be reduced by means of energy exchange with a second, already colder and lighter species. Because the general effect has successfully been demonstrated in single-species experiments [11.12, 11.27, 11.28], we are confident that the multispecies generalization proposed here is well within reach of current technology. New phases can also be expected in the case of a crystallization of a multispecies quantum gas close to absolute zero [11.29]. We expect that simultaneous additional cooling of one species will help to cool all others.

Acknowledgments

We thank Peter Asenbaum, Nikolai Kiesel and Matthias Sonnleitner for discussions and Andreas Grießer for graphical support on the sketch. We acknowledge support by the Austrian Science Fund FWF through the projects SFB FoQuS P13 and P20391.

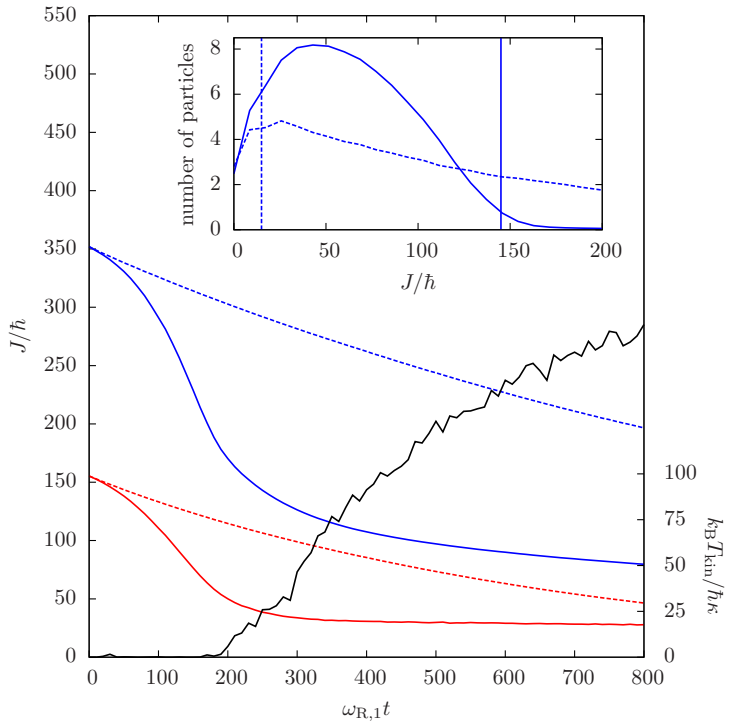

Figure 11.4: Time evolution of the kinetic energy (lower red pair of curves) and phase space volume $\langle J \rangle$ (upper blue pair) of a heavy species alone (dashed lines) and in the presence of a lighter species (solid lines). The rising solid curve depicts the intra-cavity intensity (a.u.) for sympathetic cooling. The threshold and enhanced cooling due to the second species is clearly visible. The inset depicts the distribution of the heavy particles at final time. The vertical lines are the action values separating trapped from untrapped particle orbits. In the case of the presence of the second species, almost all particles are finally trapped, whereas in the other case, almost no particle is trapped. Parameters: $N_1 = 1500$, $N_2 = 100$, $m_2 = 80m_1$, $\sqrt{N_1}\eta_1 = 400\omega_R$, $\sqrt{N_2}\eta_2 = 245\omega_R$, $\kappa = 100\omega_R$ and $\delta = -\kappa$.

Bibliography

References for Chapter 1

[1.1] M. Planck, *Zur Theorie des Gesetzes der Energieverteilung im Normalspectrum*, Verhandl. der Deutschen Physikal. Gesellsch. **2**, 237 (1900).

[1.2] M. Planck, *Ueber das Gesetz der Energieverteilung im Normalspectrum*, Ann. d. Phys. **309**, 553 (1901).

[1.3] A. Einstein, *Über einen die Erzeugung und Verwandlung des Lichtes betreffenden heuristischen Gesichtspunkt*, Ann. d. Phys. **322**, 132 (1905).

[1.4] P. A. M. Dirac, *The Quantum Theory of the Emission and Absorption of Radiation*, Proc. R. Soc. Lond. **114**, 243 (1927).

[1.5] P. A. M. Dirac, *The quantum theory of dispersion*, Proc. R. Soc. Lond. **114**, 710 (1927).

[1.6] E. Fermi, *Quantum Theory of Radiation*, Rev. Mod. Phys. **4**, 87 (1932).

[1.7] F. J. Dyson, *The S Matrix in Quantum Electrodynamics*, Phys. Rev. **75**, 1736 (1949).

[1.8] R. P. Feynman, *Mathematical Formulation of the Quantum Theory of Electromagnetic Interaction*, Phys. Rev. **80**, 440 (1950).

[1.9] R. Frisch, *Experimenteller Nachweis des Einsteinschen Strahlungsrückstoßes*, Zeitschrift für Physik **86**, 42 (1933).

[1.10] T. H. Maiman, *Stimulated Optical Radiation in Ruby*, Nature **187**, 493 (1960).

[1.11] A. L. Schawlow and C. H. Townes, *Infrared and Optical Masers*, Phys. Rev. **112**, 1940 (1958).

[1.12] A. Ashkin, *Trapping of Atoms by Resonance Radiation Pressure*, Phys. Rev. Lett. **40**, 729 (1978).

[1.13] A. Ashkin, *Optical Trapping and Manipulation of Neutral Particles Using Lasers* (World Scientific, Singapore, 2006), First edition.

[1.14] R. Grimm, M. Weidemüller and Y. B. Ovchinnikov, *Optical dipole traps for neutral atoms*, Adv. At. Mol. Opt. Phys. **42**, 95 (2000).

[1.15] H. Yin, M. D. Wang, K. Svoboda, R. Landick, S. M. Block and J. Gelles, *Transcription against an applied force*, Science **270**, 1653 (1995).

[1.16] G. Thalhammer, R. Steiger, S. Bernet and M. Ritsch-Marte, *Optical macro-tweezers: trapping of highly motile micro-organisms*, J. Opt. **13**, 044024 (2011).

[1.17] A. Ashkin, *Atomic-Beam Deflection by Resonance-Radiation Pressure*, Phys. Rev. Lett. **25**, 1321 (1970).

[1.18] T. W. Hänsch and A. L. Schawlow, *Cooling of gases by laser radiation*, Opt. Comm. **13**, 68 (1975).

[1.19] D. Wineland and H. Dehmelt, *Proposed* $10^{14}\Delta\nu/\nu$ *laser fluorescence spectroscopy on* Tl^{+} *mono-ion oscillator*, Bull. Am. Phys. Soc **20**, 637 (1975).

[1.20] J. Dalibard and C. Cohen-Tannoudji, *Laser cooling below the Doppler limit by polarization gradients: simple theoretical models*, J. Opt. Soc. Am. B **6**, 2023 (1989).

[1.21] C. Cohen-Tannoudji and W. D. Phillips, *New mechanisms for laser cooling*, Phys. Today **43**, 33 (1990).

[1.22] S. Chu, *Nobel Lecture: The manipulation of neutral particles*, Rev. Mod. Phys. **70**, 685 (1998).

[1.23] C. Cohen-Tannoudji, *Nobel Lecture: Manipulating atoms with photons*, Rev. Mod. Phys. **70**, 707 (1998).

[1.24] W. D. Phillips, *Nobel Lecture: Laser cooling and trapping of neutral atoms*, Rev. Mod. Phys. **70**, 721 (1998).

[1.25] K. B. Davis, M. O. Mewes, M. R. Andrews, N. J. van Druten, D. S. Durfee, D. M. Kurn and W. Ketterle, *Bose-Einstein Condensation in a Gas of Sodium Atoms*, Phys. Rev. Lett. **75**, 3969 (1995).

[1.26] M. H. Anderson, J. R. Ensher, M. R. Matthews, C. E. Wieman and E. A. Cornell, *Observation of Bose-Einstein condensation in a dilute atomic vapor*, science **269**, 198 (1995).

[1.27] E. A. Cornell and C. E. Wieman, *Nobel Lecture: Bose-Einstein condensation in a dilute gas, the first 70 years and some recent experiments*, Rev. Mod. Phys. **74**, 875 (2002).

[1.28] W. Ketterle, *Nobel lecture: When atoms behave as waves: Bose-Einstein condensation and the atom laser*, Rev. Mod. Phys. **74**, 1131 (2002).

[1.29] A. Einstein, *Quantentheorie des einatomigen idealen Gases, 2. Abhandlung*, in: *Sitzungsberichte der Preussischen Akademie der Wissenschaften. Sitzung der physikalisch-mathematischen Klasse vom 8. Januar* (1925), 3.

[1.30] A. Einstein, *Zur Quantentheorie des idealen Gases*, in: *Sitzungsberichte der Preussischen Akademie der Wissenschaften. Sitzung der physikalisch-mathematischen Klasse vom 29. Januar* (1925), 18.

[1.31] Bose, *Plancks Gesetz und Lichtquantenhypothese*, Zeitschrift für Physik **26**, 178 (1924).

[1.32] F. Pereira Dos Santos, J. Léonard, J. Wang, C. J. Barrelet, F. Perales, E. Rasel, C. S. Unnikrishnan, M. Leduc and C. Cohen-Tannoudji, *Bose-Einstein Condensation of Metastable Helium*, Phys. Rev. Lett. **86**, 3459 (2001).

[1.33] T. Weber, J. Herbig, M. Mark, H.-C. Nägerl and R. Grimm, *Bose-Einstein condensation of cesium*, Science **299**, 232 (2003).

[1.34] S. Sugawa, R. Yamazaki, S. Taie and Y. Takahashi, *Bose-Einstein condensate in gases of rare atomic species*, Phys. Rev. A **84**, 011610 (2011).

[1.35] K. Aikawa, A. Frisch, M. Mark, S. Baier, A. Rietzler, R. Grimm and F. Ferlaino, *Bose-Einstein Condensation of Erbium*, Phys. Rev. Lett. **108**, 210401 (2012).

[1.36] C. Cohen-Tannoudji, *Atomic Motion in Laser Light*, in: *Systèmes Fondamentaux en Optique Quantique/Fundamental Systems in Quantum Optics, Les Houches, session LIII* ed. by J. Dalibard, J. M. Raimond and J. Zinn-Justin (North-Holland, Amsterdam, 1992).

[1.37] I. Bloch, J. Dalibard and W. Zwerger, *Many-body physics with ultracold gases*, Rev. Mod. Phys. **80**, 885 (2008).

[1.38] S. Chu, L. Hollberg, J. E. Bjorkholm, A. Cable and A. Ashkin, *Three-dimensional viscous confinement and cooling of atoms by resonance radiation pressure*, Phys. Rev. Lett. **55**, 48 (1985).

[1.39] D. Jaksch, C. Bruder, J. I. Cirac, C. W. Gardiner and P. Zoller, *Cold Bosonic Atoms in Optical Lattices*, Phys. Rev. Lett. **81**, 3108 (1998).

[1.40] J. Hubbard, *Electron correlations in narrow energy bands*, Proc. R. Soc. Lond. A **276**, 238 (1963).

[1.41] D. Jaksch and P. Zoller, *The cold atom Hubbard toolbox*, Ann. Phys. **315**, 52 (2005).

[1.42] I. Bloch, *Ultracold quantum gases in optical lattices*, Nature Physics **1**, 23 (2005).

[1.43] M. P. A. Fisher, P. B. Weichman, G. Grinstein and D. S. Fisher, *Boson localization and the superfluid-insulator transition*, Phys. Rev. B **40**, 546 (1989).

[1.44] M. Greiner, O. Mandel, T. Esslinger, T. W. Hänsch and I. Bloch, *Quantum phase transition from a superfluid to a Mott insulator in a gas of ultracold atoms*, Nature **415**, 39 (2002).

[1.45] T. Kinoshita, T. Wenger and D. S. Weiss, *Observation of a one-dimensional Tonks-Girardeau gas*, Science **305**, 1125 (2004).

[1.46] B. Paredes, A. Widera, V. Murg, O. Mandel, S. Fölling, I. Cirac, G. V. Shlyapnikov, T. W. Hänsch and I. Bloch, *Tonks–Girardeau gas of ultracold atoms in an optical lattice*, Nature **429**, 277 (2004).

[1.47] E. Haller, R. Hart, M. J. Mark, J. G. Danzl, L. Reichsöllner, M. Gustavsson, M. Dalmonte, G. Pupillo and H.-C. Nägerl, *Pinning quantum phase transition for a Luttinger liquid of strongly interacting bosons*, Nature **466**, 597 (2010).

[1.48] Z. Hadzibabic, P. Krüger, M. Cheneau, B. Battelier and J. Dalibard, *Berezinskii–Kosterlitz–Thouless crossover in a trapped atomic gas*, Nature **441**, 1118 (2006).

[1.49] R. Feynman, *Simulating physics with computers*, Int. J. Theor. Phys. **21**, 467 (1982).

[1.50] J. I. Cirac and P. Zoller, *Quantum Computations with Cold Trapped Ions*, Phys. Rev. Lett. **74**, 4091 (1995).

[1.51] D. Jaksch, H.-J. Briegel, J. I. Cirac, C. W. Gardiner and P. Zoller, *Entanglement of Atoms via Cold Controlled Collisions*, Phys. Rev. Lett. **82**, 1975 (1999).

[1.52] C. A. Muschik, I. de Vega, D. Porras and J. I. Cirac, *Quantum Processing Photonic States in Optical Lattices*, Phys. Rev. Lett. **100**, 063601 (2008).

[1.53] K. Günter, T. Stöferle, H. Moritz, M. Köhl and T. Esslinger, *Bose-Fermi Mixtures in a Three-Dimensional Optical Lattice*, Phys. Rev. Lett. **96**, 180402 (2006).

[1.54] J. M. Hutson, *Ultracold Chemistry*, Science **327**, 788 (2010).

[1.55] J. Ye, H. J. Kimble and H. Katori, *Quantum state engineering and precision metrology using state-insensitive light traps*, Science **320**, 1734 (2008).

[1.56] M. Takamoto, F. L. Hong, R. Higashi and H. Katori, *An optical lattice clock*, Nature **435**, 321 (2005).

[1.57] E. T. Jaynes and F. W. Cummings, *Comparison of quantum and semiclassical radiation theories with application to the beam maser*, Proc. IEEE **51**, 89 (1963).

[1.58] R. J. Thompson, G. Rempe and H. J. Kimble, *Observation of normal-mode splitting for an atom in an optical cavity*, Phys. Rev. Lett. **68**, 1132 (1992).

[1.59] C. J. Hood, M. S. Chapman, T. W. Lynn and H. J. Kimble, *Real-Time Cavity QED with Single Atoms*, Phys. Rev. Lett. **80**, 4157 (1998).

[1.60] C. J. Hood, T. W. Lynn, A. C. Doherty, A. S. Parkins and H. J. Kimble, *The atom-cavity microscope: Single atoms bound in orbit by single photons*, Science **287**, 1447 (2000).

[1.61] P. W. H. Pinkse, T. Fischer, P. Maunz and G. Rempe, *Trapping an atom with single photons*, Nature **404**, 365 (2000).

[1.62] P. W. H. Pinkse, T. Fischer, P. Maunz, T. Puppe and G. Rempe, *How to catch an atom with single photons*, J. Mod. Opt. **47**, 2769 (2000).

[1.63] P. Horak, G. Hechenblaikner, K. M. Gheri, H. Stecher and H. Ritsch, *Cavity-induced atom cooling in the strong coupling regime*, Phys. Rev. Lett. **79**, 4974 (1997).

[1.64] G. Hechenblaikner, M. Gangl, P. Horak and H. Ritsch, *Cooling an atom in a weakly driven high-Q cavity*, Phys. Rev. A **58**, 3030 (1998).

[1.65] M. Gangl and H. Ritsch, *Cold atoms in a high-Q ring cavity*, Phys. Rev. A **61**, 043405 (2000).

[1.66] M. Gangl, P. Horak and H. Ritsch, *Cooling neutral particles in multimode cavities without spontaneous emission*, J. Mod. Opt. **47**, 2741 (2000).

[1.67] P. Horak and H. Ritsch, *Scaling properties of cavity-enhanced atom cooling*, Phys. Rev. A **64**, 033422 (2001).

[1.68] P. Domokos, P. Horak and H. Ritsch, *Semiclassical theory of cavity-assisted atom cooling*, J. Phys. B **34**, 187 (2001).

[1.69] P. Domokos, P. Horak and H. Ritsch, *Semiclassical Theory of Cavity-assisted Light Forces on Atoms and Applications*, Fortschr. Phys. **49**, 935 (2001).

[1.70] P. Domokos and H. Ritsch, *Collective cooling and self-organization of atoms in a cavity*, Phys. Rev. Lett. **89**, 253003 (2002).

[1.71] P. Domokos and H. Ritsch, *Mechanical effects of light in optical resonators*, J. Opt. Soc. Am. B **20**, 1098 (2003).

[1.72] V. Vuletić and S. Chu, *Laser Cooling of Atoms, Ions, or Molecules by Coherent Scattering*, Phys. Rev. Lett. **84**, 3787 (2000).

[1.73] B. L. Lev, A. Vukics, E. R. Hudson, B. C. Sawyer, P. Domokos, H. Ritsch and J. Ye, *Prospects for the cavity-assisted laser cooling of molecules*, Phys. Rev. A **77**, 023402 (2008).

[1.74] P. F. Barker and M. N. Shneider, *Cavity cooling of an optically trapped nanoparticle*, Phys. Rev. A **81**, 023826 (2010).

[1.75] P. Maunz, T. Puppe, I. Schuster, N. Syassen, P. W. H. Pinkse and G. Rempe, *Cavity cooling of a single atom*, Nature **428**, 50 (2004).

[1.76] M. Wolke, J. Klinner, H. Keßler and A. Hemmerich, *Cavity cooling below the recoil limit*, to be published in Science (2012).

[1.77] C. Maschler and H. Ritsch, *Cold Atom Dynamics in a Quantum Optical Lattice Potential*, Phys. Rev. Lett. **95**, 260401 (2005).

[1.78] C. Maschler, H. Ritsch, A. Vukics and P. Domokos, *Entanglement assisted fast reordering of atoms in an optical lattice within a cavity at T=0*, Opt. Comm. **273**, 446 (2007).

[1.79] J. Larson, B. Damski, G. Morigi and M. Lewenstein, *Mott-Insulator States of Ultracold Atoms in Optical Resonators*, Phys. Rev. Lett. **100**, 050401 (2008).

[1.80] C. Maschler, I. B. Mekhov and H. Ritsch, *Ultracold Atoms in Optical Lattices generated by Quantized Light Fields*, Eur. Phys. J. D **46**, 545 (2008).

[1.81] J. Larson, S. Fernández-Vidal, G. Morigi and M. Lewenstein, *Quantum stability of Mott-insulator states of ultracold atoms in optical resonators*, New J. Phys. **10**, 045002 (2008).

[1.82] S. Fernández-Vidal, G. De Chiara, J. Larson and G. Morigi, *Quantum ground state of self-organized atomic crystals in optical resonators*, Phys. Rev. A **81**, 043407 (2010).

[1.83] I. B. Mekhov, C. Maschler and H. Ritsch, *Probing quantum phases of ultracold atoms in optical lattices by transmission spectra in cavity quantum electrodynamics*, Nature Physics **3**, 319 (2007).

[1.84] I. B. Mekhov and H. Ritsch, *Quantum optics with ultracold quantum gases: towards the full quantum regime of the light–matter interaction*, J. Phys. B **45**, 102001 (2012).

[1.85] A. T. Black, H. W. Chan and V. Vuletić, *Observation of Collective Friction Forces due to Spatial Self-Organization of Atoms: From Rayleigh to Bragg Scattering*, Phys. Rev. Lett. **91**, 203001 (2003).

[1.86] J. K. Asbóth, P. Domokos, H. Ritsch and A. Vukics, *Self-organization of atoms in a cavity field: Threshold, bistability, and scaling laws*, Phys. Rev. A **72**, 053417 (2005).

[1.87] K. J. Arnold, M. P. Baden and M. D. Barrett, *Self-Organization Threshold Scaling For Thermal Atoms*, arXiv:1205.4186 [physics.atom-ph] (2012).

References for Chapter 2

[2.1] E. T. Jaynes and F. W. Cummings, *Comparison of quantum and semiclassical radiation theories with application to the beam maser*, Proc. IEEE **51**, 89 (1963).

[2.2] L. Bergmann and C. Schaefer, *Optics of waves and particles* (Walter de Gruyter, Berlin, 1999).

[2.3] M. Orszag, *Quantum Optics* (Springer-Verlag, Berlin Heidelberg, 2000), First edition.

[2.4] R. J. Thompson, G. Rempe and H. J. Kimble, *Observation of normal-mode splitting for an atom in an optical cavity*, Phys. Rev. Lett. **68**, 1132 (1992).

[2.5] P. Horak, G. Hechenblaikner, K. M. Gheri, H. Stecher and H. Ritsch, *Cavity-induced atom cooling in the strong coupling regime*, Phys. Rev. Lett. **79**, 4974 (1997).

[2.6] G. Hechenblaikner, M. Gangl, P. Horak and H. Ritsch, *Cooling an atom in a weakly driven high-Q cavity*, Phys. Rev. A **58**, 3030 (1998).

[2.7] P. Domokos and H. Ritsch, *Mechanical effects of light in optical resonators*, J. Opt. Soc. Am. B **20**, 1098 (2003).

[2.8] D. F. Walls and G. J. Milburn, *Quantum Optics* (Springer-Verlag, Berlin, 1994), First edition.

[2.9] C. W. Gardiner and P. Zoller, *Quantum Noise* (Springer-Verlag, Berlin, 2000), Second edition.

[2.10] A. Kossakowski, *On quantum statistical mechanics of non-Hamiltonian systems*, Rep. Math. Phys. **3**, 247 (1972).

[2.11] G. Lindblad, *On the generators of quantum dynamical semigroups*, Commun. Math. Phys. **48**, 119 (1976).

[2.12] Bose, *Plancks Gesetz und Lichtquantenhypothese*, Zeitschrift für Physik **26**, 178 (1924).

[2.13] J. Dalibard, Y. Castin and K. Mølmer, *Wave-function approach to dissipative processes in quantum optics*, Phys. Rev. Lett. **68**, 580 (1992).

[2.14] R. Dum, P. Zoller and H. Ritsch, *Monte Carlo simulation of the atomic master equation for spontaneous emission*, Phys. Rev. A **45**, 4879 (1992).

[2.15] K. Mølmer, Y. Castin and J. Dalibard, *Monte Carlo wave-function method in quantum optics*, J. Opt. Soc. Am. B **10**, 524 (1993).

[2.16] H. Carmichael, *An Open System Approach to Quantum Optics* (Springer-Verlag, Berlin Heidelberg, 1993), First edition.

[2.17] A. Vukics, C. Maschler and H. Ritsch, *Microscopic physics of quantum self-organization of optical lattices in cavities*, New J. Phys. **9**, 255 (2007).

[2.18] A. Vukics and H. Ritsch, *C++QED: an object-oriented framework for wavefunction simulations of cavity QED systems*, Eur. Phys. J. D **44**, 585 (2007).

[2.19] A. Vukics, *C++QEDv2: The multi-array concept and compile-time algorithms in the definition of composite quantum systems*, Computer Physics Communications **183**, 1381 (2012).

[2.20] D. Jaksch, C. Bruder, J. I. Cirac, C. W. Gardiner and P. Zoller, *Cold Bosonic Atoms in Optical Lattices*, Phys. Rev. Lett. **81**, 3108 (1998).

[2.21] D. Jaksch and P. Zoller, *The cold atom Hubbard toolbox*, Ann. Phys. **315**, 52 (2005).

[2.22] I. Bloch, J. Dalibard and W. Zwerger, *Many-body physics with ultracold gases*, Rev. Mod. Phys. **80**, 885 (2008).

[2.23] C. Maschler and H. Ritsch, *Cold Atom Dynamics in a Quantum Optical Lattice Potential*, Phys. Rev. Lett. **95**, 260401 (2005).

[2.24] C. Maschler, I. B. Mekhov and H. Ritsch, *Ultracold Atoms in Optical Lattices generated by Quantized Light Fields*, Eur. Phys. J. D **46**, 545 (2008).

[2.25] J. Larson, S. Fernández-Vidal, G. Morigi and M. Lewenstein, *Quantum stability of Mott-insulator states of ultracold atoms in optical resonators*, New J. Phys. **10**, 045002 (2008).

[2.26] S. Fernández-Vidal, G. De Chiara, J. Larson and G. Morigi, *Quantum ground state of self-organized atomic crystals in optical resonators*, Phys. Rev. A **81**, 043407 (2010).

[2.27] I. B. Mekhov and H. Ritsch, *Quantum optics with ultracold quantum gases: towards the full quantum regime of the light–matter interaction*, J. Phys. B **45**, 102001 (2012).

[2.28] P. Horak and H. Ritsch, *Scaling properties of cavity-enhanced atom cooling*, Phys. Rev. A **64**, 033422 (2001).

[2.29] C. Cohen-Tannoudji, *Atomic Motion in Laser Light*, in: *Systèmes Fondamentaux en Optique Quantique/Fundamental Systems in Quantum Optics, Les Houches, session LIII* ed. by J. Dalibard, J. M. Raimond and J. Zinn-Justin (North-Holland, Amsterdam, 1992).

[2.30] P. Domokos, T. Salzburger and H. Ritsch, *Dissipative motion of an atom with transverse coherent driving in a cavity with many degenerate modes*, Phys. Rev. A **66**, 043406 (2002).

[2.31] W. D. Phillips, *Nobel Lecture: Laser cooling and trapping of neutral atoms*, Rev. Mod. Phys. **70**, 721 (1998).

[2.32] B. L. Lev, A. Vukics, E. R. Hudson, B. C. Sawyer, P. Domokos, H. Ritsch and J. Ye, *Prospects for the cavity-assisted laser cooling of molecules*, Phys. Rev. A **77**, 023402 (2008).

[2.33] P. Maunz, T. Puppe, I. Schuster, N. Syassen, P. W. H. Pinkse and G. Rempe, *Cavity cooling of a single atom*, Nature **428**, 50 (2004).

References for Chapter 3

[3.1] J.-L. Basdevant and J. Dalibard, *Quantum Mechanics* (Springer-Verlag, Berlin Heidelberg, 2002), First edition.

[3.2] F. Bloch, *Über die Quantenmechanik der Elektronen in Kristallgittern*, Zeitschrift für Physik **52**, 555 (1929).

[3.3] I. Bloch, J. Dalibard and W. Zwerger, *Many-body physics with ultracold gases*, Rev. Mod. Phys. **80**, 885 (2008).

[3.4] R. Schulze, *Cold Atoms in a Ring-Cavity Generated Optical Lattice*, Diploma thesis, University of Innsbruck, 2009.

[3.5] G. H. Wannier, *The Structure of Electronic Excitation Levels in Insulating Crystals*, Phys. Rev. **52**, 191 (1937).

[3.6] W. Kohn, *Analytic Properties of Bloch Waves and Wannier Functions*, Phys. Rev. **115**, 809 (1959).

[3.7] J. Hubbard, *Electron correlations in narrow energy bands*, Proc. R. Soc. Lond. A **276**, 238 (1963).

[3.8] M. P. A. Fisher, P. B. Weichman, G. Grinstein and D. S. Fisher, *Boson localization and the superfluid-insulator transition*, Phys. Rev. B **40**, 546 (1989).

[3.9] D. Jaksch, C. Bruder, J. I. Cirac, C. W. Gardiner and P. Zoller, *Cold Bosonic Atoms in Optical Lattices*, Phys. Rev. Lett. **81**, 3108 (1998).

[3.10] W. Zwerger, *Mott–Hubbard transition of cold atoms in optical lattices*, J. Opt. B **5**, S9 (2003).

[3.11] M. Greiner, O. Mandel, T. Esslinger, T. W. Hänsch and I. Bloch, *Quantum phase transition from a superfluid to a Mott insulator in a gas of ultracold atoms*, Nature **415**, 39 (2002).

[3.12] F. Schwabl, *Quantenmechanik für Fortgeschrittene (QM II)* (Springer-Verlag, Berlin, 2008), Fifth edition.

[3.13] C. J. Pethick and H. Smith, *Bose–Einstein Condensation in Dilute Gases* (Cambridge University Press, Cambridge, 2002).

[3.14] D. Jaksch and P. Zoller, *The cold atom Hubbard toolbox*, Ann. Phys. **315**, 52 (2005).

[3.15] C. Cohen-Tannoudji, J. Dupont-Roc and G. Grynberg, *Photons and Atoms: Introduction to Quantum Electrodynamics* (Wiley, New York, 1989).

[3.16] D. F. Walls and G. J. Milburn, *Quantum Optics* (Springer-Verlag, Berlin, 1994), First edition.

[3.17] C. Cohen-Tannoudji, J. Dupont-Roc and G. Grynberg, *Atom-Photon Interactions: Basic Processes and Applications* (Wiley-VCH Verlag, Weinheim, 2004).

[3.18] C. W. Gardiner and P. Zoller, *Quantum Noise* (Springer-Verlag, Berlin, 2000), Second edition.

[3.19] M. J. Mark, E. Haller, K. Lauber, J. G. Danzl, A. J. Daley and H.-C. Nägerl, *Precision Measurements on a Tunable Mott Insulator of Ultracold Atoms*, Phys. Rev. Lett. **107**, 175301 (2011).

[3.20] F. Gerbier and Y. Castin, *Heating rates for an atom in a far-detuned optical lattice*, Phys. Rev. A **82**, 013615 (2010).

[3.21] H. Pichler, A. J. Daley and P. Zoller, *Nonequilibrium dynamics of bosonic atoms in optical lattices: Decoherence of many-body states due to spontaneous emission*, Phys. Rev. A **82**, 063605 (2010).

References for Chapter 4

[4.1] L. Bergmann and C. Schaefer, *Optics of waves and particles* (Walter de Gruyter, Berlin, 1999).

[4.2] P. Domokos and H. Ritsch, *Mechanical effects of light in optical resonators*, J. Opt. Soc. Am. B **20**, 1098 (2003).

[4.3] J. D. Jackson, *Classical Electrodynamics* (Wiley, New York, 1999), Third edition.

[4.4] M. Gangl and H. Ritsch, *Cold atoms in a high-Q ring cavity*, Phys. Rev. A **61**, 043405 (2000).

[4.5] M. Gangl, P. Horak and H. Ritsch, *Cooling neutral particles in multimode cavities without spontaneous emission*, J. Mod. Opt. **47**, 2741 (2000).

[4.6] P. Domokos, T. Salzburger and H. Ritsch, *Dissipative motion of an atom with transverse coherent driving in a cavity with many degenerate modes*, Phys. Rev. A **66**, 043406 (2002).

[4.7] D. Kruse, M. Ruder, J. Benhelm, C. von Cube, C. Zimmermann, P. W. Courteille, T. Elsässer, B. Nagorny and A. Hemmerich, *Cold atoms in a high-Q ring cavity*, Phys. Rev. A **67**, 051802 (2003).

[4.8] B. Nagorny, T. Elsässer, H. Richter, A. Hemmerich, D. Kruse, C. Zimmermann and P. Courteille, *Optical lattice in a high-finesse ring resonator*, Phys. Rev. A **67**, 031401 (2003).

[4.9] P. Domokos, P. Horak and H. Ritsch, *Semiclassical theory of cavity-assisted atom cooling*, J. Phys. B **34**, 187 (2001).

[4.10] D. Jaksch, C. Bruder, J. I. Cirac, C. W. Gardiner and P. Zoller, *Cold Bosonic Atoms in Optical Lattices*, Phys. Rev. Lett. **81**, 3108 (1998).

[4.11] C. Maschler and H. Ritsch, *Cold Atom Dynamics in a Quantum Optical Lattice Potential*, Phys. Rev. Lett. **95**, 260401 (2005).

[4.12] C. Maschler, H. Ritsch, A. Vukics and P. Domokos, *Entanglement assisted fast reordering of atoms in an optical lattice within a cavity at $T=0$*, Opt. Comm. **273**, 446 (2007).

[4.13] J. Larson, B. Damski, G. Morigi and M. Lewenstein, *Mott-Insulator States of Ultracold Atoms in Optical Resonators*, Phys. Rev. Lett. **100**, 050401 (2008).

[4.14] C. Maschler, I. B. Mekhov and H. Ritsch, *Ultracold Atoms in Optical Lattices generated by Quantized Light Fields*, Eur. Phys. J. D **46**, 545 (2008).

[4.15] J. Larson, S. Fernández-Vidal, G. Morigi and M. Lewenstein, *Quantum stability of Mott-insulator states of ultracold atoms in optical resonators*, New J. Phys. **10**, 045002 (2008).

[4.16] S. Fernández-Vidal, G. De Chiara, J. Larson and G. Morigi, *Quantum ground state of self-organized atomic crystals in optical resonators*, Phys. Rev. A **81**, 043407 (2010).

References for Chapter 5

[5.1] D. Jaksch, C. Bruder, J. I. Cirac, C. W. Gardiner and P. Zoller, *Cold Bosonic Atoms in Optical Lattices*, Phys. Rev. Lett. **81**, 3108 (1998).

[5.2] D. Jaksch and P. Zoller, *The cold atom Hubbard toolbox*, Ann. Phys. **315**, 52 (2005).

[5.3] I. Bloch, J. Dalibard and W. Zwerger, *Many-body physics with ultracold gases*, Rev. Mod. Phys. **80**, 885 (2008).

[5.4] M. Lewenstein, L. Santos, M. A. Baranov and H. Fehrmann, *Atomic Bose-Fermi Mixtures in an Optical Lattice*, Phys. Rev. Lett. **92**, 050401 (2004).

[5.5] J. K. Asboth, H. Ritsch and P. Domokos, *Collective excitations and instability of an optical lattice due to unbalanced pumping*, Phys. Rev. Lett. **98**, 203008 (2007).

[5.6] P. Domokos and H. Ritsch, *Mechanical effects of light in optical resonators*, J. Opt. Soc. Am. B **20**, 1098 (2003).

[5.7] P. Horak and H. Ritsch, *Dissipative dynamics of Bose condensates in optical cavities*, Phys. Rev. A **63**, 023603 (2001).

[5.8] T. Bourdel, T. Donner, S. Ritter, A. Öttl, M. Köhl and T. Esslinger, *Cavity QED detection of interfering matter waves*, Phys. Rev. A **73**, 43602 (2006).

[5.9] Y. Colombe, T. Steinmetz, G. Dubois, F. Linke, D. Hunger and J. Reichel, *Strong atom–field coupling for Bose–Einstein condensates in an optical cavity on a chip*, Nature **450**, 272 (2007).

[5.10] S. Gupta, K. L. Moore, K. W. Murch and D. M. Stamper-Kurn, *Cavity nonlinear optics at low photon numbers from collective atomic motion*, Phys. Rev. Lett. **99**, 213601 (2007).

[5.11] K. Baumann, C. Guerlin, F. Brennecke and T. Esslinger, *Dicke quantum phase transition with a superfluid gas in an optical cavity*, Nature **464**, 1301 (2010).

[5.12] D. Nagy, G. Kónya, G. Szirmai and P. Domokos, *Dicke-Model Phase Transition in the Quantum Motion of a Bose-Einstein Condensate in an Optical Cavity*, Phys. Rev. Lett. **104**, 130401 (2010).

[5.13] D. Meiser, J. Ye and M. J. Holland, *Spin squeezing in optical lattice clocks via lattice-based QND measurements*, New J. Phys. **10**, 073014 (2008).

[5.14] C. Maschler and H. Ritsch, *Cold Atom Dynamics in a Quantum Optical Lattice Potential*, Phys. Rev. Lett. **95**, 260401 (2005).

[5.15] C. Maschler, I. B. Mekhov and H. Ritsch, *Ultraold Atoms in Optical Lattices generated by Quantized Light Fields*, Eur. Phys. J. D **46**, 545 (2008).

[5.16] J. Larson, S. Fernández-Vidal, G. Morigi and M. Lewenstein, *Quantum stability of Mott-insulator states of ultracold atoms in optical resonators*, New J. Phys. **10**, 045002 (2008).

[5.17] R. J. Schulze, C. Genes and H. Ritsch, *Optomechanical approach to cooling of small polarizable particles in a strongly pumped ring cavity*, Phys. Rev. A **81**, 063820 (2010).

[5.18] C. Maes, J. K. Asbóth and H. Ritsch, *Self ordering threshold and superradiant backscattering to slow a fast gas beam in a ring cavity with counter propagating pump*, Opt. Express **15**, 6019 (2007).

[5.19] J. Klinner, M. Lindholdt, B. Nagorny and A. Hemmerich, *Normal Mode Splitting and Mechanical Effects of an Optical Lattice in a Ring Cavity*, Phys. Rev. Lett. **96**, 023002 (2006).

[5.20] S. Slama, S. Bux, G. Krenz, C. Zimmermann and P. W. Courteille, *Superradiant Rayleigh Scattering and Collective Atomic Recoil Lasing in a Ring Cavity*, Phys. Rev. Lett. **98**, 053603 (2007).

[5.21] G. Hechenblaikner, M. Gangl, P. Horak and H. Ritsch, *Cooling an atom in a weakly driven high-Q cavity*, Phys. Rev. A **58**, 3030 (1998).

[5.22] M. Gangl and H. Ritsch, *Cold atoms in a high-Q ring cavity*, Phys. Rev. A **61**, 043405 (2000).

[5.23] D. Kruse, M. Ruder, J. Benhelm, C. von Cube, C. Zimmermann, P. W. Courteille, T. Elsässer, B. Nagorny and A. Hemmerich, *Cold atoms in a high-Q ring cavity*, Phys. Rev. A **67**, 51802 (2003).

[5.24] D. Meiser, J. Ye and M. Holland, *Combining lattice clocks with cavity QED: Prospects for a mHz-linewidth laser*, in: *APS Meeting Abstracts* (2009), 1121.

[5.25] R. Bonifacio, *Photon statistics and quantum fluctuations in a Collective Atomic Recoil Laser (CARL)*, Opt. Comm. **146**, 236 (1998).

[5.26] T. Grießer, H. Ritsch, M. Hemmerling and G. R. M. Robb, *A Vlasov approach to bunching and selfordering of particles in optical resonators*, Eur. Phys. J. D **58**, 349 (2010).

[5.27] M. G. Moore, O. Zobay and P. Meystre, *Quantum optics of a Bose-Einstein condensate coupled to a quantized light field*, Phys. Rev. A **60**, 1491 (1999).

[5.28] K. Zhang, W. Chen and P. Meystre, *Dynamics of a bistable Mott insulator to superfluid phase transition in cavity optomechanics*, Opt. Comm. **283**, 665 (2009).

[5.29] J. Larson, B. Damski, G. Morigi and M. Lewenstein, *Mott-Insulator States of Ultracold Atoms in Optical Resonators*, Phys. Rev. Lett. **100**, 050401 (2008).

[5.30] J. Larson and M. Lewenstein, *Dilute gas of ultracold two-level atoms inside a cavity: generalized Dicke model*, New J. Phys. **11**, 063027 (2009).

[5.31] C. Maschler, H. Ritsch, A. Vukics and P. Domokos, *Entanglement assisted fast reordering of atoms in an optical lattice within a cavity at T=0*, Opt. Comm. **273**, 446 (2007).

[5.32] A. Vukics, W. Niedenzu and H. Ritsch, *Cavity nonlinear optics with few photons and ultracold quantum particles*, Phys. Rev. A **79**, 013828 (2009).

[5.33] B. W. Shore, P. Meystre and S. Stenholm, *Is a quantum standing wave composed of two traveling waves?*, J. Opt. Soc. Am. B **8**, 903 (1991).

[5.34] A. Vukics and P. Domokos, *Simultaneous cooling and trapping of atoms by a single cavity-field mode*, Phys. Rev. A **72**, 031401 (2005).

[5.35] S. Deachapunya, P. Fagan, A. Major, E. Reiger, H. Ritsch, A. Stefanov, H. Ulbricht and M. Arndt, *Slow beams of massive molecules*, Eur. Phys. J. D **46**, 307 (2008).

[5.36] P. Horak and H. Ritsch, *Scaling properties of cavity-enhanced atom cooling*, Phys. Rev. A **64**, 033422 (2001).

[5.37] C. W. Gardiner and P. Zoller, *Quantum noise* (Springer-Verlag, Berlin, 2000), Second edition.

[5.38] G. Szirmai, D. Nagy and P. Domokos, *Quantum noise of a Bose-Einstein condensate in an optical cavity, correlations, and entanglement*, Phys. Rev. A **81**, 043639 (2010).

[5.39] I. B. Mekhov, C. Maschler and H. Ritsch, *Cavity-Enhanced Light Scattering in Optical Lattices to Probe Atomic Quantum Statistics*, Phys. Rev. Lett. **98**, 100402 (2007).

[5.40] I. B. Mekhov and H. Ritsch, *Quantum Nondemolition Measurements and State Preparation in Quantum Gases by Light Detection*, Phys. Rev. Lett. **102**, 20403 (2009).

[5.41] J. Dalibard and C. Cohen-Tannoudji, *Dressed-atom approach to atomic motion in laser light: the dipole force revisited*, J. Opt. Soc. Am. B **2**, 1707 (1985).

[5.42] J. Larson and S. Stenholm, *Validity of adiabaticity in cavity QED*, Phys. Rev. A **73**, 33805 (2006).

[5.43] J. Larson, *Dynamics of the Jaynes–Cummings and Rabi models*, Phys. Scr. **76**, 146 (2007).

[5.44] P. Horak and H. Ritsch, *Self-induced Bragg-type scattering in dark optical superlattices*, Phys. Rev. A **55**, 2176 (1997).

[5.45] C. Cohen-Tannoudji and S. Reynaud, *Dressed-atom description of resonance fluorescence and absorption spectra of a multi-level atom in an intense laser beam*, J. Phys. B **10**, 345 (1977).

[5.46] Y. Castin and J. Dalibard, *Quantization of atomic motion in optical molasses*, Europhys. Lett. **14**, 761 (1991).

[5.47] W. Kohn, *Analytic Properties of Bloch Waves and Wannier Functions*, Phys. Rev. **115**, 809 (1959).

[5.48] A. Vukics, C. Maschler and H. Ritsch, *Microscopic physics of quantum self-organization of optical lattices in cavities*, New J. Phys. **9**, 255 (2007).

[5.49] C. J. Pethick and H. Smith, *Bose–Einstein Condensation in Dilute Gases* (Cambridge University Press, Cambridge, 2002).

[5.50] S. Fernández-Vidal, G. De Chiara, J. Larson and G. Morigi, *Quantum ground state of self-organized atomic crystals in optical resonators*, Phys. Rev. A **81**, 043407 (2010).

[5.51] A. Vukics and H. Ritsch, *C++QED: an object-oriented framework for wave-function simulations of cavity QED systems*, Eur. Phys. J. D **44**, 585 (2007).

References for Chapter 6

[6.1] P. Domokos and H. Ritsch, *Mechanical effects of light in optical resonators*, J. Opt. Soc. Am. B **20**, 1098 (2003).

[6.2] I. B. Mekhov and H. Ritsch, *Quantum optics with ultracold quantum gases: towards the full quantum regime of the light–matter interaction*, J. Phys. B **45**, 102001 (2012).

[6.3] S. Gupta, K. L. Moore, K. W. Murch and D. M. Stamper-Kurn, *Cavity Nonlinear Optics at Low Photon Numbers from Collective Atomic Motion*, Phys. Rev. Lett. **99**, 213601 (2007).

[6.4] I. D. Leroux, M. H. Schleier-Smith and V. Vuletić, *Implementation of Cavity Squeezing of a Collective Atomic Spin*, Phys. Rev. Lett. **104**, 073602 (2010).

[6.5] J. Eschner, G. Morigi, F. Schmidt-Kaler and R. Blatt, *Laser cooling of trapped ions*, J. Opt. Soc. Am. B **20**, 1003 (2003).

[6.6] J. D. Thompson, B. M. Zwickl, A. M. Jayich, F. Marquardt, S. M. Girvin and J. G. E. Harris, *Strong dispersive coupling of a high-finesse cavity to a micromechanical membrane*, Nature **452**, 72 (2008).

[6.7] S. Gröblacher, J. B. Hertzberg, M. R. Vanner, G. D. Cole, S. Gigan, K. C. Schwab and M. Aspelmeyer, *Demonstration of an ultracold micro-optomechanical oscillator in a cryogenic cavity*, Nature Phys. **5**, 485 (2009).

[6.8] O. Romero-Isart, A. C. Pflanzer, M. L. Juan, R. Quidant, N. Kiesel, M. Aspelmeyer and J. I. Cirac, *Optically levitating dielectrics in the quantum regime: Theory and protocols*, Phys. Rev. A **83**, 013803 (2011).

[6.9] M. Wallquist, K. Hammerer, P. Zoller, C. Genes, M. Ludwig, F. Marquardt, P. Treutlein, J. Ye and H. J. Kimble, *Single-atom cavity QED and optomicromechanics*, Phys. Rev. A **81**, 023816 (2010).

[6.10] A. Nunnenkamp, K. Børkje, J. G. E. Harris and S. M. Girvin, *Cooling and squeezing via quadratic optomechanical coupling*, Phys. Rev. A **82**, 021806 (2010).

[6.11] H. Krauter, C. A. Muschik, K. Jensen, W. Wasilewski, J. M. Petersen, J. I. Cirac and E. S. Polzik, *Entanglement Generated by Dissipation and Steady State Entanglement of Two Macroscopic Objects*, Phys. Rev. Lett. **107**, 080503 (2011).

[6.12] M. B. Plenio, S. F. Huelga, A. Beige and P. L. Knight, *Cavity-loss-induced generation of entangled atoms*, Phys. Rev. A **59**, 2468 (1999).

[6.13] M. Abdi, S. Barzanjeh, P. Tombesi and D. Vitali, *Effect of phase noise on the generation of stationary entanglement in cavity optomechanics*, Phys. Rev. A **84**, 032325 (2011).

[6.14] K. Børkje, A. Nunnenkamp and S. Girvin, *Proposal for Entangling Remote Micromechanical Oscillators via Optical Measurements*, Phys. Rev. Lett. **107**, 123601 (2011).

[6.15] C. Joshi, J. Larson, M. Jonson, E. Andersson and P. Öhberg, *Entanglement of distant optomechanical systems*, Phys. Rev. A **85**, 033805 (2012).

[6.16] S. Mancini and P. Tombesi, *High-sensitivity force measurement using entangled probes*, Europhys. Lett. **61**, 8 (2003).

[6.17] S. Mancini, V. Giovannetti, D. Vitali and P. Tombesi, *Entangling Macroscopic Oscillators Exploiting Radiation Pressure*, Phys. Rev. Lett. **88**, 120401 (2002).

[6.18] R. J. Schulze, C. Genes and H. Ritsch, *Optomechanical approach to cooling of small polarizable particles in a strongly pumped ring cavity*, Phys. Rev. A **81**, 063820 (2010).

[6.19] W. Niedenzu, R. Schulze, A. Vukics and H. Ritsch, *Microscopic dynamics of ultracold particles in a ring-cavity optical lattice*, Phys. Rev. A **82**, 043605 (2010).

[6.20] M. Gangl and H. Ritsch, *Cold atoms in a high-Q ring cavity*, Phys. Rev. A **61**, 043405 (2000).

[6.21] C. W. Gardiner and P. Zoller, *Quantum noise* (Springer-Verlag, Berlin, 2000), Second edition.

[6.22] I. Wilson-Rae, N. Nooshi, W. Zwerger and T. J. Kippenberg, *Theory of Ground State Cooling of a Mechanical Oscillator Using Dynamical Backaction*, Phys. Rev. Lett. **99**, 093901 (2007).

[6.23] M. Pinard, A. Dantan, D. Vitali, O. Arcizet, T. Briant and A. Heidmann, *Entangling movable mirrors in a double-cavity system*, EPL **72**, 747 (2005).

[6.24] M. Bhattacharya and P. Meystre, *Multiple membrane cavity optomechanics*, Phys. Rev. A **78**, 041801 (2008).

[6.25] K. Mølmer, Y. Castin and J. Dalibard, *Monte Carlo wave-function method in quantum optics*, J. Opt. Soc. Am. B **10**, 524 (1993).

[6.26] A. Vukics and H. Ritsch, *C++QED: an object-oriented framework for wave-function simulations of cavity QED systems*, Eur. Phys. J. D **44**, 585 (2007).

[6.27] A. Vukics, *C++QEDv2: The multi-array concept and compile-time algorithms in the definition of composite quantum systems*, Computer Physics Communications **183**, 1381 (2012).

[6.28] G. Vidal and R. F. Werner, *Computable measure of entanglement*, Phys. Rev. A **65**, 032314 (2002).

[6.29] M. Gangl, P. Horak and H. Ritsch, *Cooling neutral particles in multimode cavities without spontaneous emission*, J. Mod. Opt. **47**, 2741 (2000).

[6.30] R. M. Sandner *et al.*, in preparation (2012).

[6.31] W. Alge, K. M. Gheri and M. A. M. Marte, *The non-degenerate optical parametric oscillator in the strong-coupling regime*, J. Mod. Opt. **44**, 841 (1997).

[6.32] G. Adesso and F. Illuminati, *Entanglement in continuous-variable systems: recent advances and current perspectives*, J. Phys. A: Math. Theor. **40**, 7821 (2007).

[6.33] R. Simon, *Peres-Horodecki Separability Criterion for Continuous Variable Systems*, Phys. Rev. Lett. **84**, 2726 (2000).

[6.34] A. Vukics, C. Maschler and H. Ritsch, *Microscopic physics of quantum self-organization of optical lattices in cavities*, New J. Phys. **9**, 255 (2007).

References for Chapter 7

[7.1] M. Wallquist, K. Hammerer, P. Zoller, C. Genes, M. Ludwig, F. Marquardt, P. Treutlein, J. Ye and H. J. Kimble, *Single-atom cavity QED and optomicromechanics*, Phys. Rev. A **81**, 023816 (2010).

[7.2] C. W. Gardiner and P. Zoller, *Quantum Noise* (Springer-Verlag, Berlin, 2000), Second edition.

[7.3] G. Adesso and F. Illuminati, *Entanglement in continuous-variable systems: recent advances and current perspectives*, J. Phys. A: Math. Theor. **40**, 7821 (2007).

[7.4] R. Simon, *Peres-Horodecki Separability Criterion for Continuous Variable Systems*, Phys. Rev. Lett. **84**, 2726 (2000).

[7.5] G. Vidal and R. F. Werner, *Computable measure of entanglement*, Phys. Rev. A **65**, 032314 (2002).

References for Chapter 8

[8.1] E. Wigner, *On the Quantum Correction For Thermodynamic Equilibrium*, Phys. Rev. **40**, 749 (1932).

[8.2] W. P. Schleich, *Quantum Optics in Phase Space* (Wiley-VCH, Berlin, 2001), First edition.

[8.3] C. W. Gardiner and P. Zoller, *Quantum Noise* (Springer-Verlag, Berlin, 2000), Second edition.

[8.4] D. F. Walls and G. J. Milburn, *Quantum Optics* (Springer-Verlag, Berlin, 1994), First edition.

[8.5] P. E. Kloeden and E. Platen, *Numerical solution of stochastic differential equations* (Springer-Verlag, Berlin, 1992), First edition.

[8.6] F. Cattivelli and A. H. Sayed, *Self-organization in bird flight formations using diffusion adaptation*, 3rd IEEE International Workshop on Computational Advances in Multi-Sensor Adaptive Processing (CAMSAP), 49 (2009).

[8.7] J. M. Lehn, *Toward self-organization and complex matter*, Science **295**, 2400 (2002).

[8.8] P. Bak, C. Tang and K. Wiesenfeld, *Self-organized criticality*, Phys. Rev. A **38**, 364 (1988).

[8.9] P. Domokos and H. Ritsch, *Collective cooling and self-organization of atoms in a cavity*, Phys. Rev. Lett. **89**, 253003 (2002).

[8.10] A. T. Black, H. W. Chan and V. Vuletić, *Observation of Collective Friction Forces due to Spatial Self-Organization of Atoms: From Rayleigh to Bragg Scattering*, Phys. Rev. Lett. **91**, 203001 (2003).

[8.11] S. Stenholm, *The semiclassical theory of laser cooling*, Rev. Mod. Phys. **58**, 699 (1986).

[8.12] P. Domokos, P. Horak and H. Ritsch, *Semiclassical theory of cavity-assisted atom cooling*, J. Phys. B **34**, 187 (2001).

[8.13] P. Domokos, P. Horak and H. Ritsch, *Semiclassical Theory of Cavity-assisted Light Forces on Atoms and Applications*, Fortschr. Phys. **49**, 935 (2001).

[8.14] J. K. Asbóth, P. Domokos, H. Ritsch and A. Vukics, *Self-organization of atoms in a cavity field: Threshold, bistability, and scaling laws*, Phys. Rev. A **72**, 053417 (2005).

[8.15] H. W. Chan, A. T. Black and V. Vuletić, *Observation of Collective-Emission-Induced Cooling of Atoms in an Optical Cavity*, Phys. Rev. Lett. **90**, 063003 (2003).

[8.16] A. T. Black, J. K. Thompson and V. Vuletić, *Collective light forces on atoms in resonators*, J. Phys. B **38**, S605 (2005).

References for Chapter 9

[9.1] R. Grimm, M. Weidemüller and Y. B. Ovchinnikov, *Optical dipole traps for neutral atoms*, Adv. At. Mol. Opt. Phys. **42**, 95 (2000).

[9.2] J. D. Miller, R. A. Cline and D. J. Heinzen, *Far-off-resonance optical trapping of atoms*, Phys. Rev. A **47**, 4567 (1993).

[9.3] P. Domokos and H. Ritsch, *Mechanical effects of light in optical resonators*, J. Opt. Soc. Am. B **20**, 1098 (2003).

[9.4] P. Domokos and H. Ritsch, *Collective Cooling and Self-Organization of Atoms in a Cavity*, Phys. Rev. Lett. **89**, 253003 (2002).

[9.5] A. T. Black, H. W. Chan and V. Vuletić, *Observation of Collective Friction Forces due to Spatial Self-Organization of Atoms: From Rayleigh to Bragg Scattering*, Phys. Rev. Lett. **91**, 203001 (2003).

[9.6] J. K. Asbóth, P. Domokos, H. Ritsch and A. Vukics, *Self-organization of atoms in a cavity field: Threshold, bistability, and scaling laws*, Phys. Rev. A **72**, 053417 (2005).

[9.7] V. Vuletić and S. Chu, *Laser Cooling of Atoms, Ions, or Molecules by Coherent Scattering*, Phys. Rev. Lett. **84**, 3787 (2000).

[9.8] B. L. Lev, A. Vukics, E. R. Hudson, B. C. Sawyer, P. Domokos, H. Ritsch and J. Ye, *Prospects for the cavity-assisted laser cooling of molecules*, Phy. Rev. A **77**, 023402 (2008).

[9.9] T. Salzburger and H. Ritsch, *Collective transverse cavity cooling of a dense molecular beam*, New J. Phys. **11**, 055025 (2009).

[9.10] T. Grießer, H. Ritsch, M. Hemmerling and G. R. M. Robb, *A Vlasov approach to bunching and selfordering of particles in optical resonators*, Eur. Phys. J. D **58**, 349 (2010).

[9.11] P. Domokos, P. Horak and H. Ritsch, *Semiclassical theory of cavity-assisted atom cooling*, J. Phys. B **34**, 187 (2001).

[9.12] W. P. Schleich, *Quantum Optics in Phase Space* (Wiley-VCH, Berlin, 2001), First edition.

[9.13] P. E. Kloeden and R. Pearson, *The numerical solution of stochastic differential equations*, J. Austral. Math. Soc. Ser. B **20**, 8 (1977).

[9.14] W. Rümelin, *Numerical treatment of stochastic differential equations*, SIAM J. Numer. Anal. **19**, 604 (1982).

[9.15] D. C. Montgomery, *Theory of the Unmagnetized Plasma* (Gordon and Breach, New York, 1971), First edition.

[9.16] A. M. C. de Souza and C. Tsallis, *Student's t-and r-distributions: Unified derivation from an entropic variational principle*, Physica A **236**, 52 (1997).

[9.17] E. Lutz, *Anomalous diffusion and Tsallis statistics in an optical lattice*, Phys. Rev. A **67**, 051402 (2003).

[9.18] P. Douglas, S. Bergamini and F. Renzoni, *Tunable Tsallis Distributions in Dissipative Optical Lattices*, Phys. Rev. Lett. **96**, 110601 (2006).

[9.19] J. F. Luciani and R. Pellat, *Kinetic equation of finite Hamiltonian systems with integrable mean field*, J. Physique **48**, 591 (1987).

[9.20] P.-H. Chavanis, *Kinetic theory with angle-action variables*, Physica A **377**, 469 (2007).

[9.21] T. Grießer, W. Niedenzu and H. Ritsch, *Selforganisation and sympathetic cooling of multispecies ensembles in a cavity*, arXiv:1106.2340 [quant-ph] (2011).

[9.22] H. A. Posch and W. Thirring, *Stellar stability by thermodynamic instability*, Phys. Rev. Lett. **95**, 251101 (2005).

[9.23] P. Horak and H. Ritsch, *Scaling properties of cavity-enhanced atom cooling*, Phys. Rev. A **64**, 033422 (2001).

References for Chapter 10

[10.1] T. Grießer, H. Ritsch, M. Hemmerling and G. R. M. Robb, *A Vlasov approach to bunching and selfordering of particles in optical resonators*, Eur. Phys. J. D **58**, 349 (2010).

[10.2] D. C. Montgomery, *Theory of the Unmagnetized Plasma* (Gordon and Breach, New York, 1971), First edition.

[10.3] P. E. Kloeden and E. Platen, *Numerical solution of stochastic differential equations* (Springer-Verlag, Berlin, 1992), First edition.

References for Chapter 11

[11.1] H. J. Metcalf and P. van der Straten, *Laser cooling and trapping* (Springer-Verlag, New York, 1999).

[11.2] G. Thalhammer, R. Steiger, S. Bernet and M. Ritsch-Marte, *Optical macro-tweezers: trapping of highly motile micro-organisms*, J. Opt. **13**, 044024 (2011).

[11.3] J. Doyle, B. Friedrich, R. V. Krems and F. Masnou-Seeuws, *Quo vadis, cold molecules?*, Eur. Phys. J. D **31**, 149 (2004).

[11.4] T. J. Kippenberg and K. J. Vahala, *Cavity optomechanics: back-action at the mesoscale*, Science **321**, 1172 (2008).

[11.5] E. S. Shuman, J. F. Barry and D. DeMille, *Laser cooling of a diatomic molecule*, Nature **467**, 820 (2010).

[11.6] V. Vuletić and S. Chu, *Laser cooling of atoms, ions, or molecules by coherent scattering*, Phys. Rev. Lett. **84**, 3787 (2000).

[11.7] B. L. Lev, A. Vukics, E. R. Hudson, B. C. Sawyer, P. Domokos, H. Ritsch and J. Ye, *Prospects for the cavity-assisted laser cooling of molecules*, Phys. Rev. A **77**, 023402 (2008).

[11.8] S. Nimmrichter, K. Hammerer, P. Asenbaum, H. Ritsch and M. Arndt, *Master equation for the motion of a polarizable particle in a multimode cavity*, New J. Phys. **12**, 083003 (2010).

[11.9] V. Vuletić, H. W. Chan and A. T. Black, *Three-dimensional cavity Doppler cooling and cavity sideband cooling by coherent scattering*, Phys. Rev. A **64**, 033405 (2001).

[11.10] S. Slama, S. Bux, G. Krenz, C. Zimmermann and P. W. Courteille, *Superradiant Rayleigh scattering and collective atomic recoil lasing in a ring cavity*, Phys. Rev. Lett. **98**, 053603 (2007).

[11.11] K. Baumann, C. Guerlin, F. Brennecke and T. Esslinger, *Dicke quantum phase transition with a superfluid gas in an optical cavity*, Nature **464**, 1301 (2010).

[11.12] A. T. Black, H. W. Chan and V. Vuletić, *Observation of collective friction forces due to spatial self-organization of atoms: From Rayleigh to Bragg scattering*, Phys. Rev. Lett. **91**, 203001 (2003).

[11.13] S. Deachapunya, P. J. Fagan, A. G. Major, E. Reiger, H. Ritsch, A. Stefanov, H. Ulbricht and M. Arndt, *Slow beams of massive molecules*, Eur. Phys. J. D **46**, 307 (2008).

[11.14] J. K. Asbóth, P. Domokos, H. Ritsch and A. Vukics, *Self-organization of atoms in a cavity field: Threshold, bistability, and scaling laws*, Phys. Rev. A **72**, 053417 (2005).

[11.15] T. Salzburger and H. Ritsch, *Collective transverse cavity cooling of a dense molecular beam*, New J. Phys. **11**, 055025 (2009).

[11.16] E. Haller, M. Gustavsson, M. J. Mark, J. G. Danzl, R. Hart, G. Pupillo and H.-C. Nägerl, *Realization of an excited, strongly correlated quantum gas phase*, Science **325**, 1224 (2009).

[11.17] P. Domokos, P. Horak and H. Ritsch, *Semiclassical theory of cavity-assisted atom cooling*, J. Phys. B **34**, 187 (2001).

[11.18] W. Niedenzu, T. Grießer and H. Ritsch, *Kinetic theory of cavity cooling and selforganisation of a cold gas*, EPL **96**, 43001 (2011).

[11.19] T. Grießer, H. Ritsch, M. Hemmerling and G. R. M. Robb, *A Vlasov approach to bunching and selfordering of particles in optical resonators*, Eur. Phys. J. D **58**, 349 (2010).

[11.20] Y. L. Klimontovich, *Statistical theory of open systems* (Kluwer Academic Publishers, Dordrecht, 1995), First edition.

[11.21] L. D. Landau, *On the vibrations of the electronic plasma*, J. Phys. USSR **10**, 574 (1946).

[11.22] V. B. Krapchev and A. K. Ram, *Adiabatic theory for a single nonlinear wave in a Vlasov plasma*, Phy. Rev. A **22**, 1229 (1980).

[11.23] P.-H. Chavanis, *Kinetic theory with angle-action variables*, Physica A **377**, 469 (2007).

[11.24] R. Balescu, *Irreversible processes in ionized gases*, Phys. Fluids **3**, 52 (1960).

[11.25] A. Lenard, *On Bogoliubov's kinetic equation for a spatially homogeneous plasma*, Ann. Phys. **10**, 390 (1960).

[11.26] J. F. Luciani and R. Pellat, *Kinetic equation of finite Hamiltonian systems with integrable mean field*, J. Physique **48**, 591 (1987).

[11.27] D. Kruse, M. Ruder, J. Benhelm, C. von Cube, C. Zimmermann, P. W. Courteille, T. Elsässer, B. Nagorny and A. Hemmerich, *Cold atoms in a high-Q ring cavity*, Phys. Rev. A **67**, 051802 (2003).

[11.28] S. Ritter, F. Brennecke, K. Baumann, T. Donner, C. Guerlin and T. Esslinger, *Dynamical coupling between a Bose–Einstein condensate and a cavity optical lattice*, Appl. Phys. B **95**, 213 (2009).

[11.29] S. Gopalakrishnan, B. L. Lev and P. M. Goldbart, *Emergent crystallinity and frustration with Bose–Einstein condensates in multimode cavities*, Nat. Phys. **5**, 845 (2009).

List of publications

Publications during the PhD

Preprint

- W. Niedenzu, R. M. Sandner, C. Genes and H. Ritsch, *Quantum-correlated motion and heralded entanglement of distant optomechanically coupled objects*, arXiv:1205.6596 [quant-ph] (2012).

Articles

- T. Grießer, W. Niedenzu and H. Ritsch, *Cooperative self-organization and sympathetic cooling of a multispecies gas in a cavity*, New J. Phys. **14**, 053031 (2012).
- W. Niedenzu, T. Grießer and H. Ritsch, *Kinetic theory of cavity cooling and self-organisation of a cold gas*, EPL **96**, 43001 (2011).
- W. Niedenzu, R. Schulze, A. Vukics and H. Ritsch, *Microscopic dynamics of ultracold particles in a ring-cavity optical lattice*, Phys. Rev. A **82**, 043605 (2010).

Publications before starting the PhD

- A. Vukics, W. Niedenzu and H. Ritsch, *Cavity nonlinear optics with few photons and ultracold quantum particles*, Phys. Rev. A **79**, 013828 (2009). Selected for Virt. J. Quantum Inf. **9** (2009).
- W. Niedenzu, *Nonlinear Dynamics of Ultracold Atoms in a Quantized Lattice Potential*, Diploma thesis, University of Innsbruck (2008).

Poster presentations

- *Entanglement and momentum correlations in a ring resonator*, International Conference on Quantum Optics (Obergurgl, Austria, 12–18 February 2012).
- *Kinetic theory of cavity cooling and selforganisation of a cold gas*, ECOQAS11 (Dresden, Germany, 10–14 October 2011).
- *Kinetic theory of cavity cooling and selforganisation of a cold gas*, Dynamics and Simulation of Ultra-Cold Matter Workshop (Windsor, United Kingdom, 8–11 August 2011).
- *Kinetic theory of cavity cooling and selforganisation of a cold gas*, SFB Meeting (Innsbruck, Austria, 7–8 July 2011).
- *Kinetic theory of cavity cooling and selforganisation of a cold gas*, SFB Meeting (Vienna, Austria, 19–20 May 2011).
- *Microscopic dynamics of ultracold particles in a ring-cavity optical lattice*, FOMO 2011 Conference (Obergurgl, Austria, 20–26 March 2011).
- *Microscopic dynamics of ultracold particles in a ring-cavity optical lattice*, EMALI Conference 2010 (Barcelona, Spain, 23–25 September 2010).
- *Microscopic dynamics of ultracold particles in a ring-resonator-generated optical lattice*, 8th SFB-FoQuS Meeting (Innsbruck, Austria, 8–9 July 2010).
- *Dynamics of ultracold atoms in a ring-cavity generated optical lattice*, International Conference on Quantum Optics (Obergurgl, Austria, 21–27 February 2010).